AD-A130 546 ATMOSPHERIC CHEMILUMINESCENCE: COCHISE (COLD CHEMICAL INFRARED SIMULATION.. (U) AIR FORCE GEOPHYSICS LAB HANSCOM AFB MA R A ARMSTRONG ET AL. 13 OCT 82 1/2

UNCLASSIFIED AFGL-TR-82-0305 F/G 4/1 NL

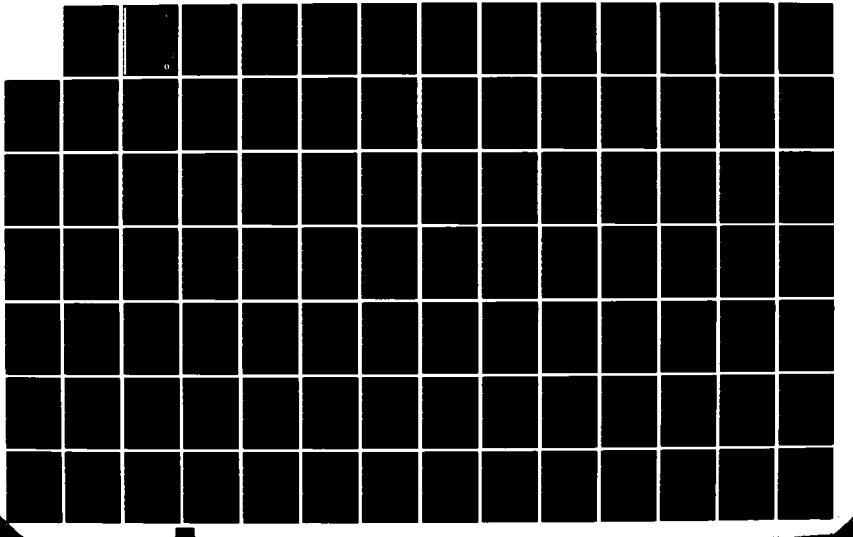

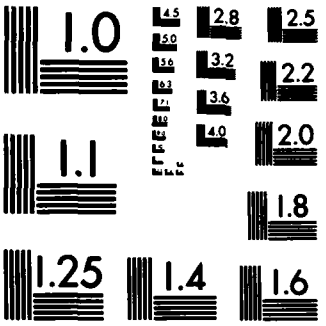

MICROCOPY RESOLUTION TEST CHART
NATIONAL BUREAU OF STANDARDS-1963-A

AFGL-TR-82-0305
PHYSICAL SCIENCES RESEARCH PAPERS, NO. 660

Atmospheric Chemiluminescence: COCHISE and Related Experiments

R.A. ARMSTRONG
J.P. KENNEALY
F.X. ROBERT
A. CORMAN
W.T. RAWLINS
L.G. PIPER
G.E. CALEDONIA
B. D. GREEN
H.C. MURPHY
J.I. STEINFELD
R. STACHNIK
S.M. ADLER-GOLDEN

13 OCTOBER 1982

OPTICAL PHYSICS DIVISION PROJECT 2310
AIR FORCE GEOPHYSICS LABORATORY
HANSCOM AFB, MASSACHUSETTS 01731

AIR FORCE SYSTEMS COMMAND, USAF

Unclassified

SECURITY CLASSIFICATION OF THIS PAGE (When Data Entered)

REPORT DOCUMENTATION PAGE		READ INSTRUCTIONS BEFORE COMPLETING FORM
1. REPORT NUMBER AFGL-TR-82-0305	2. GOVT ACCESSION NO. AD-A130546	3. RECIPIENT'S CATALOG NUMBER
4. TITLE (and Subtitle) ATMOSPHERIC CHEMILUMINESCENCE: COCHISE AND RELATED EXPERIMENTS		5. TYPE OF REPORT & PERIOD COVERED Scientific. Final 1 Nov 79-30 Sep 82
		6. PERFORMING ORG. REPORT NUMBER PSRP, No. 660
7. AUTHOR(s) R.A. Armstrong, J.P. Kennealy, F.X. Robert, A. Corman, W. T. Rawlins,[1] L. G. Piper,[1] G. E. Caledonia,[1] B. D. Green,[1] H. C. Murphy,[1] J. I. Steinfeld,[2] R. Stachnik,[2] S. M. Adler-Golden[3]		8. CONTRACT OR GRANT NUMBER(s)
9. PERFORMING ORGANIZATION NAME AND ADDRESS Air Force Geophysics Laboratory (OPR-1) Hanscom AFB Massachusetts 01731		10. PROGRAM ELEMENT, PROJECT, TASK AREA & WORK UNIT NUMBERS 61102F 2310G410
11. CONTROLLING OFFICE NAME AND ADDRESS Air Force Geophysics Laboratory (OPR-1) Hanscom AFB Massachusetts 01731		12. REPORT DATE 13 October 1982
		13. NUMBER OF PAGES 200
14. MONITORING AGENCY NAME & ADDRESS(if different from Controlling Office)		15. SECURITY CLASS. (of this report) Unclassified
		15a. DECLASSIFICATION/DOWNGRADING SCHEDULE

16. DISTRIBUTION STATEMENT (of this Report)

Approved for public release; distribution unlimited.

17. DISTRIBUTION STATEMENT (of the abstract entered in Block 20, if different from Report)

18. SUPPLEMENTARY NOTES

1. Physical Sciences, Inc. Research Park Andover, MA 01810
2. Dept of Chemistry Mass Institute of Tech Cambridge, MA 02139
3. Spectral Sciences 99 S. Bedford St. Burlington, MA 01803

19. KEY WORDS (Continue on reverse side if necessary and identify by block number)

COCHISE	Ozone excitation	Vibrational excitation
FAKIR	Nitric oxide	Laser excitation
FACELIF	Nitrogen (^{2}D)	Nitrogen (A)
Chemiluminescence	Argon emission	Oxygen (^{1}S)

20. ABSTRACT (Continue on reverse side if necessary and identify by block number)

This final report includes: (a) a discussion of the analysis of recent COCHISE data relevant to O_3 and NO infrared emission; (b) a review of recent FAKIR measurements on the quenching reactions of $N_2(A)$ with O_2, O and on the formation of $O(^1S)$ in the quenching of $N_2(A)$ by O; (c) the development and exercising of a model for the prediction of upper atmospheric NO radiation in quiescent and aurorally excited atmospheres; (d) the design requirements for FACELIF, a flow reactor with laser photoexcitation capabilities; and (e) design criteria for color center laser absorption experiments.

DD FORM 1 JAN 73 1473 EDITION OF 1 NOV 65 IS OBSOLETE

Unclassified

SECURITY CLASSIFICATION OF THIS PAGE (When Data Entered)

Contents

Atmospheric Chemiluminescence: COCHISE and Related Experiments

1. Introduction

During the last three years, thermochemical sources of infrared radiation from the upper atmosphere have been investigated in an AFGL program called Laboratory Investigations of Infrared Atmospheric Processes, Work Unit 2310G410. The program was initiated with two experiments; COld CHemical Infrared Simulation Experiment (COCHISE) and Flowing Atmospheric Kinetic InfraRed (FAKIR). Over the period, new experiments were added utilizing laser technology as it applies to atmospheric phenomena. These experiments and resulting analysis are described in detail in the following chapters. The tasks addressed in this report are:

Task 1. Using the COCHISE facility, measure the chemiluminescent radiation of NO and O_3 resulting from the reactions:

(1) $N(^2D) + O_2 \rightarrow NO + O$

(2) $O + O_2(+M) \rightarrow O_3(+M)$.

Measurements include the fundamental and overtone bands of NO and a survey of the potential infrared radiative bands of O_3.

Task 2. Interpret and analyze infrared measurements of NO and O_3 chemiluminescence. Such analysis includes deduction of vibrational populations within radiating bands and interpretation of the fluorescence in terms of reaction mechanism.

(Received for publication 8 October 1982)

Task 3. Using the FAKIR facility, study the reactions between $N_2(A\ ^3\Sigma_u^+)$ and oxygen molecules and atoms. Measure the rate constants for these reactions and reaction products and delineate branching ratios where possible.

Task 4. Perform additional subsidiary measurements on the COCHISE and FAKIR facilities as required for the successful completion of Tasks 1, 2, and 3. Such efforts include calibration tests and other measurements required for system or discharge diagnoses.

Task 5. Design and fabricate an apparatus using a krypton-ion laser pumped color center laser operating in the 2-3.5μm region, to perform high resolution absorption and emission experiments on O_3 and CO_2.

Task 6. Develop a steady-state model for the prediction of NO infrared radiation in the upper atmosphere. Include NO excitation sources specific to both the quiescent and aurorally excited upper atmosphere in the model, and include the coupled excitation and relaxation of the individual NO vibrational levels. Predict NO fluorescence for typical atmospheric conditions and dosing rates and compare the predictions with field data.

Task 7. Examine other infrared emissions arising from microwave discharged N_2/O_2.

Task 8. Design and fabricate the FACELIF facility. The FACELIF discharge-flow apparatus includes both a resonance fluorescence diagnostic and the capability to create free radicals via laser photolysis.

The experiments were completed on-site at AFGL. Due to the depth and breadth of experimental activity, external organizations performed parts of the investigation under contract, with a closely integrated scientific approach. The various components are thus inseparable, giving rise to the rather lengthy list of contributing authors. Because many of them contributed to each chapter, the chapters do not contain separate lists of authors.

The report, a final comprehensive description of the investigations performed, consists of several chapters, each a self-contained description of an experiment. Several appendixes follow, which are preprints or reprints of journal articles that give added detail and interpretation to the report.

Contents

2. COCHISE Experiments

1. INTRODUCTION

The COCHISE facility[1] is a relatively large, cryogenically cooled test chamber that may be used to study the state of the reaction products created as the result of a variety of possible gas phase reactions such as chemi-excitation processes, for example,

$$A + BC \rightarrow AB^* + C \quad , \tag{1}$$

$$A + B \xrightarrow{M} AB^* \quad , \tag{2}$$

and vibrational exchange or electronic state quenching reactions

$$A^* + B \rightarrow A + B^* \tag{3}$$

where the quantities A, B, and C represent atoms or molecules and the asterisk implies electronically or vibrationally excited states. An exhaustive description

1. Kennealy, J.P., DelGreco, F.P., Caledonia, G.E., and Rawlins, W.T. (1979) COCHISE: laboratory spectroscopic studies of atmospheric phenomena with high-sensitivity cryogenic instrumentation, Proc. Soc. Photo-Opt. Instrumentation Eng., G.A. Vanasse, Ed., 191:151.

of the design and capabilities of the facility was recently prepared and is given in Appendix A. This information is summarized below.

The basic COCHISE reaction cell (Figure 1) is cylindrically symmetric. Reagent gases are introduced through four sets of opposing inlet jets. The gases from these jets mix along the cell centerline where the reaction of interest occurs. The cell walls, held at temperatures near 20 K, remove the reactant gases from the interaction zone by cryopumping. Microwave discharge excitation is possible in one of each set of jets, allowing the formation of various atoms and free radicals as potential chemical reactants.

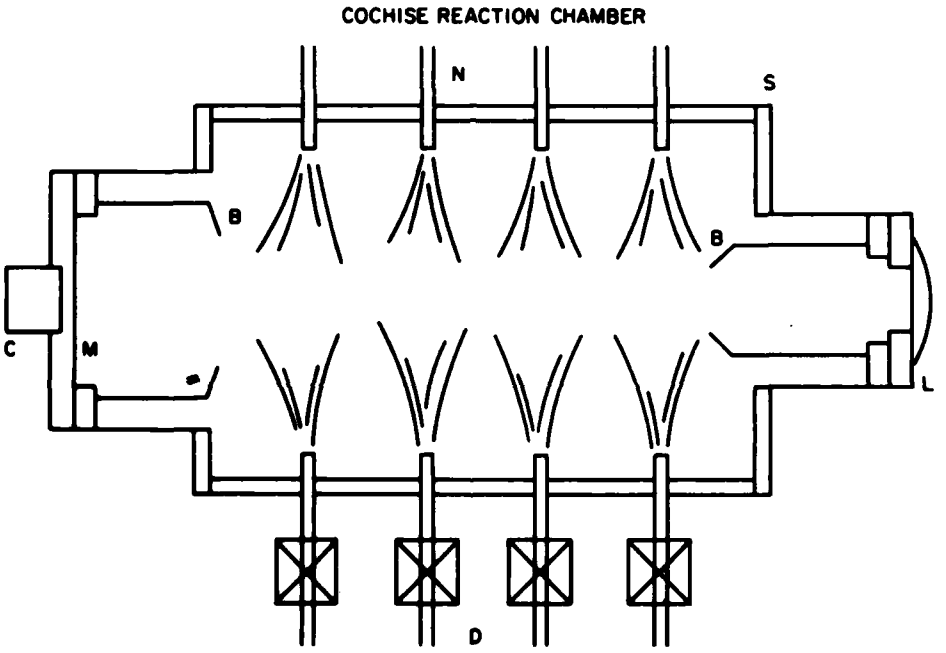

Figure 1. Scale Drawing of Chemiluminescence Reaction Cell. Ar/N_2 mixtures are excited by microwave discharges, D, and mix with the counterflow of O_2 from nozzles N in an axisymmetric reaction zone at the chamber center. Baffles, B, restrict detection system field-of-view to the on-axis reaction volume. M is a plane mirror which increases the intensity of the radiation collected by lens L. Spectral response calibration is performed using blackbody source, C, embedded behind a small hole in the end mirror

The COCHISE facility has two features which give it unique capabilities for the study of detailed reaction phenomena. The first of these is the cryopumping system, which allows operation of the reaction cell at low pressures, 10^{-6} atm, and

reagent gas temperatures, 40-100 K, without any system contamination resulting from wall effects. These operating conditions, coupled with gas residence times of the order of 1 msec or less, allow the examination of reaction product distributions under nearly single-collision conditions, that is, under conditions where the product distribution of states is unaffected by additional inelastic processes occurring in subsequent collisions.

The second feature involves the ability of the system to monitor the infrared fluorescence of excited species having concentrations as small as $10^6/cm^3$. This feature is achieved by connecting the fluorescence monitor, a 0.5-meter Czerny-Turner scanning monochromator, directly to the reaction cell and enclosing the whole in a vacuum shroud held at 20 K. Thus, the radiation background against which the spectrometer must discriminate is never greater than that of a 20 K blackbody. This low background, coupled with an ac detection system synchronized to the repetitively pulsed microwave discharge source, provides the capability for measurement of extremely small excited state concentrations.

The band systems most recently under investigation in the COCHISE facility are the first overtone band of NO, near 2.7 μm, and the asymmetric stretch (ν_3) band of O_3, near 10 μm. The ongoing studies of these bands have been discussed previously;[2] recent developments in the analysis of COCHISE data are described in the following sections.

2. NO ($\Delta v = 2$) CHEMILUMINESCENCE

The emission from the NO ($\Delta v = 2$) band system, observed in COCHISE experiments from the interaction of O_2 with discharged N_2/Ar mixtures in the low-pressure mixing region,[2] is likely due to nascent NO(v) formed in the reaction volume by the reaction (s)

$$N(^2D, {}^2P) + O_2 \rightarrow NO(v) + O \qquad (4)$$

as was shown to be the case for NO ($\Delta v = 1$) radiation observed at 5.4 μm in similar experiments.[3] Since the nascent vibrational distribution must be identical for

---

2. Rawlins, W.T., Piper, L.G., Green, B.D., Wilemski, G., Goela, J.S., and Caledonia, G.E. (1980) LABCEDE and COCHISE Analysis II, Volume I. Final Report, Physical Sciences Inc., Contract No. 19628-77-C-0089, AFGL-TR-80-0063(I), AD A112253.

3. Kennealy, J.P., DelGreco, F.P., Caledonia, G.E., and Green, B.D. (1978) Nitric oxide chemi-excitation occurring in the reaction between metastable nitrogen atoms and oxygen molecules, J. Chem. Phys. 69:1574.

the two band systems, the resulting spectral data may be used to determine the ratio of the spontaneous emission coefficients for the two bands as functions of emitting vibrational level. These ratios have not been measured for $v \geq 2$; only theoretical predictions[4] are available. However, the COCHISE data are affected by the presence of other radiation in the same spectral range as the NO overtone emission; this effect is most pronounced for the short wavelength portion of the band (that is, at lower vibrational levels, $v < 6$).[2]

A typical survey spectrum of the spectral region from 2 to 4 μm is shown in Figure 2 for the interaction of O_2 with a discharged N_2/Ar mixture. The NO overtone band can be seen extending from 2.65 μm to 3.25 μm; the remaining bands are not related to NO. A first-pass evaluation of the origin of this radiation is discussed here.

Experiments in which Ar was used instead of O_2 as a counterflow gas yielded spectra similar to that in Figure 2, except that the NO radiation was not observed; however, some weak spectral features were observed between 2.6 and 3.2 μm. Removal of N_2 from the discharge mixture resulted in a spectrum of readily

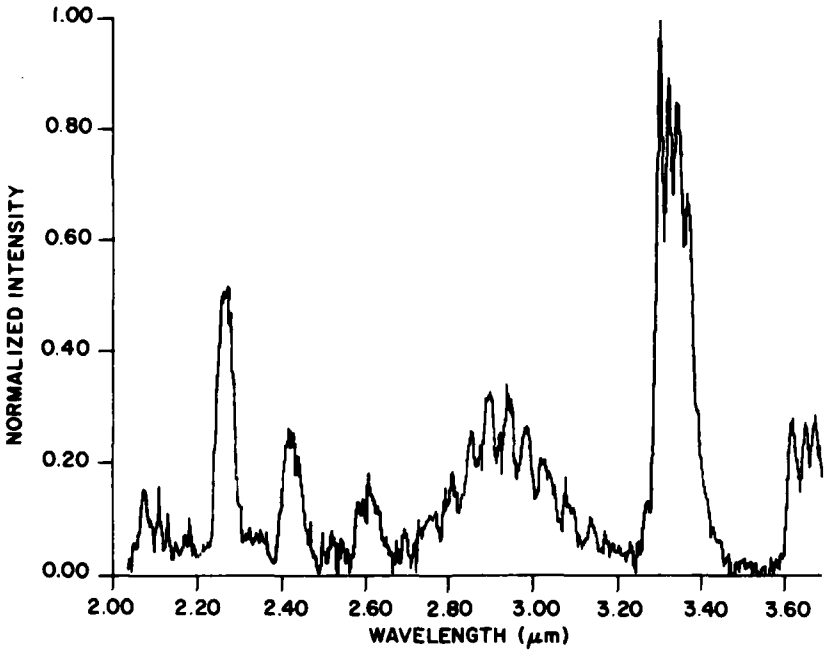

Figure 2. SWIR Spectrum Observed From the Interaction of Discharged N_2/Ar With O_2. Experiment 257704, 1 mm slits, 90 K

4. Billingsley II, F.P. (1976) Calculated vibration rotation intensities for NO($X^2\pi$), J. Molec. Spectrosc. 61:53.

identifiable Ar I atomic lines;[5,6] a partial list of the observed lines is given in Table 1. Since the radiative lifetimes of these transitions are expected to be of the order of 1 μsec,[7] it is difficult to postulate a mechanism for the occurrence of this radiation in the field of view; however, similar spectra have been observed in electron-irradiated argon in the LABCEDE facility.[8] It should be noted that the appearance of these lines can be turned to advantage as a means of calibrating the wavelength setting and resolution of the monochromator.

Table 1. Ar I Lines Identified to Date in COCHISE Spectra, 2-4 μm

λ, μm	σ, cm^{-1}	Energy Levels, cm^{-1}
2.06	4849.224	107289 - 112138
2.10	4763.756	107054 - 111818
2.15	4642.507	107496 - 112138
2.21	4528.328	107289 - 111818
	4521.069	112138 - 116660
2.31	4321.611	107496 - 111818
2.38	4192.601	112750 - 116942
2.51	3978.971	113020 - 116999
2.55	3919.695	113643 - 117562
2.57	3895.898	114975 - 118870
2.69	3715.117	113468 - 117183
2.85	3508.066	113643 - 117151
2.86	3494.032	114975 - 118469
2.88	3474.281	113468 - 116942
2.98	3356.066	120229 - 123557
3.13	3191.520	113468 - 116660
3.31	3023.087	116660 - 119683
	3016.733	113643 - 116660

5. Outred, M. (1978) Tables of atomic spectral lines for the 10000 Å to 40000 Å region, J. Phys. Chem. Ref. Data 7:1.
6. Moore, C.E. (1971) Atomic Energy Levels, Vol. I, NSRDS-NBS 35.
7. Wiese, W.L., Smith, M.W., and Miles, B.M. (1969) Atomic Transition Probabilities, Vol. II, NSRDS-NBS 22.
8. Green, B.D., private communication.

Most of the Ar I lines listed in Table 1 are masked in the spectrum of Figure 2 by the prominent band features, which appear to be related to N_2 in the microwave discharge gas. We have conducted a search through all the known infrared band systems of N I[5] and N_2[9]. The only possible contributors identified in this search are the following band systems of N_2: First Positive ($B\ ^2\Pi_g - A\ ^3\Sigma_u^+$), McFarlane ($a\ ^1\Pi_g - a'\ ^1\Sigma_u^-$, $w\ ^1\Delta_i - a\ ^1\Pi_g$), Wu-Benesch ($W\ ^3\Delta_u - B\ ^3\Pi_g$), and an unclassified system whose states are believed to be quintets. The band heads for these systems are plotted in Figure 3, superimposed upon the spectrum from Figure 2. It can be seen from this comparison that, while the evidence for the other band systems is marginal at best, the correlation between the observed features and the Wu-Benesch band heads is excellent. However, the features at 3.3 and 3.7 μm appear too complex to be due to Wu-Benesch emission alone. A tabulation of the known emission bands of the Wu-Benesch system is given in Table 2. Since the radiative lifetime of the $W\ ^3\Delta_u$ state is believed to be about 1 msec,[9] it is possible that excitation processes occurring in the discharge region could be responsible for the appearance of the radiation in the field of view.

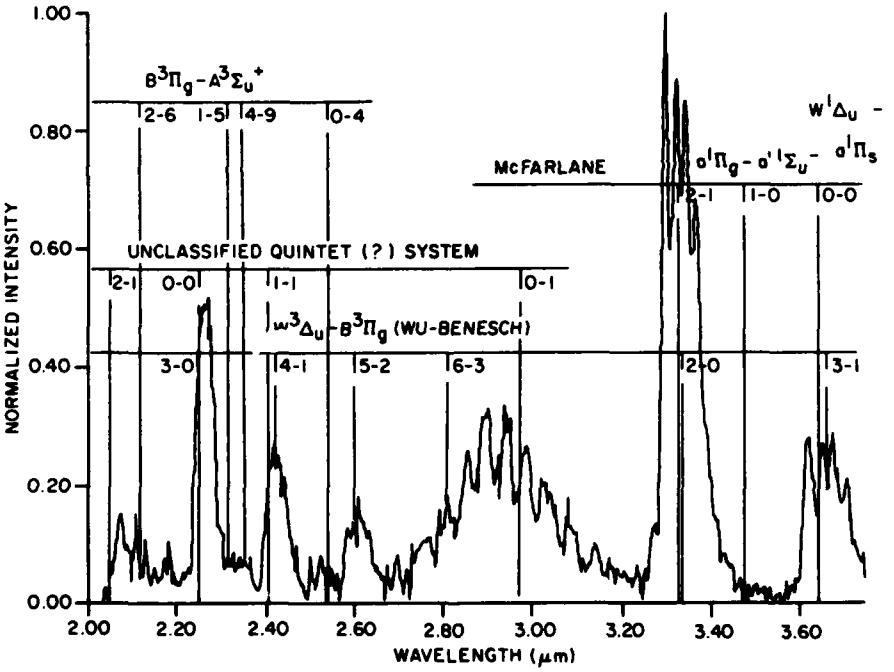

Figure 3. Comparison of N_2 Infrared Band Heads With the Spectrum of Figure 2

9. Lofthus, A., and Krupenie, P.H. (1977) The spectrum of molecular nitrogen, J. Phys. Chem. Ref. Data 6:113.

Table 2. Known Emission Band Origins of the W $^3\Delta_u$ - B $^3\Pi_g$ System (Wu-Benesch)[9]

λ_o (μm)	σ_o (cm^{-1})	Δv	v' - v''
3.33	3007	+2	2 - 0
3.66	2734		3 - 1
4.06	2463		4 - 2
2.25	4439	+3	3 - 0
2.42	4139		4 - 1
2.60	3852		5 - 2
2.81	3565		6 - 3

It can be seen from Tables 1 and 2 that the Ar I and N_2 Wu-Benesch radiation which we have tentatively identified will interfere with the NO ($\Delta v = 2$) measurements between 2.6 and 3.3 μm. For this reason, it is necessary to thoroughly characterize these systems in the absence of the NO emission in order to permit quantitative corrections for their presence. The spectra can be characterized on COCHISE by a systematic study at high resolution, with Ar counterflow and Ar and N_2/Ar mixtures alternately used as discharge gases. Special attention will be given to the possibility of any effects due to impurities in the discharged gas. The reproducibility, identities, relative intensities, and phases of the various features should be well-established. In addition, bench-scale studies of Ar/N_2 discharges on the FAKIR facility (see Section 3) using the scanning monochromator (2-4 μm) would be useful to confirm the COCHISE spectra and to establish the mechanisms for the observed radiation.

3. $O_3(\nu_3)$ EMISSION

The recombination of atomic and molecular oxygen may give rise to vibrationally excited ozone in the upper atmosphere via the sequence:

$$O + O_2 + M \rightarrow O_3(v') + M \quad (5)$$

$$O_3(v') + M \rightarrow O_3(v'') + M \quad (6)$$

$$O_3(v') \rightarrow O_3(v'') + h\nu \quad . \quad (7)$$

Recent rocketborne measurements[10] of infrared atmospheric emissions indicate that chemiluminescence in the ν_3 fundamental band of O_3 [Reaction (7)] may be a significant source of 10-12 μm radiation in the sunlit atmosphere between 60 and 100 km.

The COCHISE facility possesses a unique capability for the investigation of Reactions (5) through (7), because of its high sensitivity near 10 μm. A recent preliminary investigation[2,11] of the recombination processes yielded the first laboratory spectra ever obtained of O_3 vibraluminescence. In these experiments, O_2/Ar mixtures (0.5-73 percent O_2) were passed through the microwave discharges to produce O; O_2 and Ar were alternately used as counterflow gases. The important findings of that study are: (1) most or all of the observed O_3 emission (limited to the ν_3 band nea. 10 μm) was the net result of recombination and collisional deactivation [Reactions (4) and (5)] occurring in the discharge sidearms; (2) the observable steady-state vibrational populations under these conditions extended as high as $v' \sim 6$; and (3) the vibrational analysis was complicated by the possibility of excitation of the manifolds of the combination states $(\nu_1 + \nu_3)$ and $(\nu_2 + \nu_3)$. Discussions of the kinetics of the microwave discharge region and an analysis of the effects of difference bands are presented below. The results were published in a journal article[11] which is reproduced in Appendix C.

Much of the O_3 emission observed in the COCHISE experiments should arise from some combination of Reactions (5) through (7); these processes can take place to some extent in the low-pressure interaction region, but will occur with much faster rates in the discharge tubes immediately downstream of the microwave excitation sources. The rates of the probable production and loss processes in the discharge tubes can be roughly estimated for the experimental conditions described above; the results of such a kinetic analysis are summarized in Table 3. For dilute O_2/Ar mixtures (O_2/Ar $\sim$ 0.01) at $\sim$1 Torr, past experience with room-temperature microwave discharges indicates that fractional O_2 dissociations of 0.1 - 0.5 are typically attained (see, for example, Piper, et al[12]); for purposes of discussion, we will use the value 0.2 as a conservative estimate for our discharge conditions. At 80 K, the total O_3 production rate by recombination of O with O_2 (in Ar) is then on the order of $3 \times 10^{15}/(cm^3\ sec)$ (using the termolecular

10. Nadile, R.M., Stair, Jr., A.T., Wheeler, N.B., Frodsham, D.G., Wyatt, C.L., Baker, D.J., and Grieder, W.F. (1978) SPIRE-Spectral Infrared Rocket Experiment (Preliminary Results), AFGL-TR-78-0107, AD A058504.

11. Rawlins, W.T., Caledonia, G.E., and Kennealy, J.P. (1981) Observation of spectrally resolved infrared chemiluminescence from vibrationally excited $O_3(\nu_3)$, J. Geophys. Res. 86:5247.

12. Piper, L.G., Krech, R.H., and Taylor, R.L. (1979) Generation of N_3 in the thermal decomposition of NaN_3, J. Chem. Phys. 71:2099.

Table 3. Estimated Rates of Major $O_3(v)$ Production and Loss Processes in Discnarge Tubes for a Dilute (1 Percent O_2) O_2/Ar Mixture at 1 Torr

Reaction	Estimated Rate Constant at 80 K	Reference	Estimated Rate
$O + O_2 + Ar \rightarrow O_3(v) + Ar$	$\leq 4 \times 10^{-32}$ cm^6/sec	Huie et al[13]	$\leq 3 \times 10^{15}/(cm^3\ sec)$
$O_3(v') + Ar \rightarrow O_3(v'') + Ar$	$6 \times 10^{-15}/(cm^3\ sec)$	Rosen and Cool[15]	700/sec
$O_3(v') + O_2 \rightarrow O_3(v'') + O_2$	$2 \times 10^{-14}/(cm^3\ sec)$	Rosen and Cool[15]	20/sec
$O_3(v') + O \rightarrow$ products	$1 \times 10^{-11}/(cm^3\ sec)$	West et al[16]	5000/sec
$O_3(v')$ + wall $\rightarrow$ products	$D \sim 20\ cm^2/sec$	See text	$\leq$300/sec
Pumping loss of $O_3(v')$	---	Measured flow velocity	500/sec

rate constant expression of Huie et al[13]); we anticipate that a large fraction of the O_3 initially formed is vibrationally excited. The possibility of electronically excited precursors to $O_3(v)$ in the recombination sequence cannot be ruled out at this time; however, the analysis given here, which deals with the net recombination process, is not affected by this issue. Other possible production mechanisms for $O_3(v)$, such as direct excitation of O_3 by electron impact or by collisions with discharge-excited species such as $O_2(v)$ or $O_2(b\ ^1\Sigma_g^+)$, are not expected to occur with competitive rates under O_2-lean conditions.

The $O_3(v)$ production rate is balanced by homogeneous relaxation with the major species Ar, O_2, and O, by heterogeneous removal at the tube wall, and by flow out of the tube into the low-pressure zone. In general, the detailed kinetic information required to assess the rates of the collisional processes for all v does not exist; however, some relaxation rate measurements have been reported for single-quantum excitation in the ν_3 mode.[14-16] Rosen and Cool[14,15] found that the ν_3 and ν_1 modes equilibrated very rapidly, and that subsequent collisional deactivation to the ν_2 mode proceeded at rather slow rates comparable with those of the deactivation of the ν_2 mode itself. From the data of Rosen and Cool,[15] we estimate first-order deactivation rates for $O_3(v)$ of about 700/sec and about 20/sec for collisions with Ar and O_2, respectively; however, the possible influence on these rates of low temperature and/or high vibrational levels is unknown. By far, the dominant quenching process for $O_3(v)$ under our conditions appears to be deactivation by and/or reaction with atomic oxygen, for which we estimate a rate on the order of 5×10^3/sec, using the room temperature rate constant for either process.[16] Diffusion of $O_3(v)$ through Ar to the tube wall is expected to occur with a rate similar to that for diffusion of CO_2;[17] at 80 K, this gives an estimated surface deactivation rate of, at most, about 300/sec, if deactivation of $O_3(v)$ occurs upon every collision with the wall. Finally, from the measured gas flow rates, the pumping loss rate for $O_3(v)$ is about 500/sec. Thus, for the conditions employed in the majority of our experiments, we estimate that: (1) the dominant

---

13. Huie, R.E., Herron, J.T., and Davis, D.D. (1972) Absolute rate constants for the reaction $O + O_2 + M \rightarrow O_3 + M$ over the temperature range 200-346 K, J. Phys. Chem. 76:2653.

14. Rosen, D.I., and Cool, T.A. (1973) Vibrational deactivation of $O_3(101)$ molecules in gas mixtures, J. Chem. Phys. 59:6097.

15. Rosen, D.I., and Cool, T.A. (1975) Vibrational deactivation of O_3 molecules in gas mixtures. II., J. Chem. Phys. 62:466.

16. West, G.A., Weston, Jr., R.E., and Flynn, G.W. (1976) Deactivation of vibrationally excited ozone by $O(^3P)$ atoms, Chem. Phys. Lett. 42:488.

17. Hirschfelder, J.O., Curtiss, C.F., and Bird, R.B. (1954) Molecular Theory of Gases and Liquids, John Wiley and Sons, Inc., New York.

$O_3(v)$ deactivation process is by collision with O, which may well lead to chemical reaction or multi-quantum deactivation; (2) the ν_3 mode should reach equilibrium with the ν_1 mode within the 2 msec flow time, but the ν_2 and ν_3 modes may not be fully equilibrated during this time; and (3) wall deactivation is a relatively minor process on this time scale. From these estimated production and loss rates, we derive a maximum steady-state $O_3(v)$ concentration on the order of $5 \times 10^{11}/cm^3$ in each inlet tube, if all the recombinations form vibrationally excited O_3; this corresponds to upper-bound concentrations near $1 \times 10^9/cm^3$ in the low-pressure observation region. For comparison, the integrated intensity of a typical spectrum (for 0.7 percent O_2 in the discharge gas) corresponds to $[O_3(v)]$ of about $5 \times 10^8/cm^3$ in the observation region, with an uncertainty of a factor of 2 in the absolute-calibration of the optical system.

The $O_3(\nu_3)$ spectral analysis has been described in detail elsewhere.[2,3] The observed spectra were analyzed by comparison with simulated spectra computed from a combination of well-established spectroscopic data[18] for the (001) → (000) transition and the assumption of anharmonic scaling laws for the properties of the higher vibrational levels. However, a more rigorous treatment must include the contributions of the (101) → (100) and (011) → (010) difference bands, respectively centered at 9.92 and 9.75 μm.[19] The vibrational bands included in the present analysis are listed in Table 4, and a partial energy level diagram of the $O_3(v)$ system is shown in Figure 4.

A comparison of computed and observed spectra for the 0.7 percent O_2 case is shown in Figure 5; the contributions of the individual vibrational transitions are also depicted. It can be seen that the band overlap in the vicinity of 9.9 μm is significant due to competing contributions of the 011, 101, and 002 emissions. The inclusion of the difference bands leads to a somewhat improved spectrum match in the 9.8-10.0 μm region, compared with that previously achieved by neglecting those bands;[2] this result suggests that the implications of the data are that the ν_1, ν_2 and $2\nu_2$ modes may be at least partially excited in these experiments. The vibrational population distributions derived from the spectral fit of Figure 5 are shown in Figure 6, compared with those derived from the "pure ν_3" spectral model of Ref. 2. While the overall envelope is roughly the same in both cases, it can be seen that the 101 state is found to be in approximate thermal equilibrium with the ν_3 manifold while the 011 population appears to be much lower.

---

18. McClatchey, R.A., Benedict, W.S., Clough, S.A., Burch, D.E., Calfee, R.F., Fox, K., Rothman, L.S., and Garing, J.S. (1973) AFCRL Atmospheric Absorption Line Parameters Compilation, AFCRL-TR-73-0096, AD 762904.

19. Flaud, J.M., Camy-Peret, C., and Rothman, L.S. (1980) Improved ozone line parameters in the 10- and 4.8-μm regions, Appl. Opt. 19:655.

Table 4. O_3 Bands Used in Analysis

Upper State		Lower State	Band Center (μm)	A (sec^{-1})
	001	000	9.60	11.2
Optional	011	010	9.75	10.5
	101	100	9.92	9.8
Scaled From 001	002	001	9.83	20.7
	003	002	10.07	28.9
	004	003	10.33	35.8
	005	004	10.60	41.4
	006	005	10.88	45.9

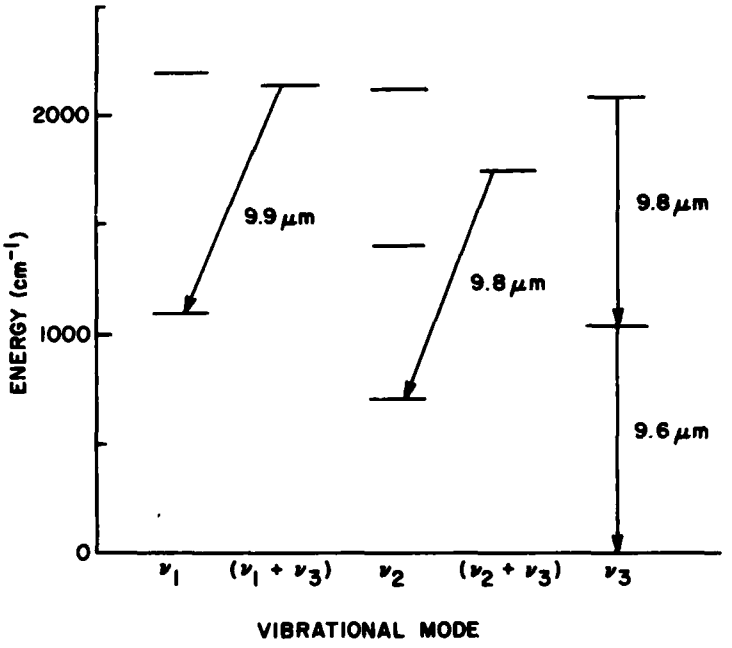

Figure 4. Energy Levels of O_3

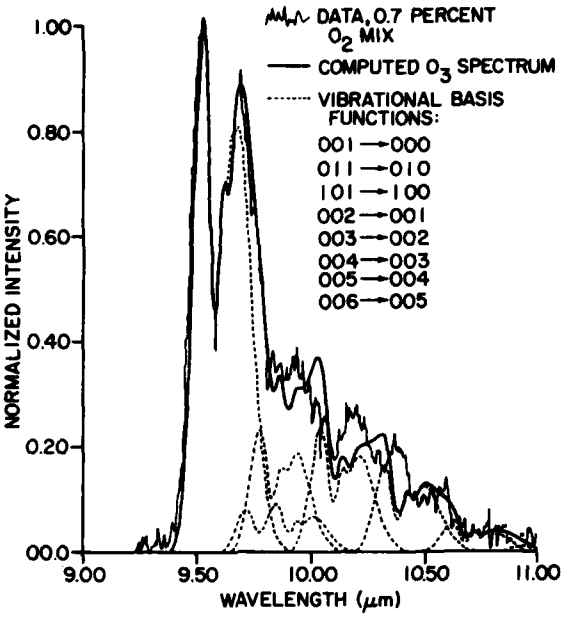

Figure 5. Comparison of Computed and Observed Spectra, Experiment 107016. In the computed spectrum, the rotational temperature is 90 K and the resolution is 0.04 μm

For our flow conditions, this result is consistent with the known intermode energy transfer kinetics of O_3 as discussed above. That is, during the available flow time, the ν_1 and ν_3 modes can become quasi-equilibrated following the initial recombination while the much slower transfer into the ν_2 mode is incomplete. Thus, contributions of bending-excited combination states to the observed spectra may be small, but those of stretching-excited states may be important. However, it is clear from the comparison in Figure 6 that the "pure ν_3" approach of Ref. 2 allows the definition of the overall envelope, analogous to a characteristic "temperature", exhibited by the observed spectrum. It must be emphasized for all of the above discussion that the derived populations for all states with $\nu_3 \geq 2$ are only estimates, since the radiative lifetimes of these states were estimated using anharmonic scaling laws; as a result, the ultimate yield of the spectral fitting is limited to relative trends in the derived population distributions.

Further COCHISE experiments will characterize the difference band contributions to the observed 10 μm emission. Repetition of previous experiments with higher resolution and lower rotational temperature (possibly, 0.02 μm and 60 K) will allow more separation of the overlapped bands. Furthermore, a study of the

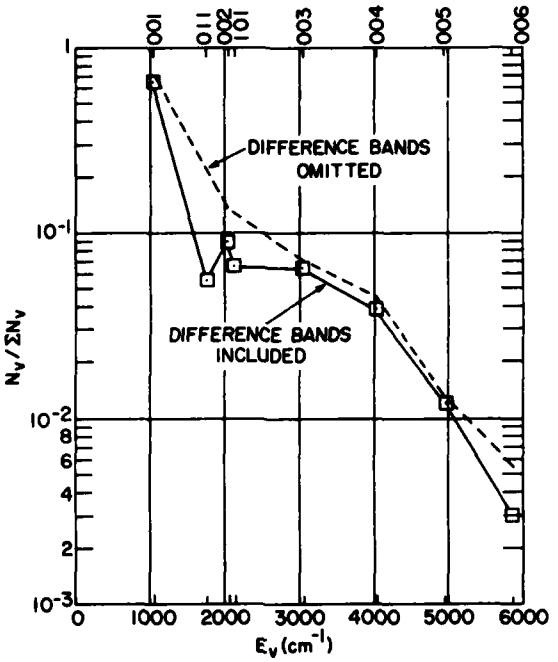

Figure 6. Derived Populations for the Fit Shown in Figure 5 (Squares). The dashed line represents the shape of the population distribution obtained in Ref. 2 by omitting the contributions of difference band emission

$(\nu_1 + \nu_3)$ summation band at 4.7 μm, under the same experimental conditions used for the 10 μm studies, will yield information on the level of excitation of the stretching-excited manifold in the ν_3 spectra.

4. N_2/O_2 DISCHARGE EXPERIMENTS

Infrared emission from electron-irradiated air has not been well-characterized spectrally in the laboratory, particularly at long wavelengths. We have performed a series of survey experiments on the COCHISE facility to identify the prominent radiating species. These experiments were done by passing air/Ar mixtures through the microwave discharges and using O_2 as the counterflow gas.

Spectral measurements were made using the 10 μm grating, and two spectral ranges were covered. The spectral range 4-6 μm was observed in the second order using sapphire to cut off long wavelength first order contributions, and the range 8-16 μm was observed directly in first order using an 8 μm long pass filter

to eliminate higher order contributions from short wavelength emissions. Typical spectra for the two wavelength regions are shown in Figures 7 and 8. These data are not corrected for the relative responsivity of the optical system. The prominent features observed in the MWIR (Figure 7) include band systems near 4.2, 4.5, 4.8, and the system extending from 5.6 to about 6 μm, which is clearly the NO fundmental band system that arises from the reaction[3]

$$N(^2D) + O_2 \rightarrow NO(v) + O \quad , \tag{1}$$

that occurs both in the central interaction zone and in the discharge tubes. The prominent feature centered at 4.5 μm appears to be the fundamental ν_3 band of N_2O. N_2O is known to be formed in electric discharges of air, but the formation mechanism is not well understood. The features near 4.2 and 4.8 μm are not readily identifiable from these data, but an interesting possibility is that some of this emission may arise from NO^+ formed in the reaction

$$N^+ + O_2 \rightarrow NO^+(v) + O \quad . \tag{2}$$

This reaction is highly exothermic and can excite up to 28 vibrational levels in NO^+, giving rise to emission extending from 4.2 up to about 6 μm. Clearly, more systematic experiments at higher spectral resolution are required to fully understand the spectrum of Figure 7.

In the LWIR (Figure 8), the only feature in the spectrum is the $O_3(\nu_3)$ fundamental band which arises from the recombination reaction

$$O + O_2 + M \rightarrow O_3(v) + M \quad ,$$

occurring in the discharge sidearms.[11] This observation is essentially the same as that for discharged O_2/Ar mixtures discussed above. It is possible that a spectral feature exists near 8 μm; however, this is at the limit of detectability and amplified scans of that region fail to reveal a definite spectral feature.

5. MWIR AND LWIR SPECTRA OF AR I

In the course of performing experiments to study O_3 emissions near 4.8 and 9.6 μm, we have observed a number of new spectral features that appear to be atomic transitions of Ar. MWIR and LWIR spectra are shown in Figures 9 and 10, respectively (uncorrected for relative system responsivity). These features are found to be present even for pure Ar discharge and counterflow gas. While no systematic studies have been made of the MWIR lines, the LWIR lines are found

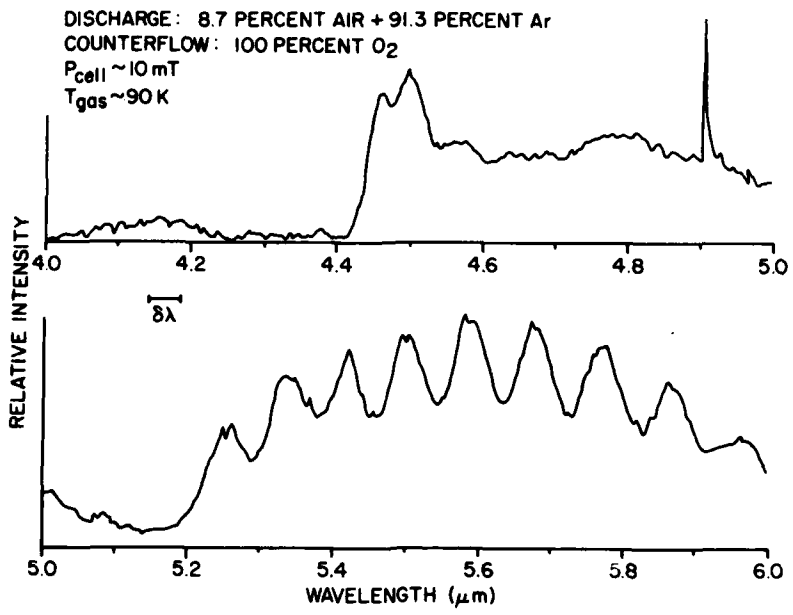

Figure 7. MWIR Spectrum (Uncorrected) for Discharged Air/Argon. The spectral resolution is 0.027 μm

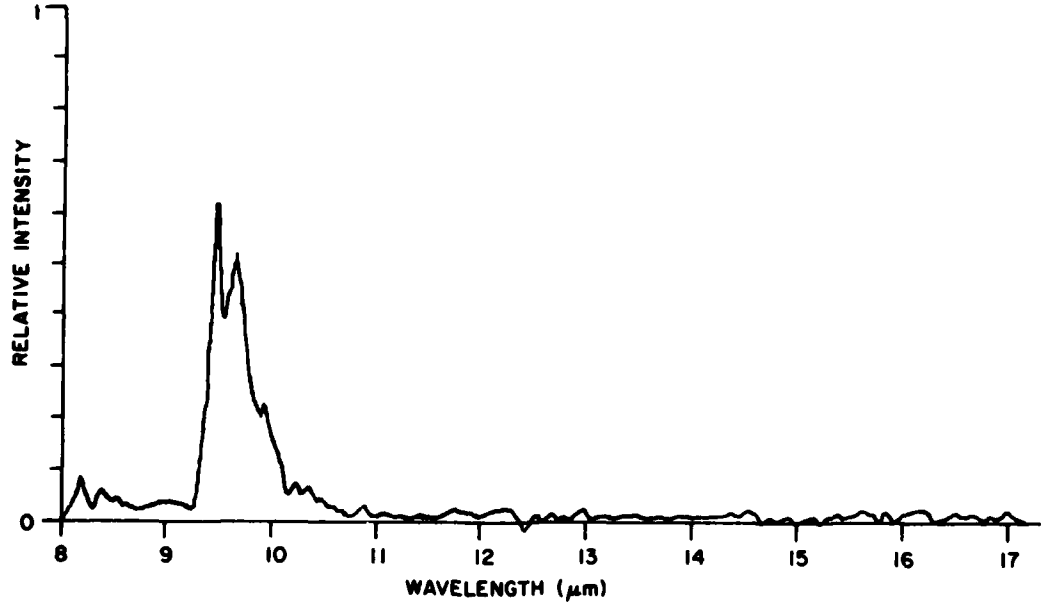

Figure 8. LWIR Spectrum (Uncorrected) for Discharged Air/Argon. Flow and pressure conditions are the same as given in Figure 7. The spectral resolution is 0.08 μm

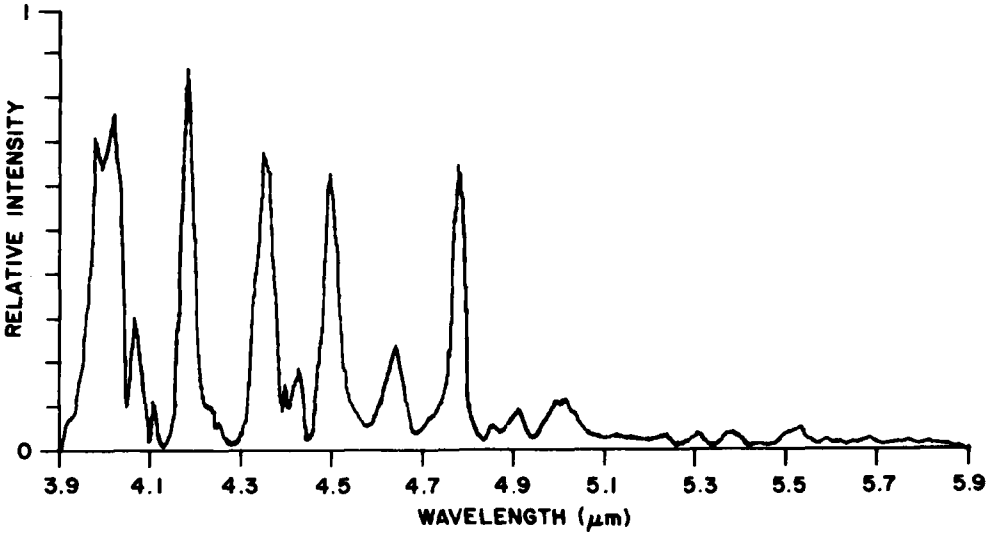

Figure 9. MWIR Spectrum (Uncorrected) of Ar I Lines. Discharge = 5 percent O_2/Ar; counterflow: 100 percent O_2. $P_{cell} \cong 3$ mTorr. The spectral resolution is 0.027 μm

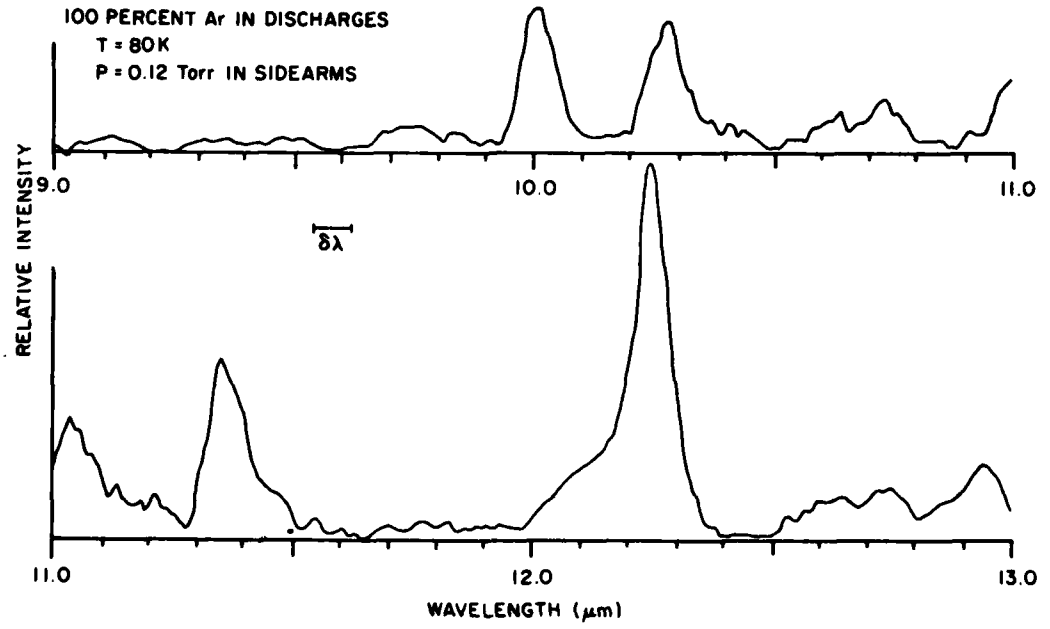

Figure 10. LWIR Spectrum (Uncorrected) of Ar I Lines. The spectral resolution is 0.08 μm

to decrease with increasing O_2 levels (Figure 11) and increase dramatically with decreasing Ar pressure in the discharge sidearms (Figure 12). The O_2 effect may be related to quenching of the emission by O or O_2. The Ar effect is difficult to interpret because changing the Ar pressure in the discharge sidearms simultaneously changes the flow velocity (that is, the residence time) and the ratio of charge to number density E/N in the discharge plasma, as well as other characteristics of the discharge.

The observed transitions appear to arise from high Rydberg-like energy levels of neutral argon. However, since the spectroscopic literature does not extend much beyond 4 μm, considerable analysis will be required to make the spectral assignments. The Rydberg series of hydrogen-like, $n \rightarrow n - 1$ transitions, which should appear in the spectral of all highly excited atomic gases, is given by

$$\lambda = 0.09113 \frac{n^2(n-1)^2}{2n-1} , \qquad (3)$$

where λ is the line position in μm and n is the principal quantum number of the emitting state ($n \geq 5$). The first few lines, for $n = 4, 5, 6, 7, \ldots$, are at 4.05, 7.46, 12.36, 19.05, ... μm, respectively. However, these are idealized transitions which are most closely approximated by transitions involving states with large orbital angular momentum (high ℓ-values); other transitions at nearby wavelengths may be expected for Rydberg states with lower ℓ or spin-orbit coupling. The Rydberg wavelengths of 4.05 and 12.36 μm correlate well with the strong transitions we observe at about 4.0 and 12.2 μm.

It is not yet clear what the excitation mechanism for the Ar Rydberg states in COCHISE could be. Possible processes could include direct electron impact excitation of Ar and recombination of Ar^+ or Ar_2^+; however, these processes should occur primarily in the discharge tubes rather than in the central mixing region. Since the radiative lifetimes of these transitions are probably on the order of 1-10 μsec, it is difficult to understand how significant amounts of the emitting species can survive the transit time of approximately 0.5 msec from the end of the discharge tubes to the detector field of view. Alternatively, it is possible that the observed Ar emission levels are due to a small fraction ($\lesssim 10^{-3}$) of scattered light from the discharge tubes themselves. This may be the case for at least the LWIR emission, since the emission intensity appears to be unaffected by the flow rate of the counterflow gas. A more systematic study of the flow dependencies of these features should confirm whether they indeed arise from scattered discharge light, and high-resolution, slow-scan studies using a careful wavelength calibration can be used to establish the transition frequencies and multiplet structures more accurately.

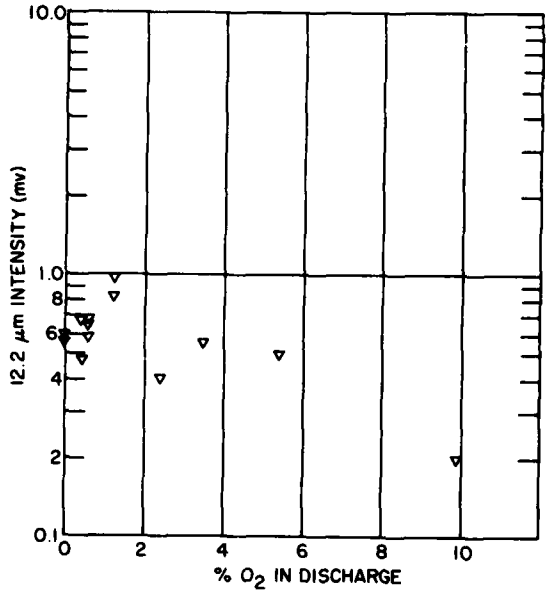

Figure 11. Ar I Intensity at 12.2 μm as a Function of O_2 Level in the Discharge Tubes, P_{Ar} = 1.3 Torr

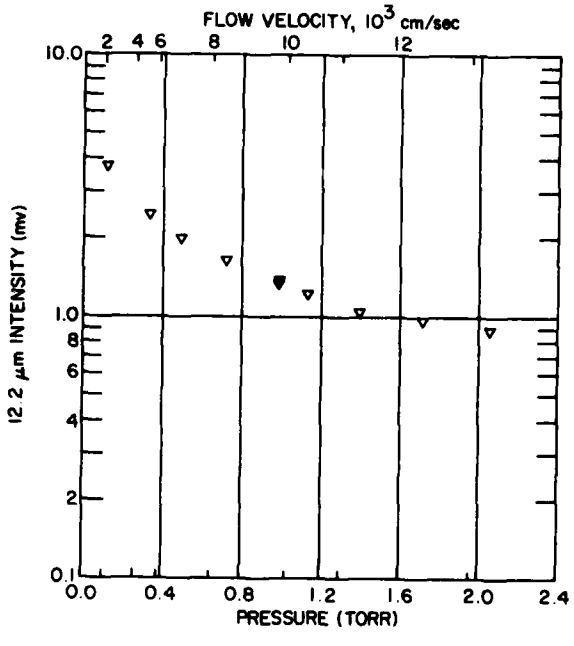

Figure 12. Ar I Intensity at 12.2 μm as a Function of Total Ar Pressure in Discharge Sidearms. Discharge gas is 100 percent Ar; no counterflow

References

1. Kennealy, J.P., DelGreco, F.P., Caledonia, G.E., and Rawlins, W.T. (1979) COCHISE: laboratory spectroscopic studies of atmospheric phenomena with high-sensitivity cryogenic instrumentation, Proc. Soc. Photo-Opt. Instrumentation Eng., G.A. Vanasse, Ed., 191:151.
2. Rawlins, W.T., Piper, L.G., Green, B.D., Wilemski, G., Goela, J.S., and Caledonia, G.E. (1980) LABCEDE and COCHISE Analysis II, Volume I. Final Report, Physical Sciences Inc., Contract No. 19628-77-C-0089, AFGL-TR-80-0063(I), AD A112253.
3. Kennealy, J.P., DelGreco, F.P., Caledonia, G.E., and Green, B.D. (1978) Nitric oxide chemi-excitation occurring in the reaction between metastable nitrogen atoms and oxygen molecules, J. Chem. Phys. 69:1574.
4. Billingsley II, F.P. (1976) Calculated vibration rotation intensities for $NO(X^2\pi)$, J. Molec. Spectrosc. 61:53.
5. Outred, M. (1978) Tables of atomic spectral lines for the 10000 Å to 40000 Å region, J. Phys. Chem. Ref. Data 7:1.
6. Moore, C.E. (1971) Atomic Energy Levels, Vol. I, NSRDS-NBS 35.
7. Wiese, W.L., Smith, M.W., and Miles, B.M. (1969) Atomic Transition Probabilities, Vol. II, NSRDS-NBS 22.
8. Green, B.D., private communication.
9. Lofthus, A., and Krupenie, P.H. (1977) The spectrum of molecular nitrogen, J. Phys. Chem. Ref. Data 6:113.
10. Nadile, R.M., Stair, Jr., A.T., Wheeler, N.B., Frodsham, D.G., Wyatt, C.L., Baker, D.J., and Grieder, W.F. (1978) SPIRE-Spectral Infrared Rocket Experiment (Preliminary Results), AFGL-TR-78-0107, AD A058504.
11. Rawlins, W.T., Caledonia, G.E., and Kennealy, J.P. (1981) Observation of spectrally resolved infrared chemiluminescence from vibrationally excited $O_3(\nu_3)$, J. Geophys. Res. 86:5247.

12. Piper, L.G., Krech, R.H., and Taylor, R.L. (1979) Generation of N_3 in the thermal decomposition of NaN_3, J. Chem. Phys. 71:2099.

13. Huie, R.E., Herron, J.T., and Davis, D.D. (1972) Absolute rate constants for the reaction $O + O_2 + M \rightarrow O_3 + M$ over the temperature range 200-346 K, J. Phys. Chem. 76:2653.

14. Rosen, D.I., and Cool, T.A. (1973) Vibrational deactivation of $O_3(101)$ molecules in gas mixtures, J. Chem. Phys. 59:6097.

15. Rosen, D.I., and Cool, T.A. (1975) Vibrational deactivation of O_3 molecules in gas mixtures. II., J. Chem. Phys. 62:466.

16. West, G.A., Weston, Jr., R.E., and Flynn, G.W. (1976) Deactivation of vibrationally excited ozone by $O(^3P)$ atoms, Chem. Phys. Lett. 42:488.

17. Hirschfelder, J.O., Curtiss, C.F., and Bird, R.B. (1954) Molecular Theory of Gases and Liquids, John Wiley and Sons, Inc., New York.

18. McClatchey, R.A., Benedict, W.S., Clough, S.A., Burch, D.E., Calfee, R.F., Fox, K., Rothman, L.S., and Garing, J.S. (1973) AFCRL Atmospheric Absorption Line Parameters Compilation, AFCRL-TR-73-0096, AD 762904.

19. Flaud, J.M., Camy-Peret, C., and Rothman, L.S. (1980) Improved ozone line parameters in the 10- and 4.8-μm regions, Appl. Opt. 19:655.

Contents

3. FAKIR Experiments

1. INTRODUCTION

The reactions of $N_2(A\ ^3\Sigma_u^+)$ with atomic and molecular oxygen could be significant sources of odd nitrogen and vibrationally excited NO in the upper atmosphere.[1] For the interaction between $N_2(A)$ and molecular oxygen, five possible reaction channels are

1. Swider, W. (1976) Atmospheric formation of NO from $N_2(A\ ^3\Sigma)$, Geophys. Res. Lett. 3:335.

$$N_2(A\ ^3\Sigma_u^+)_{v'=0} + O_2(X\ ^3\Sigma_g^-) \rightarrow N_2(X\ ^1\Sigma_g^+) + O_2(X\ ^3\Sigma_g^-) + 6.2\ eV \quad , \qquad (1a)$$

$$\rightarrow N_2(X\ ^1\Sigma_g^+) + 2\ O(^3P) + 1.1\ eV \quad , \qquad (1b)$$

$$\rightarrow N_2O + O(^3P) + 3.0\ eV \quad , \qquad (1c)$$

$$\rightarrow N_2O + O(^1D) + 1.0\ eV \quad , \qquad (1d)$$

$$\rightarrow 2NO\ (X\ ^2\Pi) = 4.2\ eV \quad . \qquad (1e)$$

Molecular oxygen is the main deactivator of $N_2(A\ ^3\Sigma_u^+)$ in the atmosphere below 100 km,[1] so that reactions (1c) and (1d) could be significant sources of atmospheric N_2O, with possible vibrational excitation of the product. Further reactions of N_2O with $N(^2D)$ and $O(^1D)$ lead to the formation of NO.[1] Direct formation of NO via reaction (1e) should be extremely slow due to the dynamic constraints which inhibit four-center exchange reactions.

Measurements of the room-temperature rate constants for this reaction vary between 1.9 and 7.6×10^{-12} cm^3/molecule sec (Table 1).[2-12] Because most of the experiments were non-state-specific tracer measurements, some of this scatter probably results in the variation in deactivation rate constant with vibrational level.

Meyer et al[2] have observed that oxygen atoms are a major product from Reaction (1), but did not put their observations on a quantitative basis. Recent experiments by Zipf[12a] have indicated that about 60 percent of Reaction (1) goes through channels (c) and (d) to make N_2O; Ianuzzi and Kaufman's[12b] very recent results dispute this, however, with the claim that N_2O formation is less than 5 percent of the total product formation in Reaction (1).

The possible reactions of $N_2(A)$ with oxygen atoms are summarized as follows:

$$N_2(A\ ^3\Sigma_u^+)_{v'=0} + O(^3P) \rightarrow N_2(X\ ^1\Sigma_g^+) + O(^3P) + 6.2\ eV \quad , \qquad (2a)$$

$$\rightarrow N_2(X\ ^1\Sigma_g^+) + O(^1D) + 4.2\ eV \quad , \qquad (2b)$$

$$\rightarrow N_2(X\ ^1\Sigma_g^+) + O(^1S) + 2.0\ eV \quad , \qquad (2c)$$

$$\rightarrow NO(X\ ^2\Pi) + N(^4S) + 2.9\ eV \quad , \qquad (2d)$$

$$\rightarrow NO\ (X\ ^2\Pi) + N(^2D) + 0.5\ eV \quad . \qquad (2e)$$

Because of the large number of references cited above, they will not be listed here. See References, page 72.

Table 1. Rate Constants for Reactions of $N_2(A\ ^3\Sigma_u^+)$ v = 0, 1 With O and O_2*

k_{O_2}	k_O	Comments	Reference
6.0	22	$Hg(6\ ^3P_1)$ tracer k_O from k_O/k_{O_2} = 3-4 and listed number for k_{O_2} claim $k_{v=1}/k_{v=0} \approx 1.3$	Meyer, Setser and Stedman[2]
2.9 (v=0)	15	claimed $k_{v=1} = k_{v=0}$ Looked at Vegard-Kaplan 0, 6 and 1, 5 emission with interference filters Probably some interference from NO γ-bands	Dunn and Young[4]
3.8		NO γ-band tracer	Young, Black and Slanger[6]
3.3		NO γ-band tracer	Slanger, Wood and Black[7]
3.7		NO γ-band tracer claim $k_{v=1} = k_{v=0}$	Callear and Wood[8]
6.5		Hg $(6\ ^3P_1)$ tracer	Meyer, Klosterboer and Setser[9]
7.6		Hg $(6\ ^3P_1)$ tracer - This value was measured relative to $k_{N_2(A)+N} = 5 \times 10^{-11}$ $cm^3/(molecule\ sec)$	Meyer, Setser and Clark[10]
1.9 (v=0) 7.6 (v=1)		Measured $N_2(A)$ with absorption on nitrogen 1^+ system	Dreyer, Perner and Roy[3]
3.5 4.5 (v=0) 5.1 (v=1)		Broadband filter - "Mostly v+0". Could have been contaminated with NO γ-bands v = 0 and v=1 with monochromator. Could have large uncertainty in reaction time.	Clark and Setser[11]
1.9 (v=0) 4.0 (v'=1)		Direct observation of Vegard-Kaplan emission decay in pulsed discharge	Zipf[12]
2.3 (v=0) 4.1 (v=1)	28 34	Direct observation of decay of Vegard-Kaplan emission in discharge-flow reactor	Present results

*The listed rate constants are for T = 300 K. They are in units of 10^{-12} $cm^3/$(molecule sec).

Reactions (2d) and (2e) may be major sources of NO and $N(^2D)$ in auroras and in the quiet daytime E-region;[1] in addition, some of the exothermicity of these reactions may appear as vibrational energy in the product NO molecules. The further reaction of $N(^2D)$, formed in Reaction (2e), with ambient O_2 can also give rise to vibrationally excited NO.

The rate constant for quenching $N_2(A\ ^3\Sigma_u^+)$ by oxygen atoms has been reported as 2.2×10^{-11} $cm^3/(molecule\ sec)$,[2] and 1.5×10^{-11} $cm^3/(molecule\ sec)$.[4] However, Meyer et al's[3] number was measured relative to k_1 which they took to be 6.0×10^{-12} $cm^3/(molecule\ sec)$ and should be reduced by a factor of 2 to conform to currently accepted values of k_1. The determination of Dunn and Young[4] was made in a complicated system that could provide reactive species, in addition to $N_2(A)$, which might complicate the kinetics. Some aeronomic estimates[1] have favored a value closer to 10^{-10} $cm^3/(molecule\ sec)$; although recent rocket measurements by Sharpe et al[13] and O'Neil et al[14] are in conflict on this. Sharp et al[13] favor the high value, while O'Neil et al[14] support the earlier laboratory measurements.

Only Meyer et al[2,5] have investigated the products of the reaction between $N_2(A)$ and oxygen atoms. They observed excitation of $O(^1S)$ by its characteristic emission at 557.7 nm, and estimated that 25^{+25}_{-10} percent of the total $N_2(A)$ quenching by oxygen atoms occurs by this path. Their system was not sufficiently free from extraneous NO contamination to rule out the possibility of NO product formation as well. In addition they neglected to correct their data for $O(^1S)$ quenching, so their result must be considered to be only a lower limit.

During the course of a program to study product formation in Reactions (1) and (2) we remeasured the rate constants at 300 K for these reactions for both vibrational levels 0 and 1. Our results are somewhat at variance with the commonly accepted value for k_1 of 3.5×10^{-12} $cm^3/(molecule\ sec)$. We show that this accepted value results from a tracer effect in most other experiments which measured an effective rate constant for the combined vibrational levels 0 and 1. Our results show that vibrational level 1 is quenched by molecular oxygen almost twice as fast as vibrational level 0, and that the state-specific rate constants bracket the average value given by most other experimenters.

Our results for k_2 are about double the previously reported laboratory values and show much less vibrational level dependence than k_1. In addition, we have

---

13. Sharp, W.E., Rees, M.H., and Stewart, A.I. (1979) Coordinated rocket and satellite measurements of an auroral event 2. The rocket observations and analysis, J. Geophys. Res. 84:1977.

14. O'Neil, R.R., Lee, E.T.P., and Huppi, E.R. (1979) Auroral $O(^1S)$ production and loss processes: ground-based measurements of the artificial auroral experiment PRECEDE, J. Geophys. Res. 84:823.

made a direct determination of k_{2c} and obtained a value k_{2c}/k_2 which is three times larger than Meyer et al's estimate.

2. EXPERIMENTAL

2.1 Apparatus

The experiments were done in a discharge-flow apparatus with the $N_2(A)$ number densities being monitored by spectroscopic observations of individual vibrational bands of the Vegard-Kaplan (N_2 A $^3\Sigma_u^+$ - X $^1\Sigma_g^+$) system of nitrogen. The reactor (see Figure 1) is a 2-in. diameter quartz tube which is pumped by a Roots blower that is capable of producing linear flow velocities up to 8×10^3 cm/sec at pressures of 1 Torr. A 0.5-m monochromator (Minuteman) is mounted on a set of rails parallel to the flow tube. Spectral observations of the luminous gases in the flow tube therefore can be made as a function of linear distance along the tube by sliding the monochromator up and down on its rails. Distances are converted to reaction times by dividing by the flow velocity. Light intensities are measured photoelectrically using a thermoelectrically cooled EMI 9558 QA photomultiplier and an SSR 1105 photon-counting rate meter.

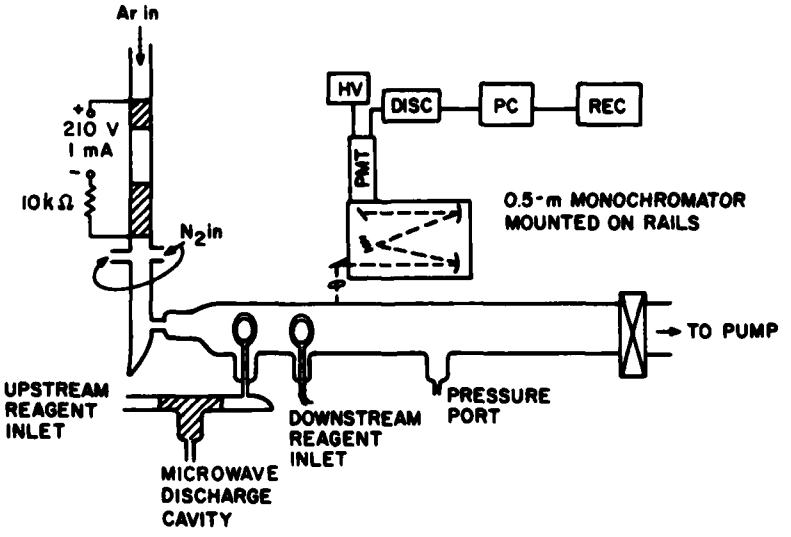

Figure 1. Schematic of Discharge-Flow Apparatus Used in Studies of $N_2(A)_{v=0,1}$ With O and O_2

The metastable nitrogen molecules are produced in the reaction between metastable $Ar(^3P_{0,2})$ and molecular nitrogen.[15,16] This transfer results in the production of nearly equal populations of the $C\ ^3\Pi_u$ and $B\ ^3\Pi_g$ states of N_2[17] which quickly cascade radiatively to the metastable $A\ ^3\Sigma_u^+$ state. A hollow-cathode discharge source was built to produce the argon metastables. While most experimenters have used tantalum for the electrodes,[16,18] we found 0.005-in. thick aluminum shim made an excellent electrode material. The shim was rolled into a cylinder whose diameter was the same as the inside diameter of the glass tubing through which the gas flowed (13 mm). The cathode (the down-stream electrode) is 40 mm long, the anode 15 mm long, and the two electrodes are separated by 45 mm. The discharge is operated in the dc mode with the anode biased at +210 V. A load resistor of 10 kΩ gives the discharge stability and limits the current. The current in the present experiments is about 3 mA. The argon was purified by flowing it through a trap filled with a 5Å molecular sieve and cooled with dry ice. Since the experiments involved metastable nitrogen, it was not necessary to remove the nitrogen impurity from the argon carrier. Cooling the trap with liquid nitrogen rather than dry ice would have removed the nitrogen. The metastables may be detected by the appearance of the characteristic reddish-violet flame which results when nitrogen is added downstream from the discharge. At the concentrations of N_2 at the point of addition, about $10^{15}/cm^3$, the flame length is about 2 cm. This length is just governed by diffusional mixing of the two streams of gas, since at these nitrogen concentrations the collisional quenching times for nitrogen on argon are on the order of tens of microseconds.[19] Typically, the argon flow rate is about 1500 μmol/sec, the nitrogen flow rate about 250 μmol/sec, and the flow tube pressure about 1.5 Torr. Typical flow velocities ranged from 1100 to 1500 cm/sec. These were obtained by throttling the Roots blower, or by shutting the blower off and using only the forepump on the flow tube.

A typical spectrum of the Vegard-Kaplan bands emanating from the flow tube is shown in Figure 2. The spectrum shows that the first three vibrational levels

15. Setser, D.W., Stedman, D.H., and Coxon, J.A. (1970) Chemical applications of metastable argon atoms. IV. Excitation and relaxation of triplet states of N_2, J. Chem. Phys. 53:1004.

16. Stedman, D.H., and Setser, D.W. (1968) Chemical applications of metastable argon atoms. II. A clean system for the formation of $N_2(A\ ^3\Sigma_u^+)$. Chem. Phys. Lett. 2:542.

17. Kolts, J.H., Brashears, H.C., and Setser, D.W. (1977) Redetermination of the $N_2(C)$ and $N_2(B)$ branching ratio from the Ar $(^3P_{0,2})$ + N_2 reaction, J. Chem. Phys. 67:2931.

18. Stedman, D.H., and Setser, D.W. (1971) Chemical applications of metastable rare gas atoms, Prog. React. Kinet. 6:193.

19. Piper, L.G., Velazco, J.E., and Setser, D.W. (1973) Quenching cross-sections for electronic energy transfer reactions between metastable argon atoms and noble gases and small molecules, J. Chem. Phys. 59:3323.

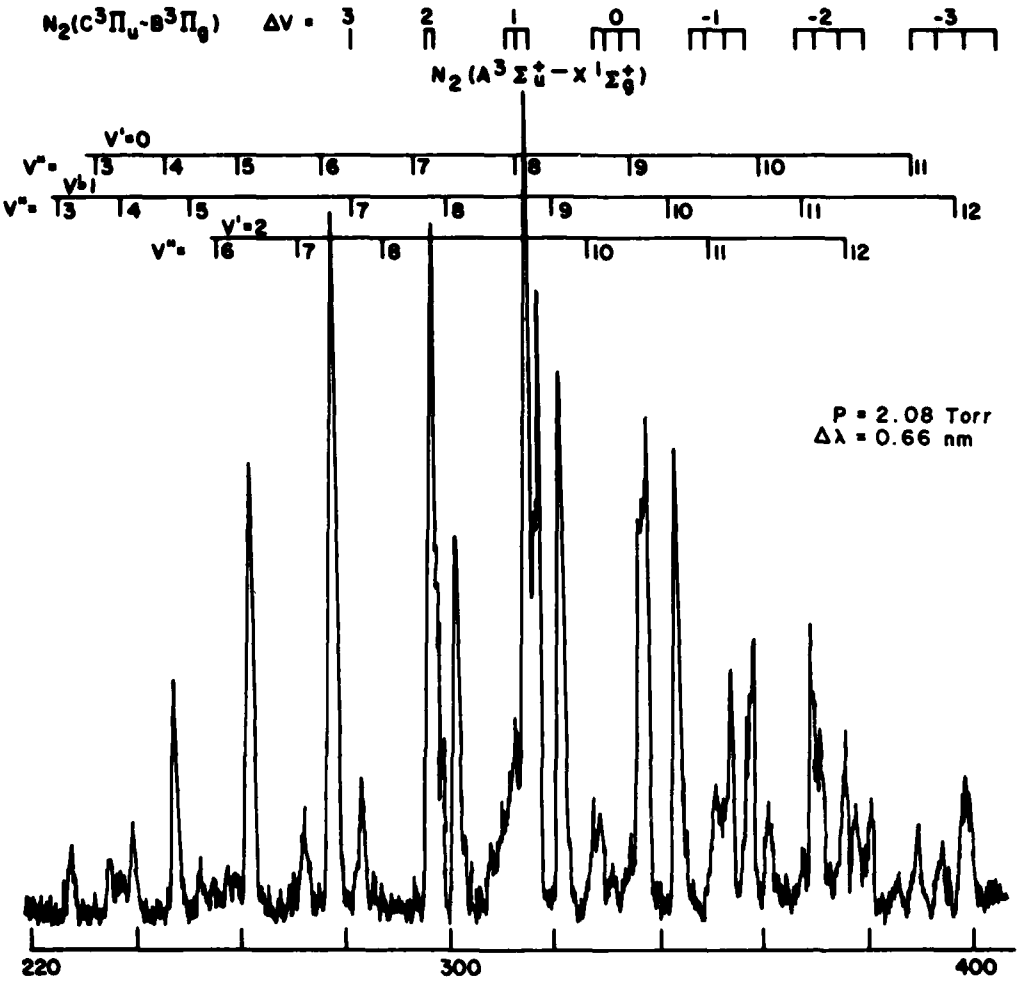

Figure 2. Spectrum of Vegard-Kaplan Bands Emitted in Discharge-Flow Reactor About 20 msec Downstream From the Discharge

of $N_2(A)$ are populated in our system with relative populations of approximately 100:50:10 for v'=0, 1, and 2 respectively. This is in contrast to the relative populations reported by Stedman and Setser of 100:95:10 for the same three levels, respectively.[15,16] We performed some experiments which showed that the ratio $[N_2(A)]_{v=1}/[N_2(A)]_{v=0}$ increases under conditions of higher total pressure and higher mole fractions of nitrogen in the flow, and when the nitrogen inlet is separated from the Ar metastable discharge by a Wood's horn light trap. These general conditions obtained in the work by Stedman and Setser, and, for the most part, did not in the present experiments. In particular, the intervention of a light

trap between the hollow-cathode discharge and the nitrogen addition point enhances the ratio $[N_2(A)]_{v=1}/[N_2(A)]_{v=0}$ by more than a factor of 2.

Molecular oxygen was introduced into the reactor through a 1-in. diameter loop injector fabricated from 2 mm OD polyethylene tubing. The flow of molecular oxygen (1-5 μmol/sec) was mixed with a substantial flow of helium (≈ 100 μmol/sec) prior to injection into the flow tube. The helium flow gave greater injection velocity and thus better mixing than O_2 injected with no helium carrier. This point was checked visually using the O/NO afterglow as a mixing diagnostic. Any effects on the kinetic measurements from small perturbations to the flow at the injection point were minimized by confining the measurement region to 30-45 cm (≈ 20-30 msec) downstream of the injector. The injector used initially in these experiments was a simple nozzle which faced upstream and injected the reagents into the center of the flow tube. Although, under certain conditions, air-afterglow observations indicated reasonable mixing with this design, the kinetic plots were curved in such a way as to indicate a slowing of the rate constant at higher reagent flows. After installation of the loop injector, this curvature disappeared. Previous workers have also observed that curvature in decay plots will result from poor mixing.[20] The use of the 2-in. tube instead of the more conventional 1-in. tube makes the mixing more critical.

Atomic oxygen was made by dissociation of O_2 in a microwave discharge through a small amount of O_2 in helium. The oxygen atoms were injected into the flow tube through the same loop injector used in the molecular oxygen studies. The small diameter of the loop caused a fairly large pressure drop between the discharge zone and the flow tube which caused significant amounts of atomic oxygen recombination between the discharge and the flow tube. The effective degree of dissociation of O_2 as determined by measurements of the O_2 flow rate and the determination of atomic oxygen number density in the flow tube was only about 13 percent. One typically expects effective dissociations about 3 times larger than this using conventional injection techniques.[21] Because the rate constant for deactivation of $N_2(A)$ by O is an order of magnitude larger than that for deactivation by O_2 (see Sections 3.2 and 4.3), the small degree of O_2 dissociation in the reactor did not cause problems in determining atomic oxygen quenching rate constants. The atomic oxygen was detected using the air-afterglow technique[22,23] (see below) which required the injection of NO through a second loop injector in the flow tube about 10 cm downstream from the oxygen injector.

The molecular oxygen was purified by pumping on liquid O_2 prior to expanding the middle portion of the liquid O_2 into a 5-*l* storage bulb. The nitric oxide used in the O-number-density determinations was purified by slowly flowing NO through

---

References 20 to 23 will not be listed here. See References, page 72.

an ascarite trap, and then a trap at dry ice temperature prior to storage in another 5-ℓ bulb. Freezing the NO at liquid nitrogen-temperature showed negligible amounts of NO_2 contamination.

Argon and nitrogen flow rates were measured using mass-flow meters (Teledyne Hastings-Raydist) whose calibrations were checked with a wet test meter. The flow rates of helium through the injectors were measured with rotameters that had also been calibrated against a wet test meter. Molecular oxygen and NO flow rates were measured by timing the pressure increase into calibrated volumes. Flow tube pressures were measured using an MKS Baratron®. The number density of reactant i is given by

$$N_i = \frac{f_i p_{tot}}{\sum_i f_i} \times \frac{N_o}{RT} \tag{3}$$

where the f_i represent reagent flow rates, p_{tot} is the total flow tube pressure in torr, N_o Avogadro's number, R the gas constant [6.236×10^4 torr cm^3/(mol K)], and T the absolute temperature.

2.2 Flow Analysis

In our apparatus there is essentially unit probability of $N_2(A)$ deactivation in collisions with the reactor walls. Thus a radial gradient in $N_2(A)$ number density is set up in the flow tube, and this radial gradient when coupled with a parabolic velocity profile resulting from laminar flow within the flow tube affects the analysis of the rate constant measurements. The proper fluid dynamic analysis of this situation has been considered exhaustively in the literature.[20,24-30] In

24. Bolden, R.C., Hemsworth, R.S., Shaw, M.J., and Twiddy, N.D. (1970) Measurements of thermal-energy ion-neutral reaction rate coefficients for rare-gas ions, J. Phys. B 3:45.

25. Farragher, A.L. (1970) Ion-molecule reaction rate studies in a flowing afterglow system, Trans. Faraday Soc. 66:1411.

26. Huggins, R.W., and Cahn, J.H. (1967) Metastable measurements in flowing helium afterglow, J. Appl. Phys. 38:180.

27. Walker, R.E. (1961) Chemical reaction and diffusion in a catalytic tubular reactor, Phys. Fluids 4:1211.

28. Poirier, R.V., and Carr, R.W. (1971) The use of tubular flow reactors for kinetic studies over extended pressure ranges, J. Phys. Chem. 75:1593.

29. Cher, M., and Hollingsworth, C.S. (1969) Chemiluminescent reactions of excited helium with nitrogen and oxygen, Adv. Chem. Ser. 80:118.

30. Kolts, J.H., and Setser, D.W. (1978) Decay rates of Ar (4s, $^3P_2$), Ar(4s, $^3P_0$), Kr(5s, $^3P_2$), and Xe(6s, $^3P_2$) atoms in argon, J. Chem. Phys. 68:4848.

the ideal case, the parabolic velocity profile is fully developed, and the rate constants determined under the assumption of plug flow conditions must be multiplied by a factor of 1.6 to give the true rate constant. The time required for the development of a parabolic velocity profile in the reactor is usually translated into a traversal distance, $z = 0.227\,aR$, where z is the distance from the inlet of the tube, a is the tube radius, and R is the Reynolds number of the flow. In our experiments, R ranges from 35 to 55 and typical entry lengths vary from 20 to 32 cm. All our measurements were done 30-45 cm downstream of the reagent inlet, thus ensuring that the flow was fully developed even if there was some perturbation to the flow from reagent addition. Thus all our reported rate constants have been increased from the plug flow values by a factor of 1.6. Possible corrections for the effects of axial diffusion, slip and axial velocity gradients are entirely negligible under our conditions.[20] Inlet effects are taken care of by our having made the measurements at a number of positions along the flow tube.

2.3 Absolute $N_2(A\,^3\Sigma_u^+)$ Number Density

The absolute number density of $N_2(A)$ in the reactor can be determined by measuring the absolute volume emission rate of the Vegard-Kaplan bands:

$$[N_2(A)] = \frac{I_{N_2(A)}}{A_{N_2(A)}} \quad . \tag{4}$$

The observed signal is related to the true volume emission rate through

$$I_{obs} = I_{true}\,\frac{\Omega}{4\pi}\,\eta_\lambda\,T_\lambda\,V \tag{5}$$

where $\frac{\Omega}{4\pi}$ is the effective solid angle subtended by the detection system, η_λ is the quantum efficiency of the photomultiplier at the wavelength of interest, T_λ is the transmission of the optical system (accounting for effects such as mirror reflectivities and grating efficiency) and V is the observed volume of luminous gas in the reactor. The wavelength dependence of the product $\frac{\Omega}{4\pi}\,\eta_\lambda\,T_\lambda\,V$ is given by the relative monochromator response function R_λ. Absolute values of that product are best obtained from a calibration experiment such as the O/NO air afterglow at one or several specific wavelengths. Absolute values at wavelengths other than those chosen for calibration experiments are obtained by scaling with R_λ.

The relative spectral response of the monochromator was calibrated between 200 and 800 nm using standard quartz-halogen and D_2 continuum lamps (Optronic Laboratories Inc.). Additional confirmation of the UV calibration was made by

comparing the intensities of several transitions from common upper levels of the NO γ-bands, excited by the interaction between $N_2(A)$ and NO, and scaled by the appropriate Franck-Condon factors.[31,32] The absolute spectral response of the detection system was measured at 580 nm using the O/NO air afterglow.

When atomic oxygen and nitric oxide are mixed, a continuum emission extending from 375 nm to beyond 3000 nm is observed.[22,23,33-39] The intensity of this emission is directly proportional to the product of the number densities of atomic oxygen and nitric oxide, and independent of pressure of bath gas, at least at pressures above about 0.2 Torr. Thus, the volume-emission rate of the air afterglow is given by

$$I_{true} = k_\lambda [O][NO]\ \Delta\lambda \qquad (6)$$

where k_λ is the air afterglow rate constant in units of $cm^3/(molecule\ sec\ nm)$ and $\Delta\lambda$ is the monochromator band width. Literature values for this rate constant span a range of more than a factor of 2,[33-39] but recent studies[38] indicate that the original work of Fontijn et al[33] is probably correct at wavelengths shorter than $\approx$ 800 nm. We use a value of 1.25×10^{-19} $cm^3/(molecule\ sec\ nm)$ at λ = 580 nm. Combining Eqs. (5) and (6) gives the observed air afterglow intensity:

---

31. Bubert, H. (1972) Population and predissociation of vibronic states of nitric oxide, J. Chem. Phys. 56:1113.

32. Möhlmann, G.R., Van Sprang, H.A., Bloemen, E., and de Heer, F.J. (1978) Experimental determination of the electronic transition moment for the NO($A\ ^2\Sigma^+ - X\ ^2\pi$) system. Lifetimes of the NO($A\ ^2\Sigma^+$, v'=0, 1, 2) levels, Chemical Physics 32:239.

33. Fontijn, A., Meyer, C.B., and Schiff, H.I. (1964) Absolute quantum yield measurements of the NO - O reaction and its use as a standard for chemiluminescent reactions, J. Chem. Phys. 40:64.

34. Vanpee, M., Hill, K.D., and Kineyko, W.R. (1971) Absolute rate constant measurements for the radiative combination of atomic oxygen with nitric oxide, AIAA Journal 9:135.

35. Golde, M.F., Roche, A.E., and Kaufman, F. (1973) Absolute rate constant for the O + NO chemiluminescence in the near infrared, J. Chem. Phys. 59:3953.

36. Golomb, D., and Brown, J.H. (1975) The temperature dependence of the NO - O chemiluminous recombination. The RMC mechanism, J. Chem. Phys. 63:5246.

37. Woolsey, G.A., Lee, P.H., and Slafer, W.D. (1977) Measurement of the rate constant for NO - O chemiluminescence using a calibrated piston source of light, J. Chem. Phys. 67:1220.

38. Sutoh, M., Morioka, Y., and Nakamura, M. (1980) Absolute rate constant for the chemiluminescent reaction of atomic oxygen with nitric oxide, J. Chem. Phys. 72:20.

39. Pravilov, A.M., and Smirnova, L.G. (1978) Spectral distribution of the chemiluminescence rate constant in the O + CO(+M) and O + NO(+He) reactions, Kinet. and Catal. 19:202.

$$I_\lambda^{O/NO} = k_\lambda [O][NO] \Delta\lambda \frac{\Omega}{4\pi} \eta_\lambda T_\lambda V \quad . \tag{7}$$

Air afterglow calibration experiments give a calibration factor,

$$\kappa_\lambda = \frac{I_\lambda^{O/NO}}{[O][NO]} = k_\lambda \Delta\lambda \frac{\Omega}{4\pi} \eta_\lambda T_\lambda V \quad , \tag{8}$$

the determination of which will be described below.

Absolute number densities of emitters are obtained from Eq. (4) using absolute volume emission rates and known transition probabilities. The air afterglow calibration factor κ_λ and the moderately well established value of the air afterglow rate constant k_λ, are used to convert observed emission intensities to volume emission rates:

$$I_{true} = \frac{I_{obs}\, k_{\lambda_c}\, \Delta\lambda_c\, R_{\lambda_c}}{\kappa_{\lambda_c} R_{\lambda_{obs}}} \tag{9}$$

where λ_c represents the wavelength of the calibration experiments and λ_{obs} is the wavelength of the transition of interest. I_{obs} must be the total integrated band intensity. In this work we usually measured $N_2(A)$ intensities in terms of peak intensities. A calibration factor consisting of the ratio of the integrated band intensity to the product of the spectrometer band width and the peak intensity was determined for cases in which total intensities were needed. In calibration experiments, the band areas were integrated numerically using spectral scans which were greatly expanded along the wavelength axis.

A series of calibration experiments made over a period of time established the calibration factor κ_{580} to ±10 percent. An additional uncertainty of ±25 percent exists in the absolute value of the air-afterglow rate constant k_{580}. Further uncertainties in the determination of the absolute number density of $N_2(A)$ enter through the relative monochromator response function (≈ 20 percent), Vegard-Kaplan band transition probabilities (20 percent), minor uncertainties in the calibration factors to convert observed peak heights to band areas, and in the uncertainty introduced by the radial density gradient of the $N_2(A)$ (≈ 10 percent).

The air-afterglow calibration experiments were run on gases with an essentially uniform concentration across the flow tube. The $N_2(A)$ on the other hand, has a strong radial density gradient across the tube, with a maximum number density in the center of the reactor and a zero number density at the reactor walls.

The form of the radial density profile is given approximately by the Bessel function $J_o(\lambda\, r/a)$[20] where λ is the first root of the Bessel function, 2.405. We corrected the number density calculation by comparing the area under the radial profile to the area under a square having unit height and unit radius. The area under the Bessel function is approximately 0.6 times the area under the unit square. Thus, to obtain an average $N_2(A)$ number density in the reactor, we multiply the initially calculated number density by 1.6.

A nominal value for peak intensity of the 0,6 Vegard-Kaplan band was 1 kHz. Given that the A-value for this transition is 0.16/sec,[40] the ratio of integrated intensity to peak intensity is 1.3, κ_{580} for a 1 mm slit width is 1.9×10^{-28} kHz $cm^6/molecule^2$, the observation bandwidth was 1.7 nm, and the ratio of the monochromator response at 276 nm to that at 580 nm is 0.2, we get an absolute $N_2(A)_{v'=0}$ number density of 1.9×10^9 molecules/cm^3. Making the correction for the radial density gradient, and also including a correction to account for the approximately one-third of the total $N_2(A)$ number density in $v'=1$, gives a final value for the total $N_2(A)$ number density in our flow tube of 4.5×10^9 molecules/cm^3. The total uncertainty in this value from the sources mentioned above is about 40 percent.

2.4 Air-Afterglow Calibration Procedure

In air-afterglow calibration experiments, the intensity at the calibration wavelength is measured when known quantities of both atomic oxygen and nitric oxide are added to the reactor. Known quantities of atomic oxygen are prepared by titration of nitrogen atoms with excess nitric oxide,

$$N + NO \rightarrow N_2 + O \qquad (10)$$

$[k_{10} = 3.5 \times 10^{-11}\ cm^3/(molecule\ sec)]$[41-43] .

---

40. Shemansky, D.E. (1969) N_2 Vegard-Kaplan system in absorption, J. Chem. Phys. 51:689.

41. Husain, D., and Slater, N.K.H. (1980) Kinetic study of ground state atomic nitrogen, $N(2\ ^4S_{3/2})$ by time-resolved atomic resonance fluorescence, JCS Faraday II 76:606.

42. Lee, J.H., Michael, J.V., Payne, W.A., and Stief, L.J. (1978) Absolute rate of the reaction of $N(^4S)$ with NO from 196-400 K with DF-RF and FP-RF techniques, J. Chem. Phys. 69:3069.

43. Clyne, M.A.A., and McDermid, I.S. (1975) Mass spectrometric determinations of the rates of elementary reactions of NO and NO_2 with ground state $N\ ^4S$ atoms, JCS Faraday I 71:2189.

In the absence of added nitric oxide, N-atom recombination produces chemiluminescence from the nitrogen first-positive bands, the intensity of which is proportional to the square of the N-atom number density,

$$N + N + M \rightarrow N_2(B\ ^3\Pi_g) \tag{11}$$

$$N_2(B\ ^3\Pi_g) \rightarrow N_2(A\ ^3\Sigma_u^+) + h\nu \qquad \text{(first positive bands)} \quad . \tag{12}$$

Upon addition of NO the first positive emission intensity decreases until such point as the quantity of NO added balances the amount of N-atoms initially in the flow. At this point, the end point of the NO titration, all N initially in the reactor has been converted to N_2, releasing a number of O atoms equal to the number of N atoms, and no emission is observed in the reactor. As more NO is added to the reactor, the air-afterglow emission begins to be observed, and the intensity of the emission will vary linearly with the amount of NO added. Such a titration plot is shown in Figure 3. The equation describing the change in the air-afterglow intensity as a function of added NO for NO additions beyond the titration end point is

$$I_{O/NO} = \kappa[O][NO] = \kappa[N]_o([NO]_o - [N]_o) \tag{13}$$

where κ is the constant of proportionality relating the air-afterglow intensity to the product $[O][NO]$, $[N]_o$ is the number density of N-atoms initially in the reactor prior to NO addition, and $[NO]_o$ refers to the NO number density which would obtain in the absence of Reaction (10). The factor κ then is determined to be the ratio of the square of the slope to the intercept of the line describing the change in air-afterglow intensity with $[NO]$.

Two major complications can lead to problems in using the above technique to calibrate the apparatus for absolute photon-emission rates or for [O] measurements. If the initial N-atom number density is greater than about 10^{14} atoms/cm^3, some O_2 spectral features from O-atom recombination will begin to be observable above the air-afterglow continuum,[44,45] and can lead to incorrect air-afterglow intensity determinations. A more serious problem, however, lies in the slow removal of O-atoms in a three body recombination with NO. The important reactions are

---

44. Slanger, T.G. (1978) Generation of O_2 ($C\ ^1\Sigma_u^-$, $C\ ^3\Delta_u$, $A\ ^3\Sigma_u^+$) from oxygen atom recombination, J. Chem. Phys. 69:4779.

45. Piper, L.G. (1978) Unpublished results.

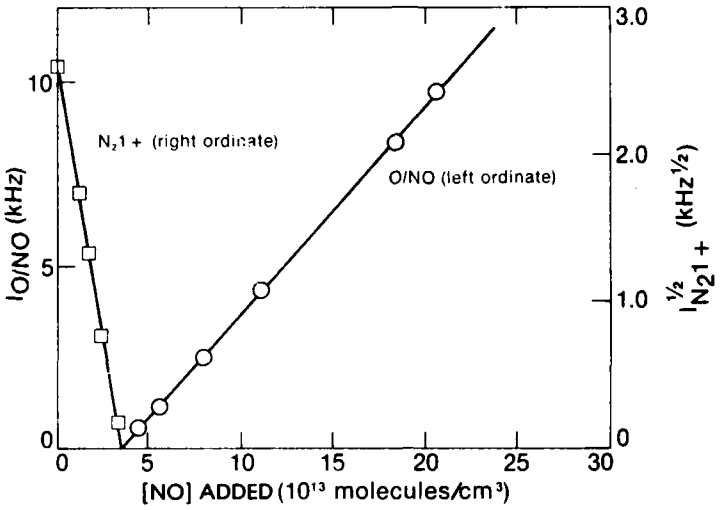

Figure 3. Variation in Emission at 580 ± 5 nm as a Function of Added [NO]

$$O + NO + M \rightarrow NO_2 + M \qquad (14)$$

$$[k_{14} = 7 \times 10^{-32} \text{ cm}^6/(\text{molecule}^2 \text{ sec}) \text{ for M = Ar}]^{46}$$

$$O + NO_2 \rightarrow NO + O_2 \qquad (15)$$

$$[k_{15} = 9.5 \times 10^{-12} \text{ cm}^3/(\text{molecule}^1 \text{ sec}^1)]^{46} \quad .$$

The second reaction is fast and essentially acts to maintain a constant NO number density, and to double the effective rate at which O is removed in Reaction (14). This effect becomes a problem at higher pressures ($\gtrsim$ 1.5 Torr), longer mixing times ($\gtrsim$ 30 msec) and large NO concentrations ($\gtrsim 10^{14}$ molecules/cm^3).

Unfortunately, it is just these adverse conditions which give the best signal-to-noise ratio in the calibration experiments. The calibrations for the experiments described in this report were corrected when necessary for the effects of removal of O in Reactions (14) and (15). However, conditions were such that the corrections never amounted to more than 5 percent.

46. Baulch, D. L., Drysdale, D. D., Horne, D. G., and Lloyd, A. C. (1973) Evaluated Kinetic Data for High Temperature Reactions. II. Homogeneous Gas Phase Reactions of the H_2 - N_2 - O_2 System. Butterworths, London.

3. QUENCHING OF $N_2(A)$ BY MOLECULAR OXYGEN

3.1 Experimental Techniques

The two important processes leading to deactivation of the $N_2(A)$ in our reactor are Reaction (1) and diffusion to the reactor walls with subsequent deactivation at the walls. Quenching by Ar, N_2[47] and He[48] in the reactor is entirely negligible. The differential equation describing the rate of change in metastable nitrogen number density with time is

$$d\frac{[N_2(A)]}{dt} = -\{k_w + k_1[O_2]\}[N_2(A)] \quad , \tag{16}$$

and, under pseudo first-order conditions $\{[N_2(A)] \ll [O_2]\}$, its solution is

$$\ln\frac{[N_2(A)]}{[N_2(A)]_o} = -\{k_w + k_1[O_2]\}\ z/\bar{v} = K_I(z/\bar{v}) \tag{17}$$

where k_w is the first-order wall deactivation rate, z the distance down the flow tube and $\bar{v}$ is the bulk flow velocity. The wall deactivation rate k_w is inversely proportional to pressure, but is independent of molecular oxygen number density. Equation (17) gives us two options for making the measurements, moveable-detector measurements or fixed-point determinations. In the moveable-detector measurements, $[O_2]$ and the total pressure are fixed and the pseudo-first-order decay rate, K_I, is measured by noting the change in $\ln[N_2(A)]$ as a function of z. Then the rate constant k_1 is given by a number of such pseudo-first-order decay-rate measurements at fixed total pressure, but varying oxygen number density:

$$\frac{dK_I}{d[O_2]} = k_1 \quad . \tag{18}$$

In the fixed-point measurements, the mixing distance is fixed and the decay in $\ln[N_2(A)]$ is measured as a function of $[O_2]$. This gives a decay constant

---

47. Levron, D., and Phelps, A.V. (1978) Quenching of $N_2(A\ ^3\Sigma_u^+,\ v = 0, 1)$ by N_2, Ar, and H_2, J. Chem. Phys. 69:2260.

48. Roy, C.R., Dreyer, J.W., and Perner, D. (1975) Rate constants for the quenching of $N_2(A\ ^3\Sigma_u^+;\ V_A = 1\text{-}6, 8)$ by rare gases, J. Chem. Phys. 63:2131.

$$\Gamma = \frac{d \ln[N_2(A)]}{d[O_2]} = k_1 z/\bar{v} \quad . \tag{19}$$

Because of problems with finite mixing time, it is best to make such measurements for several different mixing distances. Then from a plot of Γ vs z, the rate constant is determined from the slope and the virtual point of mixing is obtained from the intercept on the abscissa.

The rate constants obtained from the above analyses assume a plug flow model. As described above, they must be multiplied by a factor of 1.6 to account for fluid dynamic effects in the reactor.

3.2 Results of $N_2(A) + O_2$ Measurements

Figures 4 and 5 illustrate the moveable-detector method for the rate constant measurements, while Figures 6 and 7 illustrate the fixed-point technique. In both sets of measurements, the v'=0 level was monitored using the 0,6 Vegard-Kaplan band. Five such measurements in all gave $k_1(v'=0) = (2.31 \pm 0.06) \times 10^{-12}$ cm^3/(molecule sec) where the error estimate given is one standard deviation from the mean of the five sets of measurements.

Figure 8 shows the fixed-point decays of the v'=0 and v'=1 levels under the same conditions of mixing time and total pressure. Nine such measurements indicated that $k_1(v'=1)/k_1(v'=0) = 1.79 \pm 0.09$ where again the error estimate is one standard deviation from the mean. Given the result for $k_1(v'=0)$ above, we get that $k_1(v'=1)$ is $(4.14 \pm 0.32) \times 10^{-12}$ cm^3/(molecule sec).

The total uncertainty (rms) including uncertainties in the experimental parameters, such as temperature, pressure, and flow rate, as well as the statistical variation in the measurements, is 16 percent for the v'=0 measurements and 18 percent for the v'=1 measurements.

3.3 Discussion of $N_2(A) + O_2$ Measurements

Table 1 shows that our values are substantially in disagreement with most other measurements in the literature, although our values for the rate constants for v'=0 and v'=1 deactivation bracket the other values reported. Most of the other experimenters used either NO γ-band or Hg 6 $^3P_1$ tracers, although Dunn and Young[4] and Clark and Setser[11] used interference filters to isolate spectral lines or portions of the spectrum, Dreyer, Perner, and Roy[3] used an absorption diagnostic to monitor the $N_2(A)$ number density, and Zipf[12] monitored $N_2(A)$ emission with a monochromator.

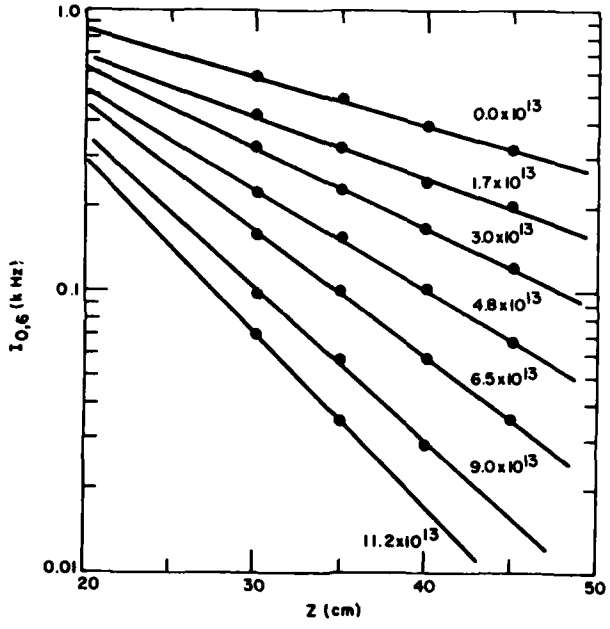

Figure 4. The Decay of $N_2(A)_{v=0}$ as a Function of Mixing Distance and $[O_2]$. The numbers by each line correspond to different $[O_2]$. P = 1.33 Torr. $\bar{V}$ = 1540 cm/sec, and $z_o \approx 10$ cm

The use of interference filters can lead to erroneous results in the $N_2(A)$ system because there is a strong possibility of NO contamination that can lead to NO γ-band signals within the band pass of the interference filter that can be much stronger than the signal from the $N_2(A)$ being monitored. In our system, even with a 1.7 nm band pass, signals from the NO-γ 0,4 and 0,5 bands significantly perturb the effective peak intensity of the Vegard-Kaplan 0,6 band between them at NO number densities on the order of 10^{10} molecules/cm^3. The obliteration of the 1,5 band of the Vegard-Kaplan system (used by Dunn and Young to monitor $N_2(A)v'=1$) by the 0,2 and 0,3 γ-bands is almost complete at such low number densities of NO. It is probably impossible in discharge-excited mixtures of N_2 and O_2 to avoid formation of significant amounts of NO ($\gtrsim 10^{10}$ molecules/cm^3). In our system, even very small leaks in the argon line, or sometimes slightly less pure gases will give significant γ-band contamination of the Vegard-Kaplan spectrum even though the gas handling system appears to be tight. In this case, small traces of air are converted to NO in the metastable argon discharge. We therefore feel that the experiments of Dunn and Young in which mixtures of N_2 and O_2 were discharged to make the $N_2(A)$, almost certainly were, in fact, tracer measurements.

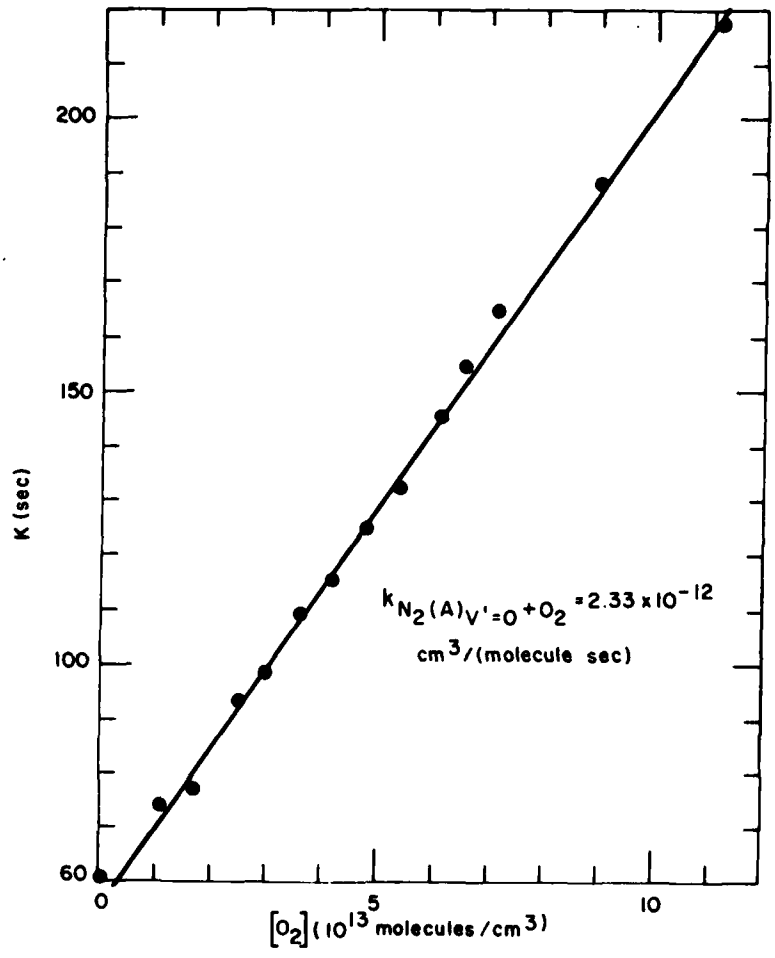

Figure 5. $N_2(A)_{v=0}$ Decay Rates as a Function of $[O_2]$. P = 1.33 Torr

A strong possibility exists that the major experiments of Clark and Setser[11] were also tracer experiments because they could not spectrally scan the region they were monitoring to ensure they had adequate gas purity. Clark and Setser do report two direct measurements in which the 0,6 and 1,9 Vegard-Kaplan bands were monitored directly as a function of molecular oxygen number density. These determinations, however, were done using the fixed observation point technique but only one injector-to-observation-region distance, so that the data could be seriously affected by a large mixing-length correction.

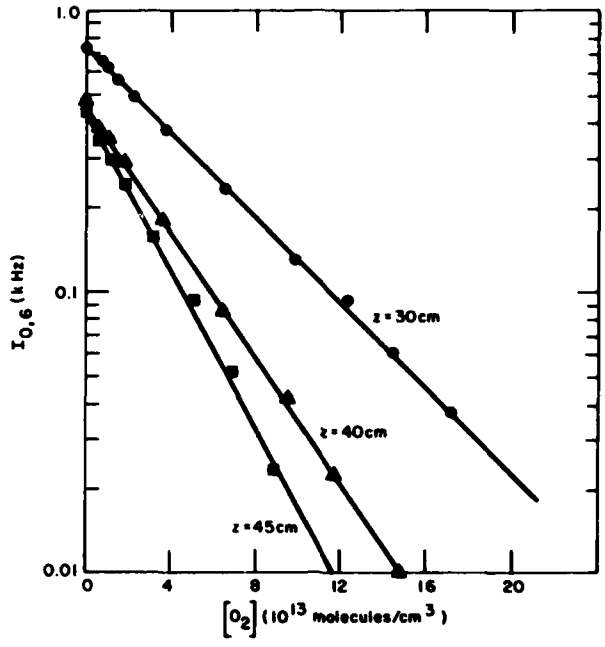

Figure 6. Decay of $N_2(A)_{v=0}$ as a Function of $[O_2]$ for Several Different Mixing Distances. P = 1.44 Torr. $\bar{V}$ = 1330 cm/sec

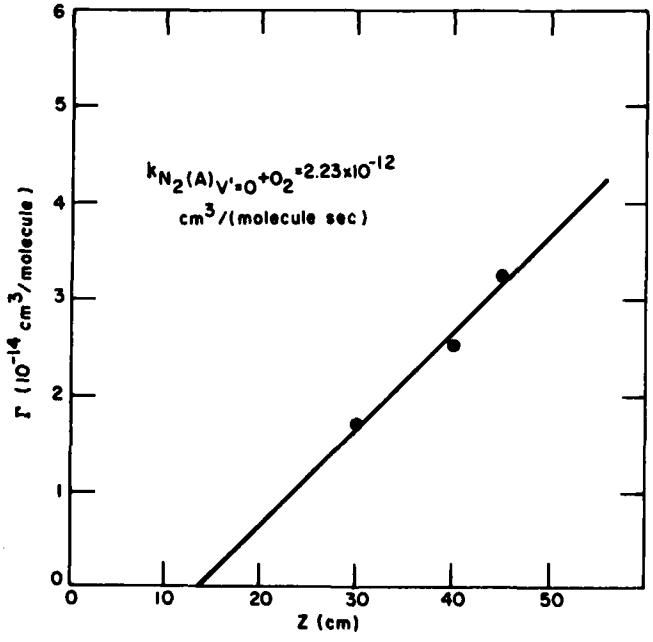

Figure 7. Decay Constants for $N_2(A)_{v=0}$ Removal by O_2 as a Function of Mixing Distance. P = 1.44 Torr. $\bar{V}$ = 1330 cm/sec

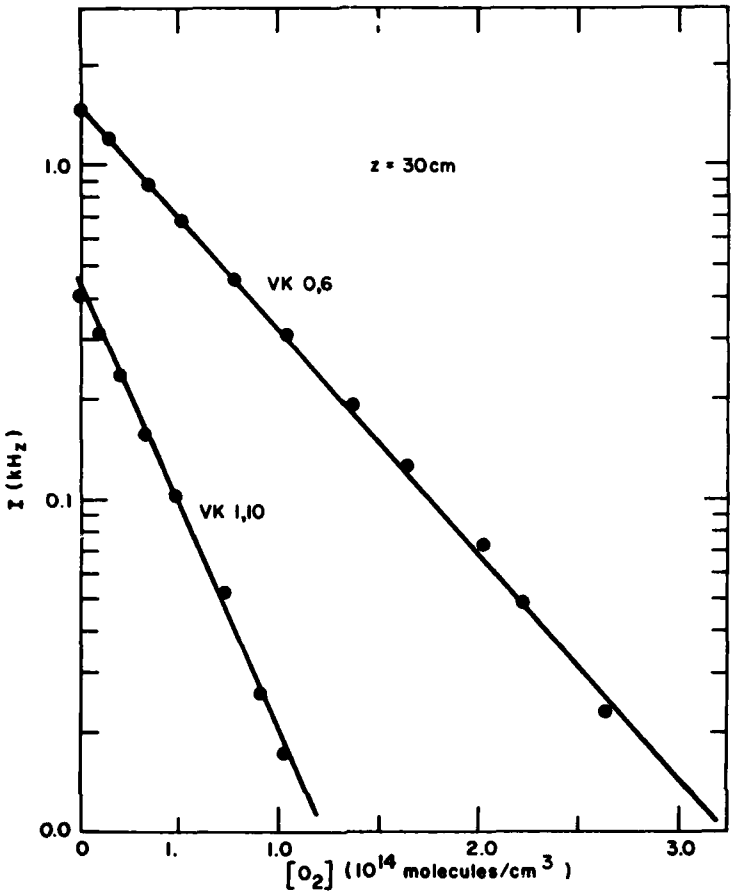

Figure 8. The Decay of $N_2(A)_{v=0}$ and v=1 as a Function of O_2 for a Mixing Distance of 30 cm. P = 1.52 Torr. $\bar{V}$ = 3271 cm/sec

On balance, we feel that all previous measurements of the rate constant for deactivation of $N_2(A)$ by O_2 could be seriously affected by the use of a tracer, or by NO impurities making measurements in effect tracer measurements, except for those done by Dreyer et al[3] and Zipf.[12] Our results agree with Dreyer et al for v'=0, but they obtained a value for v'=1 a factor of 2 larger than ours. In general, rather large deviations from the Beer-Lambert law can occur in absorption systems which use discharge lamps as the source of radiation, and such deviations can strongly affect the analysis used to extract rate constants. Dreyer et al do not discuss corrections to their lamp diagnostic. Our measurements are direct and contain no such hidden complications in the analysis; they also agree well with Zipf's recent observations which also were direct.

We designed an experiment to test the effects of using a tracer to follow $N_2(A)$ decay. We measured the decay of the 0,6 and 1,10 Vegard-Kaplan bands as a function of molecular oxygen number density, and under identical conditions, the decay of the 1,0 γ-band of NO when a small trace of NO was added to the reactor. The number density of NO added to the reactor was $\lesssim 5 \times 10^{10}$ molecules/cm^3, sufficient to give a strong tracer signal, but sufficiently small that NO quenching of $N_2(A)$ had little effect on the overall kinetics.

Two fixed-point decay plots are shown in Figures 9 and 10. It is obvious from the plots that the $N_2(A)$ decay rate as monitored by the γ-band tracer is intermediate between the decays shown for the individual $N_2(A)$ vibrational levels. Figure 11 shows how fixed-point decay constants vary with mixing distance. The γ-band-monitored decay constants are midway between the v'=0 and v'=1 decay

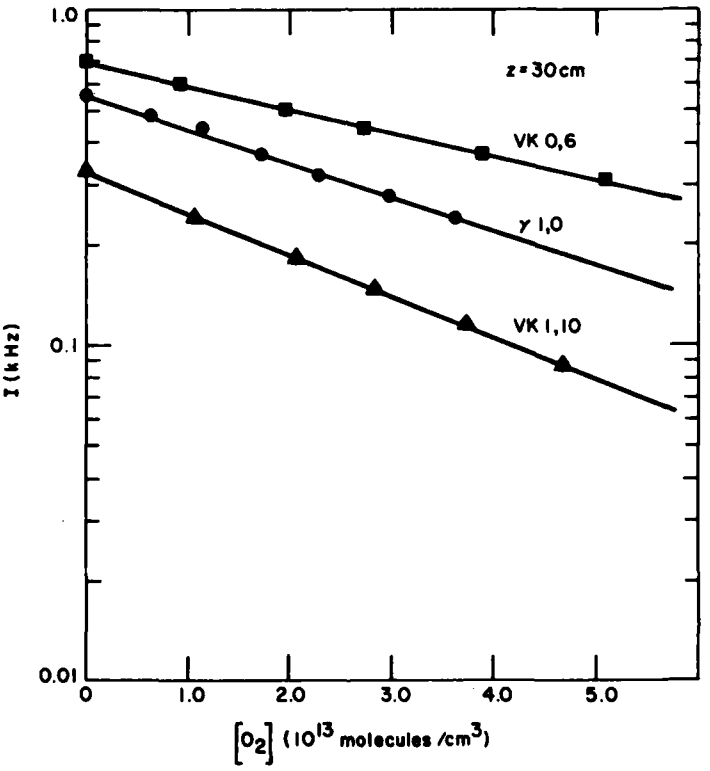

Figure 9. Fixed-point Decay of $N_2(A)$ as a Function of $[O_2]$ for v=0, v=1 and a Combination of Vibrational Levels Using the NO γ 1,0 Band as a Tracer. P = 1.30 Torr. $\bar{V}$ = 1714 cm/sec, [NO] $\lesssim 5 \times 10^{10}$ molecules/cm^3

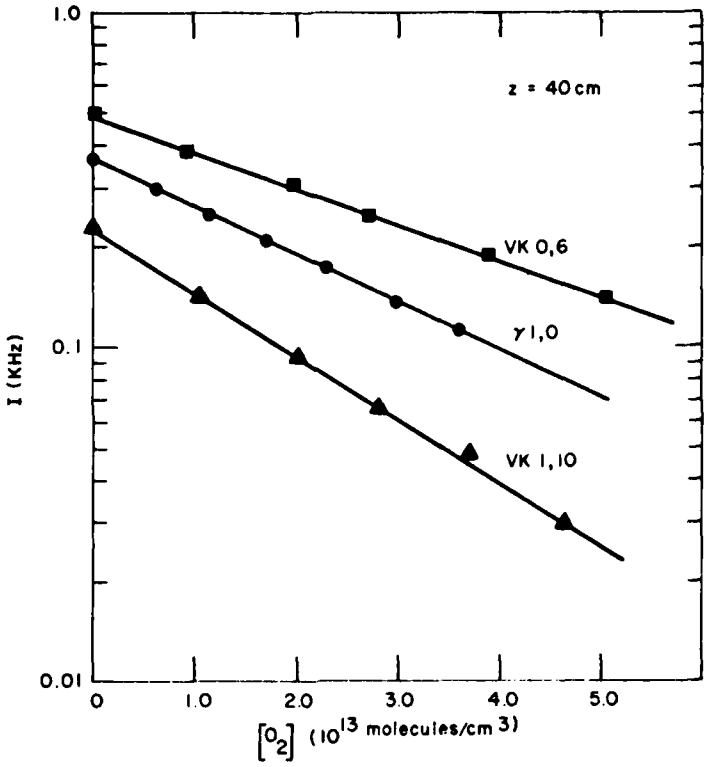

Figure 10. Fixed-Point Decay of $N_2(A)$ as a Function of $[O_2]$ for v=0, v=1, and a Combination of Both Vibrational Levels Using the NO γ 1, 0 Band as a Tracer. P = 1.30 Torr, $\bar{V}$ = 1714 cm/sec, $[NO] \lesssim 5 \times 10^{10}$ molecules/cm^3

constants, and at longer mixing times the tracer measurements approach more closely the decay of the v'=0 level.

Our system is not optimum for showing the tracer effect because our kinetic observations are made far downstream of the point of mixing (our effective reaction times vary from 11-20 msec) and our initial $[N_2(A)_{v'=0}]/[N_2(A)_{v'=1}]$ was 1.74 which implies that only about 35 percent of the total $N_2(A)$ number density was in the v'=1 state. In contrast to this Callear and Wood[8] and Young et al[6] estimated that roughly two thirds of their $N_2(A)$ number density was in v'=1 while Setser's group[2,5,9,11] had nearly equal number densities of the two states. Our tracer decay constants at the two shortest reaction times imply a $N_2(A)$ deactivation rate constant by O_2 of 3.3×10^{-12} cm^3/(molecule sec) using the mixing correction determined from the Vegard-Kaplan 0, 6 and 1, 10 measurements.

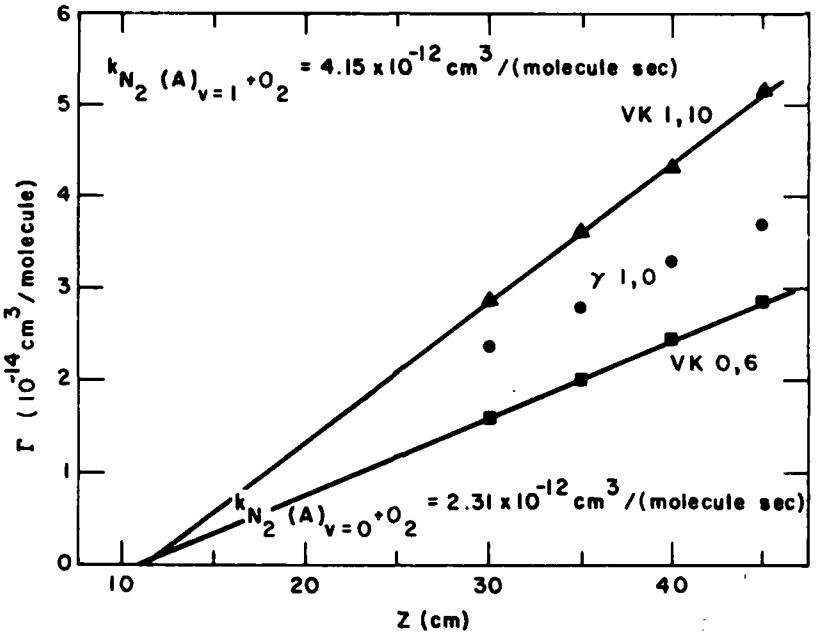

Figure 11. Decay Constants for $N_2(A)$ Removal by O_2 as a Function of Reaction Distance for v=0, v=1 and a Mixture of Vibrational Levels Using the NO γ 1,0 Band as a Tracer. P = 1.30 Torr, $\bar{V}$ = 1714 cm/sec, [NO] $\lesssim 5 \times 10^{10}$ molecules/cm^3

4. QUENCHING OF $N_2(A)$ BY ATOMIC OXYGEN

4.1 Determination of Atomic Oxygen Number Density

O-atom number densities in the experiments on the removal of $N_2(A)$ by atomic oxygen were determined by measuring the air-afterglow signal at 580 nm, with a 5 nm bandpass at at least three different NO number densities. Even though small amounts of ozone could be by-products of the O-atom discharge, there can be no interference from the O_3 + NO chemiluminescent reaction in the technique for determining the O-atom number density. The continuum generated from the O_3 + NO reaction has a short wavelength cutoff of 600 nm.[49] The [O] was taken to be the slope of the line representing the air-afterglow intensity as a function of [NO] divided by κ. A series of calibrations taken over a period of time established κ to ±10 percent. The slopes of the $I_{O/NO}$ vs [NO] plots for the determination of

49. Clough, P. N., and Thrush, B. A. (1967) Mechanism of the Chemiluminescent reaction between nitric oxide and ozone, Trans. Faraday Soc. 63:915.

[O] had for the most part standard deviations less than 5 percent. Thus, the determination of [O] is in principle accurate to ±12 percent. Because the measurements of [O] were not made simultaneously with the kinetic measurements, it is possible that short-term variations in [O] could lead to differences between the number densities of O measured and those actually in the reactor during the kinetic measurements. We shall assume these differences to be random and, therefore, included in the experimental scatter in the data analysis.

4.2 Experimental Technique for Measurements of the Quenching of $N_2(A)$ by Atomic Oxygen

Atomic oxygen for the studies of the quenching of $N_2(A)$ by atomic oxygen is produced by dissociating molecular oxygen by means of a microwave discharge through a trace of O_2 in helium. Thus, when the discharge is on, there are three important processes for $N_2(A)$ removal: deactivation at the wall, quenching by atomic oxygen, and quenching by molecular oxygen. With the discharge on, the equation describing the change in $N_2(A)$ number density with distance down the flow tube is given by

$$\bar{v} \ln \frac{[N_2(A)]}{[N_2(A)]_o} = - \{k_w + k_1[O_2] + k_2[O]\} z \quad . \tag{20}$$

When the discharge is turned off, the $N_2(A)$ number density is given by Eq. (17) as discussed earlier

$$\bar{v} \ln \frac{[N_2(A)]}{[N_2(A)]_o} = - \{k_w + k_1[O_2]_o\} z \quad . \tag{17}$$

When the discharge is on, the molecular oxygen number density is given by

$$[O_2] = [O_2]_o - \tfrac{1}{2}[O] \tag{21}$$

where $[O_2]_o$ is the number density of O_2 with the discharge off. Substituting Eq. (21) into Eq. (20) and taking the difference between Eqs. (20) and (17) results in an expression which relates the ratio of the $N_2(A)$ number density with the discharge on to that with it off to the rate constant of interest, k_2, the atomic oxygen number density, and the reaction time, that is,

$$\bar{v} \ln \frac{[N_2(A)]^{on}}{[N_2(A)]_o} - \bar{v} \ln \frac{[N_2(A)]^{off}}{[N_2(A)]_o} = \bar{v} \ln \frac{[N_2(A)]^{on}}{[N_2(A)]^{off}} = - \{k_2 - \tfrac{1}{2} k_1\}[O] z \quad . \tag{22}$$

Plots of the left hand side of Eq. (22) against [O] give lines whose slopes equal $\left(k_2 - \frac{1}{2} k_1\right) z = \Gamma'$. The slope from a plot of Γ' versus z can be used to obtain the unknown rate constant k_2, given the previously determined rate constant k_1.

4.3 Results of Measurements on $N_2(A) + O$

Figures 12 and 13 show the plots of the left hand side of Eq. (22) vs [O] at two different reaction distances, and Figure 14 shows the plot of Γ' vs z for measurements on the 0,6 band of $N_2(A)$; Figures 15, 16, and 17 show similar plots for measurements made on the 1,10 band. The slopes of the lines of Γ' vs z are $(1.7 \pm 0.1) \times 10^{-11}$ cm^3/(molecule sec) for v'=0 and $(2.0 \pm 0.1) \times 10^{-11}$ cm^3/(molecule sec) for v'=1, where the uncertainty given is one standard deviation in the least squares fit. The removal rate constants are then determined by multiplying these slopes by 1.6 to correct for flow effects (Section 4.2), and adding half of the rate constant for removal by molecular oxygen. These rate constants have been given above as 2.3×10^{-12} and 4.1×10^{-12} cm^3/(molecule sec) for v'=0 and 1, respectively (Section 3.2). The final results for the removal of $N_2(A\ ^3\Sigma_u^+)$ by atomic oxygen are $(2.8 \pm 0.2) \times 10^{-11}$ cm^3/(molecule sec) for v'=0 and $(3.4 \pm 0.2) \times 10^{-11}$ cm^3/(molecule sec) for v'=1. The total uncertainty (rms), including uncertainties in temperature, pressure, flow rate, O-atom number density, etc. is ±15 percent for v'=0 and 19 percent for v'=1.

4.4 Discussion of the $N_2(A) + O$ Results

At least two other species which are known to be produced to some extent in oxygen discharges also could be potential quenchers of $N_2(A)$. These species are ozone and $O_2(a\ ^1\Delta)$. The electronically excited molecular oxygen is formed primarily through the heterogeneous recombination of atomic oxygen while the ozone is formed from the three body reaction

$$O + O_2 + M \rightarrow O_3 + M \quad (k_{23} = 3.6 \times 10^{-34} \text{ cm}^6/(\text{molecule}^2 \text{ sec}); \text{ M} = \text{Ar})^{50} \quad . \tag{23}$$

---

50. Arnold, I., and Comes, F.J. (1979) Temperature dependence of the reactions $O(^3P) + O_3 \rightarrow 2O_2$ and $O(^3P) + O_2 + M \rightarrow O_3 + M$, Chem. Phys. 42:231.

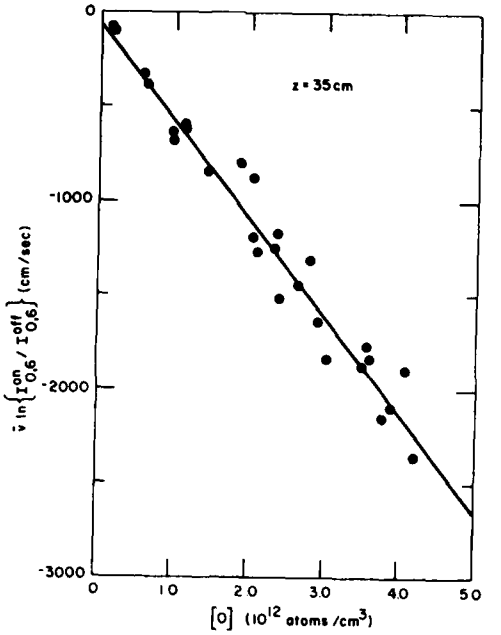

Figure 12. The Decay of $N_2(A)_{v=0}$ as a Function of [O] for a Mixing Distance of 35 cm

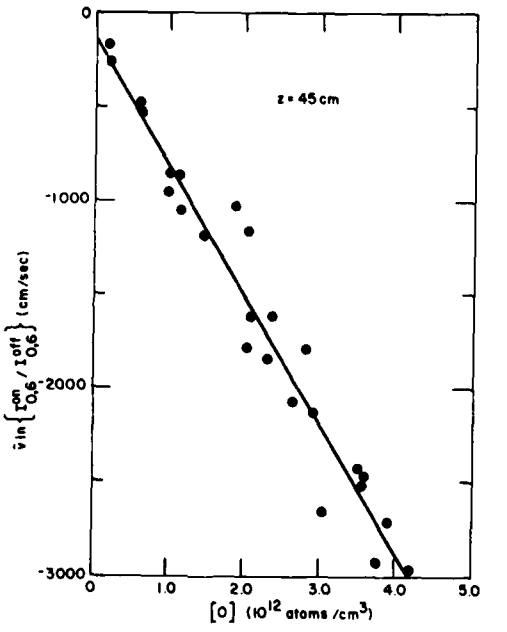

Figure 13. The Decay of $N_2(A)_{v=0}$ as a Function of [O] for a Mixing Distance of 45 cm

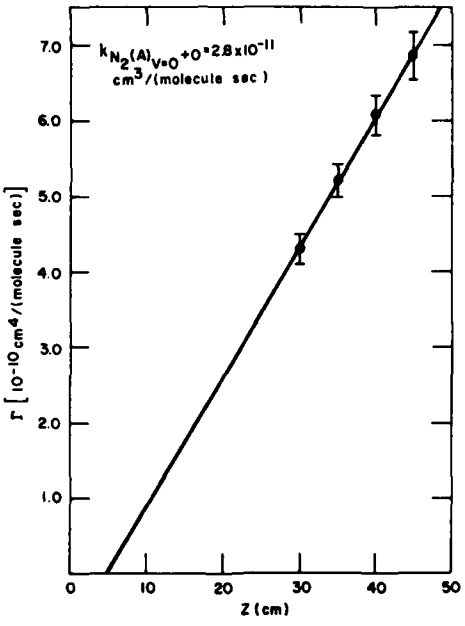

Figure 14. Decay Constants for $N_2(A)_{v=0} + O$ as a Function of Reaction Distance

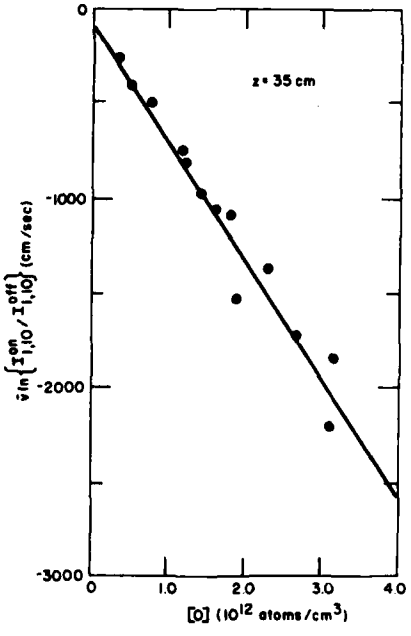

Figure 15. The Decay of $N_2(A)_{V=1}$ as a Function of [O] for a Mixing Distance of 35 cm

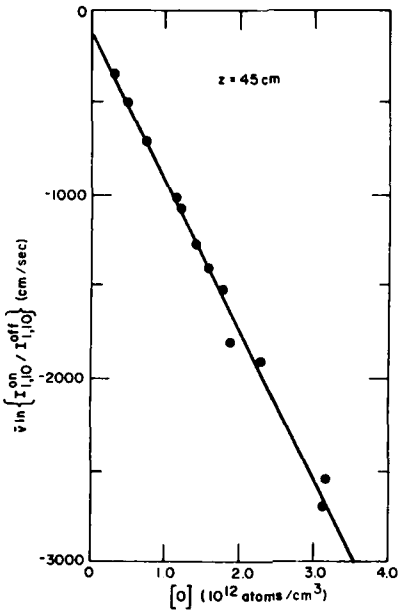

Figure 16. The Decay of $N_2(A)_{v=1}$ as a Function of [O] for a Mixing Distance of 45 cm

The ozone is destroyed by reaction with atomic oxygen

$$O + O_3 \rightarrow 2O_2 \quad (k_{24} = 8.4 \times 10^{-15} \text{ cm}^3/(\text{molecule sec})^{50} \quad , \tag{24}$$

by reaction with $O_2(a\ ^1\Delta)$,[51] and by reaction with hydrogeneous impurities in the discharged gas.[52] This latter removal process probably has the largest effect, but is the most difficult to assess. Given sufficient reaction time, Reactions (23) and (24) combine to give an upper limit to the steady-state concentration of O_3 which is given by the ratio $k_{23}[M][O_2]/k_{24}$. We estimate that the pressure in the tube containing the atom discharge is about 7.8 Torr. Thus, the ratio $k_{23}[M][O_2]/k_{24}$ is 0.011 where we have made the assumption that the third body

51. Becker, K.H., Groth, W., and Schurath, U. (1972) Reactions of $O_2(a\ ^1\Delta)$ with ozone, Chem. Phys. Lett. 14:489.

52. McCrumb, J.L., and Kaufman, F. (1972) Kinetics of the $O + O_3$ reaction, J. Chem. Phys. 57:1270.

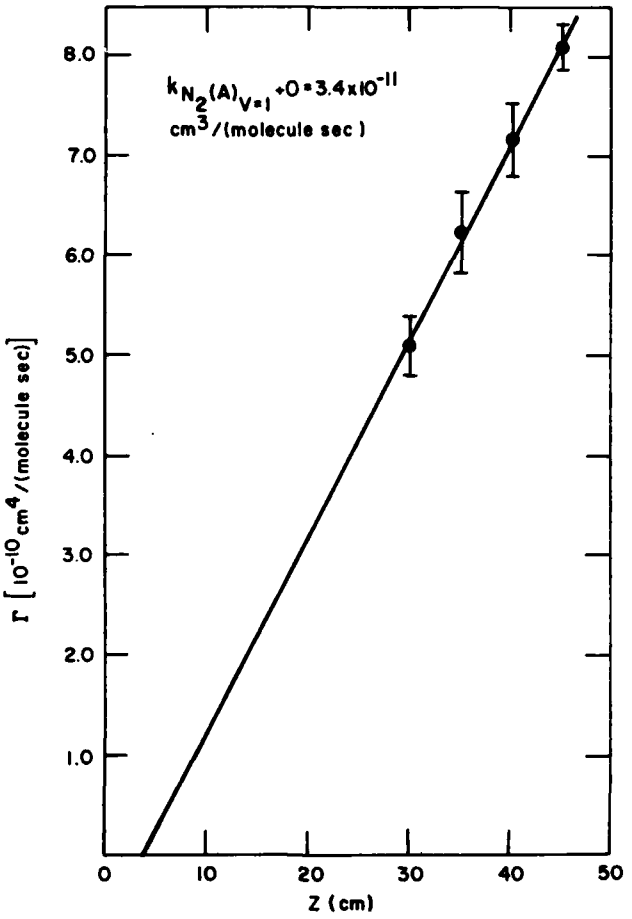

Figure 17. Decay Constants for $N_2(A)_{V=1,0} + O$ as a Function of Reaction Distance

efficiency of helium in Reaction (23) is similar to that for argon. This assumption probably is good to ±30 percent.[53]

The point of the above argument is that in the worst case, the ozone number density in the reactor will be only 1 percent of the molecular oxygen number density, whereas the atomic oxygen number density is typically about 25 percent of the molecular oxygen number density. Thus, even if the rate constant for

53. Baulch, D. L., Drysdale, D. D., Duxbury, J., and Grant, S. J. (1976) Evaluated kinetic data for high temperature reactions, III. Homogeneous gas phase reactions of the O_2-O_3 system, The CO-O_2-H_2 System, and of Sulfur-containing Species, London, Butterworths.

quenching $N_2(A)$ by ozone is 1×10^{-10} $cm^3/(molecule\ sec)$, the measurement of the rate constant for quenching of $N_2(A)$ by O will be too large by only 12 percent. Given that our neglect of the removal of ozone by $O_2(a\,^1\Delta)$ and by hydrogeneous impurities created in the discharge has caused the above estimate of the ozone number density to be an upper limit, we feel confident in rejecting ozone as a significant quencher of $N_2(A)$ in this series of measurements.

Electronically excited molecular oxygen, $O_2(a\,^1\Delta)$ could also be a potential quencher of $N_2(A)$. The extra energy in the excited oxygen is insufficient to open up any new product channels other than those already given in Reactions (1a-1e), and, in fact, product channel (1d) becomes spin-forbidden for $O_2(a\,^1\Delta)$ as the quencher of $N_2(A)$. In addition, in the approximation of a linear transition state, product channels (1a and 1c) become symmetry-forbidden for $O_2(a\,^1\Delta)$ quencher, but not for $O_2(^3\Sigma_g^-)$. Thus, if anything, we would expect $O_2(a\,^1\Delta)$ to be less reactive towards $N_2(A)$ than is $O_2(X\,^3\Sigma_g^-)$. Arguments given below indicate that $[O_2(a\,^1\Delta)]/[O] \lesssim 0.16$. Thus, for quenching of $N_2(A)$ by $O_2(^1\Delta)$ to have less than a 10 percent effect on the results given for the rate constant for quenching $N_2(A)$ by O requires a rate constant of 2×10^{-11} $cm^3/(molecule\ sec)$ for the $N_2(A) + O_2(a\,^1\Delta)$ reaction. The fastest known reaction of $O_2(a\,^1\Delta)$ has a rate constant of 3×10^{-15} $cm^3/(molecule\ sec)$.

Recently, Sharp et al[13,54,55] have analyzed data relating to a rocket flight into an aurora to conclude that the rate constant for quenching $N_2(A)$ by atomic oxygen is 2×10^{-10} $cm^3/(molecule\ sec)$. Our results clearly show their analysis is incorrect. The simulated aurora rocket experiments of O'Neil et al[14] yield results in excellent accord with the present determination of k_2.

5. EXCITATION OF $O(^1S)$ IN THE REACTION BETWEEN $N_2(A)$ AND O

One of the products of the reaction between $N_2(A)$ and atomic oxygen is $O(^1S)$.[5] We have observed how the intensity of the auroral green line, $O(^1S \rightarrow {}^1D)$, at 558 nm varies with $N_2(A)$ number density, atomic oxygen number density, and time. The processes that must be considered in the data analysis are

54. Torr, D.G., and Sharp, W.E. (1979) The concentration of atomic oxygen in the auroral lower thermosphere, Geophys. Res. Lett. 6:860.

55. Sharp, W.E., and Torr, D.G. (1979) Determination of the auroral $O(^1S)$ production sources for coordinated rocket and satellite measurements, J. Geophys. Res. 84:5345.

$$N_2(A) + O(^3P) \rightarrow O(^1S) + N_2(X) \qquad (2c)$$

$$\rightarrow \text{other products} \quad , \qquad (2a, b, d, e)$$

$$N_2(A) + O_2 \rightarrow \text{products} \quad , \qquad (1)$$

$$N_2(A) + \text{wall} \xrightarrow{k_w^A} N_2(X) \quad ,$$

$$O(^1S) + O(^3P) \rightarrow 2O(^3P \text{ or } ^1D) \quad , \qquad (25)$$

$$O(^1S) + O_2 \rightarrow \text{products} \quad , \qquad (26)$$

$$O(^1S) + \text{wall} \xrightarrow{k_w^S} O(^3P) \quad .$$

The differential equation that describes the change in the $N_2(A)$ number density as a function of time is given by

$$\frac{d[N_2(A)]}{dt} = -(k_2[O] + k_1[O_2] + k_w^A)[N_2(A)] \quad , \qquad (27)$$

and under pseudo first order conditions, $[N_2(A)] \ll [O]$, $[O_2]$, has the solution

$$[N_2(A)] = [N_2(A)]_o e^{-K_A t} \qquad (28)$$

where $K_A = k_2[O] + k_1[O_2] + k_w^A$. The differential equation for the temporal history of the $O(^1S)$ is

$$\frac{d[O(^1S)]}{dt} = k_{2c}[O][N_2(A)] - (k_{25}[O] + k_{26}[O_2] + k_w^S)[O(^1S)] \quad . \qquad (29)$$

This equation also can be solved analytically to give

$$[O(^1S)] = \frac{k_{2c}[O][N_2(A)]_o}{K_S - K_A}\left\{e^{-K_A t} - e^{-K_S t}\right\} \qquad (30)$$

where $K_S = k_{25}[O] + k_{26}[O_2] + k_w^S$. Using the result in Eq. (28) and rearranging slightly gives the result

$$\frac{[O(^1S)]}{[N_2(A)]} = \frac{k_{2c}[O]}{K_S - K_A} \left\{ 1 - e^{-(K_S - K_A)t} \right\} . \tag{31}$$

This result ignores differences in decay rate between the different vibrational levels of $N_2(A)$. Allowing for the vibrational-level effect gives

$$\frac{[O(^1S)]}{[N_2(A)]_{v'=0}} = \frac{k_{2c}^{v'=0}[O]}{K_S - K_{A_{v'=0}}} \left\{ 1 - e^{-\left(K_S - K_{A_{v'=0}}\right)t} \right\} +$$

$$\frac{k_{2c}^{v'=1}[O]}{K_S - K_{A_{v'=1}}} \left\{ 1 - e^{-\left(K_S - K_{A_{v'=1}}\right)t} \right\} \frac{[N_2(A)]^o_{v'=1}}{[N_2(A)]^o_{v'=0}} \left\{ e^{-(\Delta k_1[O_2] + \Delta k_2[O])t} \right\} \tag{32}$$

where $K_{A_{v'=0,1}}$ are as given above but with state-specific rate constants k_1 and k_2, Δk_1 and Δk_2 are the differences in the respective rate constants between $v'=1$ and 0, respectively, and the superscript o on the $N_2(A)$ number densities represent initial conditions.

Our experimental observations consisted of measurements of the decay of the 0,6 Vegard-Kaplan band and of the $O(^1S)$ 558 nm line as a function of time over a range of O-atom number densities of $0.16 - 3.9 \times 10^{12}$ atoms/cm^3, effective reaction times of 18-29 msec, and a spectral scan over the Vegard-Kaplan bands at the beginning of each run to obtain a value for the ratio of $[N_2(A)]^o_{v'=1}/[N_2(A)]^o_{v'=0}$. The data showed only a small or negligible change in the ratio $I_0(^1S)/I_{0,6}$ which led us to believe that the exponential term in Eq. (31) did not contribute significantly to the overall kinetics. We thus did an initial, simple analysis which neglected the temporal variations in the intensity ratio, and which in addition neglected differences in reactivity between the vibrational levels, assumed all runs were done at constant pressure, and assumed a constant ratio of $[O]/[O_2]$. We subsequently did a complete analysis of the data according to Eq. (32) which gave results substantially different. We will present both analyses since the simple analysis gives a good qualitative feel for what is happening, and in addition, is readily accessible to graphical representation which provides a good visual indication of the quality of the data.

5.1 Simple Analysis of the $O(^1S)$ Kinetics

The fact that there was only a weak temporal dependence in the ratio $I_0(^1S)/I_{0,6}$ (that is, the data could be considered to be constant to within about ±5 percent) implied that the exponential term in Eq. (31) was close to zero. Thus the data could be reasonably represented by Eq. (33):

$$\frac{[O(^1S)]}{[N_2(A)]} = \frac{k_{2c}[O]}{K_S - K_A} \quad . \tag{33}$$

This equation can be rearranged slightly to give

$$\frac{[O(^1S)]}{[N_2(A)]} = \frac{k_{2c}[O]/\Delta k_w}{\Delta k_w + \Delta k_0[O]/\Delta k_w} \quad , \tag{34}$$

where $\Delta k_w = k_w^S - k_w^A$ and $\Delta k_0 = k_{25} - k_2^{eff}$ (k_{26} is negligible under our conditions[56-59] and $k_2[O] + k_1[O_2]$ can be replaced by $k_2^{eff}[O]$ — see below).

Figure 18 shows a plot of the ratio of 558 nm emission to 276 nm emission (Vegard-Kaplan 0,6 band) as a function of [O] where the data points represent the average value of the ratio measured at the four different reaction times sampled (the standard deviations of the averages were less than 5 percent). Comparison of the data in the figure with the trend to be expected from Eq. (34) shows that the second term in the denominator of Eq. (34) must be greater than zero. This is not a result that we had anticipated since literature values for k_{25} are 0.75[60] and $1.8^{61} \times 10^{-11}$ cm^3/(molecule sec) and our own determination of k_2 is 2.8 and 3.4×10^{-11} cm^3/(molecule sec) for v'=0 and 1, respectively, almost a factor of two larger than Slanger and Black's[61] measurement of k_{25}.

---

56. Filseth, S.V., Stuhl, F., and Welge, K.H. Collisional deactivation of $O(^1S)$, J. Chem. Phys. 52:239.

57. Atkinson, R., and Welge, K.H. (1972) Temperature dependence of $O(^1S)$ deactivation by CO_2, O_2, N_2 and Ar, J. Chem. Phys. 57:3689.

58. Slanger, T.G., Wood, B.J., and Black, G. (1972) The temperature dependence of $O(^1S)$ quenching by O_2, Chem. Phys. Lett. 17:401.

59. Zipf, E.C. (1979) The $OI(^1S)$ state: Its quenching by O_2 and formation by the dissociative recombination of vibrationally excited O_2^+ ions, Geophys. Res. Lett. 6:881.

60. Felder, W., and Young, R.A. (1972) Quenching of $O(^1S)$ by $O(^3P)$, J. Chem. Phys. 56:6028.

61. Slanger, T.G., and Black, G. (1976) $O(^1S)$ Quenching by $O(^3P)$, J. Chem. Phys. 64:3763.

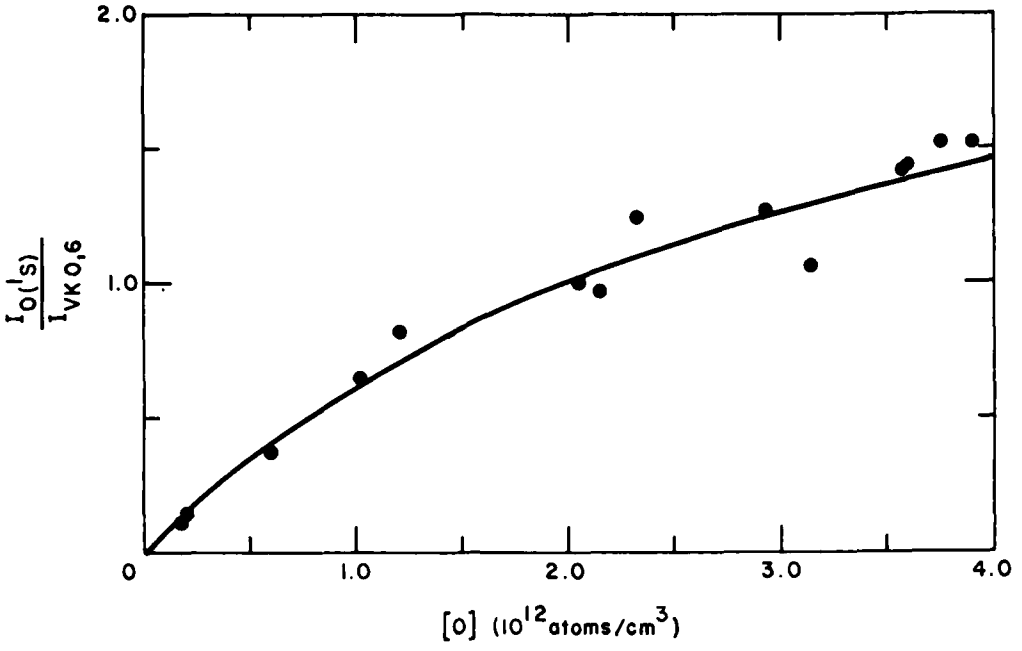

Figure 18. Variation in the Ratio of O(^{1}S) Emission as a Function of [O]. The solid line is the best-fit from the computer model. P ≈ 1.35 Torr, $\bar{V}$ ≈ 1380 cm/sec, α ≈ 0.13

There are essentially three unknowns in Eq. (34), k_w^S, k_{25}, and k_{2c}. However, the form of the data is such that it is not possible to determine the three unknowns uniquely from a non-linear least-squares fit of Eq. (32) to the data. We can, however, estimate the unknown parameter k_w^S to better than 10 percent and we have, therefore, performed non-linear least-squares fits of the data to the equation.

$$\frac{I_{O^1S}}{I_{N_2(A)}} = \frac{[O(^1S)]}{[N_2(A)]} = \frac{A_1[O]}{1 + A_2[O]} \quad , \tag{35}$$

where $A_1 = \gamma k_{2c}/\Delta k_w$ and $A_2 = \Delta k_O/\Delta k_w$. The factor γ relates observed intensities to number densities of emitting species including a correction to account for approximately one-third of the total $N_2(A)$ number density being in v'=1. The unknown parameters k_{2c} and k_{25} were extracted from the best-fit parameters using the estimated value of k_w^S and values of k_w^A and k_2^{eff} which were obtained from the data as outlined below.

Under the assumption that the fraction, α, of O_2 dissociated in the microwave discharge to make [O] is invariant to the flow rate of O_2 through the discharge (a

fairly good assumption provided that the mole fraction of O_2 in the discharge gas is less than 1 percent of the total gas flow through the discharge), the molecular-oxygen number density in the reactor will be directly proportional to the atomic-oxygen number density, that is, $[O_2] = \frac{[O]}{2}\left(\frac{1}{\alpha} - 1\right)$. Then the quantity $k_2[O] + k_1[O_2]$ in Eq. (27) can be replaced by $k_2^{eff}[O]$ where $k_e^{eff} = k_2 + \frac{1}{2}\left(\frac{1}{\alpha} - 1\right)k_1$. Figure 19 shows a plot of the decay rates of the 0,6 Vegard-Kaplan band measured in the $O(^1S)$ experiments as a function of atomic oxygen number density. Although the data are somewhat scattered, a linear trend is evident, and a linear least-squares analysis of the data gives $k_2^{eff} = (2.5 \pm 0.2) \times 10^{-11}$ cm^3/molecule sec (slope) and $k_w^A = 61 \pm 6$/sec (intercept). The value for k_2^{eff}, when multiplied by 1.6 to correct for flow effects, is in reasonable agreement with the individual determinations of k_1 and k_2 given above because only about 13 percent of the O_2 is dissociated in the microwave discharge. The value of k_w^A agrees well with our data on wall quenching[62] which indicates that the product $k_w^A p = 80 \pm 6$/sec and given that the $O(^1S)$ studies were done at approximately 1.3 Torr.

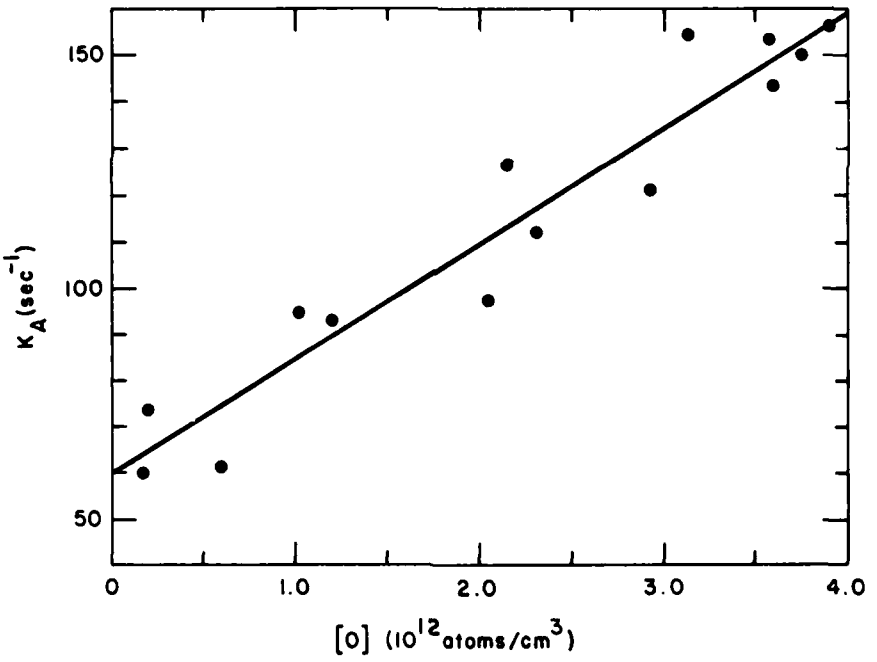

Figure 19. Rate of $N_2(A)_{v=0}$ Decay as a Function of [O]. P ≈ 1.35 Torr, $\bar{V}$ ≈ 1380 cm/sec, $\alpha \approx 0.13$

62. Piper, L.G. (1980) Unpublished results.

The rate constant for removal of $O(^1S)$ in collisions with the walls, k_w^S, is determined by the rate of diffusion in the reactor, that is,

$$k_w^S = \frac{0.62\, D_{O/Ar}}{\Lambda^2\, P} \quad , \tag{36}$$

where $\Lambda^2 = (a/\lambda_o)^2$ with λ_o being the first root of the Bessel function J_o, a the flow tube radius, $D_{O/Ar}$ the diffusion coefficient of atomic oxygen in argon, and the factor of 0.62 is included to correct for the coupling of the parabolic velocity profile with the radial density gradient of diffusing species. A value of $k_w^A p$ of 80/sec leads to a diffusion coefficient of $N_2(A)$ in argon of 140 cm^2/sec at 1 Torr in excellent agreement with the value of 143 cm^2/sec at 1 Torr for ground state N_2 diffusing into argon.[63]

Morgan and Schiff[64] have measured the diffusion coefficient of $O(^3P)$ in argon to be 209 cm^2/sec at 1 Torr and at a temperature of 280 K. Multiplying this value by $(300/280)^{3/2}$ to correct to the temperature of the present experiments[56] gives $D_{O/Ar}$ = 230 cm^2/sec at 1 Torr. Because the electronic configurations of $O(^1S)$ and $O(^3P)$ are the same, we would expect that the diffusion coefficient of $O(^1S)$ in argon would be the same as that just given for $O(^3P)$. This leads to a value for k_w^S of 97/sec under the conditions of the present experiments (1.3 Torr).

The factor γ which relates intensities to populations is given by

$$\gamma = \frac{R_\lambda^{^1S}\, A_{^1S} \times 1.5\, \beta}{R_\lambda^{0,6}\, A_{0,6}} \tag{37}$$

where R_λ^i is the relative monochromator response function and A_i is the Einstein coefficient [0.163 for the 0.6 Vegard-Kaplan band[40] and 1.18 for the $O(^1S \rightarrow {}^1D)$ transition[65]] of species i, β is a correction factor relating the measured peak height of the 0,6 band to the integrated band intensity and the factor of 1.5 is

---

63. Hirschfelder, J.O., Curtiss, C.F., and Bird, R.B. (1964) Molecular Theory of Gases and Liquids, New York: John Wiley & Sons, Inc. corrected ed. p. 579.

64. Morgan, J.E., and Schiff, H.I. (1964) Diffusion coefficients of O and N atoms in inert gases, Can. J. Chem. 42:2300.

65. Nicolaides, C., Sinanoglu, O., and Westhous, R. (1971) Theory of atomic structure including electron correlation IV. Method for forbidden transition probabilities with results for [OI], [OII], [NI], [NII], and [CI], Phys. Rev. A 4:1400.

included to account for the contribution to $O(^1S)$ production from v'=1 of $N_2(A)$. The end result for γ is 3.6.

The least-squares analysis of the data to Eq. (35) gave $A_1 = (8.3 \pm 1.0) \times 10^{-13}$ cm^3/molecule and $A_2 = (3.1 \pm 0.8) \times 10^{-13}$ cm^3/molecule, where the uncertainties given are one standard deviation from the fit. The solid line through the data in Figure 18 is Eq. (35) using these best-fit parameters. From these results we obtain $k_{2c} = 1.3 \times 10^{-11}$ cm^3/(molecule sec) and $k_{25} = 5.8 \times 10^{-11}$ cm^3/(molecule sec). The efficiency, η, for producing $O(^1S)$ from $N_2(A) + O$ is $k_{2c}/k_2 = 0.43$. The value deduced for the rate constant for quenching $O(^1S)$ by O is a factor of 3 greater than the value given by Slanger and Black.[61]

5.2 Complete Analysis of the $O(^1S)$ Data

Insertion of the best-fit value of k_{25} into the expcnential term in Eq. (31) results in a range of values of the exponential function between 0.5 and 0.9 over the range of reaction times and O-atom number densities observed in the experiments. Clearly the approximation used to obtain Eq. (34) was not valid. Consequently, we wrote a non-linear least-squares program to analyze all our data using Eq. (32). The values of the $N_2(A)$ rate constants used in the computer program were those obtained above in the rate constant measurements. The values for the wall-loss rate constants were as given previously, except that for the complete fit, small variations in total pressure from one experiment to another were incorporated by using the expression k'_w/p instead of k_w, where k'_w is the wall-loss rate constant at 1 Torr. The program also used measured values for both O and O_2 number densities, and accounted for small changes in bulk flow velocity from one set of measurements to the next. The mixing correction used was obtained from the O-atom quenching measurements. The program implicitly assumed that the ratio k_{2c}/k_2 was the same for both vibrational levels, even though the rate constants differ by about 20 percent. This assumption does not introduce significant uncertainties in the final value obtained for k_{2c}. The three unknown parameters from the complete fit are γ', k_{2c}, and k_{25} where γ' is $\gamma/1.5$, that is, the v'=1 correction is explicitly incorporated in the function to be fit.

The results of the least-squares fit gave $k_{2c} = 1.95 \times 10^{-11}$ cm^3/(molecule sec) and $k_{25} = 5.7 \times 10^{-11}$ cm^3/(molecule sec). The $O(^1S)$ production efficiency, η, from this complete fit is 0.70, a substantial increase compared to the crude fit given above, while the value deduced for k_{25} is unchanged. We did a sensitivity analysis of the data by varying in turn values of the $N_2(A)$ quenching rate constants, the $O(^1S)$ wall loss rate constant, the ratio $[N_2(A)]^o_{v'=1}/[N_2(A)]^o_{v'=0}$, and the mixing correction, while holding the others fixed at their normal values.

Variations of ±10 percent in each of the parameters affected the values of the two unknown parameters by less than 5 percent.

5.3 Discussion of the O(^{1}S) Excitation Results

Previous values of η which have appeared in the literature are the experimental determination of 0.25 given by Meyer, Setser, and Stedman[2] and the aeronomic estimates of 0.33-0.45 from the University of Michigan group[55] and 0.30 from the AFGL group.[14] Meyer, Setser, and Stedman did not correct for quenching by O(^{1}S). It is clear that a linear fit to the data of Figure 18 will give an even lower value of k_{2c} than was obtained in the analysis relevant to that figure. In the future, we hope to re-analyze as much of the existing aeronomic data as possible in order to reconcile our values for both η and k_{25} with the values currently used in aeronomic circles.

Recently, Slanger[66] has decided that his determination of k_{23} could be substantially in error. He claims that his experiments to measure k_{25} probably measured the rate constant for the quenching of O(^{1}S) by $O_2(a\ ^1\Delta)$. The $O_2(a\ ^1\Delta)$ would have been formed in his atomic oxygen flow in the heterogeneous recombination of oxygen atoms formed by titrating N with NO to the end point between the point of their formation and his observation region. Ogryzlo[67] has shown that for the products of discharges of traces of molecular oxygen in argon or helium, the ratio $[O_2(a\ ^1\Delta)]/[O]$ is a constant, independent of $[O_2]$, but increasing strongly with increasing pressure. Thus, in our experimental set up it is possible that some $O_2(a\ ^1\Delta)$ was present in our reactor in addition to atomic oxygen, and that, furthermore, the number density of the $O_2(a\ ^1\Delta)$ was directly proportional to the number density of atomic oxygen. If this is the case, then the observed effective quenching of O(^{1}S) by O(^{3}P) could have been quenching by $O_2(a\ ^1\Delta)$ instead. If Slanger's estimate[66] of a rate constant for quenching O(^{1}S) by $O_2(a\ ^1\Delta)$ of 4×10^{-10} cm^3/(molecule sec) is correct, then our measured value for k_{25} implies that $O_2(a\ ^1\Delta) \lesssim 0.16\ [O]$, with the equality holding if k_{25}, that is, quenching of O(^{1}S) by O, is actually quite small. It is by no means clear that $O_2(a\ ^1\Delta)$ is an efficient quencher of O(^{1}S). Some recent observations in Ogryzlo's laboratory[67] indicate that $O_2(a\ ^1\Delta)$ does not appear to be an efficient quencher of O(^{1}S). This issue could be checked in the present apparatus where the experiments could be repeated with a re-designed injector that would simultaneously increase the effective degree of dissociation of molecular oxygen in the discharge, and decrease drastically the pressure in the discharge region. These two effects would act in

---

66. Slanger, T.G. (1980) Private communication to L.G. Piper.
67. Ogryzlo, E.A. (1980) Private communication to L.G. Piper.

concert to reduce significantly the ratio $[O_2(a\ ^1\Delta)]/[O]$, and would presumably give $O(^1S)$ excitation data with a much smaller effective value of k_{25} if Slanger's hypothesis is correct. We hope to be able to pursue these studies in a subsequent contract.

The possible presence of $O_2(a\ ^1\Delta)$ in our reactor in no way affects the value obtained for k_{2c}. The reaction between $N_2(A)$ and $O_2(a\ ^1\Delta)$ lacks sufficient energy to give $O(^1S)$ as a product.

6. NO γ-BAND EXCITATION IN $N_2(A)$ + NO

Several experiments measured the rate constant for excitation of the NO γ-bands [NO ($A\ ^2\Sigma^+ - X\ ^2\Pi$)] in the reaction between $N_2(A)$ and NO. The major objective was to determine the sensitivity limits for detection of NO using γ-band excitation by $N_2(A)$ as the diagnostic. In addition, there is some scientific interest in studying this process because the one excitation rate constant that has been measured[11] is almost a factor of 2 larger than the published rate constants for total removal of $N_2(A)$ by NO,[3,8,68-70] A further point of interest in this study is that Callear and Wood[8] claim that the ratio of v'=0/v'=1 for the γ-bands is significantly different for excitation by $N_2(A)_{v'=0}$ than it is for $N_2(A)_{v'=1}$ even though their observations on $N_2(A)$ were indirect. We, therefore, measured the intensities of the 0,1 and 1,0 γ-bands as a function of [NO] for two different ratios of $[N_2(A)_{v'=0}]/[N_2(A)_{v'=1}]$ in order to learn more about the excitation process.

The electronically excited NO is in steady state in the reactor, so that the intensity of NO emission is directly proportional to the product of the excitation rate constant, and the $N_2(A)$ and NO number densities. Electronic quenching of the NO(A) by NO can be neglected even if the rate is gas kinetic because NO($A\ ^2\Sigma^+$) has a radiative lifetime ≈200 nsec[32] and maximum NO number densities were below 10^{11} molecules/cm^3. In state-specific terms we have

$$I_{\gamma_0} = \left(k_{00} + k_{10}\ \frac{N_1}{N_0}\right) N_0\ [NO] \qquad (38a)$$

---

68. Young, R.A., and St. John, G.A. (1968) Experiments on $N_2(A\ ^3\Sigma_u^+)$. II. Excitation of NO, J. Chem. Phys. 48:898,2572.

69. Mandel, A., and Ewing, J.J. (1977) Quenching of $N_2(A\ ^3\Sigma_u^+)$ by I_2, J. Chem. Phys. 67:3490.

70. Hill, R.M., Gutcheck, R.A., Huestis, D.L., Mukherjee, D., and Lorents, D.C. (1974) Studies of E-beam Pumped Molecular Lasers, SRI Report No. MP74-39 under ARPA Contract No. N00014-72-C-0478.

and

$$I_{\gamma_1} = \left(k_{01} + k_{11} \frac{N_1}{N_0} \right) N_0 [NO] \quad , \tag{38b}$$

where the subscripts on the rate constants represent the vibrational level of $N_2(A)$ and NO(A), respectively, N_1 and N_0 represent the number densities of $N_2(A)$ v'=1 and 0, respectively, and the subscripts on the γ's represent the vibrational level of NO(A) observed. It is evident from Eq. (38) that measurements of $dI_\gamma/d[NO]$ for both the v'=0 and 1 levels of NO(A), and at two different ratios N_1/N_0 will yield the four unknown rate constants k_{ij}.

The peak intensities of the 0, 1 and 1, 0 γ-bands were measured as a function of NO number density. The NO number density was kept below 10^{11} molecules/cm^3 to avoid significant removal of $N_2(A)$ by the NO. The Vegard-Kaplan bands were scanned with NO in the reactor to ensure that they were not attenuated by the NO. Figure 20 shows a plot of the γ-band intensities as a function of [NO]. The linearity of the plots is excellent. The 0, 1 γ-band is wholly representative of $NO(A)_{v'=0}$ because the Franck-Condon factor for the 1, 2 band is negligibly small.[31,32] Thus it does not matter that our resolution would not have been adequate to resolve the two vibrational transitions of the $\Delta v = -1$ sequence. Emission from $NO(A)_{v'=2}$ was entirely negligible compared to v'=0 and 1.

In order to correct the observed intensities of the 0, 1 and 1, 0 γ-bands to total emission intensity from NO(A) v'=0 and 1, we must multiply the observed intensities by a factor relating peak height to integrated band intensity (1.5 and 1.3 for $\gamma_{0,1}$ and $_{1,0}$ respectively), and divide by the product of the branching ratio for emission from the transition observed to that for all transitions from the upper vibrational level observed (0.298 for $\gamma_{0,1}$ and 0.479 for $\gamma_{1,0}$)[31] and the relative monochromator response function (0.26 for $\gamma_{0,1}$ at 237 nm and 0.065 for $\gamma_{1,0}$ at 215 nm). Similar corrections are necessary to convert the intensity of the 0, 6 and 1, 10 Vegard-Kaplan bands to $N_2(A)$ number densities, except that in this case absolute transition probabilities for the Vegard-Kaplan transitions must be used instead of branching ratios. The relevant correction factors of integrated intensity to peak height, relative monochromator response functions, and transition probability are, respectively, 1.30, 0.90, and 0.163[40] for the Vegard-Kaplan 0, 6 band at 276 nm and 1.42, 0.89, and 0.154[40] for the Vegard-Kaplan, 1, 10 band at 343 nm. The major uncertainties are in the relative monochromator response function, particularly at wavelengths less than 250 nm. The uncertainties in this region are on the order of 25 percent.

The correction factor relating integrated band intensities to peak heights was obtained by spreading out the spectrum and numerically integrating under each

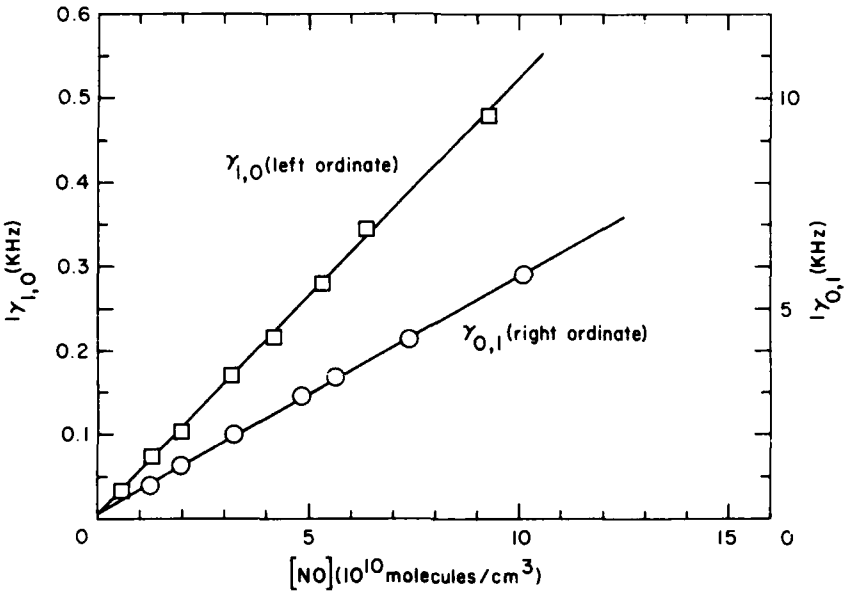

Figure 20. Intensity of NO-$\gamma_{0,1}$ and $_{1,0}$ Bands as a Function of [NO] for Constant $N_2(A)$ Number Density

peak, making corrections for overlap from adjacent bands where necessary. The correction factor is then obtained by dividing the integrated intensity by the product of the monochromator bandwidth and the peak intensity.

The results from the two sets of measurements give

$$k_{00} = (6.8 \pm 2.7) \times 10^{-11} \text{ cm}^3/(\text{molecule sec}) \quad ,$$

$$k_{01} = (1.00 \pm 0.24) \times 10^{-11} \text{ cm}^3/(\text{molecule sec}) \quad ,$$

$$k_{10} = (7.7 \pm 2.6) \times 10^{-11} \text{ cm}^3/(\text{molecule sec}) \quad ,$$

and

$$k_{11} = (1.99 \pm 0.55) \times 10^{-11} \text{ cm}^3/(\text{molecule sec}) \quad .$$

From these we obtain $k(N_2(A)_{v'=0} + NO) = (7.8 \pm 2.3) \times 10^{-11}$ cm^3/(molecule sec) and $k[N_2(A)_{v'=1} + NO] = (9.7 \pm 3.1) \times 10^{-11}$ cm^3/(molecule sec). Strictly speaking, these rate constants are NO γ-band excitation rate constants and, therefore, lower limits to the total rate constants for quenching $N_2(A)$ by NO. The values obtained for the excitation rate constants are in good agreement with the

deactivation rate constants measured by Callear and Wood (8.0×10^{-11}),[8] Young and St. John (7.0×10^{-11}),[68] Hill et al (7.5×10^{-11}),[70] Dreyer et al for $N_2(A)_{v'=1}$ (6.6×10^{-11}),[3] and Piper's measurement at 195 K [$(9 \pm 2) \times 10^{-11}$].[71] Agreement is poor with the de-excitation rate constants measured by Mandel and Ewing (4.3×10^{-11})[69] and Dreyer et al's measurement for $N_2(A)_{v'=0}$(2.8×10^{-11})[3] as well as with the excitation rate constant measured by Clark and Setser $(15 \pm 3) \times 10^{-11}$.[11] All quoted rate constants are in units of cm^3/(molecule sec).

Even admitting to the rather large error bars of the present measurements, it would seem that our results are in conflict with the excitation rate constant measured by Clark and Setser.[11] Our measurement of the excitation rate constant is, however, in excellent agreement with the majority of de-excitation rate constant measurements. Our results appear to remove the conflict between the rate constants for excitation of NO by $N_2(A)$ and de-excitation of $N_2(A)$ by NO that has previously existed.

The present results indicate that a mixture of 56 percent v'=0 and 44 percent v'=1 of $N_2(A)$ (such as obtained in Clark and Setser's measurements) will give a ratio of $NO(A)_{v'=1}/NO(A)_{v'=0}$ of 0.2/1.0 which agrees fairly well with the ratio of 0.16/1 measured by Clark and Setser.

Our data further indicate that $k_{00}/k_{01} = 6.8$ compared to the ratio of 9.5 observed by Callear and Wood.[8] Callear and Wood's value for k_{10}/k_{11} is 1.9 compared to the value of 3.9 observed here. The large error bars on our rate constants do not really put our measurements of these ratios in conflict with the measurements of Callear and Wood. Our $N_2(A)$ observations, however, are direct, whereas those of Callear and Wood were indirect.

The slope of the line for the $\gamma_{0,1}$ band in Figure 20 divided by the intensity of the 0,6 VK band is 4.6×10^{11} cm^3/molecule. Given a $VK_{0,6}$ intensity of 1 kHz and a minimum detectable $\gamma_{0,1}$ intensity of about 15 Hz we get a minimum detectable NO number density, using NO γ-band sensitization by $N_2(A)$ as the diagnostic, of $\approx 3.4 \times 10^8$ molecules/cm^3.

---

71. Piper, L.G. (1972) Kansas State University. The results are given in Ref. 11.

References

1. Swider, W. (1976) Atmospheric formation of NO from $N_2(A\ ^3\Sigma)$, Geophys. Res. Lett. 3:335.
2. Meyer, J.A., Setser, D.W., and Stedman, D.H. (1970) Energy transfer reactions of $N_2(A\ ^3\Sigma_u^+)$. II. Quenching and emission by oxygen and nitrogen atoms, J. Phys. Chem. 74:2238.
3. Dreyer, J.W., Perner, D., and Roy, C.R. (1974) Rate constants for the quenching of $N_2(A\ ^3\Sigma_u^+, v_A = 0 - 8)$ by CO, CO_2, NH_3, NO and O_2, J. Chem. Phys. 61:3164.
4. Dunn, O.J., and Young, R.A. (1976) Quenching of $N_2(A\ ^3\Sigma_u^+)$ by O_2, O, N and H, Int. J. Chem. Kin. 8:161.
5. Meyer, J.A., Setser, D.W., and Stedman, D.H. (1969) Excitation of the auroral green line of atomic oxygen ($^1S \rightarrow {}^1D$) by $N_2(A\ ^3\Sigma_u^+)$, Astrophys. J. 157:1923.
6. Young, R.A., Black, G., and Slanger, T.G. (1969) Vacuum-ultraviolet photolysis of N_2O. II. Deactivation of $N_2(A\ ^3\Sigma_u^+)$ and $N_2(B\ ^3\pi_g)$, J. Chem. Phys. 50:303.
7. Slanger, T.G., Wood, B.J., and Black, G. (1974) Temperature-dependent $N_2(A\ ^3\Sigma_u^+)$ quenching rate coefficients, J. Photochem. 2:63.
8. Callear, A.B., and Wood, P.M. (1971) Rates of energy transfer from $N_2(A\ ^3\Sigma_u^+)$ to various molecules. Initial and final quantum states in the transfer to NO $X\ ^2\Pi$ and Hg ($6\ ^1S_0$) and vibrational relaxation of $N_2(A\ ^3\Sigma_u^+)$ (v=1) in helium, Trans. Faraday Soc. 67:272.
9. Meyer, J.A., Klosterboer, D.H., and Setser, D.W. (1971) Energy transfer reactions of $N_2(A\ ^3\Sigma_u^+)$. IV. Measurement of the radiative lifetime and study of the interaction with olefins and other molecules, J. Chem. Phys. 55:2084.
10. Meyer, J.A., Setser, D.A., and Clark, W.G. (1972) Rate constants for quenching of $N_2(A\ ^3\Sigma_u^+)$ in active nitrogen, J. Phys. Chem. 76:1.

11. Clark, W.G., and Setser, D.W. (1980) Energy transfer reactions of $N_2(A\ ^3\Sigma_u^+)$ V: Quenching by hydrogen halides, methyl halides and related molecules, J. Phys. Chem. 84:2225.

12a. Zipf, E.C. (1980) A laboratory study on the formation of nitrous oxide by the reaction $N_2(A\ ^3\Sigma_u^+) + O_2 \rightarrow N_2O + O$, Nature 287:523.

12b. Kaufman, F. (1981) Personal communication.

13. Sharp, W.E., Rees, M.H., and Stewart, A.I. (1979) Coordinated rocket and satellite measurements of an auroral event 2. The rocket observations and analysis, J. Geophys. Res. 84:1977.

14. O'Neil, R.R., Lee, E.T.P., and Huppi, E.R. (1979) Auroral $O(^1S)$ production and loss processes: ground-based measurements of the artificial auroral experiment PRECEDE, J. Geophys. Res. 84:823.

15. Setser, D.W., Stedman, D.H., and Coxon, J.A. (1970) Chemical applications of metastable argon atoms. IV. Excitation and relaxation of triplet states of N_2, J. Chem. Phys. 53:1004.

16. Stedman, D.H., and Setser, D.W. (1968) Chemical applications of metastable argon atoms II. A clean system for the formation of $N_2(A\ ^3\Sigma_u^+)$. Chem. Phys. Lett. 2:542.

17. Kolts, J.H., Brashears, H.C., and Setser, D.W. (1977) Redetermination of the $N_2(C)$ and $N_2(B)$ branching ratio from the Ar $(^3P_{0,2})$ + N_2 reaction, J. Chem. Phys. 67:2931.

18. Stedman, D.H., and Setser, D.W. (1971) Chemical applications of metastable rare gas atoms, Prog. React. Kinet. 6:193.

19. Piper, L.G., Velazco, J.E., and Setser, D.W. (1973) Quenching cross-sections for electronic energy transfer reactions between metastable argon atoms and noble gases and small molecules, J. Chem. Phys. 59:3323.

20. Ferguson, E.E., Fehsenfeld, F.C., and Schmeltekopf, A.L. (1970) Flowing afterglow measurements of ion-neutral reactions, Advances in Atomic and Molecular Physics V, D.R. Bates, Ed., New York, Academic Press.

21. Piper, L.G., Krech, R.H., and Taylor, R.L. (1979) Generation of N_3 in the thermal decomposition of NaN_3, J. Chem. Phys. 71:2099.

22. Kaufman, F. (1958) The air afterglow and its use in the study of some reactions of atomic oxygen, Proc. Roy. Soc. (London) A247:123.

23. Kaufman, F. (1973) The air afterglow revisited, Chemiluminescence and Bioluminescence, M.J. Cormier, D.M. Hercules, and J. Lee, Eds., pp. 83-100.

24. Bolden, R.C., Hemsworth, R.S., Shaw, M.J., and Twiddy, N.D. (1970) Measurements of thermal-energy ion-neutral reaction rate coefficients for rare-gas ions, J. Phys. B 3:45.

25. Farragher, A.L. (1970) Ion-molecule reaction rate studies in a flowing afterglow system, Trans. Faraday Soc. 66:1411.

26. Huggins, R.W., and Cahn, J.H. (1967) Metastable measurements in flowing helium afterglow, J. Appl. Phys. 38:180.

27. Walker, R.E. (1961) Chemical reaction and diffusion in a catalytic tubular reactor, Phys. Fluids 4:1211.

28. Poirier, R.V., and Carr, R.W. (1971) The use of tubular flow reactors for kinetic studies over extended pressure ranges, J. Phys. Chem. 75:1593.

29. Cher, M., and Hollingsworth, C.S. (1969) Chemiluminescent reactions of excited helium with nitrogen and oxygen, Adv. Chem. Ser. 80:118.

30. Kolts, J.H., and Setser, D.W. (1978) Decay rates of Ar(4s, $^3P_2$), Ar(4s, $^3P_0$), Kr(5s, $^3P_2$), and Xe(6s, $^3P_2$) atoms in argon, J. Chem. Phys. 68:4848.

31. Bubert, H. (1972) Population and predissociation of vibronic states of nitric oxide, J. Chem. Phys. 56:1113.

32. Möhlmann, G.R., Van Sprang, H.A., Bloemen, E., and de Heer, F.J. (1978) Experimental determination of the electronic transition moment for the NO($A\ ^2\Sigma^+ - X\ ^2\Pi$) system. Lifetimes of the NO($A\ ^2\Sigma^+$, v'=0, 1, 2) levels, Chemical Physics 32:239.

33. Fontijn, A., Meyer, C.B., and Schiff, H.I. (1964) Absolute quantum yield measurements of the NO - O reaction and its use as a standard for chemiluminescent reactions, J. Chem. Phys. 40:64.

34. Vanpee, M., Hill, K.D., and Kineyko, W.R. (1971) Absolute rate constant measurements for the radiative combination of atomic oxygen with nitric oxide, AIAA Journal 9:135.

35. Golde, M.F., Roche, A.E., and Kaufman, F. (1973) Absolute rate constant for the O + NO chemiluminescence in the near infrared, J. Chem. Phys. 59:3953.

36. Golomb, D., and Brown, J.H. (1976) The temperature dependence of the NO - O chemiluminous recombination. The RMC mechanism, J. Chem. Phys. 63:5246.

37. Woolsey, G.A., Lee, P.H., and Slafer, W.D. (1977) Measurement of the rate constant for NO - O chemiluminescence using a calibrated piston source of light, J. Chem. Phys. 67:1220.

38. Sutoh, M., Morioka, Y., and Nakamura, M. (1980) Absolute rate constant for the chemiluminescent reaction of atomic oxygen with nitric oxide, J. Chem. Phys. 72:20.

39. Pravilov, A.M., and Smirnova, L.G. (1978) Spectral distribution of the chemiluminescence rate constant in the O + CO(+M) and O + NO(+He) reactions, Kinet. and Catal. 19:202.

40. Shemansky, D.E. (1969) N_2 Vegard-Kaplan system in absorption, J. Chem. Phys. 51:689.

41. Husain, D., and Slater, N.K.H. (1980) Kinetic study of ground state atomic nitrogen, N($2\ ^4S_{3/2}$) by time-resolved atomic resonance fluorescence, JCS Faraday II 76:606.

42. Lee, J.H., Michael, J.V., Payne, W.A., and Stief, L.J. (1978) Absolute rate of the reaction of N(^4S) with NO from 196-400 K with DF-RF and FP-RF techniques, J. Chem. Phys. 69:3069.

43. Clyne, M.A.A., and McDermid, I.S. (1975) Mass spectrometric determinations of the rates of elementary reactions of NO and NO_2 with ground state N ^4S atoms, JCS Faraday I 71:2189.

44. Slanger, T.G. (1978) Generation of O_2 ($C\ ^1\Sigma_u^-$, $C\ ^3\Delta_u$, $A\ ^3\Sigma_u^+$) from oxygen atom recombination, J. Chem. Phys. 69:4779.

45. Piper, L.G. (1978) Unpublished results.

46. Baulch, D.L., Drysdale, D.D., Horne, D.G., and Lloyd, A.C. (1973) Evaluated Kinetic Data for High Temperature Reactions. II. Homogeneous Gas Phase Reactions of the H_2 - N_2 - O_2 System. Butterworths, London.

47. Levron, D., and Phelps, A.V. (1978) Quenching of N_2($A\ ^3\Sigma_u^+$, v=0, 1) by N_2, Ar, and H_2, J. Chem. Phys. 69:2260.

48. Roy, C.R., Dreyer, J.W., and Perner, D. (1975) Rate constants for the quenching of $N_2(A\ ^3\Sigma_u^+; V_A = 1\text{-}6,8)$ by rare gases, J. Chem. Phys. 63:2131.

49. Clough, P.N., and Thrush, B.A. (1967) Mechanism of the chemiluminescent reaction between nitric oxide and ozone, Trans. Faraday Soc. 63:915.

50. Arnold, I., and Comes, F.J. (1979) Temperature dependence of the reactions $O(^3P) + O_3 \rightarrow 2O_2$ and $O(^3P) + O_2 + M \rightarrow O_3 + M$, Chem. Phys. 42:231.

51. Becker, K.H., Groth, W., and Schurath, U. (1972) Reactions of $O_2(a\ ^1\Delta)$ with ozone, Chem. Phys. Lett. 14:489.

52. McCrumb, J.L., and Kaufman, F. (1972) Kinetics of the $O + O_3$ reactions, J. Chem. Phys. 57:1270.

53. Baulch, D.L., Drysdale, D.D., Duxbury, J., and Grant, S.J. (1976) Evaluated kinetic data for high temperature reactions, III. Homogeneous gas phase reactions of the O_2 - O_3 system, The $CO\text{-}O_2\text{-}H_2$ System, and of Sulfur-containing Species, London, Butterworths.

54. Torr, D.G., and Sharp, W.E. (1979) The concentration of atomic oxygen in the auroral lower thermosphere, Geophys. Res. Lett. 6:860.

55. Sharp, W.E., and Torr, D.G. (1979) Determination of the auroral $O(^1S)$ production sources for coordinated rocket and satellite measurements, J. Geophys. Res. 84:5345.

56. Filseth, S.V., Stuhl, F., and Welge, K.H. (1970) Collisional deactivation of $O(^1S)$, J. Chem. Phys. 52:239.

57. Atkinson, R., and Welge, K.H. (1972) Temperature dependence of $O(^1S)$ deactivation by CO_2, O_2, N_2, and Ar, J. Chem. Phys. 57:3689.

58. Slanger, T.G., Wood, B.J., and Black, G. (1972) The temperature dependence of $O(^1S)$ quenching by O_2, Chem. Phys. Lett. 17:401.

59. Zipf, E.C. (1979) The $OI(^1S)$ state: Its quenching by O_2 and formation by the dissociative recombination of vibrationally excited O_2^+ ions, Geophys. Res. Lett. 6:881.

60. Felder, W., and Young, R.A. (1972) Quenching of $O(^1S)$ by $O(^3P)$, J. Chem. Phys. 56:6028.

61. Slanger, T.G., and Black, G. (1976) $O(^1S)$ Quenching by $O(^3P)$, J. Chem. Phys. 64:3763.

62. Piper, L.G. (1980) Unpublished results.

63. Hirschfelder, J.O., Curtiss, C.F., and Bird, R.B. (1964) Molecular Theory of Gases and Liquids, New York: John Wiley & Sons, Inc. corrected ed., p. 579.

64. Morgan, J.E., and Schiff, H.I. (1964) Diffusion coefficients of O and N atoms in inert gases, Can. J. Chem. 42:2300.

65. Nicolaides, C., Sinanoglu, O., and Westhous, R. (1971) Theory of atomic structure including electron correlation IV. Method for forbidden transition probabilities with results for [OI], [OII], [NI], [NII], and [CI], Phys. Rev. A 4:1400.

66. Slanger, T.G. (1980) Private communication to L.G. Piper.

67. Ogryzlo, E.A. (1980) Private communication to L.G. Piper.

68. Young, R.A., and St. John, G.A. (1968) Experiments on $N_2(A\ ^3\Sigma_u^+)$. II. Excitation of NO, J. Chem. Phys. 48:898,2572.

69. Mandel, A., and Ewing, J.J. (1977) Quenching of $N_2(A\ ^3\Sigma_u^+)$ by I_2, J. Chem. Phys. 67:3490.

70. Hill, R.M., Gutcheck, R.A., Huestis, D.L., Mukherjee, D., and Lorents, D.C. (1974) Studies of E-beam Pumped Molecular Lasers, SRI Report No. MP74-39 under ARPA Contract No. N00014-72-C-0478.

71. Piper, L.G. (1972) Kansas State University. The results are given in Ref. 11.

Contents

4. FACELIF Experiments

1. INTRODUCTION

Over the last several years, new techniques have evolved to investigate state-to-state reaction dynamics. This has been made possible by the advent of the laser as a general purpose laboratory tool. The result has been a virtual explosion of information yielding details of energy flow in chemical reactions. Realizing the potential usefulness of selecting reacting species' excitation parameters and product diagnostics by judicious use of lasers, we have designed and built a flow reactor called FACELIF (Flowing Atmospheric Chemistry Experiment by Laser-Induced Fluorescence). The experiment is designed to perform state-selective reaction dynamics in a flow tube similar to the FAKIR apparatus described in Chapter 3. The difference is in the generation of species and the product detection scheme. Laser induced fluorescence schemes have routinely been used to detect product densities around $10^9/cm^3$. This approach will be applied in this apparatus, and is discussed in detail below. The production schemes, for example, laser photolysis of O_2 to form O-atoms and stimulated emission pumping to form excited vibrational levels of NO are also described.

2. O_2 PHOTOLYSIS

To guide initial design concepts, several atomic oxygen reactions which are fundamental to understanding processes in auroras were considered:

$$N_2(A) + O(^3P) \rightarrow NO + N \quad (1)$$

$$N(^2D) + O(^3P) \rightarrow N(^4S) + O \quad (2)$$

$$NO(v) + O \rightarrow NO(v' < v) + O \quad . \quad (3)$$

The photolysis of O_2 at 157 nm using a Lumonics Excimer Laser (TE 861) is evaluated here as the atomic-oxygen source. The photolytic source of atomic oxygen is cleaner than conventional discharge sources, being free of most impurities produced in oxygen discharges including NO, H, and $O_2(a\ ^1\Delta)$. This feature is particularly important in product-formation studies such as those envisioned in Reactions (1)-(3).

The desire to produce oxygen atoms photolytically for studies on Reactions (1)-(3) imposes several constraints upon the apparatus design. Conventional techniques produce number densities on the order of 10^9 particles/cm^3 for the odd-nitrogen species in Reactions (1)-(3). This means that atomic oxygen must be the major constituent in the flow reactor if reactions are to occur at measurable rates. The magnitude of the photolytically produced atomic-oxygen number densities limits the size of the rate constant that can be measured. In the present case, potential reactions must have rate constants faster than 10^{-11} cm^3/(*molecule sec*) (see the discussion in this section).

Photolytic production of atomic oxygen should result in large fractional dissociations of the molecular oxygen to avoid major competition between Reactions (1)-(3) and the corresponding reactions of the odd nitrogen species with molecular oxygen. This limitation implies the ratio $k_O[O]/k_{O_2}[O_2] \gtrsim 1$ where the k's represent the rate constants of the odd nitrogen species with the subscripted oxygen species. Defining the fractional molecular oxygen dissociation as $\alpha = ([O_2]_o - [O_2])/[O_2]_o$, where the subscript o represents the O_2 number density prior to photolytic dissociation, we find minimum α-values of 0.05,[1,2] 0.60,[3] and 0.01[4,5] for Reactions (1)-(3) respectively.

A final constraint on the design is that the method chosen for photolysis of molecular oxygen must produce spatially uniform number densities of atomic

---

Because of the large number of references cited above, they will not be listed here. See References, page 105.

oxygen in the flow reactor. Non-uniform axial or radial number-density gradients greatly complicate the data analysis because diffusion becomes the major kinetic process of the atomic oxygen and reaction-rate processes vary spatially around the reactor.

The photolytic production of oxygen atoms for use in a flow reactor can be implemented in two ways. Conceptually, the simplest technique is just to shine the laser across the flow tube some distance upstream of the detector. Multiple passes of the laser beam back and forth across the flow tube can enhance atomic-oxygen production. The problem with this approach is that uniform irradiation of large volumes of the flow tube precludes significant fractional dissociation. The available photolysis laser will dissociate about 1 percent of the molecular oxygen in a 2-cm diameter tube (see below). The FACELIF flow reactor is configured to be 5 cm in diameter (to cut down on diffusive losses and to enhance fluorescence signals with large viewing geometries) so that the maximum fractional dissociation will be 0.0008 (see below). Reflectivity is poor in the vacuum ultraviolet so that multiple reflections will not enhance this value greatly.

An alternative technique which will give uniform atomic oxygen number densities and fractional O_2 dissociations up to 10 percent is to photolyze the molecular oxygen in a relatively long, narrow side arm from which the oxygen atoms flow into the reactor. This is the approach that we have taken for these experiments.

Although the photolysis laser is a pulsed laser, the oxygen atoms can be injected into the flow reactor continuously if the residence time in the side arm equals the time between laser pulses. We call this quasi-cw operation. Alternatively, if the residence time in the photolysis side arm is less than the time between laser pulses, the atomic oxygen number density in the reactor will be modulated. Axial diffusion fairly strongly limits the maximum O-atom number densities from modulated operation, so that little is gained by modulating the atomic oxygen. In our design calculations, we have assumed quasi-cw operation. Later we will discuss the constraints axial diffusion places upon modulated operation.

3. QUASI-CW PHOTOLYTIC PRODUCTION OF OXYGEN ATOMS

The apparatus designed is shown schematically in Figure 1. Light at 157 nm from the photolysis laser is focused by a spherical mirror through a narrow side arm containing molecular oxygen with argon or helium buffer gas. The laser-handling optics must be contained in a vacuum to prevent atmospheric absorption of the laser radiation. The photolysis mixture (O, O_2, Ar, or He) is mixed with the other reactant in the flow tube upstream of the detector. Air-afterglow intensity measurements, using a photomultiplier/interference filter combination,

determine the atomic-oxygen number density as a function of added nitric oxide number density. NO enters the flow tube through a second injector downstream of the atomic-oxygen injector.

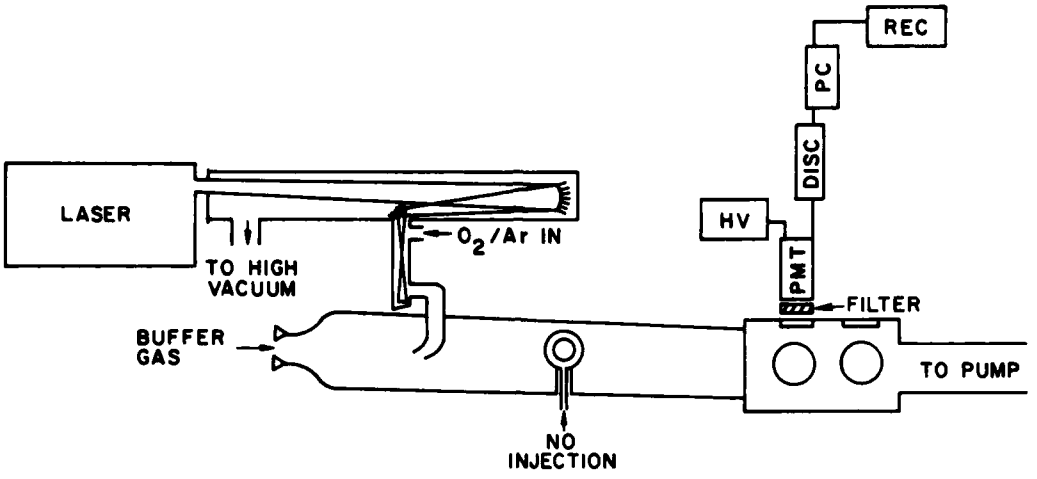

Figure 1. Flow Apparatus for Making O Atoms With a Laser

The key issues in the design considerations will be the uniformity of O-atom number densities produced by this technique, the maximum possible O-atom number densities and how they affect kinetic measurements, and how to design the laser optics to minimize transmission losses and to achieve focusing of the laser beam which will adequately fill the photolysis side arm. The major part of this section addresses these issues.

One of the important aspects of producing uniform O-atom number densities is to have uniform absorption of the laser beam in the photolysis side arm. This means that absorptions will be in the thin-target limit:

$$\frac{I_o - I}{I_o} = [O_2]'_o \, \sigma \, l' \qquad (4)$$

where I and I_o are the transmitted and initial laser-beam intensities (in units of photons per laser pulse), σ is the photo-absorption cross section of molecular

oxygen at 157 nm (6.6×10^{-18} cm^2),[6] $[O_2]'_o$ is the number density of molecular oxygen in the side arm, and ℓ' the length of the side arm. Throughout this report we shall use primes to denote quantities in the photolysis side arm, while unprimed symbols will refer to the main flow reactor. If the fractional absorption is less than 0.1, O-atom production can be considered to be uniform throughout the photolysis side arm. This leads to the constraint

$$[O_2]'_o \ell' \lesssim 1.5 \times 10^{16} \text{ molecules/cm}^2 \quad . \tag{5}$$

Atomic-oxygen number densities will be

$$[O]' = 2 \frac{I_o - I}{\pi a^2 \ell'} = \frac{2[O_2]'_o \sigma I_o I^*}{\pi a^2} \tag{6}$$

where a is the side-arm radius and I^* is the fraction of the laser-beam intensity actually delivered to the photolysis side arm compared to the laser intensity given in the manufacturer's specifications.[7] The fractional dissociation then is given by

$$\alpha = \frac{[O_2]'_o - [O_2]'}{[O_2]'_o} = \frac{[O]'}{2[O_2]'_o} = \frac{\sigma I_o I^*}{\pi a^2} \quad . \tag{7}$$

For a laser intensity of 12 mJ or 9.5×10^{15} photons/pulse we have

$$\alpha = \frac{0.02 I^*}{a^2} \tag{8}$$

or

$$a = \left(\frac{0.02 I^*}{\alpha}\right)^{1/2} \quad . \tag{9}$$

Thus the fractional dissociation that can be achieved is strongly dependent on the radius of the photolysis side arm or alternatively, the specification of a given fractional dissociation fixes the radius of the photolysis side arm. Figure 2 shows

6. Watanabe, D., Inn, E. C. Y., and Zelikoff, M. (1953) Absorption Coefficients of Oxygen in the Vacuum Ultraviolet, J. Chem. Phys. 21:1026.

7. McKee, T., Lumonics, Inc., Kanata, Ontario, Canada (1980) Private communication.

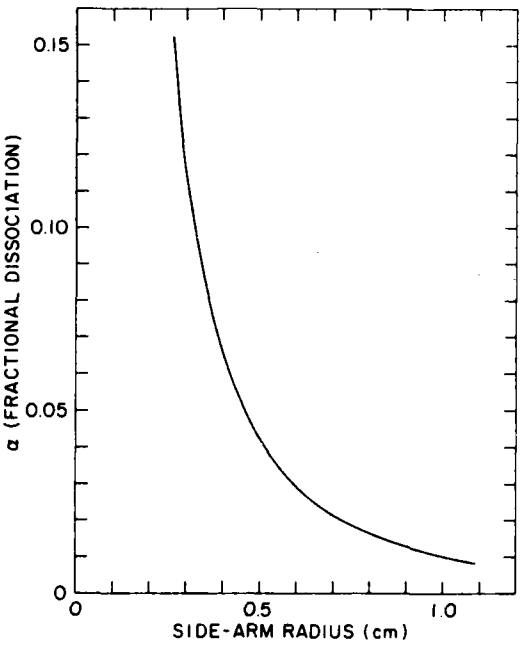

Figure 2. Variation in Fractional O_2 Dissociation With Side-Arm Radius

the relationship between fractional dissociation and photolysis-side-arm radius for I* = 0.5. A 3 mm radius will result in 10 percent dissociation whereas only 1 percent dissociation can occur in a tube with a 10 mm radius.

Negligible surface recombination of the atomic oxygen as it flows from the photolysis side arm into the flow reactor will help to ensure uniform atomic-oxygen number densities in the reactor. Surface recombination of O atoms is a first-order process[8] and the log of the ratio of atomic-oxygen number densities at the entrance and exit of the photolysis tube respectively is given by[8]

$$\ell n \frac{[O]'_o}{[O]'} = k'_w \ell'/\bar{v}' \qquad (10)$$

where $\bar{v}'$ is the gas flow velocity in the side arm and k'_w is the first-order wall-loss rate constant. The latter is given by[8]

$$k'_w = \frac{\gamma \bar{c}}{2a}$$

8. Kaufman, F. (1961) Reactions of Oxygen Atoms, Progress in Reaction Kinetics-I, G. Porter, ed., Pergamon Press Inc., New York.

where $\bar{c}$ is the mean thermal velocity of the oxygen atoms and γ is the fraction of wall collisions that result in a recombination event. The quantity γ is about 10^{-4} and we shall choose to represent it in the rest of the report as $\gamma = \gamma^* \times 10^{-4}$ where γ^* is of the order unity.[8] Thus the wall loss expression is

$$\ell n \frac{[O]'_o}{[O]'} = \frac{3.1\,\gamma^*}{a} \frac{\ell'}{\bar{v}'} \quad . \tag{11}$$

We may assume wall losses can be neglected if $[O]'_o/[O]' \lesssim 1.1$. From this constraint, Eq. (9) above, and noting that for quasi-cw operation $\ell'/\bar{v}' = 1/\text{prr}$, where prr is the pulse-repetition rate of the laser, we get

$$\ell n \frac{[O]'_o}{[O]'} = \frac{21.9\,\alpha^{1/2}\,\gamma^*}{I^{*1/2}\,\text{prr}} \tag{12}$$

or

$$\text{prr} = \frac{21.9\,\alpha^{1/2}\,\gamma^*}{I^{*1/2}\,\ell n\,\{[O]'_o/[O]'\}} \quad . \tag{13}$$

This shows a conflict between small surface recombination and large fractional dissociation. For a given fractional dissociation the pulse repetition rate must be made fairly large to minimize surface recombination. Figure 3 shows the relationship between pulse repetition rate and fractional dissociation for $I^* = 0.5$, $\gamma^* = 1.0$, and $[O]'_o/[O]' = 1.1$ (that is, only 10 percent surface recombination). The pulse-repetition-rate requirements are of course specific to quasi-cw operation. Because the maximum practical pulse-repetition rate of the available laser is about 100 Hz, the dissociation will not exceed 9-1/2 percent for this mode of operation. The relatively large pulse-repetition rates required even for modest fractional dissociations (for example, 50 Hz for 2-1/2 percent dissociation) demand a flowing gas feed on the laser to maintain constant average power and thereby constant atom flows.

The maximum possible atomic-oxygen flow rate is just the number of atoms produced in a laser pulse times the pulse repetition rate:

$$f_O = 2(I_o - I)\text{prr} = 2\,[O_2]'_o\,\sigma\,I_o\,\ell'\,I^*\,\text{prr} \quad . \tag{14}$$

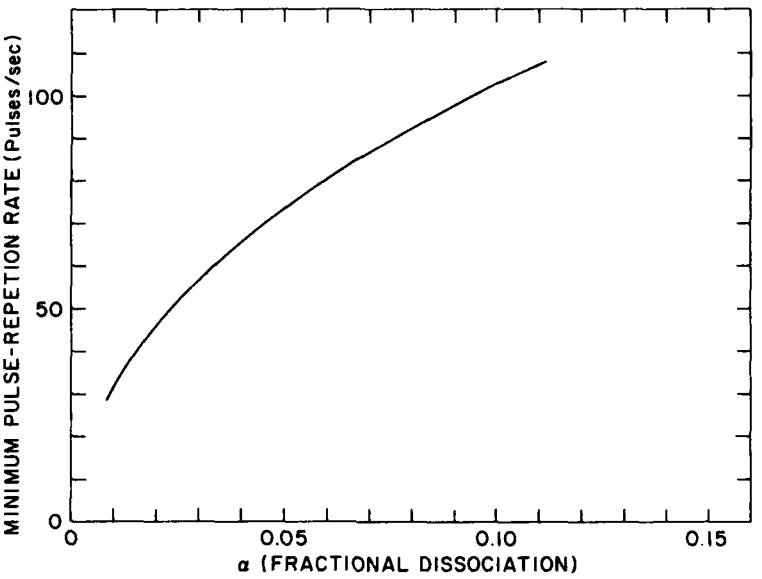

Figure 3. Relation Between Minimum Photolysis-Laser Pulse-Repetition Rate and Fractional Dissociation

Given constraint (5) above we obtain

$$f_O(\mu\text{mol/sec}) \lesssim 3.1 \times 10^{-3}\, I^*\, prr \quad . \tag{15}$$

Figure 4 shows the relationship between atomic oxygen flow and pulse repetition rate. Maximum flows are on the order of 0.1 μmol/sec.

The length of the photolysis side arm is given by

$$\ell' = \frac{\bar{v}'}{prr} \quad . \tag{16}$$

Noting that $\bar{v}' = f'RT/p'\pi a^2$ and using Eq. (9) for a gives

$$\ell' = \frac{f' RT \times 10^{-6}\, \alpha}{p'\, \pi\, (0.02\, I^*)\, prr} \quad . \tag{17}$$

We can express p' in terms of the main flow reactor pressure, p, by using the Poiseuille equation:[9]

9. Dushman, S. (1961) Scientific Foundations of Vacuum Technique, J. M. Lafferty, ed., John Wiley & Sons, Inc., New York, p. 82.

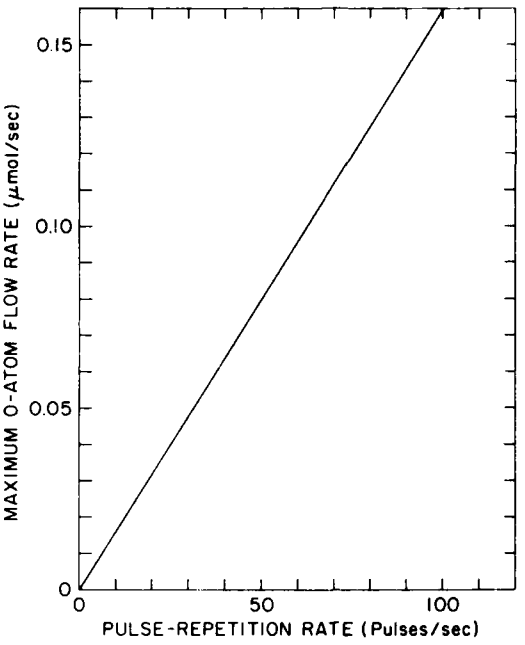

Figure 4. Variation in Maximum Atomic Oxygen Flow Rate With Photolysis-Laser Pulse-Repetition Rate

$$f'(\mu mol/sec) = \frac{13.99\, a^4}{\eta\, \ell'} \Delta p\, (2p + \Delta p) \tag{18}$$

where Δp is the pressure drop along the side arm, η is the buffer gas viscosity in Poise, and pressures are in Torr. The pressure in the side arm then is given by $p + \Delta p$. If we expand this equation and solve for Δp using the quadratic formula we obtain

$$\Delta p = -p \pm \left(p^2 + \frac{f'\, \ell'}{\zeta\, a^4} \right)^{1/2} \tag{19}$$

where

$$\zeta = \frac{13.99}{\eta} \quad .$$

We then have for p'

$$p' = p\left\{1 + \frac{f'\ell'}{\zeta a^4 p^2}\right\}^{1/2} \approx p + \frac{f'\ell'}{2\zeta a^4 p} \quad . \tag{20}$$

Inserting this expression for p' into Eq. (17) and multiplying through by the denominator gives a quadratic equation in ℓ' which can be solved to give

$$\ell' = \frac{28.26\, p^2 I^{*2}}{f'\alpha^2}\left\{\left(1 + \frac{20.93\, f'^2\, \alpha^3}{p^3\, prr\, I^{*3}}\right)^{1/2} - 1\right\} \quad . \tag{21}$$

Figure 5 shows the relationship between side-arm length and the flow rate of buffer gas through the side arm for a variety of conditions of pulse repetition rate, fractional dissociation and main flow-tube pressure. The calculations all assumed the side-arm buffer gas to be helium at room temperature ($\eta_{He} = 1.98 \times 10^{-4}$ Poise) and I* = 0.5. For typical side-arm flow rates on the order of 100-200 μmol/sec the side-arm length will be roughly 20 cm.

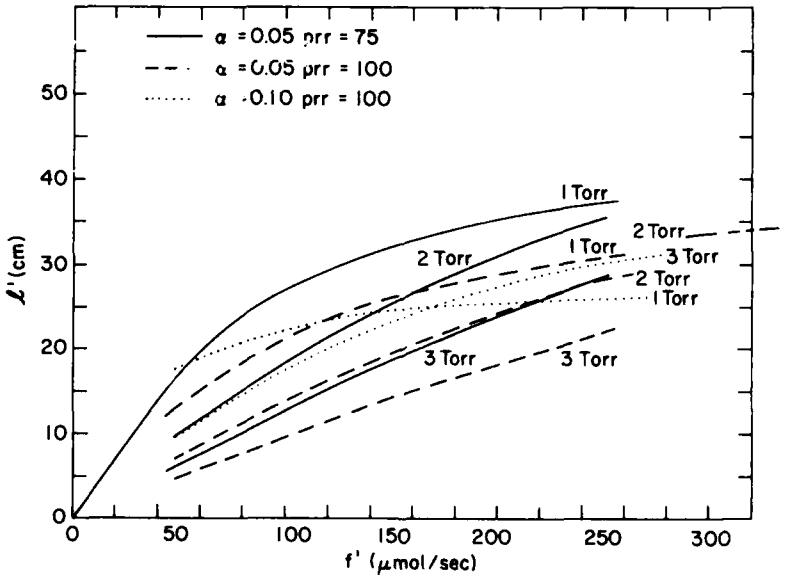

Figure 5. The Relationship Between Side-Arm Length and Gas Flow Rate Through the Side-Arm

Figure 6 describes a simplified geometry for laser focusing. The photolysis-laser beam must be focused in such a way that its effective diameter is less than 2a throughout the length of the photolysis side arm ℓ'. The spot size of the laser beam half-way along the photolysis side arm is

$$\frac{2a}{\sqrt{2}} = L\,\theta_{full} \tag{22}$$

from which we obtain

$$L = \frac{2a}{\sqrt{2}\,\theta_{full}} \quad . \tag{23}$$

The full-angle divergence of the laser is θ_{full} and the focal length of the focusing optics is L. From geometric optics we know that

$$L/D = \ell'/4a \quad , \tag{24}$$

where D is the diameter of the laser beam at the focusing optic. Using Eq. (23) above for L we obtain

$$\ell' = \frac{4\sqrt{2}\,a}{\theta_{full}\,D} \quad . \tag{25}$$

Figure 7 shows the relationship between ℓ' and a for a laser-beam diameter of 2 cm and a full-angle divergence of 6 mrad. For side-arm radii greater than 2 mm, the side-arm length can be longer than 20 cm. Thus laser focusing does not severely constrain the range of likely side-arm lengths or diameters.

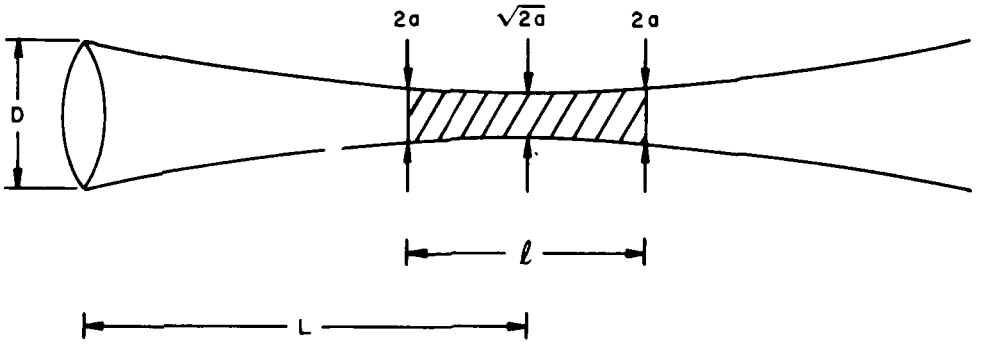

Figure 6. Geometry of Laser Focusing

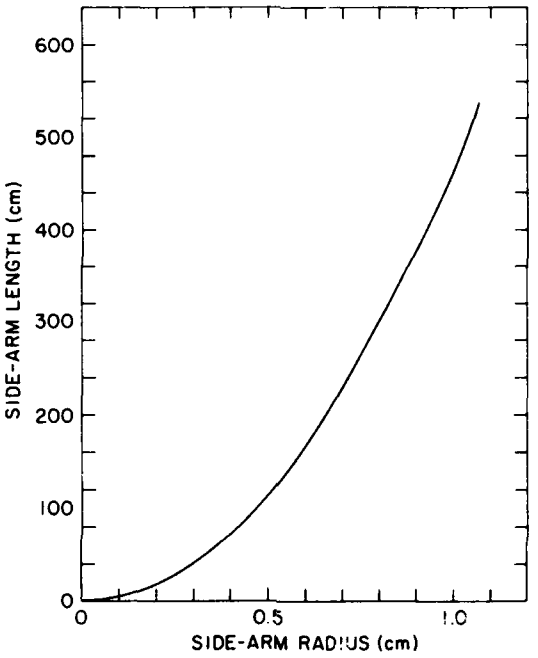

Figure 7. The Maximum Photolysis Side-Arm Length as a Function of Side-Arm Radius

The preceding discussion has shown that it is possible to inject modest flows of atomic oxygen into a flow reactor continuously using a laser-photolysis technique to produce atomic oxygen. We must still discuss the feasibility of making reaction-rate measurements in a flow reactor using these photolytically produced oxygen atoms.

The electronically or vibrationally excited minor species in Reactions (1)-(3) are deactivated with near unit probability in wall collisions. Thus diffusive losses will compete with reactive losses. We shall discuss loss processes in terms of characteristic inverse decay lengths, that is, the number of e-folds of decay per centimeter that the species undergoes as it flows down the reactor. The inverse decay lengths resulting from reaction and diffusion then are denoted δ_{rxn} and δ_D respectively. Because the minor-species number density is on the order of 10^9 molecules/cm^3 while that of the atomic oxygen is 10^{11} atoms/cm^3 or greater, pseudo first-order kinetics will obtain;[10] thus

10. See Chapter 3, Section 4 of this report.

$$\delta_{rxn} = \frac{1}{z} \ln \frac{[X]_o}{[X]} = \frac{k_o[O]}{\bar{v}} \quad , \tag{26}$$

where z is the reaction distance down the flow tube. The number density of atomic oxygen in the flow reactor is

$$[O] = \frac{f_O}{f_{tot}} p \frac{N_o}{RT} \tag{27}$$

where f_{tot} is the total gas flow rate in the reactor and N_o is Avogadro's number. Using this result in Eq. (26) and making the substitution $\bar{v} = S/\pi r^2$ where the pumping speed, S, is fRT/p and r is the flow reactor radius gives

$$\delta_{rxn} = \frac{1.49 \times 10^{13} k_O f_O}{S^2} \tag{28}$$

for S in ℓ/sec and f_O in μmol/sec. The relationship between the maximum inverse reaction length and pumping speed is shown in Figure 8 for several different rate constants. The inverse-decay length is in the useful range around 0.1 e-fold/cm only when the rate constant is larger than 10^{-11} cm^3/(molecule sec).

The characteristic inverse flow distance for diffusive losses is given by[10]

$$\delta_D = \frac{1}{z} \ln \frac{X_o}{X} = \frac{1}{\bar{v}} \frac{D_o}{\Lambda^2 p} \tag{29}$$

where D_o is the diffusion coefficient of the species of interest (in units of cm^2/sec at 1 Torr) and Λ is the characteristic diffusion length, which for an infinite cylinder is (2.405/r). Using the diffusion coefficient for $N_2(A)$ in argon[11] and the equation for the bulk flow velocity gives

$$\delta_D = \frac{84}{f_{tot}} \tag{30}$$

for f_{tot} in μmol/sec. Diffusive loss is thus minimized by operating with a large bulk flow rate. A practical upper limit for total flow rate in a standard laboratory flow reactor is 5000 μmol/sec which results in a characteristic decay distance of 60 cm per e-fold.

11. Levron, D., and Phelps, A.V. (1978) Quenching of $N_2(A\ ^3\Sigma_u^+, v=0, 1)$ by N_2, Ar and H_2, J. Chem. Phys. 69:2260.

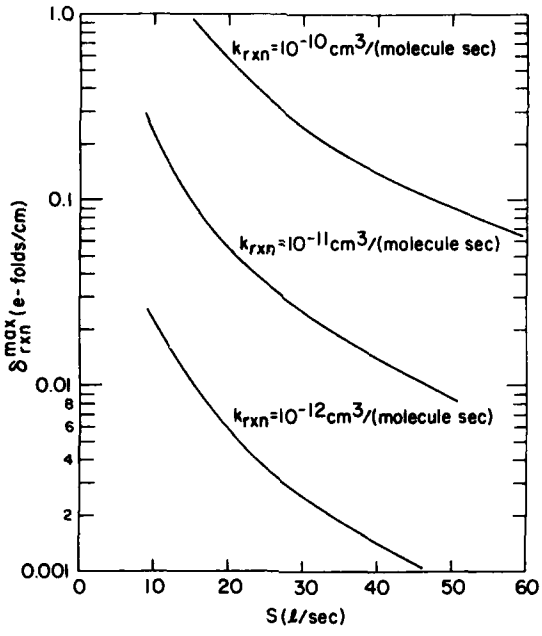

Figure 8. Inverse Reaction Distance as a Function of Reactor Pumping Speed

The ratio of the inverse-decay distances for losses due to reaction and diffusion respectively is

$$\frac{\delta_{rxn}}{\delta_D} = \frac{1.78 \times 10^{11}\, k_O f_O f_{tot}}{S^2} \quad . \tag{31}$$

This ratio is plotted in Figure 9 as a function of flow-reactor pumping speed for an assumed rate constant of 10^{-11} cm^3/(molecule sec) and for three different choices of total flow rate. This ratio is greater than unity only for total flow rates greater than about 2000 μmol/sec.

Figure 10 shows how the flow reactor pressure varies with pumping speed for three different total flow rates. The flow reactor pressures should be on the order of 1 Torr. Much higher pressures generally result in poor reagent mixing during the observation time, while low pressures result in excessive diffusional losses of the excited minor species.

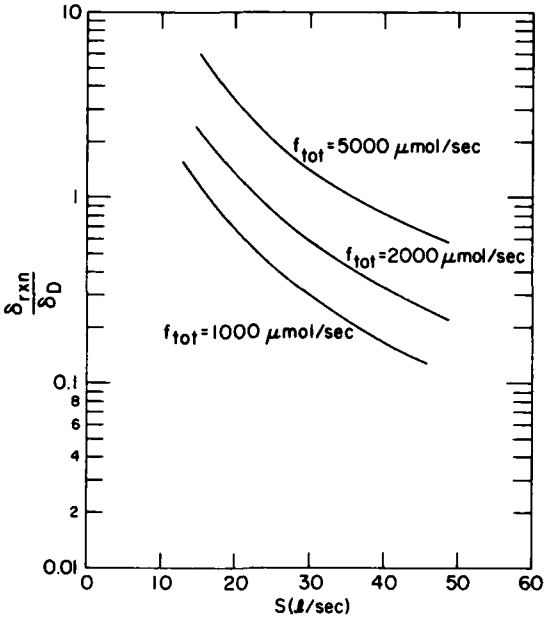

Figure 9. Ratio of Inverse Decay Distance Due to Reactive Loss to That Due to Diffusive Loss as a Function of Reactor Pumping Speed for a Reaction Rate Constant of 10^{-11} cm^3/molecule sec

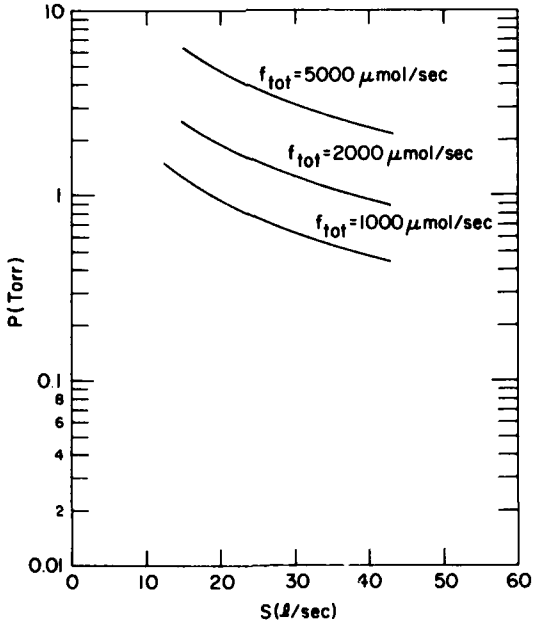

Figure 10. Flow-Tube Pressure as a Function of Reactor Pumping Speed

The curves in Figures 8-10 map the operating region for proposed flow reactor studies. The total flow rate will be around 2500 μmol/sec, the total pressure around 2 Torr, and typical decay distances about 5-10 cm per e-fold. Table 1 lists the typical operating conditions resulting from the constraints derived in this section.

Table 1. Typical Operating Conditions of FACELIF

Side Arm	Main Flow Tube
$a \approx 0.45$ cm	$r = 2.5$
$\alpha = 0.05$	$f_{tot} \approx 2500\,\mu$mol/sec
prr = 75/sec	$P_{tot} = 2$ Torr
$f_o \leq 0.12\,\mu$mol/sec	$S = 23\,\ell$/sec
$\ell' \approx 15$ cm	$\delta_{rxn} \leq 0.04$ (for $k = 10^{-11}$)
$f' \approx 100\,\mu$mol/sec	$\frac{\delta_{rxn}}{\delta_{Diff}} \approx 1.1$

4. MODULATED PHOTOLYTIC PRODUCTION OF OXYGEN ATOMS

When the side-arm residence time is short compared to the time between laser pulses, the atomic-oxygen number density in the flow reactor will be modulated. In effect, a train of plugs with relatively uniform atomic-oxygen number densities followed by plugs devoid of oxygen atoms will flow down the reactor. The constraints on uniform absorption [Eq. (5)] and heterogeneous recombination [Eq. (11)] ensure a uniform number density of oxygen atoms in the plug. In addition, axial diffusion out of the plug must be minimized to maintain uniform atomic-oxygen number densities and thereby minimize analytical complications.

Axial diffusion in the flow reactor is minimized if the number density of atomic oxygen in the center of the plug remains constant. The atomic-oxygen number density in the center of the plug changes with time as given in Eq. (32):[12]

$$\frac{[O]_c}{[O]_o} = \text{erf}\left\{\frac{z_o}{4(Dt)^{1/2}}\right\} \tag{32}$$

12. Crank, J. (1957) The Mathematics of Diffusion, The Clarendon Press, Oxford, pp. 26-28.

where $[O]_c$ is the number density in the center of the plug, $[O]_o$ is the initial plug number density, z_o is the length of the plug in the reactor, and D is the diffusion coefficient of the oxygen atoms at the reactor pressure. The time in the flow reactor is $z_{rxn}/\bar{v}$, where z_{rxn} is the distance in the flow reactor from the atom injector to the observation point, and the diffusion coefficient of oxygen atoms in argon is $(230/p)(cm^2/sec)$.[13] Thus the number density of oxygen atoms in the center of the plug decreases by only 9 percent if

$$z_o \gtrsim 75 \left(\frac{z_{rxn}}{f}\right)^{1/2} . \tag{33}$$

We will show that this constraint limits the maximum number density in the packet.

The atomic-oxygen number density in the packet is the ratio of the number of oxygen atoms produced in the photolysis pulse to the volume of the plug

$$[O] = \frac{2[O_2]'_o \ell' \sigma I_o \Phi^*}{\pi r^2 z_o} . \tag{34}$$

Equations (5) and (33) constrain Eq. (34) so that

$$[O] \lesssim 6.4 \times 10^{11} \left(\frac{f_{tot}}{z_{rxn}}\right)^{1/2} . \tag{35}$$

Figure 11 shows how the maximum number density of atomic oxygen in the plug varies with reaction length in the flow tube for two different choices of total flow rate. The maximum atomic-oxygen number density will be about 5×10^{12} atoms/cm^3 given typical reaction distances of about 50 cm.

An equation which describes the reaction kinetics in the reactor with modulated oxygen atoms results from inclusion of Eq. (35) into Eq. (26):

$$\ell n \frac{[X]_o}{[X]} = 6.8 \times 10^{11} k_O p \frac{z_{rxn}^{1/2}}{f_{tot}} . \tag{36}$$

Figure 12 shows how much the reactive species will decay in the reactor as a function of reaction distance for two different values of total flow rate at a

13. Morgan, J.E., and Schiff, H.I. (1964) Diffusion coefficients of O and N atoms in inert gases, Can. J. Chem. 42:2300.

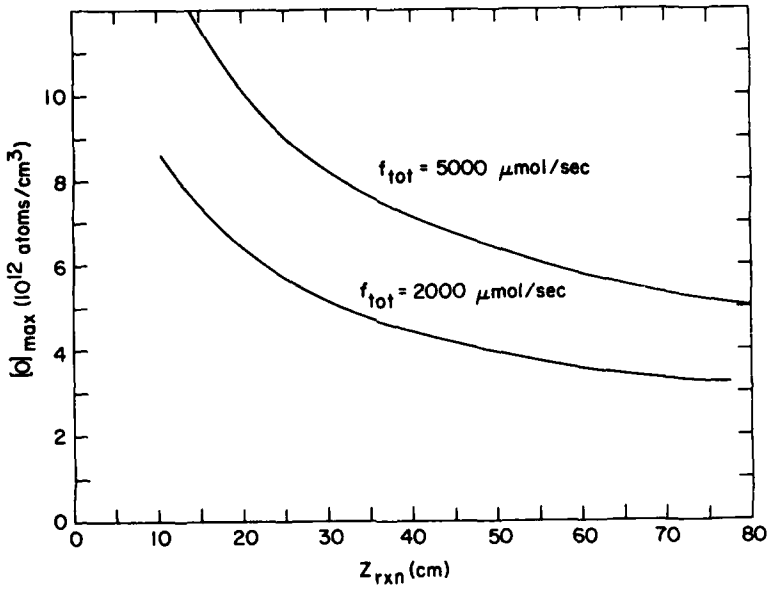

Figure 11. Maximum [O] From 157 nm Photolysis of O – Modulated Case

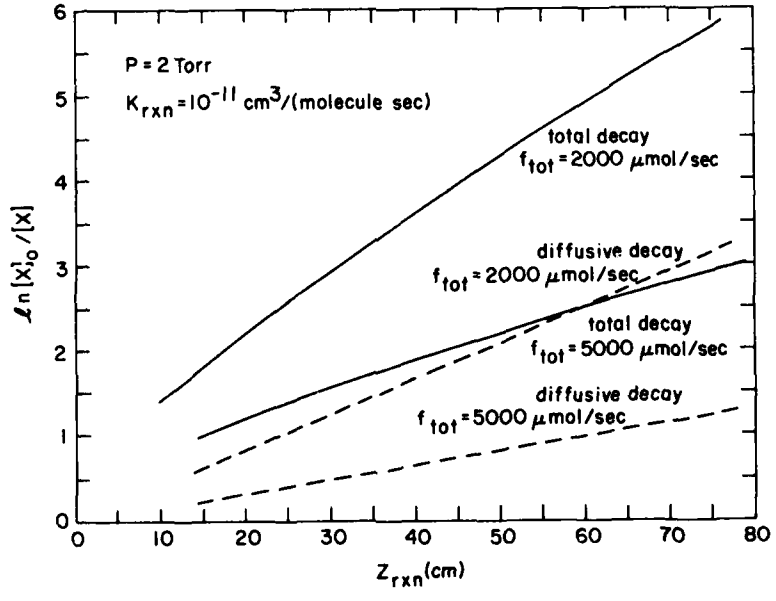

Figure 12. Maximum Decay of Species as a Function of Reaction Distance for Modulated [O]

pressure of 2 Torr and using a rate constant of 10^{-11} cm^3/(molecule sec). For a total flow rate of 2000 μmol/sec, the radicals decay by 2 orders of magnitude over a reaction distance of 75 cm; however, diffusion causes half of this decay. A 1-order-of-magnitude signal decay is a practical lower limit for accurate kinetic measurements in a flow reactor. Thus, as in the quasi-cw case, modulated operation is only suitable for measurements in systems in which the rate constant is larger than 10^{-11} cm^3/(molecule sec). However, a system with a high detection sensitivity would alleviate this limitation.

5. APPLICATION OF $N_2(A\ ^3\Sigma) + O(^3P) \rightarrow NO(v) + N(^4S)$

Nitric oxide is an important participant in atmospheric chemistry and the reaction of metastable molecular nitrogen and oxygen atoms has been suggested as a significant source of nitric oxide in the upper atmosphere.[14] It is known (from Chapter 3) that the reaction

$$N_2(A\ ^3\Sigma) + O(^3P) \rightarrow O(^1S) + N_2(X\ ^1\Sigma) \tag{37}$$

accounts for up to 75 percent of the total quenching rate of $N_2(A\ ^3\Sigma)$ by $O(^3P)$. This implies an upper limit of 5×10^{-12} cm^3/(molecule sec) for the rate constant of a chemical branch in $N_2(A\ ^3\Sigma)$ quenching. Both reactions

$$N_2(A\ ^3\Sigma) + O(^3P) \rightarrow NO(X\ ^2\Pi) + N(^4S) \qquad \Delta H = -2.9\ eV \tag{38}$$

$$N_2(A\ ^3\Sigma) + O(^3P) \rightarrow NO(X\ ^2\Pi) + N(^2S) \qquad \Delta H = -0.5\ eV \tag{39}$$

are energetically allowed. The exoergicity of Reactions (38) and (39) is sufficent to populate up to NO(v=13) and NO(v=1), respectively.

Although the non-state-specific reaction

$$N_2 + O \rightarrow NO + N \qquad \Delta H = +3.3\ eV \tag{40}$$

has been the subject of numerous kinetic studies,[15] the state-specific Reactions (38) and (39) have not. As Reaction (38) is a source of vibrationally hot NO, both the overall rate constant and nascent distribution are needed to evaluate its

14. Swider, W. (1976) Atmospheric formation of NO from $N_2(A\ ^3\Sigma)$, Geophys. Res. Letts. 3(6):335.

15. Wray, K., Feldman, E., and Lewis, P. (1970) Shock tube study of the effects of vibrational energy of N_2 on the kinetics of the $O + N_2 \rightarrow NO + N$ reaction, J. Chem. Phys. 53(11):4131.

contribution to atmospheric luminescence in the 5.4 and 2.8 μm spectral regions. The technique of laser induced fluorescence (LIF) utilizing the strong γ-band of NO ($\sigma_{peak} \sim 10^{-17}$ cm^2 molecule)[16] coupled to a conventional flowing afterglow reactor can provide such detailed kinetic information.

An upper limit on the expected concentration of NO from Reactions (38) and (39) is $0.25[N_2(A\ ^3\Sigma)]$ initial. This assumes that a) $[O(^3P)] \gg [N_2(^3\Sigma)]$ and b) quenching of $N_2(A\ ^3\Sigma)$ is essentially complete prior to the observation zone.

The usual technique for production of $N_2(A\ ^3\Sigma)$ without generating atomic nitrogen involves energy transfer from discharge produced $Ar(^3P)$ which is rapidly quenched by $N_2(X\ ^1\Sigma)$ [$k_q = 3 \times 10^{-11}$ cm^3/(molecule sec)]. The $N_2(C\ ^3\Pi_u)$ state thus formed radiatively decays via second-positive band emission to $N_2(A\ ^3\Sigma)$.[17] Concentrations of 10^9 - 10^{10} molecules/cm^3 of $N^2(A\ ^3\Sigma)$ can be produced in this manner.[18] $N_2(A\ ^3\Sigma)$ can be monitored by detection of the Vegard-Kaplan ($A\ ^3\Sigma \rightarrow X\ ^1\Sigma$) emission system, as described in the previous chapter.

Oxygen atoms can be produced in a low pressure discharge; however, long-lived excited electronic states of O_2 are produced as well.[19] Further, trace amounts of molecular nitrogen entering the flow prior to the discharge will produce NO background. An alternative method, laser photolysis of O_2 described in the previous section, assures production of O-atoms free from O_2^* and NO:

$$O_2(X\ ^3\Sigma) + 157 \text{ nm} \rightarrow O(^1D) + O(^3P)$$

$$\sigma(157 \text{ nm}) = 6 \times 10^{-18} \text{ cm}^2/\text{molecule}^{20} \quad . \tag{41}$$

The requirement that fractional dissociation of O_2, α, where

$$\alpha = (O_2)_o - (O_2)/(O_2)_o \quad ,$$

---

16. Farmer, A.J., Hasson, V., and Nicholls, R.W. (1972) Absolute oscillator strength measurements of the (v''=0, v'=1-3) bands of the ($A\ ^2\Sigma - X\ ^2\Pi$) band system of nitric oxide, J. Quant. Spectro. Radiat. Transfer 12:627.

17. Dunn, O.J., and Young, R. (1975) Quenching of $Ar(^3P_{o,2})^*$, J. Chem. Phys. 62(5):1996.

18. Meyer, J., Setser, D., and Stedman, D. (1970) Energy transfer reactions of $N_2(A\ ^3\Sigma)$ II. Quenching and emission by oxygen and nitrogen atoms, J. Phys. Chem. 74(10):2238.

19. Bader, L.W., and Ogryzlo, E.A. (1964) Reactions of $O_2(^1\Delta)$ and $O_2(^1\Sigma)$, Disc. Faraday Soc. 37:46.

20. Ogawa, S., and Ogawa, M. (1975) Absorption cross sections of $O_2(^1\Delta)$ and $O_2(^1\Sigma)$ in the region from 1087 to 1700Å, Can. J. Phys. 53:1845.

be greater than 0.01 can be fulfilled by photolyzing O_2 in a small bore sidearm (radius ~ 0.6 cm). $O(^1D)$ is quenched with unit efficiency ($\gamma = 1$) in wall collisions via

$$O(^1D) + \text{wall} \rightarrow O(^3P)\ k_w \sim c\gamma/2a \tag{42}$$

where a = 0.4 cm and c is the mean atom velocity at 298 K. This gives $k_w \sim 6 \times 10^4$/sec. Although an accurate calculation of the sidearm residence time requires the conductance of the atom injector, the residence time can be estimated to be 1 msec, as quenching by wall collisions is a first-order process

$$\ell n(O(^1D))_t/(O(^1D))_o = -k_w t \quad , \tag{43}$$

thus $O(^1D)$ is completely quenched at 1 msec.

Oxygen can also be photolyzed by ArF excimer laser emission at 193 nm. The pulse energy here is approximately 10^2 greater than at 157 nm; however, the absorption cross section is four orders of magnitude less than at 157 nm.[21]

At 10 mJ/pulse and 75 pulses/sec for the F_2 laser, the total O-atom production rate is $\sim 10^{16}$ atoms/sec. For a typical flow tube pressure of 2 Torr and total flow rate of 2500 μmole/sec, the volume flow is 2×10^4 cm^3/sec. The O-atom concentration is thus $\sim 10^{12}$ molecules/cm^3. Given a 5-cm-diameter flow tube, the linear flow velocity is $\sim 10^3$ cm/sec.

From the estimated number densities for $N_2(A\ ^3\Sigma)$ and $O(^3P)$ of 1×10^{10} and 1×10^{12} molecules/cm^3 respectively, the estimated number density of NO is 2×10^9 molecules/cm^3. The sensitivity of laser induced fluorescence can be calculated from the NO γ-band absorption cross section, laser pulse energy and NO number density. The absolute integrated absorption coefficient for the $\gamma(0,0)$ band ($k_o = 3.5 \times 10^{-16}$ cm/molecule)[21] provides an estimate of the peak absorption cross section of $\sim 10^{-17}$ cm^2/molecule. In the present experimental configuration approximately 2 cm of the laser irradiated cylinder is viewed by the PMT photocathode. The energy absorbed in the viewed volume is given by

$$E_{abs} = E_{incident}\ [\exp\ (\sigma \ell N) - 1] \quad , \tag{44}$$

where σ is the absorption cross section, ℓ is the viewed length, and N is the NO number density. Thus,

---

21. Bethke, G. (1959) Oscillator strengths in the far ultraviolet II. Oxygen Schumann-Runge bands, J. Chem. Phys. 31(3):669.

$$E_{abs} = 4 \times 10^{-8} E_{incident} \quad . \tag{45}$$

The available dye-laser system can produce a pulse of approximately 200 μJ at 226 nm.[22] This gives

$$E_{abs} = 8 \times 10^{-12} \text{ J or } 9 \times 10^{6} \text{ photons/pulse} \quad . \tag{46}$$

Multiplying by the laser repetition rate (10 Hz) and total detection efficiency (10^{-3}), a signal of approximately 10^5 photons/sec can be expected.

The total NO number in the viewed volume is 5×10^8 molecules, thus the calculated photon yield represents a fractional excitation of 0.02 and the transition is not saturated.

The previous discussion has shown that NO produced in Reactions (38) and (39) can be detected. In addition to the reactions of interest, however, there are many known reaction paths for the various species present in the flow tube. Of particular concern are those reactions which produce or deplete NO, or energy transfer reactions involving NO. The following is a list of potential interfering reactions:

$$N(^4S) + O_2(X\,^3\Sigma) \rightarrow NO(X\,^2\Pi) + O(^3P) \qquad k_{47} = 2.2 \times 10^{-11} \text{ cm}^3/\text{molecule sec}^{23} \tag{47}$$

$$NO(X\,^2\Pi) + N_2(A\,^3\Sigma) \rightarrow NO(A\,^2\Sigma) + N_2(X\,^1\Sigma) \quad k_{48} = 6 \times 10^{-11} \text{ cm}^3/\text{molecule sec}^{24} \tag{48}$$

$$NO(X\,^2\Pi) + Ar(^3P) \rightarrow NO(* \text{ or } +) + Ar \qquad k_{49} = 2 \times 10^{-10} \text{ cm}^3/\text{molecule sec}^{25} \tag{49}$$

$$NO(X\,^2\Pi) + O_2(a\,^1\Delta) \rightarrow NO(X\,^2\Pi, v=4) + O_2(^3\Sigma) \quad k_{50} = 4 \times 10^{-17} \text{ cm}^3/\text{molecule sec}^{26} \tag{50}$$

$$NO(X\,^2\Pi' v) + O_2(X\,^3\Sigma) \rightarrow NO(v-1) + O_2(v=1) \quad k_{51} = 2.4 \times 10^{-14} \text{ cm}^3/\text{molecule sec}^{27} \tag{51}$$

---

22. Quanta-Ray reference manuals; doubled R-50 dye emission + 1.06 μm YAG.

23. Whitson, M., Darnton, L., and McNeal, R. (1976) Vibrational energy distribution in the NO produced by the reaction of $N(^4S)$ with O_2, Chem. Phys. Lett. 41(3):552.

24. Dreyer, J., Perner, D., and Roy, C. (1974) Rate constants for the quenching of $N_2(A\,^3\Sigma, v_A = 0\text{-}8)$ by CO, CO_2, NH_3, NO and O_2, J. Chem. Phys. 61(8):3164.

25. Boxall, M., Chapman, C., and Wyne, R. (1975) Quenching of $Ar(^3P_1)$: Rate constants for deactivation and "Escape Factors" for trapped radiation, J. Photochem. 4:435.

26. Ogryzlo, E., and Thrush, B.A. (1973) Vibrational excitation of NO in its collisional quenching of $O_2(^1\Delta)$, Chem. Phys. Lett. 23(1):34.

27. Ogawa, T. (1976) Excitation processes of infrared atmospheric emissions, Planet Space Sci. 24:749.

AD-A138 546 ATMOSPHERIC CHEMILUMINESCENCE: COCHISE (COLD CHEMICAL INFRARED SIMULATION..(U) AIR FORCE GEOPHYSICS LAB HANSCOM AFB MA R A ARMSTRONG ET AL. 13 OCT 82 2/2

UNCLASSIFIED AFGL-TR-82-0305 F/G 4/1 NL

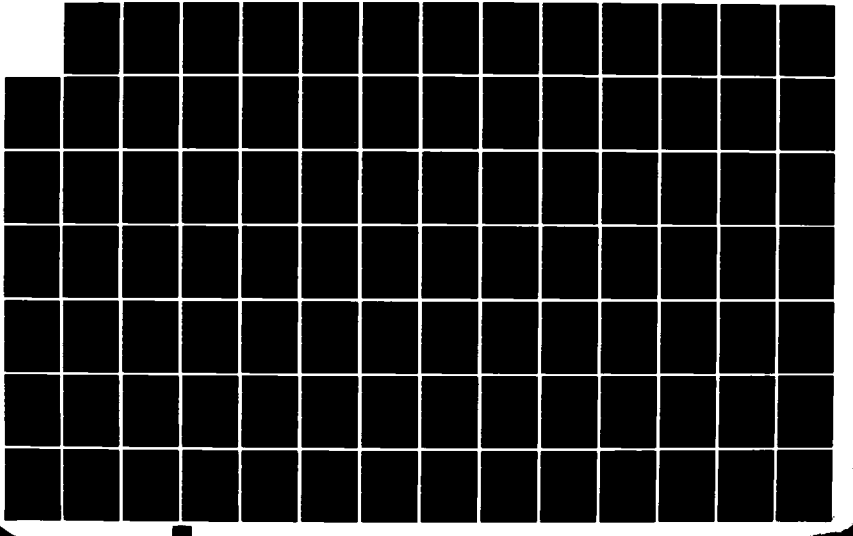

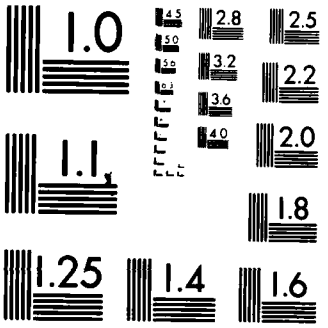

$$NO(X\,^2\Pi) + O(^3P) \rightarrow NO_2 + h\nu \qquad k_{52} = 10^{-18}\ cm^3/molecule\ sec^{28} \qquad (52)$$

$$NO(A\,^2\Sigma) + O_2(X\,^3\Sigma) \rightarrow NO(X\,^2\Pi) + O_2 \qquad k_{53} = 1.6 \times 10^{-10}\ cm^3/molecule\ sec^{29} \qquad (53)$$

$$N_2(A\,^3\Sigma) + O_2(X\,^3\Sigma) \rightarrow NO(X\,^1\Sigma) + O_2(B\,^3\Sigma) \qquad k_{54} = 5 \times 10^{-12}\ cm^3/molecule\ sec^{30} \qquad (54)$$

Some of the above rate constants are dependent on the vibrational excitation of the reactant; in such cases the value given is an average of the measured v-dependent constants.

Provided molecular nitrogen is excluded from the Ar discharge, nitrogen atoms will not be present unless formed by Reactions (38) and (39). The initial rate of Reaction (47) is therefore zero. The maximum rate at $N_2(A\,^3\Sigma) = 0.5\ N_2(A\,^3\Sigma)_{initial}$ is 5×10^8 molecules/(cm^3 sec). Based on previous estimates, the maximum rate of Reaction (38) is approximately 5×10^{10} molecules/(cm^3 sec). Reaction (48) is particularly important as it is a source of background γ-band emission and can disturb the nascent NO vibrational distribution. The estimated maximum rate of Reaction (48) is 5×10^8 molecules/(cm^3 sec).

Reaction (49) is included here to indicate the consequence of incomplete titration of $Ar(^3P)$ by N_2. As indicated, NO can quench $Ar(^3P)$ via Penning ionization or electronic excitation with nearly gas kinetic rate constant. The C → A emission of N_2 is readily detected visually, thus, determining complete titration presents no problem.

The rate of Reaction (50) is negligible and not measurable in a flowing reactor, but may be relevant to static cell experiments, as $O_2(^1\Delta)$ is a long-lived species.

Molecular oxygen is undoubtedly the most effective collision partner for vibrational relaxation of NO(v) by Reaction (51), when O_2 is present in the flow tube. O_2 number density is about 10^{14} molecules/cm^3. This implies a pseudo-first order rate constant of $2.4/sec^1$. Under the present conditions, significant relaxation of NO(v) (>10 percent) will occur beyond 30 msec from the mixing of oxygen.

Reaction (52) is the diagnostic for O-atom production. The NO_2^* formed can relax radiatively or by collisions. Except at high total pressure, Reaction (52) is too slow to deplete NO significantly.

---

23. Becker, K.H., and Groth, W. (1972) (Title not available), Proc. Int. Symp. Combustion 14.

29. Melton, L.A., and Klemperer, W. (1972) Quenching of $NO(A\,^2\Sigma)$ by $O_2(X\,^3\Sigma)$, Planet Space Sci. 20:157.

30. Julienne, P. (1976) $^3\Sigma^- - {}^3\Sigma^+$ coupling in the $O_2(B\,^3\Sigma^-)$ predissociation, J. Mol. Spectr. 63:60.

As shown in Reaction (53), NO(A $^3\Sigma$) is quenched with a gas kinetic rate constant by O_2(X $^3\Sigma$). The rate is 2×10^{13} molecules/(cm^3 sec); however, the radiative lifetime of NO(A $^3\Sigma$) is <200 nsec. During the NO(A $^3\Sigma$) lifetime only 10^{-3} of the initially excited NO molecules are quenched by O_2 under these conditions.

Reaction (54) is a potential loss mechanism for N_2(A $^3\Sigma$). The initial quenching rate is 5×10^{11} molecules/(cm^3 sec). This rate is competitive with the initial rate of Reaction (38) given above. The implication of Reaction (54) is that the presence of excessive molecular oxygen can effectively suppress Reaction (38). A large fractional dissociation (α) is therefore required.

A simple kinetic model to predict the NO yield from the reaction of N_2(A $^3\Sigma$) with O(^{3}P) can be constructed using the known or estimated rate constants for Reactions (38)-(40), (48), and (51)-(54). The additional reaction:

$$O_2(B\ ^3\Sigma) \rightarrow 2\ O(^3P) \tag{55}$$

provides a background source of O-atoms. The yield of O(^{3}P) atoms due to predissociation of O_2(B $^3\Sigma$) is dependent on vibrational quantum number, and can be estimated from measured linewidths in the Schumann-Runge bands[30] as follows:

$\Phi(v=0) \sim 0$

$\Phi(v=1) \sim 1.2$

$\Phi(v=2) \sim 0.6$.

The energy of N_2(A $^3\Sigma$, v=1) is sufficient to populate O_2(B $^3\Sigma$, v=2). The model does not include effects due to wall collisions or incomplete mixing of reagents, and plug flow is assumed.

The number densities of N_2(A $^3\Sigma$), NO(X $^2\Pi$) and NO(A $^2\Sigma$) were calculated for 20 msec following injection of Ar(^{3}P) by numerical integration of the differential rates. An integration step size of 0.01 msec was used in all the calculations.

Figures 13 and 14 illustrate the results of this calculation for various initial conditions. The point of reagent injection is treated in the calculation as a simple step function change in reagent number density. If the O_2 is initially undissociated, a steady-state NO concentration of $\sim 10^6$/cm^3 is predicted, resulting from Reactions (54), (55), and (38) or (39). The volume emissivity of NO*, due primarily to the energy-transfer step in Reaction (48), decreases exponentially from a maximum $\sim 10^5$/cm^3; this would be masked by the much more intense Vegard-Kaplan emission [curve K6 N_2(A) in Figure 13]. With $[O]_o = 10^{12}$/cm^3, the steady-state NO concentration rises to $\sim 10^8 - 10^9$/cm^3, readily detectable above

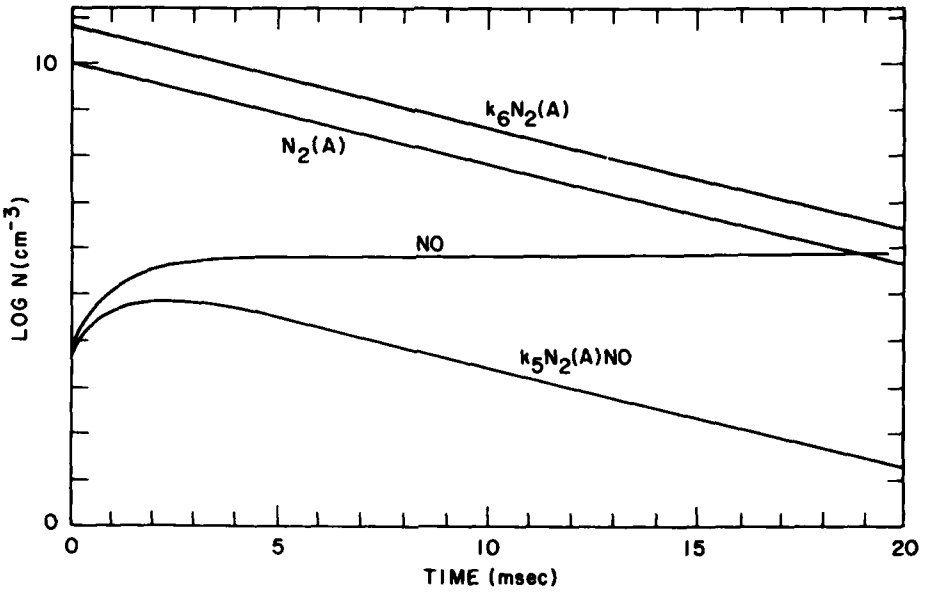

Figure 13. Number Densities for $N_2(A)$, NO(X) and NO(A) After Ar* Injection, $[O]_o = 0$

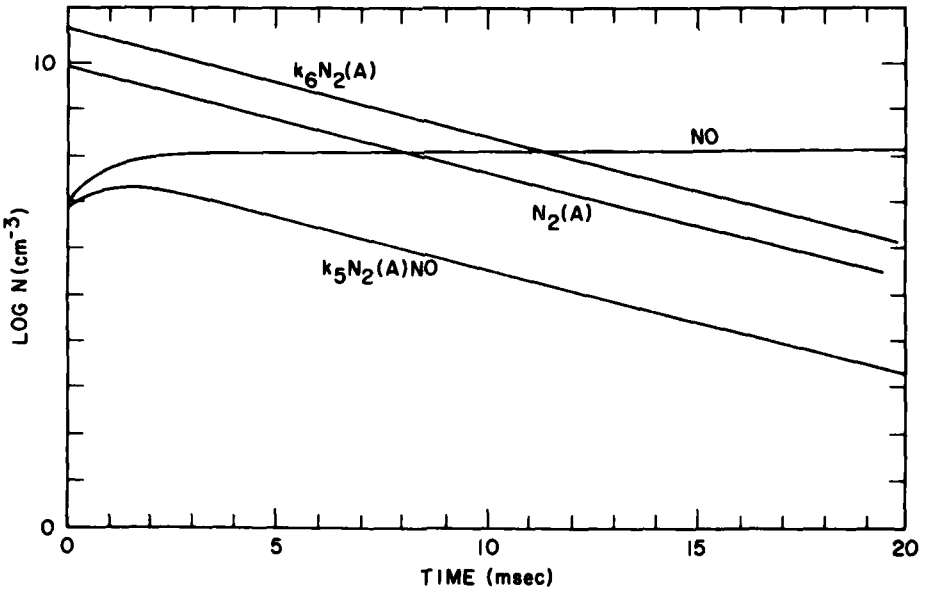

Figure 14. Number Densities for $N_2(A)$, NO(X) and NO(A) After Ar* Injection, $[O]_o = 1 \times 10^{12}$

background emission (Figure 14). The quenching of metastable N_2 by ground state O_2 limits the NO product to 10^9 molecules/cm^3 even with an initial O-atom number density of 10^{12} molecules/cm^3.

Several questions remain which must be answered experimentally before more accurate estimates of the minimum detectable rate of Reaction (38) can be made. The actual laser energy to the photolysis zone must be measured. The conductance and pressure drop in the sidearm are required to obtain the O-atom residence time and degree of recombination. The efficiency of the collection optics and photomultiplier as well as probe laser energy must be measured. It may also be possible to monitor N and O atom concentrations independently, using the 2-photon excitation method recently reported.[31]

6. RELAXATION OF SINGLE RO-VIBRATIONAL LEVELS OF NO

Currently accepted values for the vibrational relaxation rate of NO($X\ ^2\Pi, v>1$) rely on data from the decay of an initial distribution over several vibrational levels of NO. The extraction of single-level collisional relaxation requires extensive deconvolution.[4] Direct measurement of these rates is possible by initial optical preparation of a population in a selected v-state. A sensitive diagnostic technique, such as laser induced fluorescence, can be employed to probe the vibrational distribution. The feasibility of direct overtone pumping to obtain a v = 2 population and stimulated emission pumping (SEP)[32] to prepare populations in v=5 to v=10 is considered here.

6.1 Direct Overtone Pumping

The IR source selected for this study is a krypton-ion pumped F-center laser. These lasers are normally continuous-wave and provide up to 30 mW power with 1 MHz linewidth.[33] For the case well below saturation, where the excited state population, N_2, is negligible compared to the ground state population, N_1, the steady-state ratio, N_2/N_1, is given by

$$N_2/N_1 \sim \sigma I_p T \quad , \tag{56}$$

---

31. Laser Focus, (May, 1982), p. 24.

32. Kittrell, C., Abramson, E., Kinsey, J. L., McDonald, S.A., Reisner, D.E., Field, R.W., and Kayatama, D.H. (1981) Selective vibrational excitation by stimulated emission pumping, J. Chem. Phys. 75(5):2056.

33. Burleigh FCL Manual.

where σ is the absorption cross section for the selected (v, J) transition, I_p is the photon flux [photons/(cm^2 sec^1)], and T is the total relaxation rate for level 2 including radiative and collisional terms.

Using the value of 0.02 for the ratio of overtone to fundamental integrated absorption coefficients[34] and 2.5/(cm^2 atm) for the peak line intensity at 300 K, the peak line intensity for the first overtone is estimated to be 0.045/(cm^2 atm). Taking the 300 K Doppler width as the lineshape, the absorption cross section, $\sigma \sim 3 \times 10^{-19}$ cm^2, since the laser linewidth and Doppler linewidth are comparable.[35] The photon flux at 30 mW total power is 4×10^{18} photons/(cm^2 sec), assuming a laser beam cross section of 0.1 cm^2.

Collisional relaxation of NO(v=2) exceeds radiative loss at NO pressure greater than 5 mTorr. This estimate is obtained using 2500/(sec Torr) for the NO-NO quenching rate.[36] At 1 Torr NO, the loss rate T is ~400 μsec. Taking T = 100 μsec in the approximation (56), N_2/N_1 is estimated at $\sim 1 \times 10^{-4}$. At 1 Torr NO, this ratio gives an NO(v=2) number density of 10^{12} molecules/cm^3. A previous estimate of the LIF detection sensitivity showed $<10^9$ molecules/cm^3 can be detected.

Although this initial estimate indicates that overtone pumping can produce an adequate excited population, several effects such as pump transition collisional line broadening by buffer gases, NO(A $^2\Sigma^+$) fluorescence quenching by NO(X $^2\Pi$) and by O_2(X $^3\Sigma$), and reabsorption of fluorescence photons still need to be considered.

6.2 Stimulated Emission Pumping

The technique of stimulated emission pumping (SEP) has been demonstrated to be an effective method for populating selected single vibrational levels in iodine vapor[32] and small polyatomic molecules (formaldehyde, acetylene). The application of this technique to nitric oxide requires the selection of a vibronic state which can be optically prepared by a pump laser pulse and which has reasonable Franck-Condon factors for transitions to the selected vibrational levels of the ground electronic state. Examination of the Franck-Condon factors for the β-system indicates that NO(B $^2\Pi$, v=7) has $q(v', v'') > 10^{-2}$ for $v'' < 17$ except for

34. Chandralah, G., and Cho, C.W. (1973) A study of the fundamental and first overtone bands of NO in NO-rare gas mixtures at pressures up to 10,000 psi, J. Mol. Spectros. 47:134.

35. Goldman, A., and Schmidt, S.C. (1975) Infrared spectral line parameters and absorptance calculations of NO at atmospheric and elevated temperatures for the Δv=1 bands region. J. Quant. Spectrosc. Radiat. Transfer 15:127.

36. Stephenson, J.C. (1974) Vibrational relaxation of NO(X $^2\Pi$, v=1) in the temperature range 100-300°K, J. Chem. Phys. 60(11):4289.

v''-3, 6, 9, 14.[37] The band center of $\beta(7,0)$ is ~191 nm and overlaps the emission of the ArF excimer laser. This laser provides up to 200 mJ in 10 nsec at 193 nm. The $\beta(7,0)$ transition also overlaps the intense $\delta(0,0)$ band. This coincidence obscures direct measurement of the integrated absorption coefficient.[21] Using the values of k for $\beta(6,0)$ and $\beta(9,0)$ and the Franck-Condon factors, the absorption coefficient for $\beta(7,0)$ can be estimated as $\sim 5/(\text{cm}^2\ \text{atm})$. The radiative lifetime of $\beta(7,0)$ exceeds 1 μsec. Evaluating,

$$B \times I/\Delta\nu \sim 10^7/\text{sec} \quad , \tag{57}$$

using 1 cm^{-1} for the laser linewidth. The pump transition can therefore be readily saturated by the ArF pulse. The fraction of the initially prepared B state molecules that can be dumped at intensities below dump saturation is given by

$$f = B \times I\ T/\Delta\nu \tag{58}$$

where $\Delta\nu$ is the Doppler width of the pump lineshape ($\Delta\nu \sim 0.1\ \text{cm}^{-1}$). Franck-Condon factors indicate that the B coefficients for $\beta(7, 0 - 16)$ are within a factor of 10 except for v''=3, 6, 9, 14. The dump transition wavelengths are between 240 nm $\beta(7,6)$ and 389 nm $\beta(7,16)$ for which laser energies in excess of 1 mJ/pulse are readily obtained. Evaluating the expression for the dumped fraction gives 2×10^{-2} when the dump pulse is focused to 0.1 cm^2. The population that can be produced in a selected vibrational level is given by

$$N(v) = N(v=0)(2 \times 10^{-2})(0.5)P(J) \quad , \tag{59}$$

where P(J) is the rotational partition function. J is the value for the rovibronic transition most nearly in resonance with the ArF pump frequency. The above estimate indicates that sufficient number density of vibrationally excited NO molecules can be prepared using SEP to allow LIF detection.

---

37. Nicholls, R.W. (1964) Franck-Condon factors to high vibrational quantum numbers IV: NO band systems, J. Res. of Natl. Bureau of Standards - A, 68A(5):535.

References

1. Piper, L.G., Caledonia, G.E., and Kennealy, J.P. (1981) Rate constants for deactivation of $N_2(A)$ v'=0, 1 by O_2, J. Chem. Phys. 74:2888.
2. Piper, L.G., Caledonia, G.E., and Kennealy, J.P. (1981) Rate constants for deactivation of $N_2(A\ ^3\Sigma_u^+)$ v'=0, 1 by O, J. Chem. Phys. 75:2847.
3. Iannuzzi, M.P., and Kaufman, F. (1980) Rates of some reactions of $N(^2D$ and $^2P)$ near 300 K, J. Chem. Phys. 73(9):4701.
4. Green, B.D., Caledonia, G.E., Murphy, R.E., and Robert, F.X. (1982) The vibrational relaxation of NO(v=1,7) by O_2, J. Chem. Phys. 76(5):2441.
5. Fernando, R.P., and Smith, I.W.M. (1979) Vibrational relaxation of NO by atomic oxygen, Chem. Phys. Lett. 66:218.
6. Watanabe, D., Inn, E.C.Y., and Zelikoff, M. (1953) Absorption coefficients of oxygen in the vacuum ultraviolet, J. Chem. Phys. 21:1026.
7. McKee, T., Lumonics, Inc., Kanata, Ontario, Canada (1980) Private communication.
8. Kaufman, F. (1961) Reactions of oxygen atoms, Progress in Reaction Kinetics-I, G. Porter, ed., Pergamon Press Inc., New York.
9. Dushman, S. (1961) Scientific Foundations of Vacuum Technique, J.M. Lafferty, ed., John Wiley & Sons, Inc., New York, p. 82.
10. See Chapter 3, Section 4 of this report.
11. Levron, D., and Phelps, A.V. (1978) Quenching of $N_2(A\ ^3\Sigma_u^+, v=0, 1)$ by N_2, Ar and H_2, J. Chem. Phys. 69:2260.
12. Crank, J. (1957) The Mathematics of Diffusion, The Clarendon Press, Oxford, pp. 26-28, 124.
13. Morgan, J.E., and Schiff, H.I. (1964) Diffusion coefficients of O and N atoms in inert gases, Can. J. Chem. 42:2300.
14. Swider, W. (1976) Atmospheric formation of NO from $N_2(A\ ^3\Sigma)$, Geophys. Res. Letts. 3(6):335.

15. Wray, K., Feldman, E., and Lewis, P. (1970) Shock tube study of the effects of vibrational energy of N_2 on the kinetics of the $O + N_2 \rightarrow NO + N$ reaction, J. Chem. Phys. 53(11):4131.

16. Farmer, A.J., Hasson, V., and Nicholls, R.W. (1972) Absolute oscillator strength measurements of the ($v''=0, v'=1-3$) bands of the ($A\ ^2\Sigma - X\ ^2\Pi$) band system of nitric oxide, J. Quant. Spectro. Radiat. Transfer 12:627.

17. Dunn, O.J., and Young, R. (1975) Quenching of $Ar(^3P_{o,2})^*$, J. Chem. Phys. 62(5):1996.

18. Meyer, J., Setser, D., and Stedman, D. (1970) Energy transfer reactions of $N_2(A\ ^3\Sigma)$ II. Quenching and emission by oxygen and nitrogen atoms, J. Phys. Chem. 74(10):2238.

19. Bader, L.W., and Ogryzlo, E.A. (1964) Reactions of $O_2(^1\Delta)$ and $O_2(^1\Sigma)$, Disc. Faraday Soc. 37:46.

20. Ogawa, S., and Ogawa, M. (1975) Absorption cross sections of $O_2(^1\Delta)$ and $O_2(^1\Sigma)$ in the region from 1087 to 1700A, Can. J. Phys. 53:1845.

21. Bethke, G. (1959) Oscillator strengths in the far ultraviolet II. Oxygen Schumann-Runge bands, J. Chem. Phys. 31(3):669.

22. Quanta-Ray reference manuals; doubled R-50 dye emission + 1.06 μm YAG.

23. Whitson, M., Darnton, L., and McNeal, R. (1976) Vibrational energy distribution in the NO produced by the reaction of $N(^4S)$ with O_2, Chem. Phys. Lett. 41(3):552.

24. Dreyer, J., Perner, D., and Roy, C. (1974) Rate constants for the quenching of $N_2(A\ ^3\Sigma, v_A = 0\text{-}8)$ by CO, CO_2, NH_3, NO and O_2, J. Chem. Phys. 61(8):3164.

25. Boxall, M., Chapman, C., and Wyne, R. (1975) Quenching of $Ar(^3P_1)$: Rate constants for deactivation and "Escape Factors" for trapped radiation, J. Photochem. 4:435.

26. Ogryzlo, E., and Thrush, B.A. (1973) Vibrational excitation of NO in its collisional quenching of $O_2(^1\Delta)$, Chem. Phys. Lett. 23(1):34.

27. Ogawa, T. (1976) Excitation processes of infrared atmospheric emissions, Planet Space Sci. 24:749.

28. Becker, K.H., and Groth, W. (1972) (Title not available), Proc. Int. Symp. Combustion 14.

29. Melton, L.A., and Klemperer, W. (1972) Quenching of $NO(A\ ^2\Sigma)$ by $O_2(X\ ^3\Sigma)$, Planet Space Sci. 20:157.

30. Julienne, P. (1976) $^3\Sigma^- - {}^3\Sigma^+$ coupling in the $O_2(B\ ^3\Sigma^-)$ predissociation, J. Mol. Spectry 63:60.

31. Laser Focus (May, 1982) p. 24.

32. Kittrell, C., Abramson, E., Kinsey, J.L., McDonald, S.A., Reisner, D.E., Field, R.W., and Kayatama, D.H. (1981) Selective vibrational excitation by stimulated emission pumping, J. Chem. Phys. 75(5):2056.

33. Burleigh FCL Manual.

34. Chandralah, G., and Cho, C.W. (1973) A study of the fundamental and first overtone bands of NO in NO-rare gas mixtures at pressures up to 10,000 psi, J. Mol. Spectros. 47:134.

35. Goldman, A., and Schmidt, S.C. (1975) Infrared spectral line parameters and absorptance calculations of NO at atmospheric and elevated temperatures for the $\Delta v=1$ bands region, J. Quant. Spectrosc. Radiat. Transfer 15:127.

36. Stephenson, J. C. (1974) Vibrational relaxation of NO($X\ ^2\Pi, v=1$) in the temperature range 100-300°K, J. Chem. Phys. 60(11):4289.

37. Nicholls, R.W. (1964) Franck-Condon factors to high vibrational quantum numbers IV: NO band systems, J. Res. of Natl. Bureau of Standards - A, 68A(5):535.

Contents

5. Color Center Laser Experiments

1. INTRODUCTION

During the development of the COCHISE facility, we realized that there were several important issues that were not amenable to investigation in the cryogenic tank (see below). Experiments are now being designed to utilize an F-center laser (FCL) to address some of these issues. The concept is to directly interrogate molecular processes in the 2-3.5 μm region by FCL absorption or pumping experiments. These are room temperature experiments which utilize the large signal and very narrow line source to overcome sensitivity problems associated with a warm background.

One of the initial experiments planned is a direct absorption measurement for determining exact positions of $3\nu_3$, $4\nu_3$ and $5\nu_3$. Literature values[1,2] for the anharmonic constant X_{33} range from -15 cm^{-1} to -12.3 cm^{-1}. Unfortunately, this value is critical to the analysis of the COCHISE data. Measurement of the exact positions of the ν_3 energy levels as high as possible in the vibrational progression will give a more accurate value for X_{33}. Current calculated values[3] for $3\nu_3$.

1. McCaa, D.J., and Shaw, J.H. (1968) The infrared spectrum of ozone, J. Mol. Spectr. 25:374.
2. Barbe, A., Secroun, C., and Jouvre, P. (1972) Spectre d'absorption infrarouge de l'ozone gazeuz, Compte Rendu Acad. Sci. Paris 274:615.
3. Adler-Golden, S.M., and Armstrong, R.A. (1982) Spectroscopic Parameters for Ozone from Infrared and Ultraviolet Techniques, AFGL-TR-82-0231.

$4\nu_3$, and $5\nu_3$ are 3045.0, 4000, and 4919.2 cm^{-1} (3.28, 2.50, and 2.03 μm). The first two are within the tuning range of the FCL. The last, $5\nu_3$, is just beyond the range of the present crystals. However, new crystals have been developed which extend the short wavelength end down to 0.8 μm. Thus, pumping these levels is, in principle, quite possible. There are several combination modes in this region[3] as well, which will be characterized by the FCL absorption experiment.

In addition to aiding the analysis of COCHISE data, high resolution absorption experiments on ozone, including line width measurements, will give information for the AFGL absorption line compilation on which HITRAN is based. Natural linewidths, doppler broadening and pressure broadening are issues under investigation, especially for overtone and combination bands.

A second issue to be addressed in the FCL experiments is an investigation of 4.3 μm emission from CO_2 resulting from 2.7 and 2.77 μm pumping. Solar pumping of the 10^01 and 02^01 levels of CO_2 followed by ν_3 relaxation to 10^00 and 02^00 levels with emission of 4.3 μm has been assumed to be a significant source of atmospheric emission.[4] Models estimating this emission have assumed that the ν_3 relaxation is identical to the 00^01 relaxation rate. Since ν_3 is not strongly coupled to ν_1 or ν_2 in CO_2, this assumption is likely to be valid. However, there has never been an experimental verification of this. Finzi and Moore[5] have measured the intermolecular V-V relaxation process using a doubled Nd:YAG pumped optical parametric oscillator, but they did not extend their investigation to the intramolecular case. Kumer[6] attempted to apply an optical parametric oscillator to this measurement but was unable to obtain useful information due to apparatus problems. Since the peak of the FCL output is at 2.7 μm, the experiment should be easily addressed using the FCL as a pump source and a filter/detector to observe the 4.3 μm emission.

2. APPARATUS

The original laser system consisted of a Burleigh FCL-20 containing three crystals, and a Spectra-Physics 164 krypton-ion pump laser. The three crystals

---

4. James, T.C., and Kumer, J.B. (1973) Fluorescence of CO_2 near 4.3 microns: application to daytime limb radiance calculations, J. Geophy. Res. 78:8320.

5. Finzi, J., and Moore, C.B. (1975) Relaxation of $CO_2(10^01)$, $CO_2(02^01)$ and $N_2O(10^01)$ vibrational levels by near-resonant V-V energy transfer, J. Chem. Phys. 63:2285.

6. Kumer, J. Unpublished results.

are (1) KCl:Na, (2) KCl:Li, and (3) RbCl:Li which operate in the ranges 2.2-2.5, 2.5-2.8, and 2.75-3.3 μm, respectively. The specifications at the time of purchase indicated that the Spectra Physics 164 operating at 1 W was sufficient to pump all crystals. In fact, this was found not to be true since the quality control on production runs of the crystals could not be maintained at the prototype level. Crystals 2 and 3 could be pumped with the 647.1/676.1 nm line combination, but the ion tube could not sustain 1 W since that output exceeded design criteria. Crystal (1) requires 1.5 W on the 568.2 nm green line, which cannot be achieved with the Model 164. We therefore replaced the Model 164 with a Spectra Physics Model 171, which can achieve up to 7 W on all red lines and 3 W on the yellow/green lines. Operation above specification was achieved.

The Burleigh FCL-20 as delivered was inoperable since the laser cavity was misaligned. As designed, there is no way to align the laser in the field. Burleigh accepted responsibility and realigned and refurbished the laser. Upon return of the instrument, lasing was achieved. A PbS detector with standard in-house fabricated circuitry was used for laser detection.

A gas handling system was fabricated from pyrex to handle ozone generation and storage. A silent discharge technique is used to generate O_3 from a flow of pure O_2. A Variac-controlled luminous-tube transformer is wired to two copper foil electrodes on the inside and outside of a glass finger. Ozone is formed as O_2 is slowly passed through the discharge, and is subsequently trapped on silica gel maintained at -80 C with a dry ice/propanol slurry. Slight warming by lowering the slurry bath is sufficient to raise the O_3 partial pressure up to several hundreds of mTorr. Pressure is measured with a MKS Baratron 310BH-100 head and 27M-6C control unit.

The absorption experiments are designed to operate with either an intracavity absorption cell or with an extra-cavity white cell with a variable path length up to 20 m. The absorption experiments are typically performed in a chopped mode, with a reference beam split off to a second detector. A phase sensitive lock-in amplifier (PAR-HR8) operating in the channel difference mode normalizes the absorption signal to the reference beam. Spectra are recovered on a Hewlett-Packard strip chart recorder.

The pump/probe experiments on CO_2 are performed in the pulsed mode with an electro-optical shutter modulating the 2.70 and 2.77 μm pump beam. A cold filter/detector system selects the 4.3 μm emission. Further experimental details for this approach have not yet been verified.

3. INITIAL RESULTS AND ANALYSIS OF APPROACH

The initial system check consisted of evacuating the laser tuning arm and fixing the detector 20 cm from the output window. A simple single beam absorption spectrum of air was obtained which clearly showed the crystal 2&3 tuning ranges. CO_2 and H_2O absorption lines were identified and there was nothing otherwise remarkable about the spectrum. No further experimental results were available at report time.

We have performed an initial analysis comparing the extra-cavity white cell absorption approach to the intracavity absorption approach for three cases.

Case 1: Extra-cavity White Cell/With Etalon

The FCL operates on a single mode of approximately 3×10^{-5} cm^{-1} width by using an intracavity etalon. Therefore, with etalon tuning the observed linewidth will be simply the Doppler- and pressure-broadened rotational linewidth. Reasonable experimental conditions for operation of the multi-pass white cell would be, for example, 5 Torr ozone, 5 Torr oxygen, and a 10-m path length. For these conditions, the optical path, $u = 6.6$ atm cm, and linewidth, $\gamma_{TOTAL} = 5 \times 10^{-3}$ cm^{-1}. The peak absorptance is given by

$$\alpha_{peak} = 1 - \exp(-ku) \tag{1}$$

where

$$k = \frac{S\sqrt{\ell n 2}}{\pi \gamma_{TOTAL}} , \tag{2}$$

and

S = Line strength (atm^{-1} cm^{-2}) .

If one assumes that the peak absorption coefficient for the actual Voigt lineshape may be approximated by that of a Doppler lineshape, insertion of the numerical values yields

$$\alpha_{peak} = 1 - \exp(-350S) . \tag{3}$$

With this multipass, etalon-tuned configuration the sensitivity is extremely high. Therefore, even very weak lines ($S \sim 10^{-5}$) of the $3\nu_3$, $2\nu_1 + \nu_3$, and $3\nu_3 + \nu_1$ systems can be seen.

Case 2: Extra-cavity White Cell/Without Etalon

Without the etalon, the laser operates on 2 modes separated by 10 GHz (0.3 cm^{-1}), each mode of which consists of a narrow cluster of individual cavity modes spaced by 0.01 cm^{-1} and probably varying in time. The precise behavior of the laser lineshape is difficult to predict. To a crude approximation we assume that the two main modes are equal in strength, and that the effective half-width of each mode is 0.005 cm^{-1}. Then in the observed spectrum an individual rotational line will indeed be resolved, but it will appear as a doublet. The peak absorptance of each component of the doublet will be given by:

$$\alpha_{peak} = \frac{1}{2}(1 - e^{-k_{eff}u}) \tag{4}$$

where

$$k_{eff} = \frac{S\sqrt{\ell n 2}}{\pi \gamma_{eff}} \quad , \tag{5}$$

γ_{eff} being the effective linewidth for a 0.005 cm^{-1} wide ozone line convoluted with a 0.005 cm^{-1} instrument function; $\gamma_{eff} \sim 0.01$ cm^{-1}. Inserting the numerical values yields

$$\alpha_{peak} \sim \frac{1}{2}[1 - \exp(-175S)] \tag{6}$$

or

$$\alpha_{peak} \sim 90S \text{ (small S)} \quad . \tag{7}$$

Thus, a factor of roughly 4 in sensitivity is lost compared to using the etalon. However, due to the approximate nature of the lineshape model only a qualitative conclusion should be drawn.

Case 3: Intracavity Cell/Without Etalon

A short cell ($\ell \sim 10$ cm) may be placed within the laser cavity for an absorption experiment. Unfortunately, the etalon cannot be used simultaneously. The expected signal for such an intracavity experiment can be estimated using Eqs. (4) - (7), inserting an appropriate value for the optical path, u, estimated as follows. The effective number of passes n in an intracavity experiment is given by:

$$R^n = 1/e \tag{8}$$

for a single-mode laser, where R is the reflectivity of the output coupler. In this case the output coupler is a grating with $R \sim 0.9$ on the first order, yielding $n = 9$. Thus, assuming single-mode behavior, a 10 cm cell, 9 passes, and the previously stated ozone and oxygen concentrations, Eq. (7) instead becomes

$$\alpha_{peak} \sim 8S \quad . \tag{9}$$

A factor of 40 is lost compared to the extra-cavity single mode experiment, Eq. (3). Actually, Eq. (9) should be regarded as an upper limit on α_{peak}, since Eq. (8) is invalid for a multimode laser; when one mode is spoiled, another mode may be enhanced.

References

1. McCaa, D.J., and Shaw, J.H. (1968) The infrared spectrum of ozone, J. Mol. Spectr. 25:374.
2. Barbe, A., Secroun, C., and Jouvre, P. (1972) Spectre d'absorption infrarouge de l'ozone gazeuz, Compte Rendu Acad. Sci. Paris 274:615.
3. Adler-Golden, S.M., and Armstrong, R.A. (1982) Spectroscopic Parameters for Ozone from Infrared and Ultraviolet Techniques, AFGL-TR-82-0231.
4. James, T.C., and Kumer, J.B. (1973) Fluorescence of CO_2 near 4.3 microns: application to daytime limb radiance calculations, J. Geophy. Res. 78:8320.
5. Finzi, J., and Moore, C.B. (1975) Relaxation of $CO_2(10^0 1)$, $CO_2(02^0 1)$ and $N_2O(10^0 1)$ vibrational levels by near-resonant V-V energy transfer, J. Chem. Phys. 63:2285.
6. Kumer, J. Unpublished results.

Appendix A

Design and Performance Characteristics of the COCHISE Facility

A1. INTRODUCTION

Chemical excitation processes, in which some of the energy released by the reactants appears as internal energy in the product molecules, can provide important mechanisms for molecular infrared radiation and nonequilibrium energy disposal in the quiescent and disturbed upper atmosphere. There are two generic types of such processes: chemiexcitation,

$$A + BC \rightarrow AB^{\dagger} + C \tag{A1}$$

where chemical bonds are broken and/or formed, and energy transfer,

$$AB + C^{\dagger} \rightarrow AB^{\dagger} + C \tag{A2}$$

in which the chemical identities of the collision partners are unchanged but excitation energy is transferred from species C to species AB. The predominant mode of excitation of $AB^{\dagger}$ is vibrational; however, some atmospheric species (most notably N_2 and O_2) possess electronic states which can radiate in the infrared. It is often difficult to deduce detailed information about these processes from in situ atmospheric measurements of infrared emission; such data usually

have low spectral resolution and contain contributions from competing thermal and scattering mechanisms. However, laboratory investigations of individual chemical processes under carefully controlled conditions can provide detailed mechanistic and spectroscopic information; this information can, in turn, be used in conjunction with atmospheric models both to interpret the in situ data and to define further measurements.

Infrared emission spectroscopic experiments designed to investigate gas phase chemiexcitation reactions require (1) high sensitivity to the relatively weak molecular radiation from the products of Reactions (A1) and (A2); (2) adequate resolution to allow conclusive spectral analysis; and (3) specificity to the chemiexcitation process under investigation, that is, negligible interference from radiative, collisional, and surface relaxation processes. These conditions work against each other; the achievement of condition (3) necessitates the use of small pressures and/or product yields, which results in low radiation levels and increases the difficulty of achieving conditions (1) and (2). Furthermore, the limitation of IR detection sensitivity by thermal background radiation in the field of view severely inhibits spectrally resolved observations of long wavelength radiation from important atmospheric species such as CO_2 (15 μm) and O_3 (10 μm). Previous IR chemiluminescence methods such as arrested relaxation [1-3] and discharge flow [4, 5] coupled with the use of circular-variable-filter spectrometers, [5] grating monochromators, [2] and Fourier transform spectrometers, [1-4] have been highly successful in studies of chemiexcitation in hydrogen halides at wavelengths less than about 5 μm. [6] In general, however, these methods suffer from thermal background limitations; for example, at 10 μm, the spectral radiance from a typical $AB^{\dagger}$ species at a column density of about $10^8/cm^2$ (often representative

1. Carrington, T., and Polanyi, J.C. (1972) MTP International Review of Science, Physical Chemistry, Series One, Vol. 9 (J. D. Polanyi, ed.), Butterworth, London, p. 135.
2. Holmes, B.E., and Setser, D.W. (1977) Energy disposal in unimolecular and bimolecular reactions, in Physical Chemistry of Fast Reactions, Vol. 3, edited by I.W.M. Smith, Plenum Publishing Co., London.
3. Moehlmann, J.G., Gleaves, J.T., Hudgens, J.W., and McDonald, J.D. (1974) Infrared chemiluminescence studies of the reaction of fluorine atoms with monosubstituted ethylene compounds, J. Chem. Phys. 60:4790.
4. Sung, J.P., Malins, R.J., and Setser, D.W. (1979) Comparison of rate constants for reactions of hydrogen atoms with chlorine, fluorine, iodine chloride, and chlorine fluoride, J. Phys. Chem. 83:1007.
5. Berquist, B.M., Bozzelli, J.W., Piper, L.G., and Kaufman, F. (1972-1980) Unpublished work.
6. Bogan, D., and Setser, D.W. (1977) Fluorine-containing free radicals, kinetics and dynamics of reactions, ACS Symp. Ser. 66.

of such experiments) would be about nine orders of magnitude less than that from a room-temperature blackbody.

The improvement in IR detectivity due to a cryogenic background is shown in Figure A1. Since the limiting noise mechanism is the statistical fluctuation in the photon flux associated with the detector's environment, the detectivity of the system is inversely proportional to the square root of that flux. The results plotted in Figure A1 are normalized to the detectivity at 293 K. Although considerable enhancement in detectivity is obtained with an 80 K background, the effects of background radiation can be virtually eliminated by cooling the entire reaction chamber/detection system to temperatures below 40 K. As a further benefit of cryogenic temperatures, rapid cryopumping of reagent gases can be attained near 20 K, and radiation leakage from the external vacuum system can then be eliminated by isolating the reaction/detection system during the experiments.

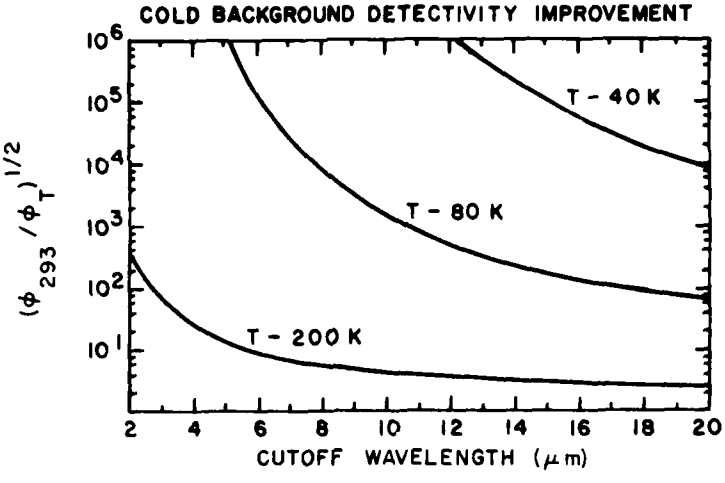

Figure A1. Reduction in Background Photon Flux by Cryogenic Operation

The COCHISE facility at the Air Force Geophysics Laboratory is a cryogenic apparatus designed for partial simulations and detailed experimental studies of high altitude IR excitation phenomena, particularly chemiexcitation and excitation transfer processes. The experimental direction taken in the development of COCHISE (COld CHemiexcitation Infrared Simulation Experiment) has been to reduce the temperatures of both the reaction chamber and the detection system

to approximately 20 K to optimize the benefits of cold background and cryopumping. A state-of-the-art infrared detector and a cryogenic scanning monochromator are coupled to a long-path reaction cell to allow spectrally resolved detection of IR radiation (2 - 20 μm) from emitting species at concentrations as low as 10^6 molecules/cm^3. The techniques of discharge flow and arrested relaxation are combined to allow mixing of the reacting species in the field of view at steady-state pressures near 3 mTorr, so that in most cases, the chemiexcited products can be formed and observed under nearly single-collision conditions. The high speed cryopumping of the reaction vessel removes the excited species from the field of view of the detection system before radiative or collisional relaxation can occur, and eliminates contamination by back-diffusion from the chamber walls.

This appendix describes the detailed design and operation of the COCHISE apparatus. In the following section, an overall description of the apparatus will be given, followed by more detailed descriptions of the various components. In the final section, some specific applications of the facility to relevant atmospheric problems will be discussed.

A2. APPARATUS DESCRIPTION

A schematic of the entire COCHISE apparatus is given in Figure A2. The reaction cell and detection system are enclosed within a cryogenic thermal shroud, which is, in turn, enclosed by a main vacuum chamber to provide thermal isolation. All surfaces within the shroud, with the exception of selected optical components and reagent gas lines, are held at temperatures as low as 20 K, which allows rapid cryopumping of all reagent and background gases except He and H_2. The reagent gases enter the reaction cell through four sets of opposing jets (see also Figure A3) and interact along the centerline of the cell; the resulting radiation is viewed through a lens by a grating monochromator detection system. The data processing, temperature control, and system housekeeping are performed by an external computer. The various components of the system are described in more detail below.

A2.1. Thermal Isolation and Control System

The cryogenic portion of the apparatus is thermally isolated inside a cylindrical main vacuum chamber ~3 m long and ~1.5 m in diameter (see Figure A2). The thermally insulating vacuum enclosure is maintained at ~10^{-10} atm by a 20-in. cold-baffled diffusion pump (Consolidated Vacuum Corp) backed by a large two

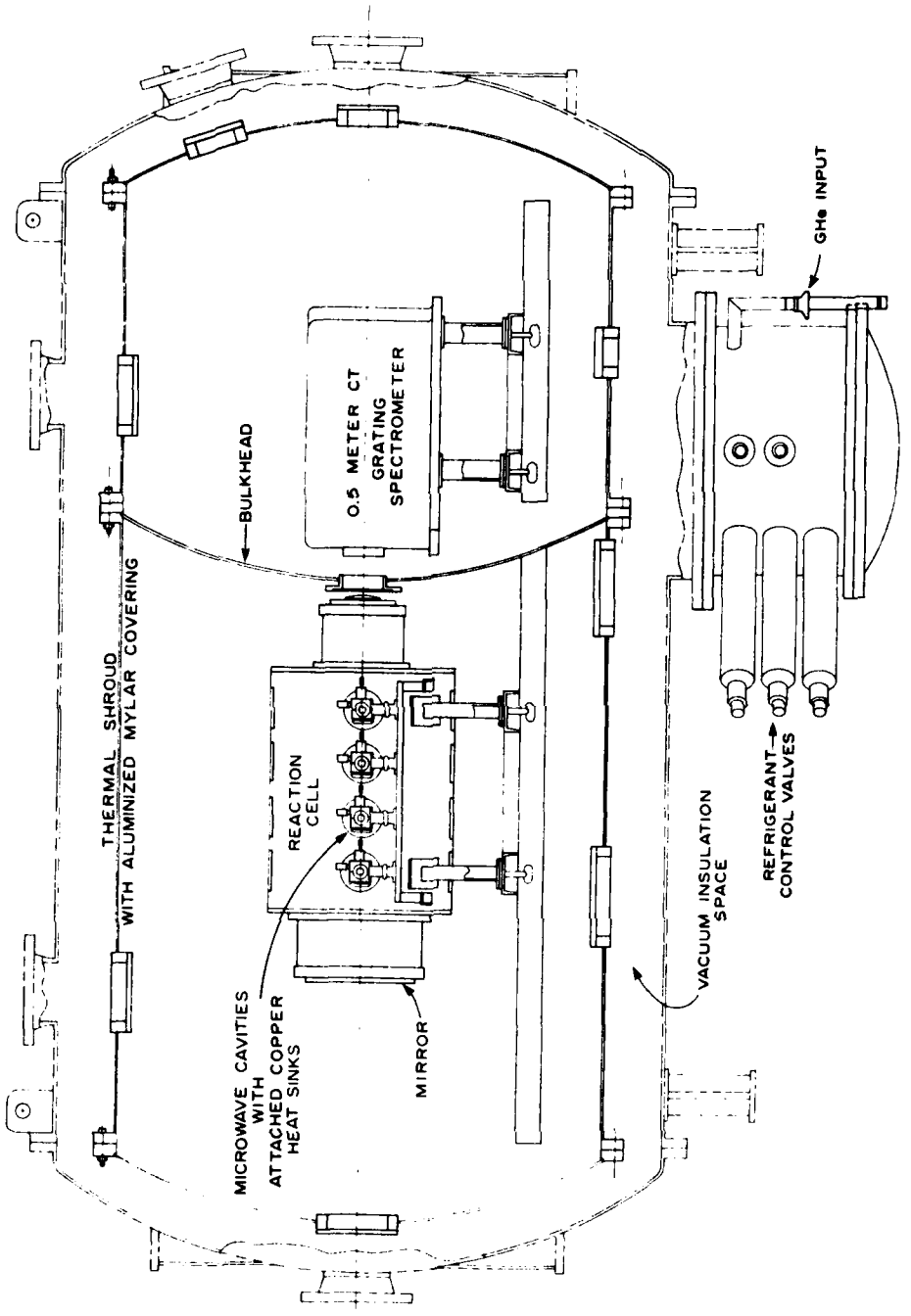

Figure A2. Schematic of COCHISE Facility

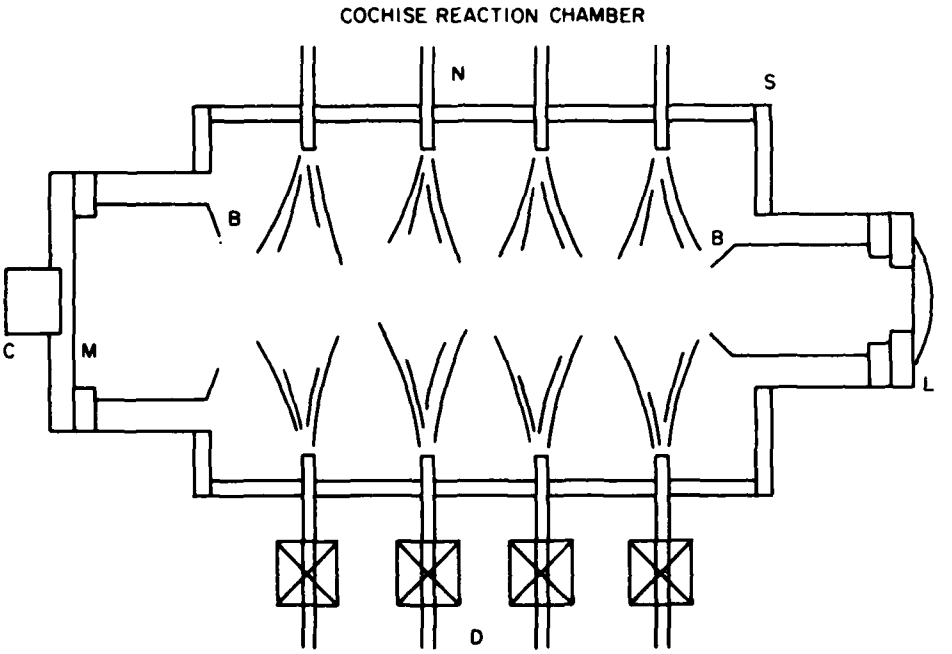

Figure A3. Scale Drawing of Chemiluminescence Reaction Cell. Ar/N_2 mixtures are excited by microwave discharges, D, and mix with the counterflow of O_2 from nozzles N in an axisymmetric reaction zone at the chamber center. Baffles, B, restrict detection system field-of-view to the on-axis reaction volume. M is a plane mirror which increases the intensity of the radiation collected by lens L. Spectral response calibration is performed using blackbody source, C, embedded behind a small hole in the end mirror

stage mechanical pump (Leybold - Heraeus DK-180). The light-tight aluminum shroud, ~2.5 m long and 1.25 m in diameter, is supported on stainless steel and phenolic stand-offs and is completely surrounded by a multi-layer thermal shield to provide insulation from the 300 K thermal radiation of the outer wall. This shield consists of 19 alternating layers of aluminized mylar, dacron bridal veil, and 0.030-in. Scott Industrial Foam and admits a total radiative load of less than 50 W from the 300 K outer wall to the 20 K shroud, a net reduction of more than 2 orders of magnitude. The shroud, reaction cell, and detection system are cooled to ~20 K by a 600 W closed-cycle helium refrigeration system (Cryogenic Technology, Inc.). Extended-stem valves permit control of coolant flow in three independent loops supplying the shroud, reaction cell, and microwave discharge heat sink (see below).

Component temperatures are monitored at roughly 25 locations by calibrated platinum resistance thermometers. DC voltage is supplied from an external source; the resulting voltage drop across each sensor is amplified, processed by analog-digital conversion in a PDP-8E (Digital Equipment Corp.) computer, converted to absolute temperature, and displayed on various storage oscilloscopes or hard copy devices. Temperatures are controlled in 13 different areas by resistive heaters mounted on the appropriate hardware, which is, in turn, isolated from surrounding areas by stainless steel or phenolic stand-offs. Power to the heaters is percentage-controlled by the computer via solid-state switches so that the temperature of each heat station is independently sampled and regulated to within ± 0.5 K.

Due to the rapid cryopumping by the 20 K walls, it is possible to vacuum-isolate the internal cryogenic chambers from each other and from the external vacuum system during the measurements in order to seal off external light leaks. This is accomplished by means of specially modified, cryogenic, latching solenoid valves of a type not commercially available. These valves, which are operated from an external control panel, can be opened and closed by separate solenoids and will remain in either position in the absence of applied power; microswitches mounted on the valve shafts provide positive readouts of the valve positions.

The physical arrangement shown in Figure A2 emphasizes flexibility in usage of the apparatus. The main vacuum chamber and cryogenic shroud have full-opening end doors and a number of access ports through which all of the services for the experiments, such as cryogenic coolant, microwave power, reagent gases, and instrumentation, are introduced. All diagnostic and control devices are mounted externally. The ready availability of extra access ports and vacuum feedthroughs allows a high degree of adaptability to future diagnostic concepts such as use of lasers or atomic resonance line sources.

A2.2. Reaction Cell and Reagent Gas Lines

A schematic of the chemiluminescence reaction chamber is given in Figure A3. The copper reaction cell is cylindrically symmetric, 60 cm in length, and 40 cm in diameter. To control the cryopumping speed (and thus the reagent gas residence time - see below), the reaction cell temperature can be independently varied; temperature uniformity to ± 0.1 K over the entire surface is achieved through proper positioning of coolant flow lines and heater elements.

The reagent gases are metered into the system by motorized Granville-Phillips leak valves; flow rates are monitored by calibrated mass flowmeters

(Brooks). One gas mixture flows through four sapphire microwave discharge sidearms on one side of the cell; another gas mixture flows through four counterflow sidearms on the opposite side of the cell. Up to three gases can be mixed prior to introduction to the discharge cavities; two gases can be separately mixed for the counterflow. Upon penetration of the outer vacuum chamber, the room-temperature gases undergo a two-stage heat exchange process. The first stage, outside the shroud, is a copper plate cooled with liquid nitrogen; the second stage, inside the cryogenic shroud, permits variable temperature selection over the range 30 - 500 K. The gases then pass through temperature-controlled copper lines to the appropriate inlet sidearms and into the reaction volume. Just prior to entering the reaction cell, gases in the sapphire discharge tubes are ionized and excited by four modified McCarroll-Evenson[7] microwave discharge cavities (Opthos Instruments) powered by Raytheon PGM 10 power supplies (2450 MHz, 100 W) with variable duty cycle. Typical operation is at 50 - 90 percent of maximum power with duty cycles of either 100 percent or 50 percent at 23 Hz, creating steady state conditions while the discharges are on; all four discharges are driven by a single pulse generator to insure synchronous operation to within a few microseconds. Excess heat generated by the discharge plasmas is transmitted to a copper heat sink plate where it is removed by the helium coolant; the heat transfer rate is controlled by an extended-stem valve on the coolant as described above. In normal operation, the discharges are held at the desired gas temperature (typically 80 - 100 K in experiments to date).

As is shown in Figure A3, the reagent gases are expanded into the interaction volume, with equal mass flow rates, through four sets of diametrically opposed inlet jets that are equally spaced along the cylindrical cell. Flow conditions in the reaction cell have been modeled[8] for a range of experimental conditions; free expansion occurs in the reaction cell and the gas reaches a limiting velocity in which all of the thermal energy in the inlet tube is converted into kinetic energy. Near the cylinder axis, an axisymmetric stagnation point occurs, and the thermal energy of the gas molecules returns to that of the gas in the inlet tubes. Gas density variations along the cylinder axis (reaction volume) are predicted to be 10 percent or less. The pressures in the reaction zone and in the sidearms are monitored by an MKS Baratron capacitance manometer. At typical flow rates

---

7. McCarroll, B. (1970) An improved microwave discharge cavity for 2450 MHz, Rev. Sci. Instr. 41:279; Fehsenfeld, F.C., Evehson, K.M., and Broida, H.P. (1965) Microwave discharge cavities operating at 2450 MHz, Rev. Sci. Instr. 36:294.

8. Caledonia, G.E., Green, B.D., Simons, G.A., Kennealy, J.P., Robert, F.X., Corman, A., and Del Greco, F.P. (1977) COCHISE Studies I; Fluid Dynamical and Infrared Spectral Analysis, AFGL-TR-77-0281, AD A053218.

used in the past, ~4 standard l/min of various $Ar/N_2/O_2$ combinations on each side, the resulting pressures are about 1 Torr in each sidearm and about 3 mTorr in the reaction zone; the corresponding gas residence times are about 2 msec from the discharge to the expansion region and about 0.3 msec in the field of view (see below).[9]

The chemiluminescent reactions occur primarily in the stagnation region where the opposing flows meet. The infrared radiation is viewed by the detection system through a 3-in. f/7 antireflection-coated germanium lens; the resulting field of view is roughly columnar along the cylinder axis so that only radiation originating within 4 cm of the axis is observed. A polished Al mirror at the far end of the cell enhances the collection efficiency of the system. Internal baffles on the mirror and lens discriminate against scattered light from the discharges. The walls of the reaction cell are not in the field of view. The spectral response of the optical system is routinely calibrated with a variable-temperature blackbody source embedded in the center of the mirror.

A2.3. Spectral Detection System

The detection system is isolated from the reaction system by an Al bulkhead which both blocks scattered radiation from the cell and prevents the passage of reagent gases into the detection system. Infrared radiation from a cylinder about 8 cm in diameter centered along the axis of the reaction cell (or from the blackbody source in the center of the end mirror, for calibration measurements) passes through the reaction cell lens into the detection system via a 3-in. antireflection-coated germanium window in the center of the bulkhead. The radiation then passes through an order-sorting filter and an optional tuning fork chopper into a cryogenic grating monochromator, where it is dispersed and focused onto a liquid-helium-cooled detector.

A2.3.1. FOREOPTICS

A series of long-wavelength-pass and/or bandpass filters is deployed by a specially constructed, solenoid-driven, rotating filter wheel. For most applications to date, long-wavelength-pass filters with sharp short wavelength cutoffs at nominally 2, 4, and 8 μm have been used to isolate the corresponding first order spectral regions 2-4, 4-8, and 8-16 μm.

---

9. Kennealy, J., Del Greco, F. P., Caledonia, G. E., and Green, B. D. (1978) Nitric oxide chemi-excitation occurring in the reaction between metastable nitrogen atoms and oxygen molecules, J. Chem. Phys. 69:1574.

A 23 Hz tuning fork chopper (American Time Products, Type 140 or Philamon, Type TFLC 34CH-7178) in front of the monochromator entrance slit can be used to modulate the incoming radiation. This chopper is used in all blackbody measurements and is optional in the chemiluminescence measurements, as will be described in Section A2.3.4.

A2.3.2. CRYOGENIC MONOCHROMATOR

In the development of a cryogenic spectrometer system for the COCHISE facility, a scanning grating monochromator proved to be the most straightforward, reliable, and economical approach. The instrument chosen was a 0.5-m asymmetric Czerny-Turner system (Minuteman # 305 CM), which is mounted on an Invar frame to minimize distortion at low temperatures. The spherical collecting and focusing mirrors and the grating are mounted in Invar supports which are in turn mounted directly to the basic frame. The entire assembly is covered with a light-tight Al housing and is held at 20 K during normal operation.

Two interchangeable replica gratings are employed, their selection depending upon the wavelength region of interest; both gratings are 6.4 cm square, which gives the instrument an aperture ratio of f/6.9. For wavelengths shorter than 8 μm, a grating blazed at 3 μm with 150 lines/mm (at room temperature) allows a nominal first-order reciprocal dispersion of 0.013 μm/mm in the exit slit plane; for longer wavelengths, a grating blazed at 10 μm with 75 lines/mm gives 0.027 μm/mm. Thus, for a slit width of 0.55 mm, the resolution element is approximately 2.6 cm^{-1} at 5 μm and approximately 1.4 cm^{-1} at 10 μm. Such resolution permits not only the determination of detailed vibrational structure for most small atmospheric molecules (typical vibrational spacings of about 10 cm^{-1}), but also often permits the observation of some rotational structure.

The entrance and exit slit assemblies consist of rotatable discs containing a series of fixed, 2 cm-high slits ranging in width from 0.1 to 3.0 mm; the slits can be independently indexed by manual controls outside the vacuum chamber. The grating is rotated by a conventional sine-drive mechanism using a precision ball screw designed specifically for cryogenic service; the scan drive controls are located outside the vacuum system. Three shafts penetrate the outer and inner walls of the system and are coupled to the slit assemblies and grating drive screw via stainless steel bellows.

A2.3.3. CRYOGENIC INFRARED DETECTOR

The infrared preamplifier-detector module was designed and fabricated at the Electrodynamics Laboratory of Utah State University. The detector element is an arsenic-doped silicon cube, 3.0 mm on an edge (Santa Barbara Research Center); an f/0.25 parabolic reflector images the monochromator exit slit onto

the detector and thus permits collection of virtually all radiation passing through the slit. A contiguous preamplifier unit utilizes an integrated JFET operational amplifier (Burr-Brown 3521R) in a direct-coupled negative-feedback operational scheme that has previously been successfully applied to ultra-high impedance cryogenic detectors.[10] The module also contains an infrared emitting diode, temperature monitors and associated electronic elements and devices. The preamplifier and detector are maintained at temperatures of ~ 220 and 9 K, respectively, by proportional control systems. An external console provides system control functions, detector bias, signal conditioning circuitry, and output indicators and terminals. This detector, when operated at about 9 K, is sensitive to 1.2 - 22 μm radiation and has a peak Noise Equivalent Power of approximately 10^{-16} W/Hz$^{1/2}$.

Liquid helium cooling of the detector package is provided by a 20 l liquid helium vessel suspended from a port in the top of the vacuum chamber. The neck of the vessel, which serves as a fill-and-vent line, is flexibly connected by a bellows to a port in the 20 K shroud to make a light-tight penetration. Thermal coupling between the detector and the liquid helium vessel is accomplished by a copper bar and thermal strap, with optional sapphire electrical standoffs to isolate the detector/preamplifier case.

A2.3.4. SIGNAL PROCESSING

The detector output is processed by phase-sensitive detection to discriminate against random-phase background noise. The radiation reaching the detector is modulated in one of two ways. In most chemiluminescence observations, the microwave discharges are pulsed at 23 Hz with a square wave, 50 percent duty cycle; since chemical reaction does not occur in the absence of the reactive species formed in the discharge plasma, this results in a square wave oscillation in the chemiluminescence signal (provided the chopping frequency is slow enough relative to the flow speed so that diffusional "blurring" of the waveform does not occur). An alternate method of data collection is to operate the discharges continuously and modulate the radiation with the chopper. However, the pulsed discharge method has the advantage of discrimination against stray radiation that is not directly linked to species produced in the discharge plasma. The chopper is also used to modulate the radiation from the internal blackbody source during calibration measurements.

The ac detector output passes through a bandpass amplifier (PARC Model 113) and into a lock-in amplifier (PARC Model 124) which is synchronized either to the

---

10. Wyatt, C.L., and Baker, D.J. (1973) Rocket Launch of an LWIR Spectrometer Into an Aurora, Internal Report, Electro-Dynamics Labs., Utah State University.

frequency of the chopper pick-up coil or to the external pulse generator used to pulse the microwave discharges. The final demodulated signal is digitally filtered, displayed, and stored in real time by the PDP-8/E computer. The combination of grating scan rate, electronic time constant, and digital filtering rate for a given spectral scan is carefully chosen so that there are at least seven averaged data points and three time constants per spectral resolution element; these criteria insure that the apparent spectral detail is indeed limited by the instrument resolution.

A3. APPLICATIONS

The spectral responsivity of the COCHISE optical/detection system, as determined from calibrations with the internal blackbody source, is plotted as a function of wavelength in Figure A4. The spectral region 2-15 μm was traversed by means of two gratings and three long-wavelength-pass filters, as described in the caption. Absolute calibration of the optical system is complicated due to the radially extended distribution of the chemiluminescent emission; however, relative responsivity determinations are straightforward. Thus, the relative responsivities shown in Figure A4 are quite representative, while the absolute scale is only accurate to within about a factor of 2 at this time. Since the noise level of the instrumentation is $\sim 10^{-6}$ V, the maximum responsivity, at $\sim 10\ \mu$m, corresponds to an optimum NESR near 10^{-11} W/(cm^2 sr μm), or $\sim 10^7$ photons/(cm^3 sec μm) for the effective optical path length of 100 cm. For typical species of interest (for example, O_3 - see discussion later in this section), the transition probability is ~ 10/sec and the bandwidth is $\sim 1\ \mu$m; thus the minimum detectable concentration of such vibrationally excited species is on the order of 10^6 molecules/cm^3. This unusually high sensitivity at such long wavelengths results from a combination of the absence of noise from thermal background radiation and the long optical path which is available for the measurements.

The versatility of the apparatus is illustrated by the spectra of Figures A5 and A7. In Figure A5, a CO(Δv=1) fluorescence spectrum, observed when a discharged N_2/Ar mixture interacts in the viewing region with a counterflowing CO/O_2 mixture, is shown. The spectral resolution of 0.007 μm (~ 3 cm^{-1}) was attained using 0.5-mm slits. The vibrational structure ($\omega_e\chi_e \sim 13.5$ cm^{-1}) is well-resolved, with contributions evident from at least the first five vibrational levels; furthermore, even the rotational structure ($B_e \sim 1.9$ cm^{-1}) is partially resolved. Since the band center of the (v' $\rightarrow$ v'') = (1$\rightarrow$ 0) transition is well-known

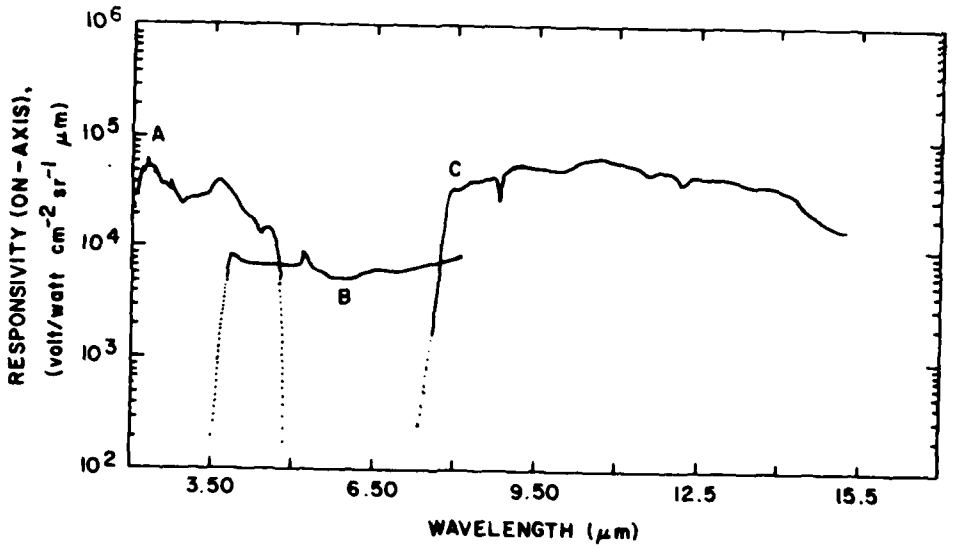

Figure A4. Approximate Spectral Responsivity of COCHISE Optical System. Curve A: 2 μm cut-on, long wavelength pass filter; 3 μm grating; 380 K blackbody source. Curve B: 4 μm cut-on, long wavelength pass filter; 3 μm grating; 380 K blackbody source. Curve C: 8 μm cut-on, long wavelength pass filter; 10 μm grating; 535 K blackbody source. A BaF_2 window in the exit slit limits the response for $\lambda \gtrsim 14$ μm

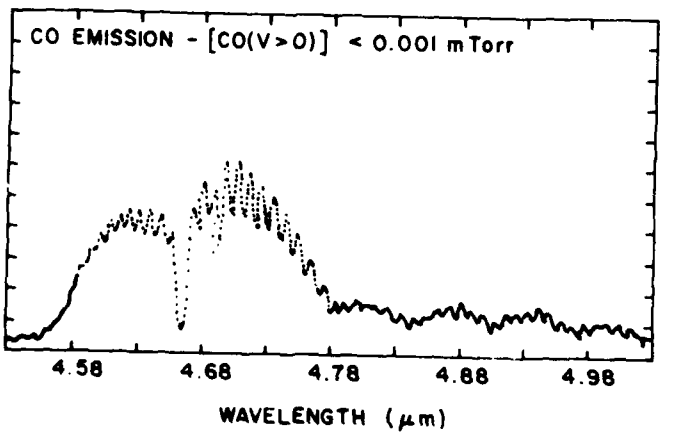

Figure A5. CO(Δv=1) Fluorescence Observed From the Interaction of Active Nitrogen With a CO/O_2 Mixture

to be 4.667 μm,[11] high-resolution spectra of the kind shown in Figure A5 provide convenient internal wavelength calibration standards for the system. The mechanism for excitation of CO(v) in these preliminary measurements appears to involve energy transfer processes similar to Reaction (A2); a systematic investigation of this process is planned for future experiments.

A fluorescence spectrum of NO(Δv=2), obtained by observing the interaction of active nitrogen and O_2 near 2.7 μm with a resolution of 0.027 μm (37 cm^{-1}), is shown in Figure A6. In this case the vibrational structure ($2\omega_e\chi_e \sim 28$ cm^{-1}) is partially resolved, with contributions evident from at least v' = 2-12, but the rotational structure ($B_e \sim 1.7$ cm^{-1}) is unresolved. A detailed COCHISE investigation of NO(Δv=1) chemiluminescence near 5.4 μm was published recently;[9] the observed fundamental and overtone band radiation is due to a chemi-excitation reaction similar to Reaction (A1):

$$N(^2D) + O_2 \rightarrow NO(v) + O \quad . \tag{A3}$$

A parallel investigation of the overtone band is now in progress, with the objective of determining the ratio of fundamental and overtone band Einstein transition probabilities as a function of vibrational level. Reaction (A3) is believed to be an important source of NO infrared radiation in the disturbed upper atmosphere; the COCHISE results[9] on this process provide input for atmospheric modeling calculations[12] which are directed toward the interpretation of in situ measurements of infrared radiation in quiescent[13] and auroral[14] atmospheres.

An O_3 ν_3 -band spectrum, observed near 10 μm in the interaction of a discharged O_2/Ar mixture with counterflowing O_2 is shown in Figure A7; in contrast to the data of Figures A5 and A6, this fluorescence appears to arise primarily from O_3(v) formed in the discharge sidearms via the recombination reaction:[15]

11. Caledonia, G. E., Green, B. D., and Murphy, R. E. (1979) A study of the vibrational level dependent quenching of CO(v=1-16) by CO_2, J. Chem. Phys. 71:4369.

12. Kennealy, J. P., and Caledonia, G. E. (1980) A model of upper atmospheric nitric oxide IR radiation, EOS 60:338; (1979) Planet Space Sci. 30.

13. Nadile, R. M., Stair, Jr., A. T., Wheeler, N. B., Frodsham, D. G., Wyatt, C. L., Baker, B. J., and Grieder, W. F. (1978) SPIRE - Spectral Infrared Rocket Experiment (Preliminary Results), AFGL-TR-78-0107, AD A058504.

14. Rawlins, W. T., Caledonia, G. E., Gibson, J. J., and Stair, Jr., A. T. (1980) Infrared emission from NO(Δv=1) in an aurora: spectral analysis and kinetic interpretation of HIRIS measurements, J. Geophys. Res. 86:1313.

15. Rawlins, W. T., Caledonia, G. E., and Kennealy, J. P. (1980) Observation of spectrally resolved infrared chemiluminescence from vibrationally excited $O_3(\nu_3)$, J. Geophys. Res. 86:5247.

$$O + O_2 + Ar \rightarrow O_3(v) + Ar \quad . \tag{A4}$$

Hence, the vibrational distribution responsible for the observed spectrum is collisionally relaxed. The spectral resolution exhibited here is 0.04 μm (4 cm^{-1}), which should be sufficient to resolve vibrational structure in O_3 ($\omega_e x_e \sim 12$-15 cm^{-1}). Although emission from the (001) vibrational level is the dominant feature in the observed spectrum, contributions from higher levels up to $v_3' = 6$ are evident at longer wavelengths. The fluorescence observed in these initial experiments represents the first spectrally resolved observations of emission from the higher vibrational levels of ozone; it is anticipated that continuing detailed studies of this system on COCHISE will yield information of fundamental relevance to upper atmospheric radiance measurements near 10 μm.

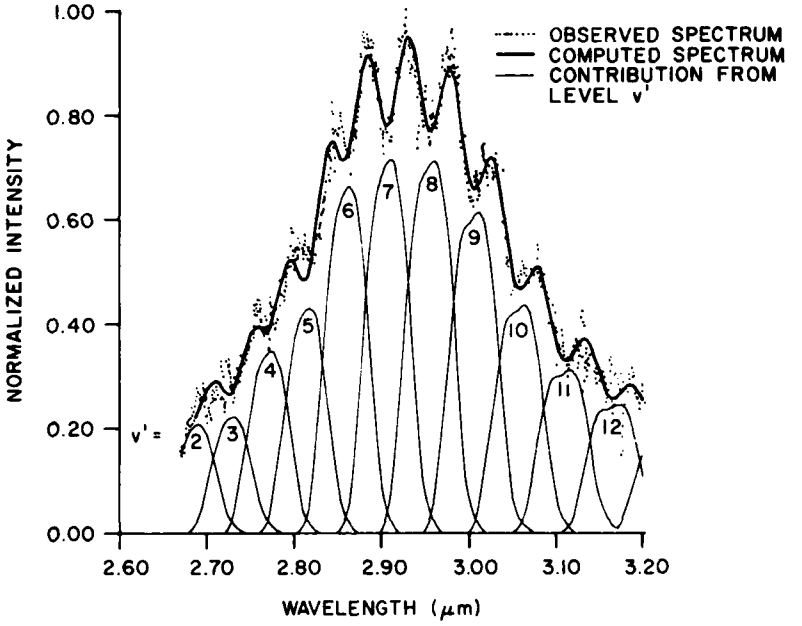

Figure A6. Comparison of Computed and Observed Spectra, Experiment 283706. In the computed spectrum, the rotational temperature is 90 K and the resolution is 0.027 μm. The standard deviation of the least squares fit is 0.033

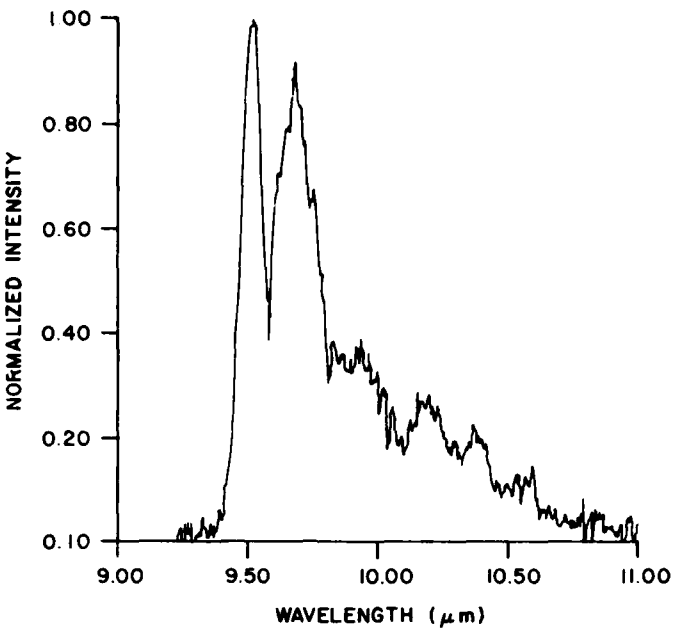

Figure A7. Observed Spectrum of $O_3(\nu_3)$ Band. Experiment 107016: 1.5 mm slits, 3 mTorr He background. Discharge: 0.7 percent O_2/Ar; counterflow: O_2

Spectra such as those of Figures A5 through A7 contain information on the populations of the vibrational states that give rise to the observed emission; these populations are, in turn, related to fundamental kinetic processes in the interaction region and/or in the discharge tubes. In the COCHISE studies, the vibrational populations are derived from a least-squares spectral fitting analysis similar to that used by other investigators.[16] In general, the emission intensity of the i^{th} spectral line is given by[17]

$$I_i = hc\,\nu_i\,A_i\,N_i \qquad (A5)$$

where ν_i and A_i are the frequency and strength of the transition, and N_i is the number density of the species of interest in the upper (emitting) vibration-rotation

16. Berquist, B.M., Piper, L.G., and Kaufman, F. unpublished work; see also Ref. 11.

17. Herzberg, G. (1951) Molecular Spectra and Molecular Structure I, Spectra of Diatomic Molecules, D. Van Nostrand Co., New York, 2nd ed.

state; if rotations are assumed to be thermalized in our experiments, N_i is given by $N_i = N_{J'}(v')N_{v'}$, where the rotational population for each vibrational level, $N_{J'}(v')$, is given by a Boltzmann factor,

$$N_{J'}(v') = \frac{g_{J'} \exp^{(-E_{J'}(v'))}}{Q_R(v')} \quad , \tag{A6}$$

and $N_{v'}$ is unknown. In Eq. (A6), $E_{J'}(v')$ and $g_{J'}$ are the rotational energy and degeneracy of the emitting state, and $Q_R(v')$ is the rotational partition function for vibrational level v'. The total spectral intensity at each point then has the form $\sum_{v'} I_i(v')$, where the vibrational basis functions $I_i(v')$ are computed from Eqs. (A5) and (A6) and are convolved over the band with the instrument resolution function. In practice, the convolved basis functions for unit vibrational populations are computed from fundamental spectroscopic constants or from line-by-line compilations such as that of McClatchey et al.;[18] the vibrational populations are then determined by a least squares method in which the quantities $\{N_{v'}\}$ are the solutions that minimize the sum of the squares of the intensity differences between experimental and computed spectra. In this way, vibrational populations are uniquely determined for each experiment, with no inherent assumptions of a functional form such as a Boltzmann distribution.

A4. CONCLUSIONS

Simulation of atmospheric infrared radiative processes in the laboratory requires high sensitivity at long wavelengths and low pressures. The COCHISE facility satisfies these criteria by means of cryogenic (20 K) operation of the entire reaction vessel and detection system; this provides minimal thermal background and rapid cryopumping of reagents, which in turn permit operation with low pressure and large optical paths. The ultimate detection sensitivity of the system is on the order of 10^6 molecules/cm^3 for vibrationally excited species.

The achievement of total cryogenic operation of such a large and complex apparatus requires careful design and testing of each component; we have documented here the end results of this developmental effort. The facility has already been successfully applied to several fundamental problems of interest to the

18. McClatchey, R.A., Benedict, W.S., Clough, S.A., Burch, D.E., Calfee, R.F., Fox, K., Rothman, L.S., and Garing, J.S. (1973) AFCRL Atmospheric Absorption Line Parameters Compilation, AFCRL-TR-73-0096, AD 762904.

atmospheric community; it is anticipated that further research in this direction will significantly improve our understanding of these and other basic processes.

References

1. Carrington, T., and Polanyi, J.C. (1972) MTP International Review of Science, Physical Chemistry, Series One, Vol. 9 (J. D. Polanyi, ed.), Butterworth, London, p. 135.
2. Holmes, B. E., and Setser, D.W. (1977) Energy disposal in unimolecular and bimolecular reactions, in Physical Chemistry of Fast Reactions, Vol. 3, edited by I.W.M. Smith, Plenum Publishing Co., London.
3. Moehlmann, J.G., Gleaves, J.T., Hudgens, J.W., and McDonald, J.D. (1974) Infrared chemiluminescence studies of the reaction of fluorine atoms with monosubstituted ethylene compounds, J. Chem. Phys. 60:4790.
4. Sung, J.P., Malins, R.J., and Setser, D.W. (1979) Comparison of rate constants for reactions of hydrogen atoms with chlorine, fluorine, iodine chloride, and chlorine fluoride, J. Phys. Chem. 83:1007.
5. Berquist, B.M., Bozzelli, J.W., Piper, L.G., and Kaufman, F. (1972-1980) Unpublished work.
6. Bogan, D., and Setser, D.W. (1977) Fluorine-containing free radicals, kinetics and dynamics of reactions, ACS Symp. Ser. 66.
7. McCarroll, B. (1970) An improved microwave discharge cavity for 2450 MHz, Rev. Sci. Instr. 41:279; Fehsenfeld, F.C., Evehson, K.M., and Broida, H.P. (1965) Microwave discharge cavities operating at 2450 MHz, Rev. Sci. Instr. 36:294.
8. Caledonia, G.E., Green, B.D., Simons, G.A., Kennealy, J.P., Robert, F.X., Corman, A., and Del Greco, F.P. (1977) COCHISE Studies I; Fluid Dynamical and Infrared Spectral Analysis, AFGL-TR-77-0281, AD A053218.
9. Kennealy, J., Del Greco, F.P., Caledonia, G.E., and Green, B.D. (1978) Nitric oxide chemi-excitation occurring in the reaction between metastable nitrogen atoms and oxygen molecules, J. Chem. Phys. 69:1574.
10. Wyatt, C.L., and Baker, D.J. (1973) Rocket Launch of an LWIR Spectrometer Into an Aurora, Internal Report, Electro-Dynamics Labs., Utah State University.
11. Caledonia, G.E., Green, B.D., and Murphy, R.E. (1979) A study of the vibrational level dependent quenching of CO(v=1-16) by CO_2, J. Chem. Phys. 71:4369.
12. Kennealy, J.P., and Caledonia, G.E. (1980) A model of upper atmospheric nitric oxide IR radiation, EOS 60:338; (1979) Planet Space Sci. 30.
13. Nadile, R.M., Stair, Jr., A.T., Wheeler, N.B., Frodsham, D.G., Wyatt, C.L., Baker, B.J., and Grieder, W.F. (1978) SPIRE - Spectral Infrared Rocket Experiment (Preliminary Results), AFGL-TR-78-0107, AD A058504.
14. Rawlins, W.T., Caledonia, G.E., Gibson, J.J., and Stair, Jr., A.T. (1980) Infrared emission from NO(Δv=1) in an aurora: spectral analysis and kinetic interpretation of HIRIS measurements, J. Geophys. Res. 86:1313.

15. Rawlins, W. T., Caledonia, G. E., and Kennealy, J. P. (1980) Observation of spectrally resolved infrared chemiluminescence from vibrationally excited $O_3(\nu_3)$, J. Geophys. Res. 86:5247.

16. Berquist, B. M., Piper, L. G., and Kaufman, F. unpublished work; see also Ref. 11.

17. Herzberg, G. (1951) Molecular Spectra and Molecular Structure I, Spectra of Diatomic Molecules, D. Van Nostrand Co., New York, 2nd ed.

18. McClatchey, R. A., Benedict, W. S., Clough, S. A., Burch, D. E., Calfee, R. F., Fox, K., Rothman, L. S., and Garing, J. S. (1973) AFCRL Atmospheric Absorption Line Parameters Compilation, AFCRL-TR-73-0096, AD 762904.

Appendix B

NO Infrared Radiation in the Upper Atmosphere

B1. INTRODUCTION

NO is created in the upper atmosphere through chemical mechanisms that are primarily initiated by the direct and indirect dissociation of molecular nitrogen by solar UV photons, cosmic rays and auroral electrons. The resulting atmospheric chemistry is such that significant concentrations of NO will be present at altitudes above 100 km under both day and night conditions at all latitudes.[1] One of the reasons this is of interest is that NO is one of the few infrared active molecules in the upper atmosphere. The NO fundamental and first overtone vibration-rotation bands fall at 5.4 and 2.7 μm, respectively, and are the dominant sources of high altitude radiation in these wavelength regions. Indeed, it has recently been demonstrated that radiative cooling by NO is the most important thermospheric cooling agent above 120 km.[2]

This appendix examines the mechanisms responsible for upper atmosphere NO vibrational band radiation under both quiescent and aurorally excited conditions and develops a radiation model for comparison with available measurements.

---

1. Cravens, T. E., and Stewart, A. I. (1978) Global morphology of nitric oxide in the lower E region, J. Geophys. Res. 83:2445.
2. Kockarts, G. (1980) Nitric oxide cooling in the terrestrial atmosphere, Geophys. Res. Lett. 7:137.

Examinations of atmospheric NO excitation and de-excitation mechanisms,[3-5] and predictions for the upper atmospheric NO fundamental band column intensity have been previously published.[5,6] Nonetheless, as described below, kinetic information developed in the last few years now allows for considerably more realistic predictions of anticipated NO radiation levels and vibrational distribution functions. Furthermore, past studies have been limited to specific atmospheric configurations and have not examined the sensitivity of the radiation predictions to both atmospheric variations and uncertainties in rate constants; such issues will be addressed in the present analysis.

A model for high altitude NO radiation in the quiescent atmosphere is presented in Section B2 and a similar model appropriate to the aurorally dosed atmosphere is developed in Sectio.. B3. Model predictions are compared with rocket based measurements of NO radiation levels in both sections. The summary and conclusions of the study are presented in Section B4.

B2. NO FLUORESCENCE IN THE QUIESCENT ATMOSPHERE

The approach taken in this modeling effort is to assume a range of steady neutral atmospheres and to examine how various vibrational excitation and de-excitation mechanisms operate on the model atmospheres to produce NO vibrational radiation. The modeling is limited to altitudes above 90 km where the vibrational bands of interest are optically thin.

The dominant collisional excitation mechanism at these altitudes appears to be the reaction

$$NO(v) + O \xrightarrow{k_{1,v}} NO(v-n) + O \quad , \tag{B1}$$

where v represents vibrational level. The room temperature rate constant for deactivation of NO(v=1) by oxygen atoms has recently been measured[7] to be

3. Degges, T.C. (1971) Vibrationally excited nitric oxide in the upper atmosphere, Appl. Opt. 10:1856.

4. Ogawa, T. (1976) Excitation processes of infrared atmospheric emissions, Planet. Space Sci. 24:749.

5. Gordiets, B.F., Markov, M.N., and Shelepin, L.A. (1978) I. R. radiation of the upper atmosphere, Planet. Space Sci. 26:933.

6. Bishop, R.H., Shaw, A.W., Han, R.Y., and Megill, L.R. (1974) Infrared processes in the auroral zone, J. Geophys. Res. 79:1729.

7. Fernando, R.P., and Smith, I.W.M. (1979) Vibrational relaxation of NO by atomic oxygen, Chem. Phys. Lett. 66:218.

6.5×10^{-11} cm^3/sec in reasonable agreement with both theory[8] and a higher temperature shock tube measurement.[9] Reaction (B1) has been written in its general form inasmuch as the theoretical study of this reaction indicates that the total rate constant for deactivation of NO vibrational level v by oxygen atoms is independent of vibrational level and that multi-quantum transitions are favored over single quantum. These issues are not relevant to the quiescent atmosphere where only v=1 is significantly excited but will become important in modeling the auroral atmosphere where higher vibrational levels are formed. Note that the rate constant for excitation of NO by O is just given by detailed balancing of the measured deactivation rate constant.

Another collisional quenching reaction of possible importance is

$$NO(v=1) + O_2 \xrightarrow{k_{2,1}} NO(v=0) + O_2 \qquad \text{(B2)}$$

which has been found[10,11] to have a room temperature rate constant of 3×10^{-14} cm^3/sec. Quenching of NO(v=1) by N_2 has been found to be inefficient[10] and plays no role in defining NO vibrational populations above 90 km. No other atmospheric species has a sufficiently high concentration to affect NO vibrational relaxation.

NO can also be created vibrationally excited[12-14] by the reaction

$$N(^4S) + O_2 \rightarrow NO + O \quad . \qquad \text{(B3)}$$

---

8. Quack, M., and Troe, J. (1975) Complex formation in reactive and inelastic scattering: statistical adiabatic channel model of unimolecular processes III, Ber. Bunsenges, Physik. Chem. 79:170.

9. Glanzer, K., and Troe, J. (1975) Vibrational relaxation of NO in collisions with atomic oxygen and chlorine, J. Chem. Phys. 63:4352.

10. Murphy, R.E., Lee, E.T.P., and Hart, A.M. (1975) Quenching of vibrationally excited nitric oxide by molecular oxygen and nitrogen, J. Chem. Phys. 63:2919.

11. Fernando, R.P., and Smith, I.W.M. (1981) Relaxation of NO(v=1) by radical species, J. Chem. Soc. Faraday Transactions 2, 77:459.

12. Hushfar, F., Rogers, J.W., and Stair, A.T., Jr. (1971) Infrared chemiluminescence of the reaction $N + O_2 \rightarrow NO + O$, Appl. Opt. 10:1843.

13. Whitson, M.E., Jr., Darnton, L.A., and McNeal, R.J. (1976) Vibrational energy distribution in the NO produced by the reaction of $N(^4S)$ with O_2, Chem. Phys. Lett. 41:552.

14. Rahbee, A., and Gibson, J.J. (1981) Rate constants for the formation of NO_4 in vibrational levels V 2 through 7 from the reaction $N(^4S) + O_2 \rightarrow NO + O$, J. Chem. Phys. 74:5143.

This reaction does not appear to be significant relative to the other mechanisms considered because of its low rate constant[15] of $4.4 \times 10^{-12}\ e^{-3220/T}\ cm^3/sec$. Specifically:

(1) The activation energy for this reaction is larger than that for direct excitation of NO(v=1) by O whereas the respective frequency factor is an order of magnitude lower;

(2) The N-atom concentration everywhere will be well below the O-atom concentration;

(3) Less than 20 percent of the NO created in Reaction (B3) will be formed vibrationally excited.[12, 14]

The remaining excitation mechanism to be considered is radiative pumping. The present modeling is limited to night-time conditions; however, in any event, "earthshine" radiation is of the same order as the solar flux at 5.4 μm, the wavelength region of the NO fundamental band (see for example, Ref. 3, Degges). The rate of NO(v=1) excitation per NO molecule due to absorption of "earthshine" radiation is

$$R_E = \frac{\pi I_\nu S}{hc\nu N_o}\ sec^{-1} \tag{B4}$$

where I_ν is the "earthshine" radiance at NO band center ν in $W/(cm^2\ sr)$, S is the band-strength of the fundamental band of NO, taken[16] as $113/(Ama\ cm^2)$, h is Planck's constant, c is the speed of light and N_o is Loschmidt's number. The "earthshine" radiance at 5.4 μm does not vary over the altitude range under study but does vary with latitude and season. Recent LOWTRAN 5 predictions[17] for six different "standard" atmospheres ranging from tropical to subarctic winter bracket the "earthshine" radiance at 5.4 μm between the values of 1.55 and $3 \times 10^{-7}\ W/(cm^2\ sr)$. The larger value has been used here for purposes of calculation. Radiative excitation of the first overtone band of NO by "earthshine" will be negligible because of the significantly lower "earthshine" radiance at 2.7 μm.

The remaining mechanisms considered in the modeling are spontaneous emission from the fundamental and first overtone bands of NO, that is,

---

15. Demore, W.B., et al (1979) Chemical kinetic and photochemical data for use in stratospheric modeling. Evaluation number 2, JPL Publ. 79-27.

16. Billingsley, F.P., II (1976) Calculated vibration-rotation intensities for $NO(x^2\pi)$, J. Molec. Spectrosc. 61:53.

17. Kneizys, F.X., Shettle, E.P., Gallery, W.O., Chetwynd, J.H., Jr., Abreu, L.W., Selby, J.E.A., Fenn, R.W., and McClatchey, R.A. (1980) Atmospheric transmittance/radiance: computer code LOWTRAN 5, AFGL-TR-80-0067, AD A088215.

$$NO(v) \xrightarrow{A_{v\rightarrow v-1}} NO(v-1) + h\nu \quad . \tag{B5}$$

$$NO(v) \xrightarrow{A_{v\rightarrow v-2}} NO(v-2) + h\nu \quad . \tag{B6}$$

The Einstein coefficients developed by Billingsley[16] have been employed.

The kinetic/radiative processes discussed above represent the dominant mechanisms which affect the vibrational mode of NO in the quiescent atmosphere. This set has been used with representative upper atmospheric configurations to provide model predictions of anticipated NO fluorescence profiles. The base for the model atmospheres, the O_2, N_2, and temperature profiles, has been taken from the 1976 U. S. Standard Atmosphere.[18] The definition of the O and NO profiles is more complicated because of the large variability of these species in the upper atmosphere.

Atomic oxygen is a major constituent of the atmosphere at altitudes above 100 km and representative profiles of this species are generally included in standard atmospheres (for example, the U. S. Standard Atmosphere, 1976). Direct measurements of mesospheric oxygen atom concentrations have built up considerably in the last decade. Swider[19] has reviewed such measurements performed prior to 1977. A number of additional measurements have been performed since then;[20-29] and these are primarily rocket-borne measurements utilizing either a mass spectrometer or an oxygen resonance lamp. In several instances these observations fall considerably below the concentrations listed in "standard atmospheres." Indeed, it has been suggested[24] that oxygen atom concentrations in auroral regions are typically lower than anticipated. Alternatively, other measurements[26, 28, 29] exhibit much higher peak oxygen atom concentrations. The observed range in peak O-atom concentrations is a factor of 20. It is not clear whether this large variation is due to natural variability or measurement uncertainties.

Two characteristic oxygen atom profiles have been chosen as "representative" for modeling purposes; these are shown in Figure B1. The higher of the two profiles is a standard,[18] while the other is taken to be representative of lower oxygen profiles reported in a number of the more recent studies. The effect of even higher O-atom concentrations will be readily educible from the trends of the model predictions. Many of the measurements reported above were limited to altitudes below 140 km; the "low O" profile was purposely chosen to approach the standard atmosphere at higher altitudes asymptotically. Note that in the case of

---

Because of the large number of references cited above, they will not be listed here. See References, page 165.

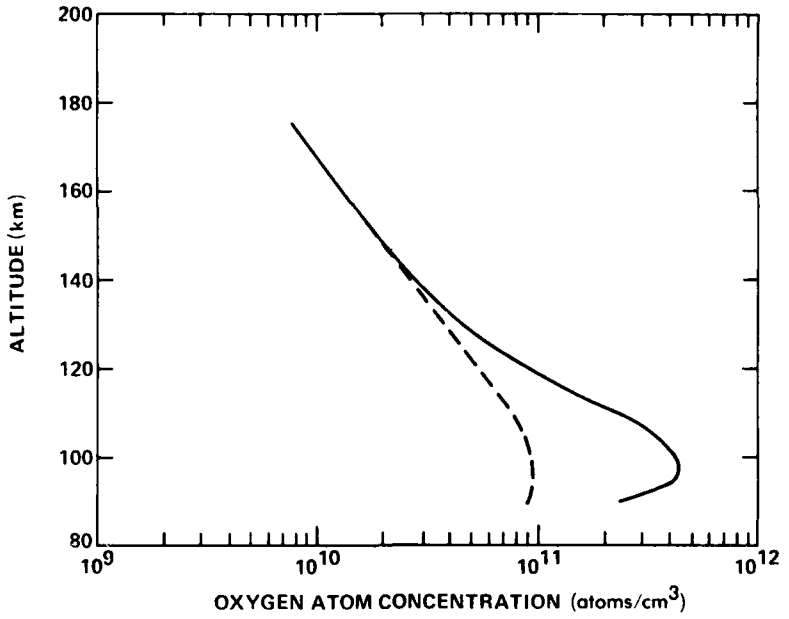

Figure B1. Representative Oxygen Atom Profiles. —— U. S. Standard Atmosphere, 1976, --- "Low O" profile

the "low O" profile, the corresponding O_2 profile was adjusted so as to maintain the proper ratio of N to O.

The NO concentration profile in the upper atmosphere is more variable than that for oxygen atoms, varying significantly with latitude and geomagnetic activity. Large enhancements in NO density are anticipated during auroral events. Upper atmospheric NO concentrations are typically deduced via UV absorption/fluorescence techniques, however, mass spectrometric measurements have been performed and furthermore, NO concentrations can also be inferred from measured ionic concentrations.[30] Upper atmospheric NO measurements prior to 1977 have been reviewed by Swider.[19] A number of measurements have been performed since then.[1,30,31,32,33,34-36] These measurements scatter over more than two orders of magnitude in the altitude range of interest. Two generic NO profiles have been used in the modeling and these are displayed in Figure B2. The lower of the two profiles is meant to be representative of the median of the available measurements while the larger is typical of NO concentrations predicted to develop in regions of strong auroral activity.[37-40]

Because of the large number of references cited above, they will not be listed here. See References, page 165.

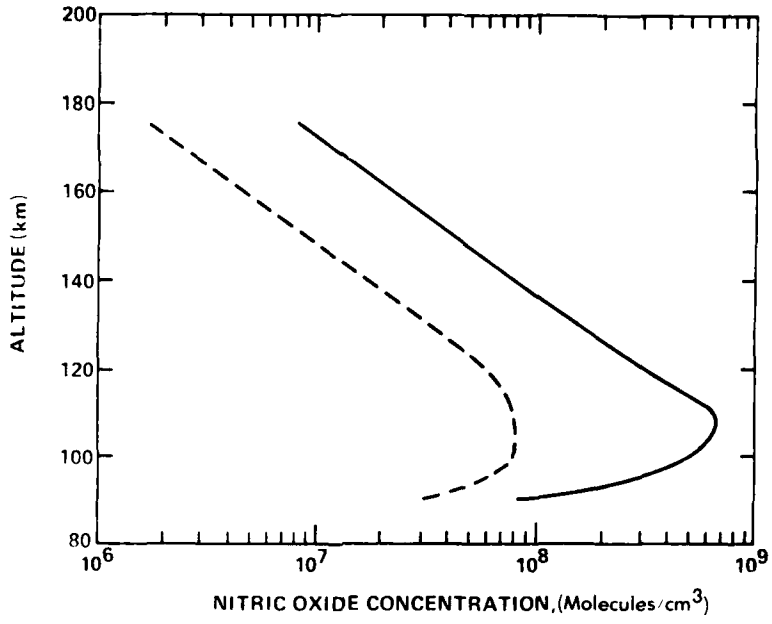

Figure B2. Generic NO Profiles, —— Auroral NO, --- Median NO

The NO and O profiles defined above have been used in conjunction with the standard atmosphere and Reactions (B1) through (B6) to provide predictions for generic NO radiation levels in the quiescent atmosphere. Figure B3 shows resultant predictions for the characteristic vibrational temperature between NO levels v=1 and 0 for the two oxygen atom profiles of Figure B1, as contrasted with the kinetic temperature. The vibrational temperatures are of course, independent of the NO profile used.

As can be seen, the NO vibrational temperature exceeds the kinetic temperature at altitudes below 110 km, reflecting the dominance of "earthshine" excitation at these altitudes. The situation reverses at higher altitudes with the NO vibrational temperature peaking at approximately 415 K, well below the kinetic temperature. Note that the difference in predictions developed for the two oxygen atom profiles is not large.

The predicted total NO fundamental band column intensities (zenith look) corresponding to these predictions are shown in Figure B4. The four curves displayed correspond to predictions for high and low O-atom profiles for both NO profiles. As can be seen, varying the O-atom profile produces little change in the radiation level. Total integrated column intensities can be of order 10^{-8} W/(cm^2 sr) and peak values are achieved at altitudes of about 120 km, that is,

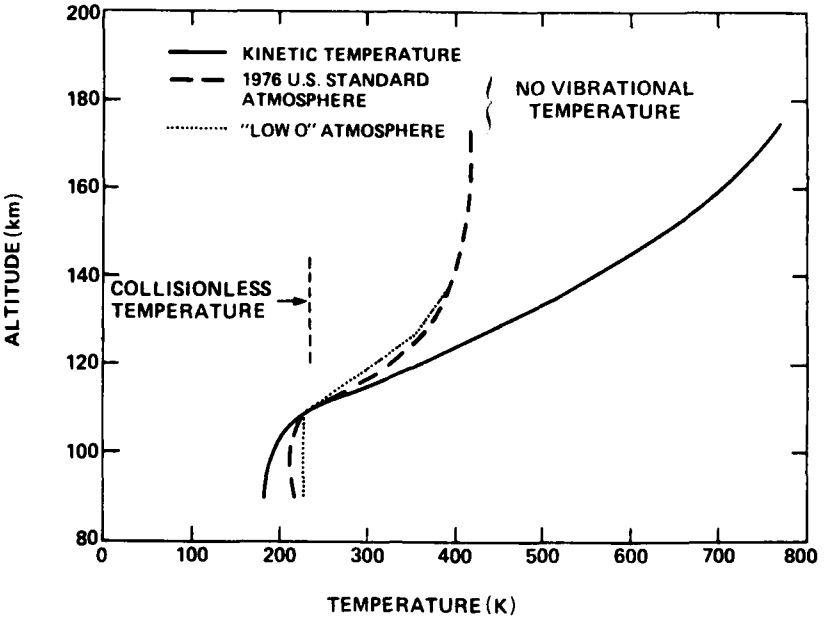

Figure B3. Kinetic and Predicted NO Vibrational Temperatures for the Quiescent Atmosphere

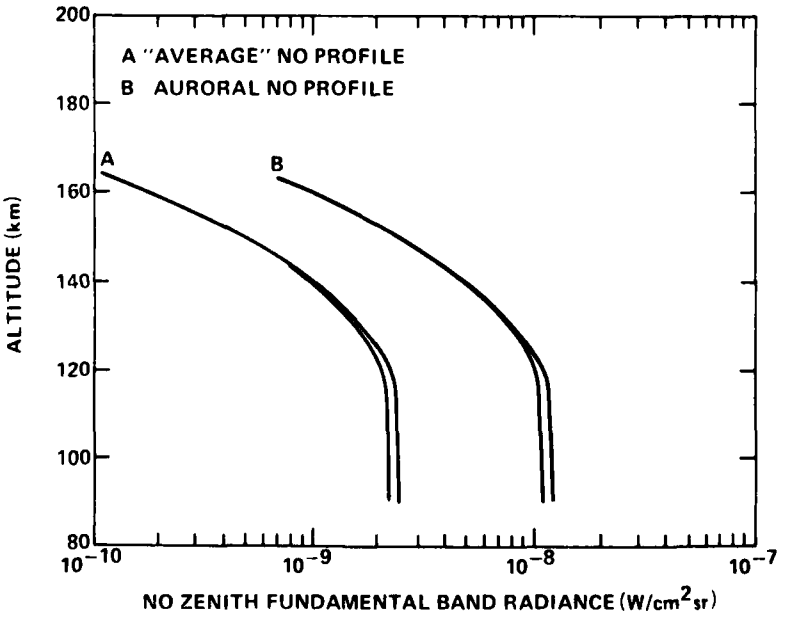

Figure B4. Predicted Zenith NO Band Column Intensity vs Altitude for Various Model Quiescent Atmospheres

the major fraction of NO radiation originates at altitudes above 120 km. This latter point is best seen by examining the predicted altitude variation in the NO volume emission rate as shown in Figure B5 for the U. S. Standard atmosphere O-atom profile and the auroral NO profile. This result is typical of all four predictions and the observed altitude variation primarily reflects the interplay of the O and NO profiles and the kinetic temperature through Reaction (B1).

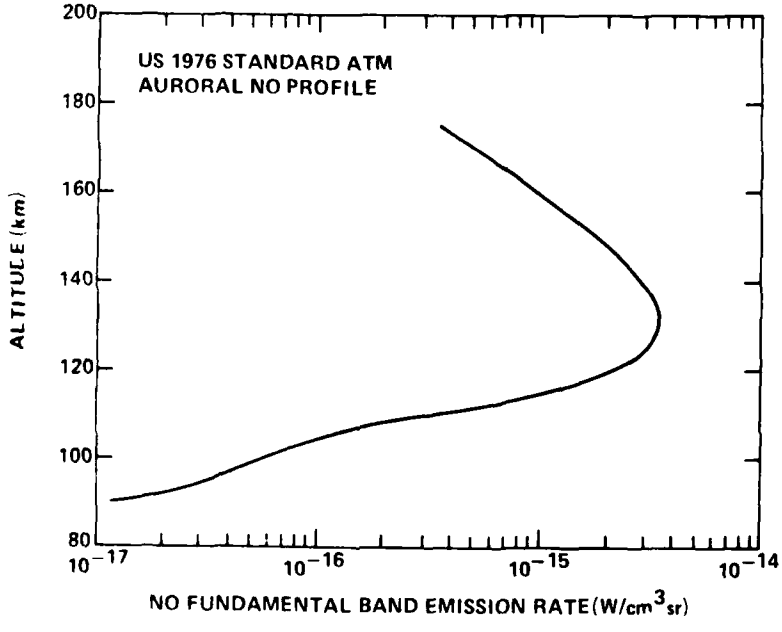

Figure B5. Local NO Fundamental Band Radiance vs Altitude, Quiescent Atmosphere

It is of some interest to compare these predictions with available measurements. Figure B6 shows three zenith-look measurements that are representative of northern latitudes. These were taken in either the quiescent atmosphere or weak auroras, on both rocket upleg and downleg, as part of the ICECAP program.[41-43] The data presented are from rocket flights 18.205-1, 18.219-1, and NJ-74 and have been scaled from peak radiances presented by Stair et al[41] and Hurd et al[42] to band radiances using representative NO bandwidths. (This scaling introduces an uncertainty of at most a factor of 2.) No significant variation is seen in the three cases, although the measurements were performed under

References 41 to 43 will not be listed here. See References, page 166.

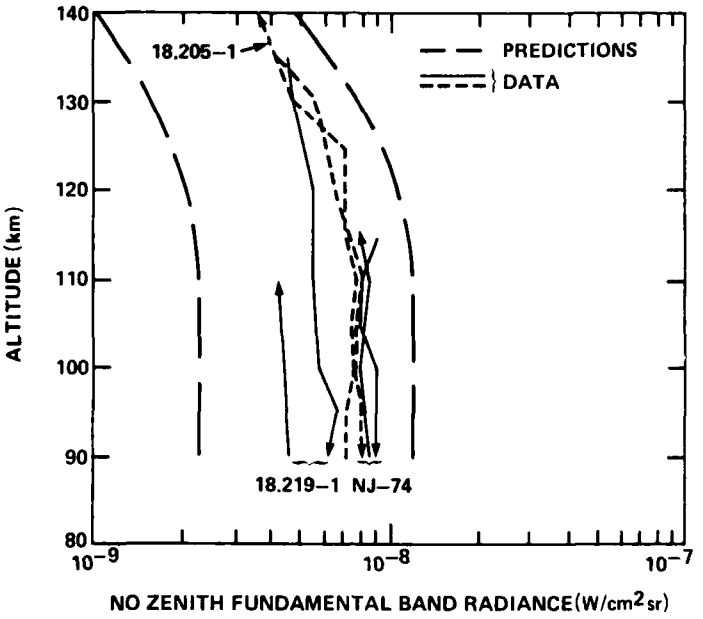

Figure B6. NO Fundamental Column Band Intensity vs Altitude, Data, and Predictions

varying levels of auroral activity. It has been concluded[42, 43] on the basis of such results that weak auroral activity does not lead to a significant enhancement in NO fundamental band fluorescence. Shown for comparisons are the highest and lowest of the predictions from Figure B4. As can be seen, the predictions nicely bracket the data and furthermore, exhibit similar trends with altitude. The data are closer in magnitude to the higher prediction as would be anticipated for measurements performed in auroral regions. It appears that the existing data base can be readily interpreted within the framework of the quiescent atmosphere model described above. Note that no predictions have been presented for the NO first overtone band; predicted NO vibrational temperatures in the quiescent atmosphere are so low that radiation levels from this band will be negligibly small.

B3. NO FLUORESCENCE IN THE AURORALLY EXCITED ATMOSPHERE

During an aurora the electron energy dosing of the upper atmosphere results in the production of a number of metastable states such as $N(^2D, ^2P)$, $N_2(A^3\Sigma)$, $O_2(^2\Delta, 2\Sigma)$ which are not necessarily present in the quiescent atmosphere.

Subsequent reactions involving those species can provide additional sources for the production of vibrationally excited NO. Specifically, the reaction

$$N(^2D) + O_2 \rightarrow NO + O \qquad \text{(B7)}$$

has been shown[44] to produce NO vibrationally excited up to at least v=12. (It has been suggested[45] that the quenching of $N_2(A)$ by O_2, O could also lead to NO formation. There has been, as yet, no evidence that such reactions occur and this possibility will not be pursued in the present effort.)

The prediction of NO radiance levels arising from Reaction (B7) involves several distinct steps. In the first place, the production efficiency of $N(^2D)/NO$ per auroral electron-ion pair must be defined. It will be seen that this quantity is a function of both the neutral and the ionic properties of the atmosphere. Next, the altitude-dependent electron-ion pair production rate must be specified; this, of course, will be a function of both the auroral intensity and penetration strength. Finally, once the production rate for NO(v) is specified, the relaxed distribution must be evaluated. This requires determination of the steady balance between Reaction (B7) and Reactions (B1), (B2), (B5), and (B6). Each of these steps are discussed in turn below.

B3.1. $N(^2D)/NO$ Production Efficiencies

The dominant mechanisms for the formation of $N(^2D)$ atoms in the aurorally excited E-region are presently thought to be dissociative recombination of NO^+,

$$NO^+ + e \rightarrow a_1\, N(^2D) + (1 - a_1)\, N(^4S) + O \quad , \qquad \text{(B8)}$$

ionic interchange reactions between nitrogen ions and atomic and molecular oxygen,

$$N_2^+ + O \rightarrow a_2\, N(^2D) + (1 - a_2)\, N(^4S) + NO^+ \qquad \text{(B9)}$$

$$N^+ + O_2 \rightarrow a_3\, (N^2D) + (1 - a_3)\, N(^4S) + O_2^+ \quad . \qquad \text{(B10)}$$

---

44. Kennealy, J. P., DelGreco, F. P., Caledonia, G. E., and Green, B. D. (1978) Nitric oxide chemiexcitation occurring in the reaction between metastable nitrogen atoms and oxygen molecules, J. Chem. Phys. 69:1574.

45. Swider, W. (1976) Atmospheric formation of NO from $N_2(A^3\Sigma)$, Geophys. Res. Lett. 3:335.

and direct electron impact dissociation of N_2, encompassing the two reactions

$$e + N_2 \rightarrow e + a_4\, N(^2D) + (2 - a_4)\, N(^4S) \qquad \text{(B11)}$$

and

$$e + N_2 \rightarrow e + a_5\, N(^2D) + (1 - a_5)\, N(^4S) + N^+ \quad . \qquad \text{(B12)}$$

The available experimental information on the branching ratios for Reactions (B8) - (B12) is relatively sparse. The $N(^2D)$ production efficiency of Reaction (B8) has been measured in the laboratory[46] to be $a_1 = 0.76$. There appear to be no laboratory measurements of the branching ratios for Reactions (B9) and (B10). Aeronomic estimates, based upon a kinetic interpretation of thermospheric measurements of $N(^2D) \rightarrow N(^4S)$ emission at 5200 Å, imply that a_2 and a_3 are near unity.[47] The uncertainty in these estimates, particularly in Reaction (B10) (see below), could be large and laboratory validation would be useful.

There have been no laboratory measurements of the branching ratios for Reactions (B11) and (B12) and aeronomic modelers typically assume[37, 38, 47] values of a_4 between 1 and 2. Several recent studies may now be used to provide a firmer estimate for the production rate of $N(^2D)$ by Reactions (B11) and (B12). The first of these is a detailed theoretical study on electron/proton energy degradation in air.[48] In this analysis a painstakingly developed set of cross-sections for electron impact excitation of O_2/N_2 were used to specify species production efficiencies in electron irradiated air. It was found in this analysis that the production efficiency for the sum of N and N^+ ions makes a rapid asymptotic approach with increasing electron energy to 1.27/ion-pair in air where, after adjusting the predictions for radiative cascade of highly excited nitrogen atoms to the ground or lowest metastable states, the production efficiencies of $N(^4S)$, $N(^2D)$, $N(^2P)$, and N^+ are predicted to be in the proportion 0.59/0.43/0.09/0.16. Thus, the analysis of Porter et al[48] implies that approximately one-half of the nitrogen atoms produced by Reactions (B11) and (B12) will be formed in metastable states.

46. Kley, D., Lawrence, G.M., and Stone, E.J. (1977) The yield of $N(^2D)$ atoms in the dissociative recombination of NO^+, J. Chem. Phys. 66:4157.

47. Frederick, J.E., and Rusch, D.W. (1977) On the chemistry of metastable atomic nitrogen in the F-region deduced from simultaneous satellite measurements of the 5200 Å airglow and atmospheric composition, J. Geophys. Res. 82:3509.

48. Porter, H.S., Jackman, C.H., and Green, A.E.S. (1976) Efficiencies for production of atomic nitrogen and oxygen by relativistic proton impact in air, J. Chem. Phys. 65:154.

It should be noted that this result is specific to a 21 percent O_2/79 percent N_2 mixture, whereas the E-region atmospheric composition does exhibit large ambient oxygen atom concentrations. An electron energy deposition code[49] was exercised to determine the potential effect of varying atmospheric composition on the efficiency for production of metastable nitrogen atoms. The most recent compilation of excitation cross-sections for O_2, O, and N_2 were used as input to this code[50] and energy allocation predictions were performed for a range of conditions corresponding to the composition of the U. S. 1976 Standard Atmosphere over the altitude range of 90-140 km. The computer model used did not yield a direct prediction of the metastable atom creation efficiency as output, but did provide relative ionization rates. Interestingly enough, it was found that for the altitude range considered, the fractional production efficiency for N_2^+ and N^+ varied only slightly, exhibiting an average value of approximately 0.75 per ion pair. Thus it may be inferred that the relative production rates for metastable atoms predicted for room air will also be reasonably valid for atmospheric conditions under which atomic oxygen concentrations can exceed those of molecular oxygen.

Recently laboratory observations have been combined with auroral data for $N(^2P)$ radiative emission to provide estimates of 1.82, 1.36, 0.72, and 0.61 $\times$ 10^{-16} cm^2 for the relevant electron impact excitation cross-sections for $N(^4S)$, $N(^2D)$, $N(^2P)$, and N^+ production, respectively, at an electron energy of 100 eV.[51] Scaling these cross-sections directly for ion pair production in air results in predicted excitation efficiencies per ion pair for $N(^4S)/N(^2D)/N(^2P)/N^+$ of 0.57/0.34/0.23/0.18 atoms, respectively. Thus this analysis suggests that 0.57 metastable nitrogen atoms are created per ion pair in close agreement with the prediction of Porter et al[48] although this latter analysis predicts a larger proportion of the metastables to be in the ^2D configuration. Furthermore, the total production rate of N and N^+ as deduced from the cross-sections of Zipf et al[51] is 1.32 per ion pair, again in good agreement with the analysis of Porter et al.[48]

In the present analysis all nitrogen atom metastables have been treated as if they are in the ^2D configuration. The effect of this approximation on the following predictions is not anticipated to be large, inasmuch as the only important auroral sources of $N(^2P)$ appear to be Reactions (B11) - (B12) and even for these reactions

---

49. Peterson, L. R., Sawada, T., Bass, J. N., and Green, A. E. S. (1973) Electron energy deposition in a gaseous mixture, Computer Phys. Comm. 5:239.

50. Jackman, C. H., Garvey, R. H., and Green, A. E. (1977) Electron impact on atmospheric gases I. Updated cross-sections, J. Geophys. Res. 82:5081.

51. Zipf, E. C., Espy, P. J., and Boyle, C. F. (1980) The excitation and collisional deactivation of metastable $N(^2P)$ atoms in auroras, J. Geophys. Res. 85:687.

$N(^2D)$ is predicted to be the dominant metastable produced. Based upon the results discussed above, a production efficiency of 0.55 $N(^2D)$ atoms per ion pair produced in air has been assumed for the direct electron impact dissociation of N_2 by Reactions (B11) and (B12); this value is taken to be invariant over the altitude range of 90-180 km.

From a modeling point of view, it is very convenient to discuss $N(^2D)$ production relative to the ion pair production rate q_e and thus the reaction efficiencies of Reactions (B8) - (B10) will also be recast into production efficiency per ion pair in air. The positive ions created in electron irradiated air are those of atomic and molecular oxygen and nitrogen: however, in the E-region a number of ion/neutral charge exchange and interchange reactions occur on time scales short relative to electron-ion recombination with the result that the primary E-region positive ions are found to be O_2^+ and NO^+,[52] with NO^+ being the dominant of the two in auroral regions.[37, 53, 54] If NO^+ were the only positive ion then the rate of production of $N(^2D)$ via Reaction (B8) would be $a_1 = 0.76$ per ion pair. Since finite concentrations of O_2 will be present, the actual production rate will be given by the quantity $F_1 a_1$ per ion pair where F_1 is defined by

$$F_1 = (1 + k_a \overset{+}{O_2}/k_b NO^+)^{-1} \quad , \tag{B13}$$

where k_a and k_b are the rate constants for electron-ion recombination of O_2 and NO^+, respectively. Note that for the E-region, F_1 will typically be near unity, both because the quantity O_2/NO will be less than one and because $k_b \approx 2\ k_a$.[54] The quantity F_1 can be evaluated directly either by using model predictions or, as in the present analysis, through the use of measured profiles of ionic concentrations.

With regard to the ionic interchange in Reaction (B9), approximately 75 percent of the ion pairs created in electron irradiated air are in the form N_2^+/N^+, and it is predicted that 0.16 N^+ are created per ion pair;[48] thus the production rate of N_2^+ is 0.59 per ion pair. The N_2^+ so formed will either react with oxygen atoms, Reaction (B9), or with oxygen molecules via

---

52. Swider, W. (1975) The D- and E-regions, p. 259 of Atmospheres of Earth and the Planets, B.M. McCormac, Ed., D. Reidel Publ. Co., Dordrecht-Holland.

53. Narcisi, R.S., Sherman, C., Wlodyka, L.E., and Ulwick, J.C. (1974) Ion composition in an IBC class II aurora 1. Measurements, J. Geophys. Res. 79:2843.

54. Swider, W., and Narcisi, R.S. (1974) Ion composition in an IBC class II aurora. 2. Model, J. Geophys. Res. 79:2849.

$$N_2^+ + O_2 \xrightarrow{k_{14}} O_2^+ + N_2 \quad . \tag{B14}$$

Therefore the $N(^2D)$ production rate per ion pair due to Reaction (B9) may be specified by

$$F_2 = 0.59\, a_2\, (1 + k_{14}\, O_2/k_9 O)^{-1} \tag{B15}$$

where k_9 and k_{14} have been measured to be $1.4 \times 10^{-10}\,(T/300)^{-0.44}$ cm^3/sec for $T < 1500$ K[55] and 5×10^{-11} cm^3/sec for $T < 900$ K,[56] respectively. It is to be noted that the contribution of Reaction (B9) to the total $N(^2D)$ production rate is controlled by the properties of the ambient atmosphere.

The last reaction to be considered, that between N^+ and oxygen molecules, Reaction (B10), does not significantly impact the analysis in that there are only 0.16 N^+ ions formed per ion pair in air. Reaction (B10) has another branch,

$$N^+ + O_2 \rightarrow NO^+ + O \tag{B16}$$

and the best experimental information[56] suggests that branches (B10) and (B16) are equally probable. Since these latter reactions represent the dominant loss mechanism for N^+ in the E-region, the assumption that a_3 is unity results in an estimated $N(^2D)$ creation rate of 0.08 per ion pair due to Reaction (B10).

Once $N(^2D)$ atoms are formed, they will subsequently react to form vibrationally excited NO via Reaction (B7) or be collisionally quenched by oxygen atoms via

$$N(^2D) + O \rightarrow N(^4S) + O \tag{B17}$$

and consequently the fraction of $N(^2D)$ atoms which ultimately react to form NO may be specified by

$$F_{NO} = \left(1 + \frac{k_{17} O}{k_7 O_2}\right)^{-1} \quad . \tag{B18}$$

---

55. McFarland, M., Albritton, D.L., Fehsenfeld, F.C., Ferguson, E.E., and Schmeltekopf, A.L. (1974) Energy dependence and branching ratio of the $N_2^+ + O$ reaction, J. Geophys. Res. 79:2925.

56. Lindinger, W., Fehsenfeld, F.C., Schmeltekopf, A.L., and Ferguson, E.E. (1974) Temperature dependence of some ionospheric ion-neutral reactions from 300-900 K, J. Geophys. Res. 79:4753.

The room temperature rate constant for Reaction (B7) is well defined; a value of $k_7 = 5.2 \times 10^{-12}$ cm^3/sec has been used in the present study.[57] Furthermore, k_7 has been found to exhibit a negligible temperature dependence over the range T = 237 - 365 K.[58]

The magnitude of the rate constant of Reaction (B17) is more controversial. Davenport et al,[59] in an experimental study, deduced that

$$k_{17} = 4 \times 10^{-12} e^{-250/T} \text{ cm}^3/\text{sec}$$

where the activation energy was evaluated from a limited data base spanning the temperature range of 315-400 K. In contrast to this Frederick and Rusch[47] performed a detailed analysis of the 5200 A ($N(^2D) \rightarrow N(^4S)$) visible airglow data obtained on Atmosphere Explorer C and D during both day and night conditions and deduced that the rate constant for Reaction (B17) must be 4×10^{-13} cm^3/sec. Indeed, they suggest that use of the rate constant of Davenport et al[59] would require the specification of a new, as yet unidentified, source of $N(^2D)$ in the upper atmosphere. Further studies of this rate constant will be required in order to clear up this discrepancy.

It can be seen that the ultimate production efficiency for vibrationally excited NO will be a function of both the neutral and ionic composition of the disturbed atmosphere. The two neutral atmospheres described earlier have once again been used for purposes of calculation. Note that the NO concentration is not relevant to this analysis. The positive ion profiles employed correspond to those measured in a specific IBC class II aurora[53] and may be considered typical. These measurements were available only between 90 and 145 km and were extrapolated to higher altitudes under the assumptions that the NO^+/O_2^+ ratio remained the same as the measured value at 145 km and that the ion pair production rate scaled linearly with atmospheric density.

The predicted efficiencies for $N(^2D)$ and NO production are shown in Figure B7. As can be seen, the predicted $N(^2D)$ production efficiency per ion pair varies between 1.1 and 1.65 and is not significantly different for the two model atmospheres employed. The altitude variation observed is primarily due to the

---

57. Husain, D., Mitra, S.K., and Yound, A.N. (1974) Kinetic study of electronically excited nitrogen atoms $N(2\,^2D_J,\ 2\,^2P_J)$, by attenuation of atomic resonance radiation in the vacuum ultra-violet, J. Chem. Soc. Farad. Trans. II 70:1721.

58. Slanger, T.G., Wood, B.J., and Black, G. (1971) Temperature coefficients for $N(^2D)$ quenching by O_2 and N_2O, J. Geophys. Res. 76:8430.

59. Davenport, J.E., Slanger, T.G., and Black, G. (1976) Quenching of $N(^2D)$ by N_2 and H_2O, J. Chem. Phys. 64:4442.

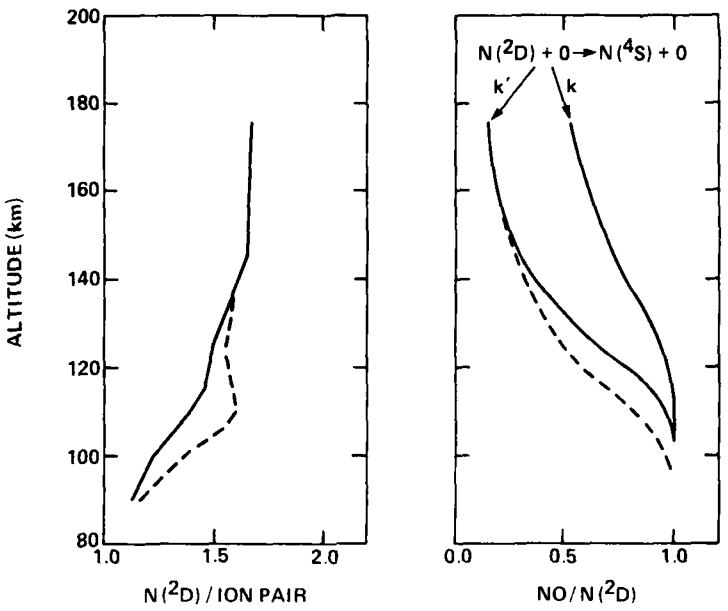

Figure B7. Predicted $N(^2D)$ and NO Production Efficiencies. ——"Low O" atmosphere; --- U. S. Standard Atmosphere; 1976. $k = 4 \times 10^{-13}$ cm^3/sec, $k' = 4 \times 10^{-12}$ exp (-250/T) cm^2/sec

increased contribution of Reaction (B9) with increasing O/O_2 ratio. The fraction of the $N(^2D)$ atoms that are converted to NO also does not exhibit a large sensitivity to the choice of atmosphere, varying at the most by 40 percent; however, the sensitivity to the specification of the rate constant for Reaction (B17) is quite pronounced, reflecting the importance of this reaction in the $N(^2D)$ kinetics. Note that only some 20 percent of the $N(^2D)$ atoms produced above 150 km will ultimately lead to production of NO.

B3.2. Ion Pair Production Rates

As stated earlier, the ion pair production rate is very specific to both the intensity and penetration strength of the aurora. In general, modelers of auroral chemistry will select a specific auroral dosing function and then calculate the associated altitude profiles of ionic and neutral species.[5,6,37,38,39] The opposite tack has been taken in the present work; positive ion profiles measured for a specific aurora (also as part of the ICECAP program) have been used to evaluate $N(^2D)$ production efficiencies. These same ionic profiles can be utilized to determine the electron-ion pair production rate. This is possible because in the steady state the ion production rate must equal the loss rate. For the present

case,[53] the dominant steady state ions are NO^+ and O_2^+ and therefore, the production rate is given by

$$q_e = (k_a O_2^+ + k_b NO^+)(e) \tag{B19}$$

where k_a and k_b are the electron-ion recombination rate coefficients previously used in Reaction (B13) and e is the electron density, which at the altitudes of interest may be equated to the total positive charge.

Equation (B19) has been evaluated using the rate constants reported by Swider and Narcisi[54] and the ion densities of Narcisi et al.[53] The ion densities were only available for altitudes below 145 km and q_e was assumed to scale linearly with atmospheric density at higher altitudes. The resulting altitude profile for the auroral electron-ion pair production rate is shown in Figure B8. The values are specific to a diffuse IBC class II aurora and it has been previously shown[54] that the use of Eq. (B19) provides values of q_e in good agreement with those determined independently from observations of the precipitating electron flux.

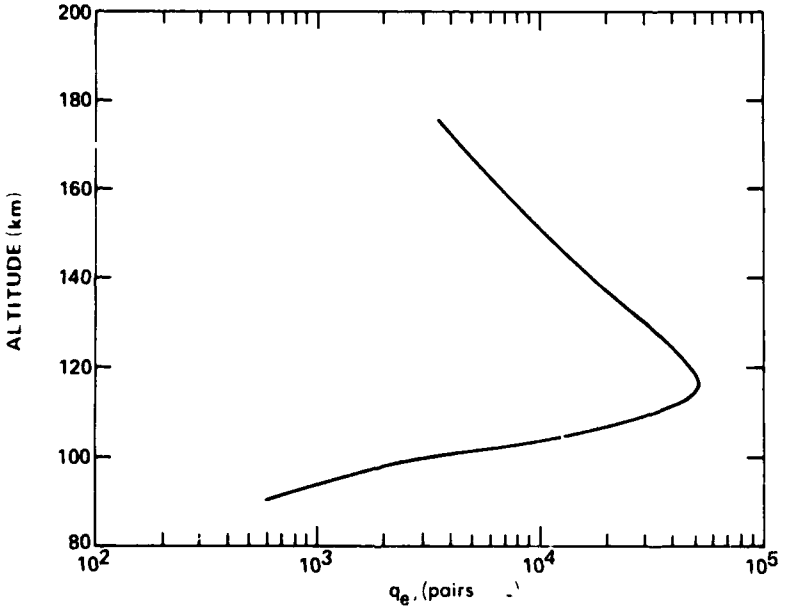

Figure B8. Deduced Electron-Ion Pair Production Rate vs Altitude for Diffuse IBC Class II Aurora

B4. NO INFRARED RADIATION

The $N(^2D)/NO$ production efficiencies and the electron-ion pair production rates developed in the previous two subsections may now be used to evaluate the additional level of NO fluorescence produced during an aurora. The kinetic mechanism that produces vibrationally excited NO is Reaction (B7) and the relative rates for producing vibrational levels 1 to 12 via this reaction have been taken from the work of Kennealy et al.[44] The dominant relaxation mechanisms for NO(v) are once again Reactions (B1), (B2), (B5), and (B6).

The rate constants for Reactions (B1) and (B2) must now be specified for vibrational levels v 1-12. As pointed out in Section B2, the available theoretical treatment[8] suggests that the rate constant for Reaction (B1) is independent of vibrational level and that the quenching of level v can lead to the population of all lower vibrational levels with multi-quantum transitions being favored. Predictions in the present analysis have been made under the limiting assumptions that quenching of NO(v) by O proceeds either in single-quantum transitions or leads directly to the ground state, that is,

$$NO(v) + O \rightarrow NO(v-1) + O \qquad \text{(B1a)}$$

or

$$NO(v) + O \rightarrow NO(0) + O \quad . \qquad \text{(B1b)}$$

When NO is quenched by O_2 [Reaction (B2)], the vibrational-level-dependent rate constants recently measured on the LABCEDE facility have been used.[60] These measurements indicate that the quenching rate constants for this process scale approximately as $v^{3/2}$. Once again it will be seen that NO quenching by O_2 is not an important process at altitudes above 100 km.

The master equation for vibrational relaxation of the population density of NO vibrational level v may be written as

$$\begin{aligned} d[NO(v)]/dt = {} & R_v + (k_{1,\,v+1}\,[O] + k_{2,\,v+1}\,[O_2] + A_{v+1,\,v})\,[NO(v+1)] \\ & + A_{v+2 \rightarrow v}\,[NO(v+2)] - (k_{1,\,v}\,[O] + k_{2,\,v}\,[O_2] + A_{v,\,v-1} \\ & + A_{v,\,v-2})\,[NO(v)] \quad , \quad v \geq 1 \quad , \end{aligned} \qquad \text{(B20)}$$

60. Green, B. D., Caledonia, G. E., and Murphy, R. E. (1981) The vibrational relaxation of NO(v 1-7) by O_2, J. Chem. Phys., 76:2441.

for the case of single quantum relaxation, for example, Reaction (B1a). Here R_v is the rate of production of NO(v) by Reaction (B7) and the quantities O and O_2 are the number densities of oxygen atoms and molecules, respectively. A similar equation pertains to multi-quantum relaxation, Reaction (B1b), with the exception that the term $k_{1,\,v+1}$ O, NO(v) on the right hand side of Eq. (B20) is eliminated. These sets of equations have been solved in the steady state limit, that is, dNO(v)/dt = 0, under the closure condition that NO(v > 12) ≡ 0, and for the two "model" atmospheres and two values of the rate constant for Reaction (B17).

Typical predictions for the auroral NO fundamental band zenith-look radiance for an IBC class II aurora evaluated under the various modeling assumptions outlined above are shown in Figure B9. Six different predictions are provided; these bracket the potential uncertainties in NO radiation intensity which can arise from kinetic uncertainties for the model atmospheres chosen. The predictions are in two sub-groups corresponding to the uncertainty in the recommended value of the rate constant for Reaction (B17). The difference between these two subgroups, a factor of 2-3 at all altitudes, thus reflects variations in the NO production rate R_v, as exemplified in Figure B7. Note that within each subgroup the specification of the model atmosphere does not provide for large differences in the band radiance. Two limiting cases are also shown. The first of these corresponds to the "low O" atmosphere, the lower rate constant for Reaction (B17) and radiative cascade as the only NO relaxation mechanism, and is meant to be an upper bound prediction within the overall constraints of the model. It is interesting to note that for this case the inclusion of collisional quenching produces less than a 20 percent change in total radiance. The second limiting case corresponds to the U. S. 1976 Standard Atmosphere, the larger rate constant for Reaction (B17), and multi-quantum collisional relaxation of NO (all previous predictions were for single quantum relaxation). This latter prediction should represent a lower bound for the radiance within the constraints of the model and is a factor of 3 below the previously discussed upper bound. Furthermore, it can be seen that multi-quantum relaxation provides for an approximately 30 percent decrease in predicted band radiance over that for single quantum relaxation.

Note that all the predicted NO fundamental band column intensities approach asymptotes at ≈ 110 km, implying that the major portion of the radiance arises at higher altitudes. This is in accord with the altitude dependence of the ion pair creation rate, shown in Figure B8. Indeed, the NO fundamental band volume emission rate is shown in Figure B10 for the two limiting cases discussed previously and it can be seen to have an altitude profile very similar to that of q_e, in line with the fact that radiative decay is a primary relaxation mechanism over the full altitude range of interest. Thus, not unexpectedly, the auroral NO radiation will closely mirror the auroral dosing profile.

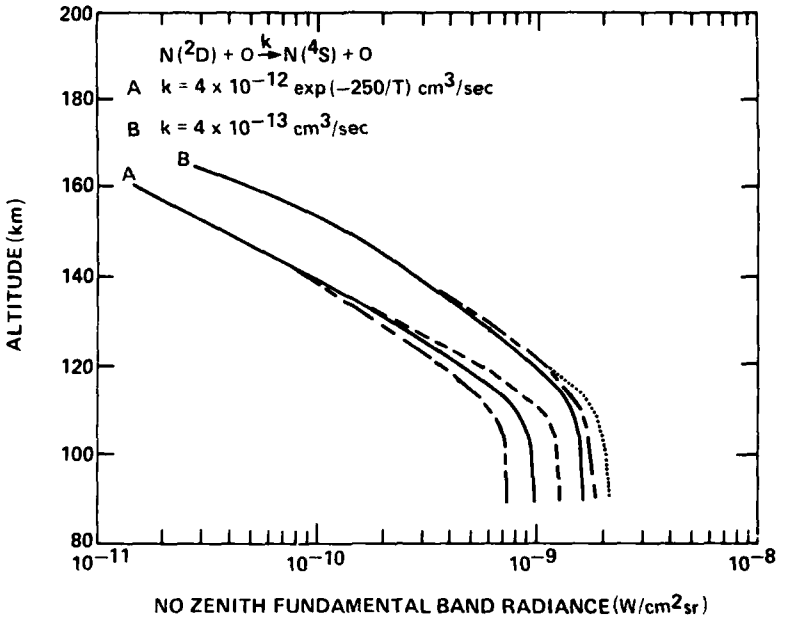

Figure B9. Predicted NO Zenith Fundamental Band Radiance vs Altitude for an IBC Class II Aurora, Single Quantum Transfer Predictions: ——, 1976 U. S. Standard Atmosphere; ---, "Low O" Atmosphere; . . ., "Low O" Atmosphere, Radiative only; — — —, Multi-Quantum Transitions, 1976 U. S. Standard Atmosphere

Similar predictions for the NO first overtone band zenith column intensity are shown in Figure B11, again for the two limiting cases. Note that the "high" and "low" predictions differ only by a factor of 2.3. It can be seen from comparison of Figures B9 and B11 that the first overtone band radiation, falling near 2.7 μm, has an intensity some 15-20 percent of that of the fundamental band. This observation is in sharp contrast to the case of the quiescent atmosphere where NO first overtone radiation is minuscule in comparison to that of the fundamental band, and is a direct result of the chemi-excitation Reaction (B7) which provides for the formation of highly vibrationally excited NO.

It can be of some interest to examine the predictions in light of local efficiencies per ion pair rather than total band radiance. Such predictions are shown for the fundamental and first overtone bands in Figures B12 and B13, respectively, for the two limiting cases and for one of the intermediate models. Shown are the number of photons radiated in each band per electron-ion pair created. It should be noted that the primary differences between the "upper" and "lower" bounds is the auroral efficiency for producing NO rather than any relaxation effects; this is

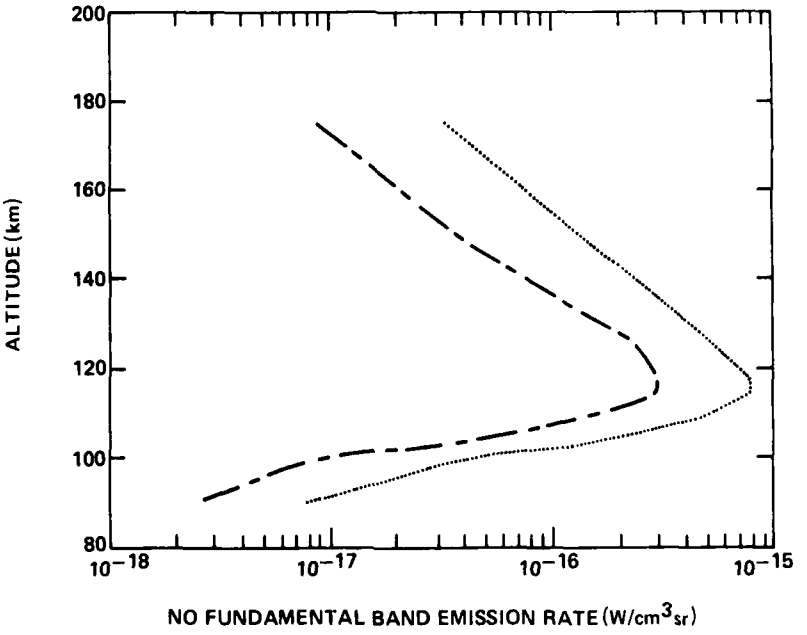

Figure B10. Local NO Fundamental Band Emission Rate vs Altitude in an IBC Class II Aurora: ..., "Low O" Atmosphere, Radiative Cascade Only, $k_{17} = 4 \times 10^{-13}$ cm^3/sec; — — — U. S. *Standard Atmosphere, Multi-quantum Relaxation,* $k_{17} = 4 \times 10^{-12} \exp(-250/T)$ cm^3/sec

also the cause of the observed decreasing photon efficiency with increasing altitude. The effect of collisional relaxation can be gauged by comparing the two predictions made for the model atmosphere, but with and without the quenching reactions included. As can be seen, collisional quenching (at least single quantum) produces at most a 30 percent reduction in radiation in either band over the altitude range considered.

The fundamental band efficiency was recently deduced to be approximately 2 photons/ion pair in a strong aurora.[61] Unfortunately this evaluation is uncertain by a factor of 2.5 and thus cannot be used to discriminate between the predictions of Figure B12.

One of the quantities of fundamental interest in the present effort is the specification of the NO vibrational population distribution during an aurora. It is, of course, the latter quantity which defines the spectral shape of the fundamental

---

61. Rawlins, W.T., Caledonia, G.E., Gibson, J.J., and Stair, A.T., Jr. (1981) Infrared emission from NO(Δv=1) in an aurora: spectral analysis and kinetic interpretation of HIRIS measurements, J. Geophys. Res. 86:1313.

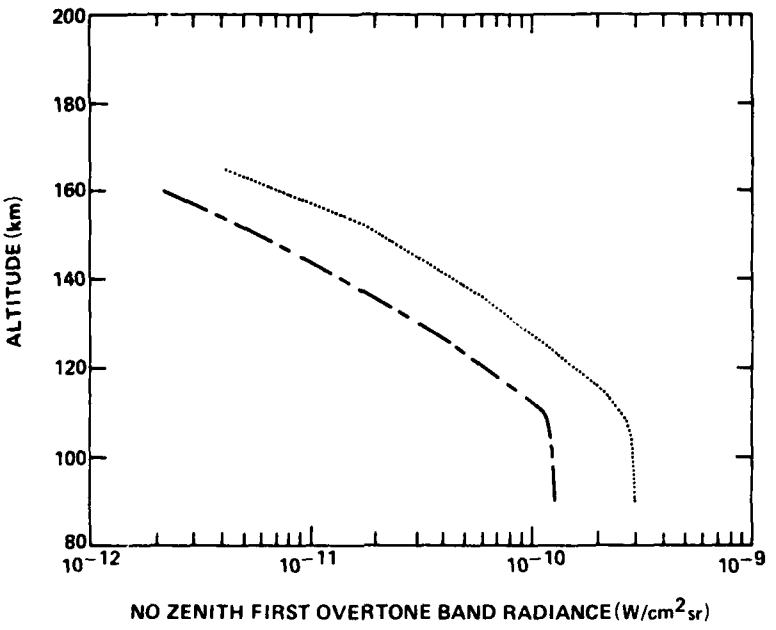

Figure B11. Predicted NO First Overtone Band Zenith Intensity vs Altitude for an IBC Class II Aurora: ...., "Low O" Atmosphere, Radiative Cascade Only, $k_{17} = 4 \times 10^{-13}$ cm^3/sec; — — —, U. S. 1976 Standard Atmosphere, Multi-Quantum Relaxation, k_{17} 4 × 10^{-12} exp (-250/T) cm^3/sec

and first overtone bands. A typical set of predicted NO vibrational populations is shown in Figure B14. These predictions span the altitude range of 100-160 km and are all normalized to the same NO creation rate for purposes of comparison. The majority of the predictions shown are for single quantum relaxation although the radiative cascade limit (labeled H = ∞) and one prediction for multi-quantum relaxation are also included. A number of salient features are evinced by this figure. First and foremost, the vibrational populations, although somewhat non-Boltzmann, are characterized by high characteristic vibrational "temperatures"; for example, the v 2/v - 1 "temperatures" span the range of 3400-7200 K for the single quantum relaxation predictions. Furthermore, the predicted distributions are nearly invariant at altitudes above about 120 km. Lastly it can be seen that the effects of collisional quenching are most pronounced at the lowest vibrational levels. Thus, with decreasing altitude the resultant band shape tends to be weighted more to the longer wavelengths.

Also shown in Figure B14 are two NO vibrational distributions inferred from HIRIS observations of NO fundamental band radiation in an IBC class III aurora.[61]

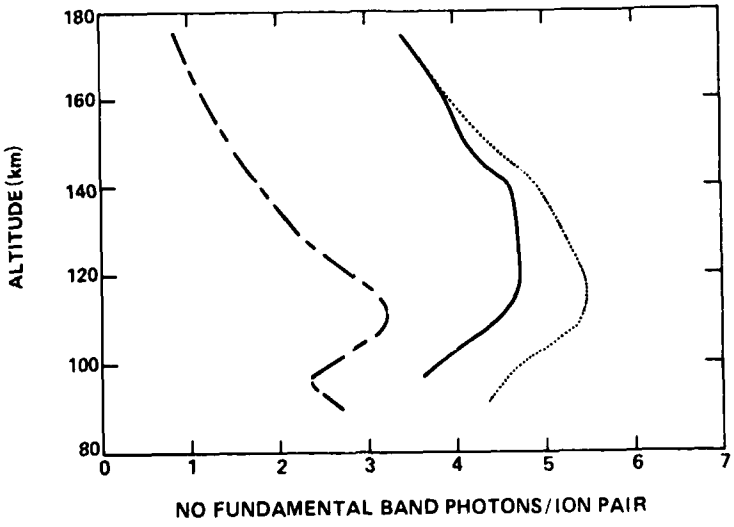

Figure B12. NO Fundamental Photons Per Ion Pair vs Altitude: ....., "Low O" Atmosphere, Radiative Cascade Only, $k_{17} = 4 \times 10^{-13}$ cm^3/sec; ——, Same Except Single Quantum Collisional Relaxation Included; —— – ——, U. S. 1976 Standard Atmosphere, Multi-Quantum Relaxation, $k_{17} = 4 \times 10^{-12} \exp(-250/T)$ cm^3/sec

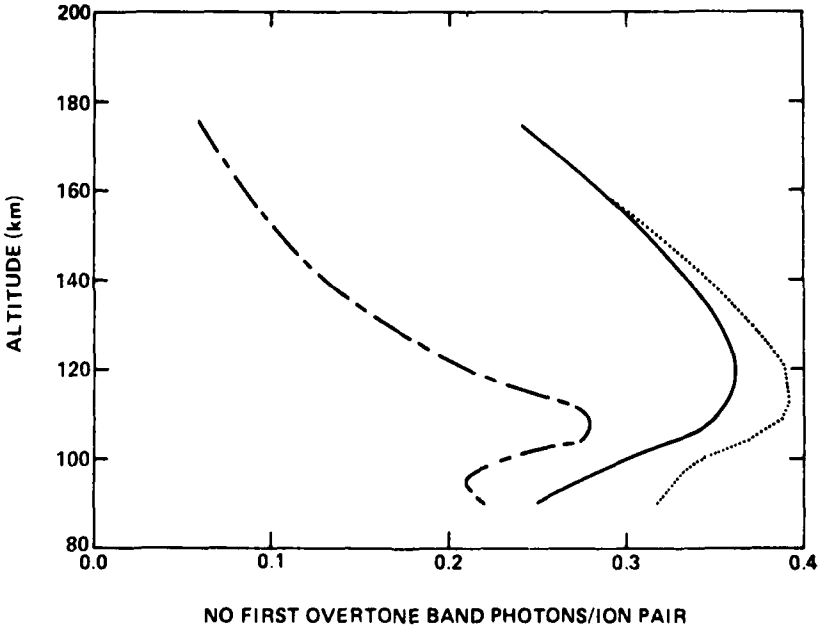

Figure B13. NO First Overtone Band Photons Per Ion Pair vs Altitude. Designations are as in Figure B12

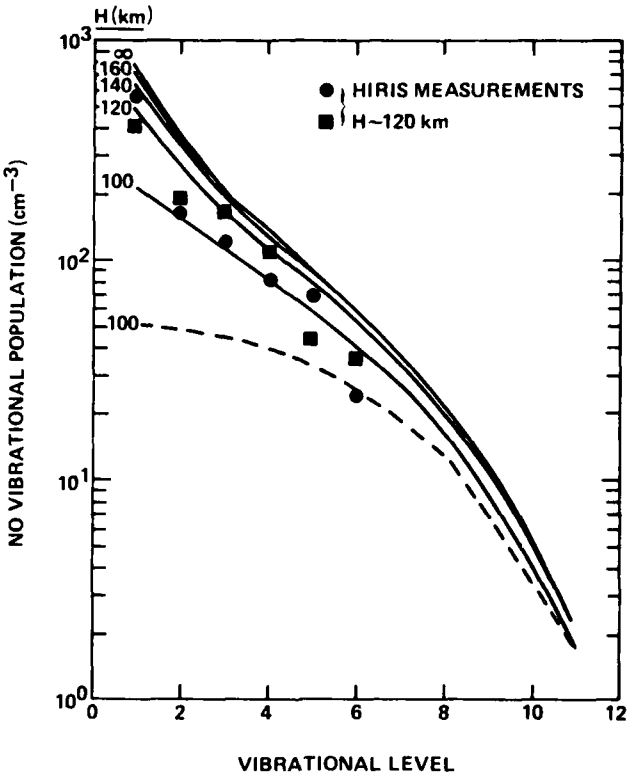

Figure B14. Predicted Auroral NO Vibrational Distributions at Several Altitudes for a Constant Creation Rate of $NO^+ = 10^4/cm^3$ sec, U. S. Standard Atmosphere; ——, Single Quantum Relaxation; - - - -, Multi-Quantum Relaxation

These measurements were taken at a platform altitude of about 120 km; however, because of instrumentation complications, they may be representative of the NO distribution at a different altitude. Nonetheless it can be seen that the data is in excellent agreement with the general trend of the theoretical predictions.

Next, we must compare the predicted auroral NO band intensities with the data base. It can be readily seen that the predicted auroral NO fundamental band zenith intensities of Figure B9 are considerably smaller than those predicted for the quiescent atmosphere as presented in Figure B4. This is consistent with the previously mentioned observation that NO radiation levels in an IBC class II aurora exhibited no enhancement over those observed for the quiescent atmosphere (see Figure B6 and text of Section B2). On the other hand, the predictions imply that an IBC class III aurora (a factor of 10 more intense) should exhibit an enhancement and indeed, this is in line with observations.

Shown in Figure B15 are upleg and downleg measurements of NO zenith fundamental band radiance observed in an IBC class III aurora (as reported in Baker et al,[42,43,62] scaled as described in Section B2) contrasted with similar measurements taken in the quiescent atmosphere and weaker aurora (< IBC II), as previously displayed in Figure B6. The auroral enhancement is clearly evident. One theoretical prediction is shown for comparison. This prediction is the sum of the previously predicted quiescent atmosphere radiance for the auroral region NO profile and the highest of the IBC II auroral NO predictions of Figure B9 multiplied by 10 for scaling to a class III aurora. The agreement between data and prediction is quite good in particular considering the fact that the aurora in question clearly exhibited a much deeper penetration profile than the IBC II aurora utilized in the modeling. Nonetheless, although the good agreement may be somewhat fortuitous, the comparison clearly demonstrates that the auroral observations can be readily interpreted within the framework of the present analysis.

62. Baker, K.D., Baker, D.J., Ulwick, J.C., and Stair, Jr., A.T. (1977) Measurements of 1.5-5.3 μm infrared enhancements associated with a bright auroral breakup, J. Geophys. Res. 82:3518.

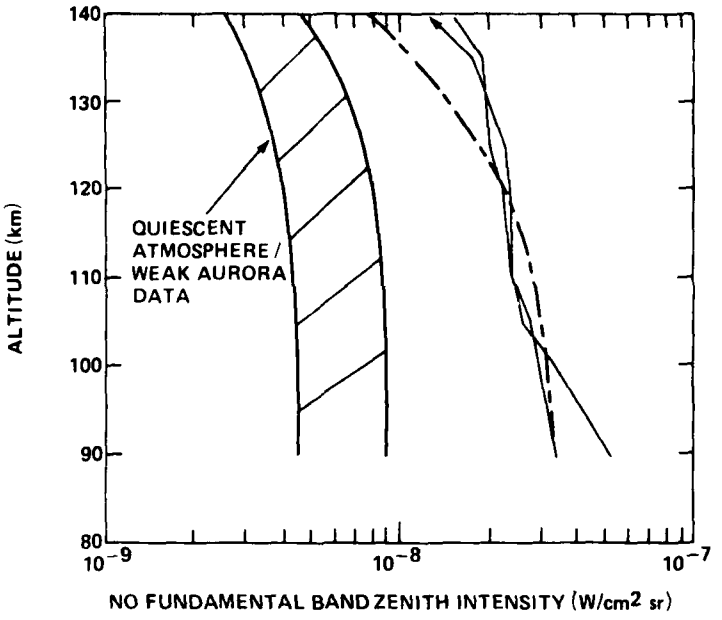

Figure B15. NO Fundamental Band Zenith Intensity vs Altitude for Several Scenarios; ——, Measured in an IBC III Aurora; --- Predicted

B5. SUMMARY AND CONCLUSIONS

A general model for the prediction of NO infrared radiation levels in the quiescent and aurorally excited upper atmosphere has been developed and exercised. The specific philosophy of the modeling was to evaluate NO radiation levels over a range of parameters characteristic of atmospheric variability and to identify those uncertainties in atmospheric properties and kinetic parameters that provide the largest uncertainties in predicted radiance levels.

In general it has been found that the available data base for upper atmospheric NO radiation can be readily understood in terms of the model and a number of salient features have been identified.

(1) The dominant excitation mechanism for NO in the quiescent upper atmosphere is the reaction $O + NO(v=0) \rightarrow O + NO(v=1)$, rather than radiative excitation.

(2) The largest change in predicted NO radiative levels is due to natural variations in the NO concentration rather than in the O concentration.

(3) Predicted NO vibrational temperatures in the quiescent atmosphere are < 420 K over the altitude range of 90-175 km.

(4) Significant enhancements over quiescent fundamental band radiative levels are not achieved in IBC class II or weaker auroras.

(5) For aurorally excited NO, first overtone radiative intensities are 15-20 percent of those of the fundamental band.

(6) Uncertainties in the collisional quenching kinetics of NO(v) do not produce large variations in total band radiation but can provide for significant changes in the spectral contents of the band.

(7) The uncertainty in the rate constant for the process $N(^2D) + O \rightarrow N(^4S) + O$ provides for factor of 2 uncertainty in auroral NO band radiances.

(8) The total auroral efficiency for producing NO infrared radiation is predicted to vary between 2.0 and 4.2 percent depending on the atmospheric properties and kinetic parameters employed.

(9) The auroral NO vibrational population distribution is predicted to be highly vibrationally excited in accord with recent observations.

References

1. Cravens, T.E., and Stewart, A.I. (1978) Global morphology of nitric oxide in the lower E region, J. Geophys. Res. 83:2446.
2. Kockarts, G. (1980) Nitric oxide cooling in the terrestrial atmosphere, Geophys. Res. Lett. 7:137.
3. Degges, T.C. (1971) Vibrationally excited nitric oxide in the upper atmosphere, Appl. Opt. 10:1856.
4. Ogawa, T. (1976) Excitation processes of infrared atmospheric emissions, Planet. Space Sci. 24:749.
5. Gordiets, B.F., Markov, M.N., and Shelepin, L.A. (1978) I. R. radiation of the upper atmosphere, Planet. Space Sci. 26:933.
6. Bishop, R.H., Shaw, A.W., Han, R.Y., and Megill, L.R. (1974) Infrared processes in the auroral zone, J. Geophys. Res. 79:1729.
7. Fernando, R.P., and Smith, I.W.M. (1979) Vibrational relaxation of NO by atomic oxygen, Chem. Phys. Lett. 66:218.
8. Quack, M., and Troe, J. (1975) Complex formation in reactive and inelastic scattering: statistical adiabatic channel model of unimolecular processes III, Bev. Bunsenges, Physik. Chem. 79:170.
9. Glanzer, K., and Troe, J. (1975) Vibrational relaxation of NO in collisions with atomic oxygen and chlorine, J. Chem. Phys. 63:4352.
10. Murphy, R.E., Lee, E.T.P., and Hart, A.M. (1975) Quenching of vibrationally excited nitric oxide by molecular oxygen and nitrogen, J. Chem. Phys. 63:2919.
11. Fernando, R.P., and Smith, I.W.M. (1981) Relaxation of NO(v=1) by radical species, J. Chem. Soc. Faraday Transactions 2, 77:459.

12. Hushfar, F., Rogers, J.W., and Stair, A.T., Jr. (1971) Infrared chemiluminescence of the reaction $N + O_2 \rightarrow NO + O$, Appl. Opt. 10:1843.

13. Whitson, M.E., Jr., Darnton, L.A., and McNeal, R.J. (1976) Vibrational energy distribution in the NO produced by the reaction of $N(^4S)$ with O_2, Chem. Phys. Lett. 41:552.

14. Rahbee, A., and Gibson, J.J. (1981) Rate constants for the formation of NO_4 in vibrational levels V = 2 through 7 from the reaction $N(^4S) + O_2 \rightarrow NO + O$, J. Chem. Phys. 74:5143.

15. Demore, W.B., et al (1979) Chemical kinetic and photochemical data for use in stratospheric modeling. Evaluation number 2, JPL Publ. 79-27

16. Billingsley, F.P., II (1976) Calculated vibration-rotation intensities for $NO(x^2\pi)$, J. Molec. Spectrosc. 61:53.

17. Kneizys, F.X., Shettle, E.P., Gallery, W.O., Chetwynd, J.H., Jr., Abreu, L.W., Selby, J.E.A., Fenn, R.W., and McClatchey, R.A. (1980) Atmospheric transmittance/radiance: computer code LOWTRAN 5, AFGL-TR-80-0067, AD A088215.

18. U.S. Standard Atmosphere, 1976, NOAA-S/T 7601562 (U.S. G.P.O. 1976).

19. Swider, W. (1977) Minor neutral mesospheric constituents at high latitudes, in COSPAR Space Research, Vol. XVII, M.J. Rycroft and A.C. Stickland, Eds., Pergamon Press, Oxford.

20. Deans, A.J., and Shepherd, G.C. (1978) Rocket measurements of oxygen and nitrogen emissions in aurora, Planet. Space Sci. 26:319.

21. Trinks, H., Offerman, D., von Zahn, U., and Steinhauer, C. (1978) Neutral composition measurements between 90 and 200 km altitude by rocket-borne mass spectrometer, J. Geophys. Res. 83:2169.

22. Keneshea, T.J., Zimmerman, S.P., and Phubrick, C.R. (1979) A dynamic model of the mesosphere and lower thermosphere, Planet. Space Sci. 27: 385.

23. Wesser, B., and Donahue, T.M. (1979) Atomic oxygen between 80 and 120 km: evidence for a latitudinal variation in vertical transport near the mesopause, J. Geophys. Res. 84:1297.

24. Torr, D.G., and Sharp, W.E. (1979) The concentration of atomic oxygen in the auroral lower thermosphere, Geophys. Res. Lett. 6:860.

25. Sharp, W.E. (1980) Absolute concentrations of $O(^3P)$ in the lower thermosphere at night, Geophys. Res. Lett. 7:485.

26. Dickinson, P.H.G., Bain, W.C., Thomas, L., Williams, E.R., Jenkins, D.B., and Priddy, N.D. (1980) The determination of the atomic oxygen concentration and associated parameters in the lower thermosphere, Proc. Roy. Soc. London A369:379.

27. Howlett, L.D., Baker, K.D., Megill, L.R., Shaw, A.W., and Pendleton, W.R. (1980) Measurement of a structured profile of atomic oxygen in the mesosphere and lower thermosphere, J. Geophys. Res. 85:1291.

28. Offerman, D., Friedrich, V., Ross, P., and von Zahn, U. (1981) Neutral gas composition measurements between 80 and 120 km, Planet. Space Sci. 29:747.

29. Thomas, R.J., and Young, R.A. (1981) Measurement of atomic oxygen and related airglows in the lower thermosphere, J. Geophys. Res. 86:7389.

30. Swider, W. (1978) Daytime nitric oxide at the base of the thermosphere, J. Geophys. Res. 83:4407.

31. Baker, K.D., Nagy, A.F., Olsen, R.O., Oran, E.S., Randhawa, J., Strobel, D.F., and Tohmatsu, T. (1977) Measurements of the nitric oxide altitude distribution in the mid-latitude mesosphere, J. Geophys. Res. 82:3281.

32. Trinks, H., von Zahn, U., Barth, C.A., and Kelly, K.K. (1978) A joint nitric oxide measurement by rocket-borne ultraviolet photometer and mass spectrometer in the lower thermosphere, J. Geophys. Res. 83:203.

33. Thomas, R.J. (1978) A high altitude rocket measurement of nitric oxide, J. Geophys. Res. 83:513.

34. Stewart, A.I., and Cravens, T.E. (1978) Diurnal and seasonal effects in E-region low-latitude nitric oxide, J. Geophys. Res. 83:2453.

35. Abdu, M.A., and Batista, I.S. (1979) Nitric oxide height distribution in the lower ionosphere from rocket ion composition results over a southern temperate latitude station, J. Geophys. Res. 84:5267.

36. Massie, S.T. (1980) Nitric oxide delta band absorption measurements in the lower thermosphere, J. Geophys. Res. 85:2155.

37. Kondo, V., and Ogawa, T. (1976) Odd nitrogen in the lower thermosphere under auroral perturbations, J. Geomag. Geoelectr. 28:253.

38. Roble, R.G., and Rees, M.H. (1977) Time dependent studies of the aurora: effects of particle precipitation on the dynamic morphology of ionospheric and atmospheric properties, Planet Space Sci. 25:991.

39. Rees, M.H., and Roble, R.G. (1979) The morphology of N and NO in auroral substorms, Planet. Space Sci. 27:453.

40. Vallance Jones, A. (1975) A model for the excitation of electron aurora and some applications, Can. J. Phys. 53:2267.

41. Stair, Jr., A.T., Ulwick, J.C., Baker, K.D., and Baker, D.J. (1975) Rocketborne observations of atmospheric infrared emissions in the auroral region, p. 335 in Atmospheres of Earth and the Planets, Ed. B.M. McCormac, D. Reidel Publ. Co., Dordrecht-Holland.

42. Hurd, A.G., Carpenter, J.W., Degges, T.C., Grieder, W.F., Reidy, W.P., Shepherd, O., Stair, A.T., Jr., O'Neil, R.R., Ulwick, J.C., Baker, D.J., and Baker, K.D. (1977) Comparison of ICECAP and EXCEDE Rocket Measurements With Computer Code Predictions, AFGL-TR-77-0060, AD A047526.

43. Reidy, W.P., Degges, T.C., Hurd, A.G., Ulwick, J.C., and Stair, A.T., Jr. (1981) Auroral nitric oxide concentration and infrared emission, J. Geophys. Res. 87:3591.

44. Kennealy, J.P., DelGreco, F.P., Caledonia, G.E., and Green, B.D. (1978) Nitric oxide chemiexcitation occurring in the reaction between metastable nitrogen atoms and oxygen molecules, J. Chem. Phys. 69:1574.

45. Swider, W. (1976) Atmospheric formation of NO from $N_2(A^3\Sigma)$, Geophys. Res. Lett. 3:335.

46. Kley, D., Lawrence, G.M., and Stone, E.J. (1977) The yield of $N(^2D)$ atoms in the dissociative recombination of NO^+, J. Chem. Phys. 66:4157.

47. Frederick, J.E., and Rusch, D.W. (1977) On the chemistry of metastable atomic nitrogen in the E-region inferred from simultaneous satellite measurements of the 5200 Å airglow and atmospheric composition, J. Geophys. Res. 82:3509.

48. Porter, H.S., Jackman, C.H., and Green, A.E.S. (1976) Efficiencies for production of atomic nitrogen and oxygen by relativistic proton impact in air, J. Chem. Phys. 65:154.

49. Peterson, L.R., Sawada, T., Bass, J.N., and Green, A.E.S. (1973) Electron energy deposition in a gaseous mixture, Computer Phys. Comm. 5:239.

50. Jackman, C.H., Garvey, R.H., and Green, A.E. (1977) Electron impact on atmospheric gases I. Updated cross-sections, J. Geophys. Res. 82:5081.

51. Zipf, E.C., Espy, P.J., and Boyle, C.F. (1980) The excitation and collisional deactivation of metastable $N(^2P)$ atoms in auroras, J. Geophys. Res. 85:687.

52. Swider, W. (1975) The D- and E-regions, p. 259 of Atmospheres of Earth and the Planets, B.M. McCormac, Ed., D. Reidel Publ. Co., Dordrecht-Holland.

53. Narcisi, R.S., Sherman, C., Wlodyka, L.E., and Ulwick, J.C. (1974) Ion composition in an IBC class II aurora 1. Measurements, J. Geophys. Res. 79:2843.

54. Swider, W., and Narcisi, R.S. (1974) Ion composition in an IBC class II aurora. 2. Model, J. Geophys. Res. 79:2849.

55. McFarland, M., Albritton, D.L., Fehsenfeld, F.C., Ferguson, E.E., and Schmeltekopf, A.L. (1974) Energy dependence and branching ratio of the $N_2^+ + O$ reaction, J. Geophys. Res. 79:2925.

56. Lindinger, W., Fehsenfeld, F.C., Schmeltekopf, A.L., and Ferguson, E.E. (1974) Temperature dependence of some ionospheric ion-neutral reactions from 300-900 K, J. Geophys. Res. 79:4753.

57. Husain, D., Mitra, S.K., and Young, A.N. (1974) Kinetic study of electronically excited nitrogen atoms $N(2\,^2D_J, 2\,^2P_J)$, by attenuation of atomic resonance radiation in the vacuum ultra-violet, J. Chem. Soc. Farad. Trans. II 70:1721.

58. Slanger, T.G., Wood, B.J., and Black, G. (1971) Temperature coefficients for $N(^2D)$ quenching by O_2 and N_2O, J. Geophys. Res. 76:8430.

59. Davenport, J.E., Slanger, T.G., and Black, G. (1976) Quenching of $N(^2D)$ by N_2 and H_2O, J. Chem. Phys. 64:4442.

60. Green, B.D., Caledonia, G.E., and Murphy, R.E. (1981) The vibrational relaxation of NO(v=1-7) by O_2, J. Chem. Phys. 76:2441.

61. Rawlins, W.T., Caledonia, G.E., Gibson, J.J., and Stair, A.T., Jr. (1981) Infrared emission from $NO(\Delta v=1)$ in an aurora: spectral analysis and kinetic interpretation of HIRIS measurements, J. Geophys. Res. 86:1313.

62. Baker, K.D., Baker, D.J., Ulwick, J.C., and Stair, Jr., A.T. (1977) Measurements of 1.5-5.3 μm infrared enhancements associated with a bright auroral breakup, J. Geophys. Res. 82:3518.

Appendix C

Observation of Spectrally Resolved Chemiluminescence From Vibrationally Excited $O_3(\nu_3)$

JOURNAL OF GEOPHYSICAL RESEARCH, VOL. 86, NO. C6, PAGES 5247–5252, JUNE 20, 1981

Observation of Spectrally Resolved Infrared Chemiluminescence From Vibrationally Excited $O_3(\nu_3)$

W. T. RAWLINS AND G. E. CALEDONIA

Physical Sciences Inc., Woburn, Massachusetts 01801

J. P. KENNEALY

Optical Physics Division, Air Force Geophysics Laboratory, Hanscom AFB, Massachusetts 01731

Infrared emission from the ν_3 band of ozone near 9.6 μm has been observed in the COCHISE cryogenic chemical reactor-spectrometer. Vibrationally excited O_3, formed principally by recombination of O_2 with discharge-produced oxygen atoms at 1 torr and 80–120 K, is expanded into a low-pressure (~5 mtorr) environment where its infrared radiation is observed without interference from infrared background effects. The observed spectral distributions are interpreted by using a least squares spectral synthesis method, in which the vibrational state populations and spectroscopic parameters are adjusted in computed spectra so as to provide the best fits to the observed spectra. The (001) → (000) transition is responsible for most of the observed intensity; however, ($\Delta v = 1$) emission from higher vibrational levels is also seen, extending to ~11 μm ($v' \sim 6$). Although the observed spectral distributions are affected by collisional deactivation occurring in the discharge region, the apparent degree of vibrational excitation observed in these experiments should have considerable bearing on investigations of infrared radiation in the upper atmosphere.

INTRODUCTION

The recombination of atomic and molecular oxygen may give rise to vibrationally excited ozone in the upper atmosphere via the sequence

$$\text{(R1)} \quad O + O_2 \rightleftarrows O_3^\dagger$$

$$\text{(R2)} \quad O_3^\dagger + M \rightarrow O_3(v') + M$$

$$\text{(R3)} \quad O_3(v') \rightarrow O_3(v'') + h\nu$$

$$\text{(R4)} \quad O_3(v') + M \rightarrow O_3(v'') + M$$

Recent rocketborne measurements [*Sadile et al.*, 1978] of infrared atmospheric emissions indicate that chemiluminescence in the ν_3 fundamental band of O_3 ((R3)) may be a significant source of 10–12 μm radiation in the sunlit atmosphere between 60 and 100 km [*Degges et al.*, 1979]. However, little information exists on the details of the production (R1)–(R2) and loss (R3)–(R4) processes under mesospheric/thermospheric conditions, as a result, it has been difficult and highly speculative to evaluate the role of this mechanism in the upper atmosphere.

The formation of vibrationally excited O_3 in several modes by (R1)–(R4) has been well established in the laboratory at relatively high pressure and room temperature [*von Rosenberg and Trainor*, 1973, 1974, 1975]; however, the extent of excitation was not spectrally defined in those experiments. We wish to report here the initial results from a series of infrared chemiluminescence experiments carried out at lower pressure, more representative of the upper atmosphere, utilizing the COCHISE infrared emission spectroscopy facility. The spectral data reported here, which are limited to the ν_3 band near 9.6 μm, represent the first laboratory measurements of spectrally resolved infrared emission from vibrationally excited O_3.

EXPERIMENTAL

The measurements were made in the COCHISE facility at the Air Force Geophysics Laboratory, an apparatus described in detail elsewhere [*Kennealy et al.*, 1978, 1979] and which will only be summarized here. This facility provides much enhanced infrared sensitivity (up to 6 orders of magnitude) by virtual elimination of thermal background radiation; this is achieved through cryogenic (20 K) operation of essentially the entire apparatus. The reaction chamber is shown schematically in Figure 1; reagent gases, flowing at total flow rates of ~8 l/min (STP), enter the chamber through four sets of diametrically opposed inlet tubes, interact in an axisymmetric stagnation region along the centerline of the cell, and are cryopumped rapidly by the 20 K wall. Matched microwave discharges (Opthos Instruments) on four of the inlets produce atomic oxygen in O_2–Ar mixtures (0.5–2% O_2); O_2 and Ar are alternately used as counterflow gases (Matheson, UHP). Inlet gas temperatures are electronically controlled and were varied from 80 to 120 K in these experiments. Approximate gas pressures and residence times were 1 torr and 2 ms in the discharge inlet, and 0.003 torr and 0.3 ms (i.e., nearly single collision conditions) in the central interaction zone.

Infrared radiation, arising from chemi-excitation reactions occurring either in the interaction zone or in the discharge inlets, is viewed along the cell axis through a Ge lens which defines a roughly columnar field-of-view, as shown by the cross-hatched area in Figure 1; a polished Al mirror at the opposite end of the cell further enhances the collection efficiency of the system. The detection system consists of a cryogenic 0.5 m scanning monochromator (Minuteman 305 CM) and a liquid-helium-cooled Si:As detector–preamplifier package. Incoming radiation is presorted by an 8 μm long-wavelength-pass interference filter in front of the entrance slit of the monochromator, and the detector output is electronically filtered (PARC 113), and processed by a phase sensitive detector (PARC 124) synchronized to the microwave discharges; the discharges are pulsed at ~2 Hz with a 50% (square wave) duty cycle to create steady state conditions while the discharges are on. The final demodulated signal is digitally filtered, displayed, and recorded on magnetic tape by a Digital Equipment Corp. PDP-11 computer.

Spectral response of the [illegible] system is established by [illegible] blackbody calibration source. These calibrations indicate a detection limit (S/N

Paper number 80C1785
0148-0227/81/080C-1785$01.00

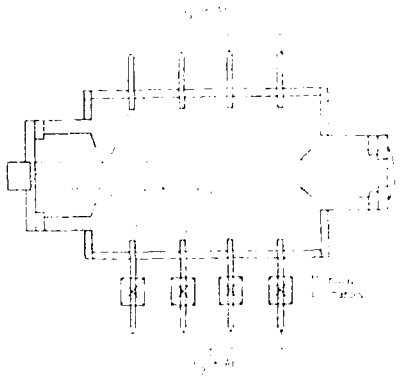

Fig. 1. COCHISE reaction chamber. The cross-hatched region delineates the field-of-view of the detector (not shown).

= 1) for $O_3(001)$ of approximately 3×10^6 molecules cm^{-3}. Typical spectral resolutions obtained in these experiments were 0.04–0.08 μm.

Results and Kinetic Analysis

Spectral scans from 8 to 16 μm were made for a variety of discharge conditions and reagent combinations as described above. Representative spectra observed in the 9- to 11-μm wavelength region are shown in Figures 2–4. The prominent feature centered at 9.6 μm is readily identifiable as the (001) → (000) band (ν_3) of O_3 [*McCaa and Shaw*, 1968]. The remaining emission, extending from ~9.8 to ~11 μm, appears to be due to vibrationally excited $O_3(\nu_1)$; this identification is borne out by the observations described below. The ν_1 (9.1 μm) and ν_2 (14.3 μm) bands of O_3 could not be observed above the noise limit in these initial experiments; from this we can only deduce the upper limits $[O_3(100)] \leq 2\,[O_3(001)]$ and $[O_3(010)] \leq 15\,[O_3(001)]$.

Much of the O_3 emission observed in the COCHISE experiments should arise from some combination of (R1)–(R4); these processes can take place to some extent in the low-pressure interaction region, but will occur with much faster rates in the discharge tubes immediately downstream of the microwave excitation sources. The rates of the probable production and loss processes in the discharge tubes can be roughly estimated for the experimental conditions described above, the results of such a kinetic analysis are summarized in Table 1. For dilute O_2/Ar mixtures (O_2/Ar ~ 0.01) at ~1 torr, past experience with room-temperature microwave discharges indicates that fractional O_2 dissociations of 0.1–0.5 are typically attained [see, for example, *Piper et al.*, 1979]; for purposes of discussion, we will use the value 0.2 as a conservative estimate for our discharge conditions. At 80 K, the total O_3 production rate by recombination of O with O_2 (in Ar) is then on the order of 3×10^{15} cm^{-3} s^{-1} (using the termolecular rate constant expression of *Hute et al.* [1972]); we anticipate that a large fraction of the O_3 initially formed is vibrationally excited. The possibility of electronically excited precursors to $O_3(v)$ in the recombination sequence (e.g., as $O_3^\dagger$ in (R1)–(R2)) cannot be ruled out at this time; however, the analysis given here, which deals with the net recombination process, is not affected by this issue. Other possible production mechanisms for $O_3(v)$, such as direct excitation of O_3 by electron impact or by collisions with discharge-excited species such as $O_2(v)$ or $O_2(b^1\Sigma_g^+)$, are expected to be at least an order of magnitude slower than the recombination path in the dilute O_2/Ar mixtures, due to the relatively small reactant concentrations for these processes.

The $O_3(v)$ production rate is balanced by homogeneous relaxation with the major species Ar, O_2, and O, by heterogeneous removal at the tube wall, and by flow out of the tube into the low-pressure zone. In general, the detailed kinetic information required to assess the rates of the collisional processes for all v does not exist; however, some relaxation rate measurements have been reported for single-quantum excitation in the ν_3 mode [*Rosen and Cool*, 1973, 1975; *West et al.*, 1976]. Rosen and Cool found that the ν_3 and ν_1 modes equilibrated very rapidly and that subsequent collisional deactivation to the ν_2 mode proceeded at rather slow rates comparable with those of the deactivation of the ν_2 mode itself. From the data of *Rosen and Cool* [1975] we estimate first-order deactivation rates for $O_3(v)$ of ~ 700 s^{-1} and ~ 20 s^{-1} for collisions with Ar and O_2, respectively; however, the possible influence on these rates of low temperature and/or high vibrational levels is unknown. By far, the dominant quenching process for $O_3(v)$ under our conditions appears to be deactivation by and/or reaction with atomic oxygen, for which we estimate a rate on the order of 5×10^3 s^{-1}, using the room-tem-

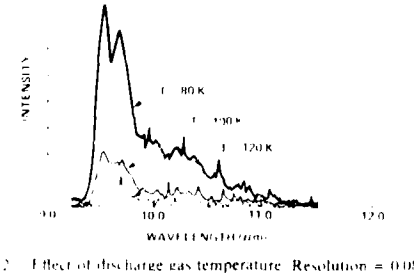

Fig. 2. Effect of discharge gas temperature. Resolution = 0.08 μm.

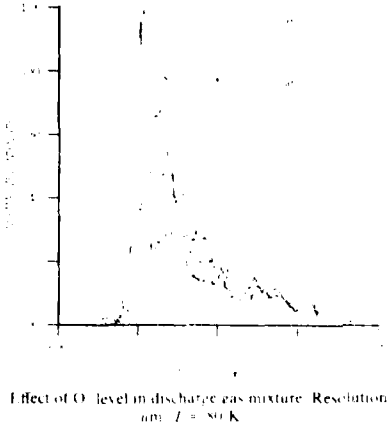

Fig. 3. Effect of O level in discharge gas mixture. Resolution = 0.04 μm. T = 80 K.

perature rate constant for either process [*West et al.*, 1976]. Diffusion of $O_3(v)$ through Ar to the tube wall is expected to occur with a rate similar to that for diffusion of CO_2 [*Hirschfelder et al.*, 1954]; at 80 K, this gives an estimated surface deactivation rate of, at most, ~ 300 s^{-1}, if deactivation of $O_3(v)$ occurs upon every collision with the wall. Finally, from the measured gas flow rates, the pumping loss rate for $O_3(v)$ is ~ 500 s^{-1}. Thus, for the conditions employed in the majority of our experiments, we estimate that (1) the dominant $O_3(v)$ deactivation process is by collision with O, which may well lead to chemical reaction or multi-quantum deactivation, (2) the ν_3 mode should reach equilibrium with the ν_1 mode within the 2 ms flow time, but the ν_2 and ν_3 modes may not be fully equilibrated during this time, and (3) wall deactivation is a relatively minor process on this time scale. From these estimated production and loss rates, we derive a maximum steady state $O_3(v)$ concentration on the order of 5×10^{11} cm^{-3} in each inlet tube, if all the recombinations form vibrationally excited O_3; this corresponds to upper-bound concentrations near 1×10^9 cm^{-3} in the low-pressure observation region. For comparison, the integrated intensity of the 0.7% O_2 spectrum in Figure 3 corresponds to $[O_3(v)] \sim 5 \times 10^8$ cm^{-3} in the observation region, with an uncertainty of a factor of 2 in the absolute calibration of the optical system.

Examination of the effects of experimental variation of counterflow species, inlet gas temperature, and O_2 fraction in the discharge gas provides further evidence that most of the observed $O_3(v)$ is indeed formed in the discharge tubes by three-body recombination and collisional deactivation. Switching the counterflow species from O_2 to Ar, for a given O_2/Ar discharge mixture, gives a spectrum of virtually the same intensity and spectral distribution as before; this is in marked contrast to the considerable reduction in signal and shift in distribution which one would expect if a significant fraction of the $O_3(v)$ formation occurred in the mixing region. This observation clearly indicates that the observed spectra result from processes occurring in the discharge tube.

Results of varying the discharge gas temperature from 80 to 120 K are illustrated in Figure 2; the observed band intensity exhibits a strong inverse temperature dependence which scales approximately as T^{-3}, or $\exp(500/T)$ over the limited temperature range studied. Although contrary to theoretical prediction of a $\sim T^{-1}$ dependence at low temperatures [*Troe*, 1977], the latter expression gives essentially the same temperature dependence as has been measured for the rate constant of the reaction

$$\text{(R5)} \qquad O + O_2 + Ar \rightarrow O_3 + Ar$$

near room temperature [*Arnold and Comes*, 1979; *Hute et al.*, 1972; *Hampson and Garvin*, 1978], this constitutes strong evidence that three-body recombination is responsible for the observed fluorescence, at least for the dilute O_2/Ar mixtures.

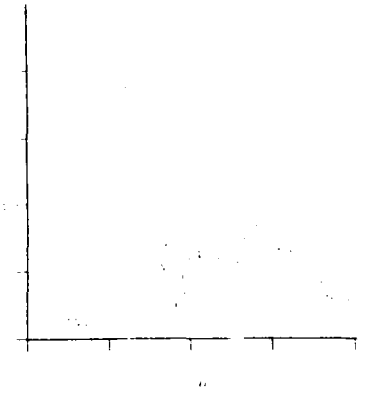

Fig. 4. Observed O_3 spectrum for high-O_2 discharge mixture. Resolution = 0.08 μm, T = 90 K.

The effects of varying the fraction of O_2 in the O_2/Ar discharge mixture (at a fixed flow rate) are demonstrated in Figures 3 and 4. For the low-O_2 mixtures (Figure 3), increasing the O_2 level caused a corresponding increase in total band intensity but a reduction in the relative contributions from the higher vibrational level. One interpretation of this effect is that the presence of more O_2 in the mixture increases the overall collisional relaxation rate in the inlet tube, as might occur if the relaxation of higher vibrational levels by O_2 is relatively fast. Alternatively, increased O_2 may lead to enhanced steady state concentrations of O_3 in $v = 1$ relative to $v > 1$, possibly via deactivation processes involving discharge-produced O; since the oxygen atom concentration has not been measured in these experiments, the variation of [O] with increasing $[O_2]$ is not clear.

In contrast to the low-O_2 cases, spectra from high-O_2 discharge mixtures (Figure 4) exhibit a distinct bimodal distribution, suggestive of (1) competing $O_3(v)$ production mechanisms, and (2) either little collisional deactivation or an unusual dependence of the deactivation rate on v. The cause of the spectral distribution shown in Figure 4 is not yet understood, but may be related to excitation of O_3 by collisions with discharge-excited O_2 (e.g., $O_2(v)$ or $O_2(b^1\Sigma_g^+)$), and/or to the occurrence of (R1) and (R2) in the mixing zone following extensive deactivation of discharge-produced $O_3(v > 1)$ in the inlet tubes. Clearly, more detailed kinetic measurements are required to resolve these issues.

TABLE 1. Estimated Rates of Major $O_3(v)$ Production and Loss Processes in Discharge Tubes for a Dilute (1%) O_2/Ar Mixture at 1 torr

Reaction	Estimated Rate Constant at 80 K	Reference	Estimated Rate
$O + O_2 + Ar \rightarrow O_3(v) + Ar$	$\sim 4 \times 10^{-33}$ cm^6 s^{-1}	*Hute et al.* [1972]	$\sim 3 \times 10^{17}$ cm^{-3} s^{-1}
$O_3(v) + Ar \rightarrow O_3 + Ar$	6×10^{-15} cm^3 s^{-1}	*Rosen and Cool* [1978]	700 s
$O_3(v) + O_2 \rightarrow O_3 + O_2$	2×10^{-14} cm^3 s^{-1}	*Rosen and Cool* [1978]	200 s
$O_3(v) + O \rightarrow$ products	1×10^{-12} cm^3 s^{-1}	*West et al.* [1976]	5000 s
$O_3(v) +$ wall $\rightarrow$ products	$D = 20$ cm^2 s^{-1}	see text	~ 300 s
Pumping loss of $O_3(v)$		measured flow velocity	500 s

SPECTRAL ANALYSIS AND DISCUSSION

The observed spectral distributions can be further identified and characterized by analysis of the $O_3(\nu_3)$ vibration-rotation spectrum; a complete spectral analysis, treating all $\Delta v_3 = 1$ transitions for all possible $(v_1 v_2)$ combinations, would yield the vibrational state populations responsible for the observed spectra. Unfortunately, due to the paucity of spectroscopic information on vibrationally excited O_3, and also to the difficulty in resolving the extensive overlap between the numerous possible bands, such a detailed treatment is not feasible for the present data. However, some preliminary conclusions about the observed energy content may be drawn from a more simplified analysis, assuming $v_1 = v_2 = 0$ and treating the asymmetric stretching vibration as a typical anharmonic oscillator.

Detailed information on the rotational line positions and strengths of the (001) → (000) band is available from the AFGL absorption line parameter compilation [*McClatchey et al.*, 1973; *Flaud et al.*, 1980*b*]; these data are consistent with the results of many recent measurements [*Depannemaecker et al.*, 1977; *Depannemaecker and Bellet*, 1977; *Barbe et al.*, 1977; *Flaud et al.*, 1980*a*]. The band centers $\tilde{\nu}_{0,v_3}$ of the $\Delta v_3 = 1$ transitions from higher vibrational levels of the ν_3 mode were calculated from the formula

$$\tilde{\nu}_{0,v_3} = \tilde{\nu}_{01} - 2x_{33}(v_3' - 1) \tag{1}$$

where v_3' is the vibrational quantum number of the upper state and x_{33} is the first-order anharmonicity constant for the asymmetric stretch (this treatment necessarily neglects the possible effects of Coriolis interaction with v_1 [*Clough and Kneizys*, 1966] on the vibrational spacings). The value of $\tilde{\nu}_{01}$, the band center of the (001) → (000) transition, is well known to be 1042.1 cm^{-1} [*Clough and Kneizys*, 1966; *McCaa and Shaw*, 1968]. The only reported values of x_{33} are 15 cm^{-1} [*McCaa and Shaw*, 1968] and 12.3 cm^{-1} [*Barbe et al.*, 1972], both of which were determined by measurements of infrared absorption from the ground state; since the data of *Barbe et al.* [1972] extend to $v_3' = 4$ and are considerably more precise, the value $x_{33} = 12.3$ cm^{-1} was used in the preliminary calculations presented here. The rotational spacings and relative line strengths obtained from *McClatchey et al.* [1973] for the (001) → (000) transition were assumed to hold for all higher v_3', thus neglecting the effects of vibration-rotation interactions. The band Einstein coefficients were estimated from the scaling law

$$A_{v_3', v_3'-1} = v_3' A_{10} \left(\frac{\tilde{\nu}_{v_3'}}{\tilde{\nu}_{01}} \right)^3 \tag{2}$$

where the Einstein coefficient of the (001) → (000) band is, from the data of *Flaud et al.* [1980*b*], $A_{10} = 11.2$ s^{-1}. The contribution to the total integrated intensity due to each $v_3' \rightarrow v_3' - 1$ band is then given by

$$I_{v_3'} \propto h c \tilde{\nu}_{v_3'} N_{v_3'} A_{v_3', v_3'-1} \tag{3}$$

where $N_{v_3'}$ is the concentration of species in state v_3'. The sum of the $dI/d\lambda$ contributions, convolved with the instrumental slit function, is matched to each observed CIRRIS spectrum by a least squares method in which the set of vibrational populations $N_{v_3'}$ is varied to achieve the best least squares fit to the spectral data [*Kennealy et al.*, 1978].

A typical comparison between computed and observed spectra is shown in Figure 5; the estimated contributions of the different vibrational transitions to the computed spectrum are illustrated in Figure 6. Contributions from at most six vibrational levels can be identified, although the anharmonicity correction appears to be incorrect (or incomplete) for $v_3' \geq 4$; use of several trial values of x_{33} between 10 and 15 cm^{-1} does not improve the general quality of the fits. Although the spectral features can perhaps be better reproduced by introducing higher-order corrections to x_{33}, some of the present mismatch probably results from the presence of $\Delta v_3 = 1$ difference bands in the data. Indeed, preliminary spectral fits in which the (101) → (100) and (011) → (101) bands, respectively, centered at 9.92 and 9.75 μm [*Flaud et al.* 1980*b*], are included, yield a somewhat improved spectral match in the 9.8- to 10.0-μm region. Although there is still considerable uncertainty, the results of this exercise suggest a significant population of the (101) state (i.e., near that of the 002 state), but a much smaller population of the (011) state; for our flow conditions, this result is consistent with the known intermode energy transfer kinetics of O_3 as discussed above [*Hui et al.*, 1975; *Rosen and Cool*, 1973, 1975]. A detailed spectral study of the $(\nu_1 + \nu_3)$ summation band near 4.7 μm will more directly address the

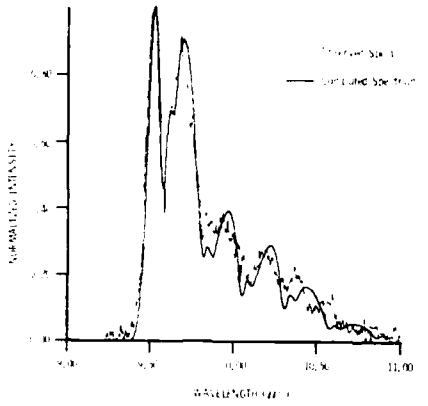

Fig. 5. Comparison of computed and observed spectra. Resolution = 0.04 μm, T = 80 K, 0.7% O_2 in discharge gas. The standard deviation of the least squares fit is 0.05.

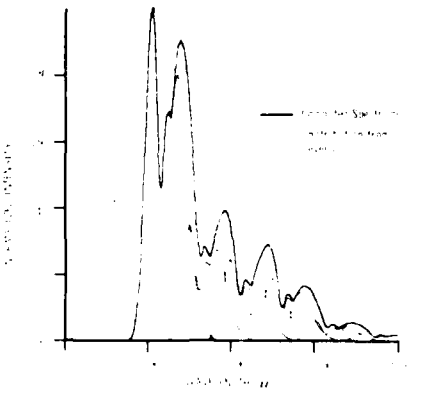

Fig. 6. Contributions of vibrational basis sets to overall computed O_3 spectrum of Figure 5.

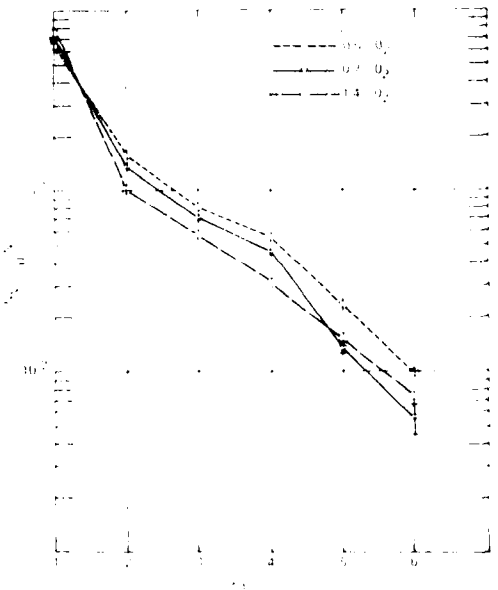

Fig. 7. Vibrational populations in the $(OO^{\ddagger}_{1})$ manifold computed for the spectra in Figure 3, showing the effects of O_2 level in the dilute discharge mixtures. These populations were derived by using the anharmonic oscillator, rigid rotator approximation as described in the text; possible contributions from difference bands were not included. The relative populations shown here are subject to uncertainties in the estimated relative Einstein coefficients. The relative statistical uncertainties in the derived populations were less than 3% for levels 1-4 and are shown by error bars for levels 5 and 6 of the 0.7% O_2 case

10-μm difference band question, as will more complete study of all O_3 emissions between 2 and 16 μm.

Some example vibrational distributions derived by the above analysis are shown in Figure 7. An accurate experimental or theoretical determination of the vibrational level dependence for the ν_1 band Einstein coefficients is a formidable problem which has not yet been solved [see, for example, *Curtiss et al.*, 1979]. As a result, the spectral fitting method can only yield relative trends in the derived vibrational population distributions, such as the increase in vibrational 'temperature' with decreasing $[O_2]$ in the low-O_2 discharge gas mixtures, as shown in Figure 7. Subject to the limitations of both the present data and the assumptions made in the spectral analysis, the average degree of excitation exhibited by each of the spectra shown here is ~1.6 quanta per $O_3(v)$, which is roughly the same as that given by Boltzmann distributions with vibrational temperatures in the 1200-2000 K range; since collisional deactivation of $O_3(v)$ has clearly affected these experiments, this estimate can only be applied as a crude lower bound for the initial distribution in atmospheric radiance predictions. Nevertheless, the extent of residual excitation observed even in these experiments is rather high (two thirds of the way towards dissociation). Further kinetic studies, aimed at isolating the formation and relaxation processes, should more clearly delineate the roles of (R1)-(R4) in the upper atmosphere.

Acknowledgments. This research was jointly supported by the Air Force Office of Scientific Research and Defense Nuclear Agency. Extensive technical contributions were provided by F. P. Delgreco and F. X. Robert.

REFERENCES

Arnold, I., and F. J. Comes, Temperature dependence of the reactions $O(^3P) + O_3 \rightarrow 2O_2$ and $O(^3P) + O_2 + M \rightarrow O_3 + M$, *Chem. Phys.*, *42*, 231, 1979.

Barbe, A., C. Secroun, and P. Jouve, Spectre d'absorption infrarouge de l'ozone gazeux, *Compte Rendue Acad. Sci. Paris*, *274*, 615, 1972.

Barbe, A., C. Secroun, and P. Jouve, Infrared and microwave high-resolution spectrum of the ν_1 band of ozone, *J. Molec. Spectrosc.*, *64*, 343, 1977.

Clough, S. A., and F. X. Kneizys, Coriolis interaction in the ν_1 and ν_3 fundamentals of ozone, *J. Chem. Phys.*, *44*, 1855, 1966.

Curtiss, L. A., S. R. Langhoff, and G. D. Carney, Ab initio SCF and CI calculations of the dipole moment function of ozone, *J. Chem. Phys.*, *71*, 5022, 1979.

Degges, T. C., A. T. Stair, Jr., R. M. Nadile, and E. R. Hegblom, Altitude dependence and spectral character of atmospheric ozone long wavelength infrared emission, *Eos Trans. AGU*, *60*, 338, 1979.

Depannemaecker, J. C., and J. Bellet, Rotational spectra of $^{16}O_3$ and of the five $^{16}O_3$ isotopic species, *J. Molec. Spectrosc.*, *66*, 106, 1977.

Depannemaecker, M. J. C., B. Duterage, and M. J. Bellet, Systematic calculations of rotational spectra of normal and substituted (^{18}O in place of ^{16}O) ozone molecules, *J. Quant. Spectrosc. Radiat. Transfer*, *17*, 519, 1977.

Flaud, J. M., C. Camy-Peret, A. Barbe, C. Secroun, and P. Jouve, Line positions and intensities for the $2\nu_2$, $\nu_1 + \nu_3$, and $2\nu_3$ bands of ozone, *J. Molec. Spectrosc.*, *80*, 185, 1980*a*.

Flaud, J. M., C. Camy-Peret, and L. S. Rothman, Improved ozone line parameters in the 10- and 4.8-μm regions, *Appl. Opt.*, *19*, 655, 1980*b*.

Hampson, R. F., Jr., and D. Garvin, (Eds.), Reaction Rate and Photochemical Data for Atmospheric Chemistry-1977, *NBS Spec. Pub. 513*, Nat. Bur. Stand., Washington, D. C., 1978.

Hirschfelder, J. O., C. F. Curtiss, and R. B. Bird, *Molecular Theory of Gases and Liquids*, John Wiley, New York, 1954.

Hui, K. K., D. I. Rosen, and T. A. Cool, Intermode energy transfer in vibrationally excited O_3, *Chem. Phys. Lett.*, *32*, 141, 1975.

Huie, R. E., J. T. Herron, and D. D. Davis, Absolute rate constants for the reaction $O + O_2 + M \rightarrow O_3 + M$ over the temperature range 200-346 K, *J. Phys. Chem.*, *76*, 2653, 1972.

Kennealy, J. P., F. P. DelGreco, G. E. Caledonia, and B. D. Green, Nitric oxide chemi-excitation occurring in the reaction between metastable nitrogen atoms and oxygen molecules, *J. Chem. Phys.*, *69*, 1574, 1978.

Kennealy, J. P., F. P. DelGreco, G. E. Caledonia, and W. T. Rawlins, COCHISE: Laboratory Spectroscopic Studies of Atmospheric Phenomena with High-Sensitivity Cryogenic Instrumentation, *Proc. Soc. Photoopt. Instr. Eng.*, *191*, 151, 1979.

McCaa, D. J., and J. H. Shaw, The infrared spectrum of ozone, *J. Molec. Spectrosc.*, *25*, 374, 1968.

McClatchey, R. A., W. S. Benedict, S. A. Clough, D. E. Burch, R. F. Calfee, K. Fox, L. S. Rothman, and J. S. Garing, AFCRL Atmospheric Absorption Line Parameters Compilation, *AFCRL-TR-73-0096*, Air Force Geophys. Lab., Hanscom AFB, Mass., 1973.

Nadile, R. M., A. T. Stair, Jr., N. B. Wheeler, D. G. Frodsham, C. L. Wyatt, D. J. Baker, and W. F. Grieder, SPIRE-Spectral infrared rocket experiment (Preliminary Results), *AFGL-TR-78-0107*, Air Force Geophys. Lab., Hanscom AFB, Mass., 1978.

Piper, L. G., R. H. Krech, and R. L. Taylor, Generation of N_3 in the thermal decomposition of NaN_3, *J. Chem. Phys.*, *71*, 2099, 1979.

Rosen, D. I., and T. A. Cool, Vibrational deactivation of $O_3(101)$ molecules in gas mixtures, *J. Chem. Phys.*, *59*, 6097, 1973.

Rosen, D. I., and T. A. Cool, Vibrational deactivation of O_3 molecules in gas mixtures. 2, *J. Chem. Phys.*, *62*, 466, 1975.

Troe, J., Theory of thermal unimolecular reactions at low pressures. 2. Strong collision rate constants, applications, *J. Chem. Phys.*, *66*, 4758, 1977.

von Rosenberg, C. W., and D. W. Trainor, Observations of vibra-

tionally excited ozone formed by recombination, *J. Chem. Phys.*, 59, 2142, 1973.
von Rosenberg, C. W., and D. W. Trainor, Vibrational excitation of ozone formed by recombination, *J. Chem. Phys.*, *61*, 2442, 1974.
von Rosenberg, C. W., and D. W. Trainor, Excitation of ozone formed by recombination, 2, *J. Chem. Phys.*, *63*, 5348, 1975.
West, G. A., R. E. Weston, Jr., and G. W. Flynn, Deactivation of vibrationally excited ozone by $O(^3P)$ atoms, *Chem. Phys. Lett.*, *42*, 488, 1976.

(Received August 18, 1980;
revised December 3, 1980;
accepted December 12, 1980.)

Appendix D

Rate Constants for Deactivation of $N_2(A)v' = 0,1$ by O_2

Rate constants for deactivation of $N_2(A)v'=0,1$ by O_2

L. G. Piper and G. E. Caledonia

Physical Sciences Inc., Woburn, Massachusetts 01801

J. P. Kennealy

Air Force Geophysics Laboratories, Bedford, Massachusetts 01730

(Received 3 October 1980; accepted 18 November 1980)

The removal of $N_2(A\ ^3\Sigma_u^+, v'=0,1)$ by O_2 has been studied in a room temperature discharge-flow apparatus by monitoring the temporal decay of the 0,0 and 1,0 bands of the Vegard–Kaplan system. Rate constants for the reaction with O_2 are (2.3 ± 0.4) and $(4.1 \pm 0.7) \times 10^{-12}$ cm^3 molecule^{-1} s^{-1} for $v'=0$ and 1, respectively. The rate constant measured for $v'=0$ is about 35% lower than commonly accepted values for the rate constant for quenching $N_2(A)$ by O_2. This discrepancy is shown to result from the fact that most other studies used a tracer to monitor the $N_2(A)$ number density. The rate of decay of the tracer reflects both the decay of the $v'=0$ and $v'=1$ levels of $N_2(A)$ and its value is midway between the decay rates of the individual vibrational levels.

I. INTRODUCTION

It has been suggested that the reactions of $N_2(A\ ^3\Sigma_u^+)$ with atomic and molecular oxygen could be significant sources of odd nitrogen and vibrationally excited NO in the upper atmosphere.[1] For the interaction between $N_2(A)$ and molecular oxygen a number of possible exoergic reaction channels may be proposed:

$$N_2(A\ ^3\Sigma_u^+)_{v'=0} + O_2(X\ ^3\Sigma_g^-) \rightarrow N_2(X\ ^1\Sigma_g^+) + O_2(X\ ^3\Sigma_g^-) + 6.2\ \text{eV}, \quad (1a)$$

$$\rightarrow N_2(X\ ^1\Sigma_g^+) + 2O(^3P) + 1.1\ \text{eV}, \quad (1b)$$

$$\rightarrow N_2O + O(^3P) + 3.0\ \text{eV}, \quad (1c)$$

$$\rightarrow N_2O + O(^1D) + 1.0\ \text{eV}, \quad (1d)$$

$$\rightarrow 2NO(X\ ^2\Pi) + 4.2\ \text{eV}. \quad (1e)$$

Since O_2 is the main deactivator of $N_2(A\ ^3\Sigma_u^+)$ in the atmosphere below 100 km,[1] significant amounts of atmospheric N_2O could be formed via Reactions (1c) and (1d), with possible vibrational excitation of the product. Further reactions of N_2O with $N(^2D)$ and $O(^1D)$ can lead to the formation of NO.[1] Direct formation of NO via Reaction (1e) is expected to be extremely slow due to the dynamic constraints which inhibit such four-center exchange reactions.

Previous measurements of the room-temperature rate constants for this reaction vary between 1.9 and 7.6 $\times 10^{-12}$ cm^3 molecule^{-1} s^{-1}[3–12] (Table I). Because most previous measurements were made using a tracer, and were therefore not state specific, some of this scatter probably results in the variation in deactivation rate constant with vibrational level.

Meyer *et al.*[2] have observed that oxygen atoms are a major product from Reaction (1), but did not put their observations upon a quantitative basis. Very recent experiments by Zipf[12] have indicated that about 60% of Reaction (1) proceeds through channels (1c) and (1d) to make N_2O.

During the course of a program to study product formation in Reaction (1), we remeasured the rate constant for this reaction for both vibrational levels 0 and 1. Our result for $k_1(v'=0)$ of 2.3×10^{-12} cm^3 molecule^{-1} s^{-1} is about 35% lower than the commonly accepted value of 3.5×10^{-12} cm^3 molecule^{-1} s^{-1}. We will show that most other measurements were non-state specific tracer measurements which measured an effective deactivation rate constant for a mixture of vibrational levels. Our results further show that vibrational level 1 is quenched by molecular oxygen almost twice as fast as vibrational level 0. Thus, the tracer measurements give a rate constant midway between those for $v'=1$ and $v'=0$, the magnitude being dependent upon the relative ratio $[N_2(A)_{v'=1}]/[N_2(A)_{v'=0}]$.

II. EXPERIMENTAL

A. Apparatus

The experiments were performed in a discharge-flow apparatus with the $N_2(A)$ number densities being monitored by spectroscopic observations of individual vibrational bands of the Vegard–Kaplan ($N_2\ A\ ^3\Sigma_u^+ - X\ ^1\Sigma_g^+$) system of nitrogen. The reactor (see Fig. 1) is a 2 in. diameter quartz tube which is pumped by a Roots blower that is capable of producing linear velocities up to 8×10^3 cm s^{-1} at pressures of 1 Torr. A 0.5 m monochromator (Minuteman) is mounted upon a set of rails parallel to the flow tube. Spectral observations of the luminous gases in the flow tube may therefore be made as a function of linear distance along the tube by sliding the monochromator up and down on its rails. Distances are converted to reaction times by dividing by the flow velocity. Light intensities are measured photoelectrically using a thermoelectrically cooled EMI 9558QA photomultiplier and an SSR 1105 photon-counting rate meter.

The metastable nitrogen molecules are produced in the reaction between metastable $Ar(^3P_{0,2})$ and molecular nitrogen.[13,14] This transfer results in the production of nearly equal populations of the $C\ ^3\Pi_u$ and $B\ ^3\Pi_g$ states of N_2[15] which quickly cascade radiatively to the metastable $A\ ^3\Sigma_u^+$ state. A hollow-cathode discharge source was built to produce the argon metastables. While most experimenters have used tantalum for the electrodes,[14,16] we found 0.005 in. thick aluminum shim

 0021 9606/81/052888 08$01.00

TABLE I. Rate constants for reactions of $N_2(A\,^3\Sigma_u^+)$ $v = 0, 1$ with O and O_2.[a]

k_{O_2}	k_O	Comments	Reference
6.0	22	Hg $(6\,^3P_1)$ tracer k_O from $k_O/k_{O_2} = 3$–4 and listed number for k_{O_2} claim $k_{v=1}/k_{v=0} \approx 1.3$	2
2.9 ($v = 0$)	15	Claimed $k_{v=1} = k_{v=0}$ Looked at VK 0,6 and 1,5 with interference filters Probably some interference from NO γ bands	4
3.8		NO γ-band tracer	6
5.3		NO γ-band tracer	7
3.7		Hg $(6\,^3P_1)$ tracer Claim $k_{v=1} = k_{v=0}$	8
6.5		Hg $(6\,^3P_1)$ tracer	9
7.6		Hg $(6\,^3P_1)$ tracer – this value was measured relative to $k_{N+(A)+N} = 5 \times 10^{-31}$ cm^6 molecule^{-1} s^{-1}	10
1.9 ($v = 0$)		Measured $N_2(A)$ with absorption on nitrogen	3
7.6 ($v = 1$)		1$^+$ system	
3.5		Broad band filter – "mostly $v = 0$" – could have been contaminated with NO γ bands	11
4.5 ($v = 0$) 5.1 ($v = 1$)		$v = 0$ and $v = 1$ with monochromator – could have large uncertainty in reaction time	
2.3 ± 0.4 ($v = 0$) 1.1 ± 0.7 ($v = 1$)		Direct observation of Vegard–Kaplan emission in discharge-flow reactor	Present results

[a] The listed rate constants are for $T = 300$ K. They are in units of 10^{-12} cm^3 molecule^{-1} s^{-1}.

made an excellent electrode material. The shim was rolled into a cylinder whose diameter was the same as the inside diameter of the glass tubing through which the gas flowed (13 mm). The cathode (the downstream electrode) is 40 mm long, the anode 15 mm long, and the two electrodes are separated by 45 mm. The discharge is operated in the dc mode with the anode biased at +210 V. A load resistor of 10 kΩ gives the discharge stability and limits the current; the current in the present experiments is about 3 mA. The argon was purified by flowing it through a trap filled with a 5 A molecular sieve and cooled with dry ice. Since the experiments involved metastable nitrogen, it was not necessary to remove the nitrogen impurity from the argon carrier.

The metastables may be detected by the appearance of the characteristic reddish-violet flame which obtains upon the addition of nitrogen downstream from the discharge. At the concentrations of N_2 at the point of addition ($\approx 10^{15}$ molecules cm^{-3}) the flame length is about

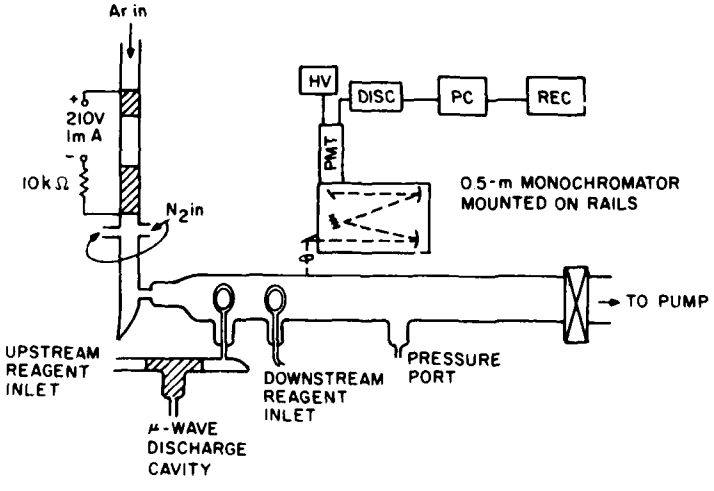

FIG. 1. Schematic of discharge-flow apparatus used in studies of $N_2(A)_{v=0,1}$ with O_2.

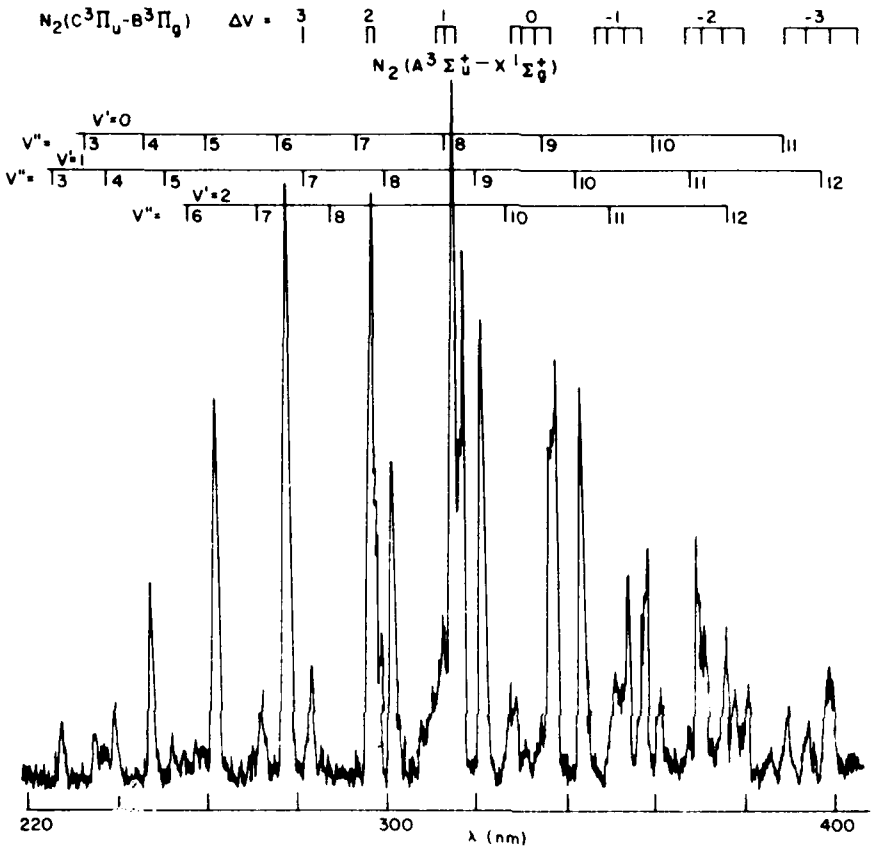

FIG. 2. Spectrum of Vegard-Kaplan bands emitted in discharge-flow reactor about 10 cm downstream from the discharge. $P = 2.08$ Torr, $\Delta\lambda = 0.66$ nm.

2 cm. This length is just governed by diffusional mixing of the two streams of gas, since at these nitrogen concentrations the collisional quenching times for nitrogen on argon are on the order of tens of microseconds.[17] Typically, the argon flow rate is ≈ 1500 μmol s^{-1}, the nitrogen flow rate ≈ 250 μmol s^{-1}, and the flow-tube pressure about 1.5 Torr. Typical flow velocities ranged from 1100–1500 cm s^{-1}. These were obtained by throttling the Roots blower, or by shutting the blower off and using only the forepump on the flow tube.

A typical spectrum of the Vegard-Kaplan bands emanating from the flow tube is shown in Fig. 2. The spectrum shows that the first three vibrational levels of $N_2(A)$ are populated in our system with relative populations of approximately 100, 50, 10 for $v' = 0$, 1, and 2, respectively. This is in contrast to the relative populations reported by Stedman and Setser of 100, 95, 10 for the same three levels, respectively.[2b,3] We performed some experiments which showed that the ratio $N_{v'=1}/N_{v'=0}$ increases under conditions of higher total pressure and higher mole fractions of nitrogen in the flow, and when the nitrogen inlet is separated from the Ar metastable discharge by a Wood's horn light trap. These general conditions obtained in the work of Stedman and Setser, and for the most part did not in the present experiments. In particular, the intervention of a light trap between the hollow cathode discharge and the nitrogen addition point enhances the ratio $N_{v'=1}/N_{v'=0}$ by more than a factor of 2.

Molecular oxygen was introduced into the reactor through a 1 in. diameter loop injector fabricated from 2 mm o.d. polyethylene tubing. The flow of molecular oxygen (1–5 μmol s^{-1}) was mixed with a substantial flow of helium (≈ 100 μmol s^{-1}) prior to injection into the flow tube. The helium flow gave greater injection velocity and thus better mixing than was the case when the O_2 was injected with nitrogen carrier. The mixing was checked visually using the O+NO chemiluminescent mixing chamber. Any effects of the kinetic measurements from small perturbations to the flow of the spectral peak were minimized by confining the measurement region to the 30–45 cm or 20–30 cm down-flow

of the injector. The molecular oxygen was purified by pumping on liquid O_2 prior to expanding the middle portion of the liquid O_2 into a 5 ℓ storage bulb.

Argon and nitrogen flow rates were measured using mass-flow meters (Teledyne Hastings-Raydist) whose calibrations were checked with a wet test meter. The flow rate of helium through the injector was measured with a rotameter which had also been calibrated against a wet test meter. Molecular oxygen flow rates were measured by timing the pressure increase into a calibrated volume. Flow tube pressures were measured using an MKS Baratron®.

B. Experimental technique

The two important processes leading to deactivation of the $N_2(A)$ in our reactor are Reaction (1) and diffusion to the reactor walls with subsequent deactivation at the walls. Quenching by Ar,[18] N_2,[18] and He[19] in the reactor is entirely negligible. The differential equation describing the rate of change in metastable nitrogen number density with time is

$$d[N_2(A)]/dt = -(k_w + k_1[O_2])[N_2(A)] . \quad (2)$$

Under pseudo-first-order conditions ($[N_2(A)] \ll [O_2]$) its solution is

$$\ln\{[N_2(A)]/[N_2(A)]_0\} = -(k_w + k_1[O_2])z/\bar{v} = K(z/\bar{v}) , \quad (3)$$

where k_w is the first-order wall deactivation rate, z the distance down the flow tube, and $\bar{v}$ is the bulk flow velocity. The wall deactivation rate constant k_w is inversely proportional to pressure, but is independent of molecular oxygen number density. Equation (3) provides us with two options for making the measurements: movable detector measurements or fixed-point determinations. In the movable detector measurements, $[O_2]$ and the total pressure are fixed and the pseudo-first-order decay rate K is measured by noting the change in $\ln[N_2(A)]$ as a function of z. Then the rate constant k_1 is given by a number of such pseudo-first-order decay rate measurements at fixed total pressure, but varying oxygen number density:

$$dK/d[O_2] = k_1 . \quad (4)$$

In the fixed-point measurements, the mixing distance is fixed and the decay in $\ln[N_2(A)]$ is measured as a function of $[O_2]$. This gives a decay constant

$$\Gamma = d\ln[N_2(A)]/d[O_2] = k_1 z/\bar{v} . \quad (5)$$

Because of problems with finite mixing time, it is best to make such measurements for several different mixing distances. Then on a plot of Γ vs z the rate constant is determined from the slope and the virtual point of mixing is obtained from the intercept on the abscissa.

The rate constants obtained from the above analysis assume a plug flow model. They must be increased by a factor of 1.6 to account for fluid dynamic effects in the reactor (see below).

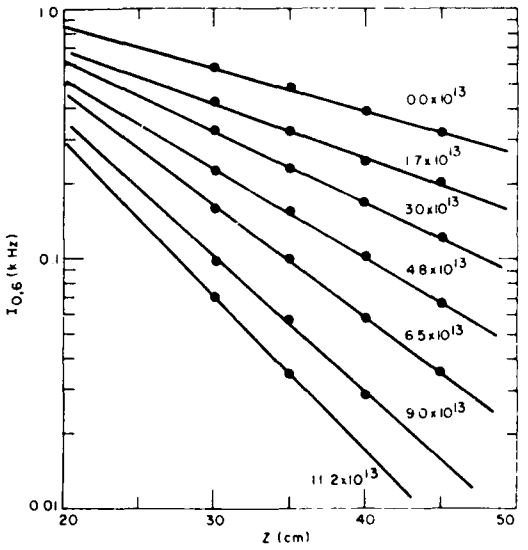

FIG. 3. The decay of $N_2(A)_{v=0}$ as a function of mixing distance and of $[O_2]$. The numbers by each line correspond to different $[O_2]$. $P = 1.33$ Torr, $\bar{v} = 1.6 \times 10^3$ cm s^{-1}, and $z_0 = 10$ cm.

C. Flow analysis

In our apparatus there is essentially unit probability of $N_2(A)$ deactivation in collisions with the reactor walls. Thus, a radial gradient in $N_2(A)$ number density is set up in the flow tube, and this radial gradient, when coupled with a parabolic velocity profile resulting from laminar flow within the flow tube, affects the analysis of the rate constant measurements. The proper fluid dynamic analysis of this situation has been considered exhaustively in the literature.[20-27] In the ideal case, the parabolic velocity profile is fully developed, and the rate constants determined under the assumption of plug flow conditions must be multiplied by a factor of 1.6 to give the true rate constant. The time required for the development of a parabolic velocity profile in the reactor is usually translated into a traversal distance $z = 0.227aR$, where z is the distance from the inlet of the tube, a is the tube radius, and R is the Reynolds number of the flow. In our experiments R ranges from 35–55 and typical entry lengths vary from 20–32 cm. All our measurements were done 30–45 cm downstream of the reagent inlet, thus ensuring that the flow was fully developed even if there was some perturbation to the flow from reagent addition. Thus, all our reported rate constants have been increased from the plug-flow values by a factor of 1.6. Possible corrections for the effects of axial diffusion, slip, and axial velocity gradients are entirely negligible under our conditions.[27] Inlet effects are accounted for by our having made the measurements at a number of positions along the flow tube.

III. RESULTS

Figures 3 and 4 illustrate the movable detector method for the rate constant measurements, while Figs. 5 and

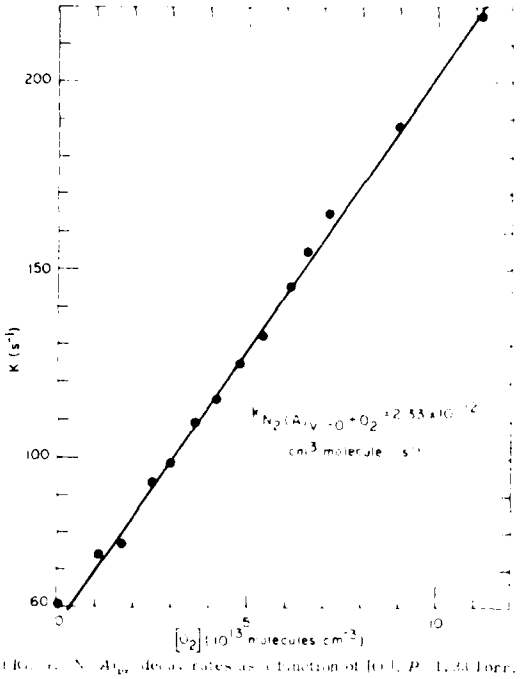

FIG. 6. $N_2(A^3\Sigma_u^+)$ decay rates as a function of $[O_2]$, $P = 1.33$ Torr.

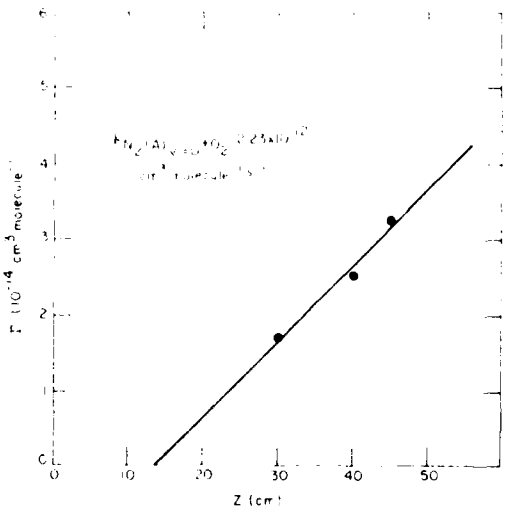

FIG. 7. Decay constants for $N_2(A^3\Sigma_u^+)$ removal by O_2 as a function of mixing distance. $P = 1.33$ Torr, $\bar{v} = 13.0 \times 10^4$ cm s^{-1}.

6 illustrate the fixed point technique. In both sets of measurements, the $v' = 0$ level was monitored using the 0, 6 Vegard–Kaplan band. Five such measurements in all gave $k_1(v' = 0) = (2.31 \pm 0.06) \times 10^{-12}$ cm^3 molecule^{-1} s^{-1}

where the uncertainty given is one standard deviation from the mean of the five sets of measurements.

Figure 7 shows the fixed-point decays of the $v' = 0$ and $v' = 1$ levels under the same conditions of mixing time and total pressure. Nine such measurements indicated that $k_1(v' = 1)/k_1(v' = 0) = 1.79 \pm 0.09$, where again the un-

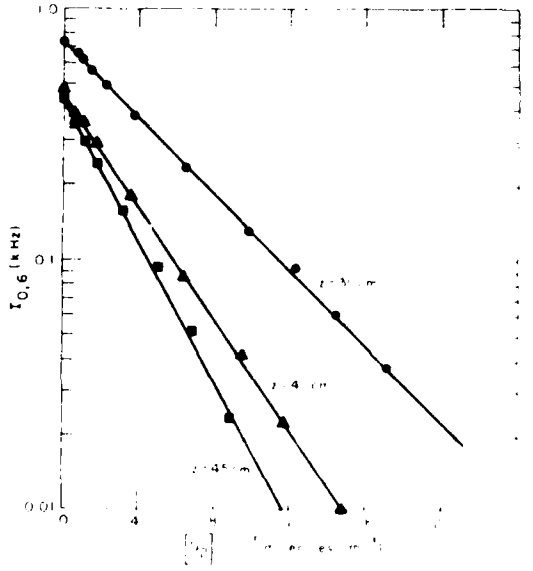

FIG. 8. Decay of $N_2(A^3\Sigma_u^+)$ [illegible] different mixing distances. $P = 1.33$ [illegible]

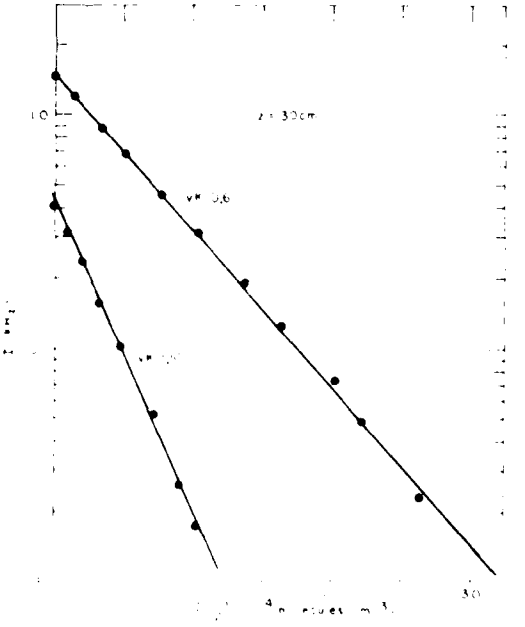

[illegible]

certainty is one standard deviation from the mean. Given the result for $k_1(v'=0)$ above, we get that $k_1(v'=1)$ is $(4.14 \pm 0.32) \times 10^{-12}$ cm^3 molecule^{-1} s^{-1}.

The total uncertainty (rms) including uncertainties in the experimental parameters, i.e., temperature, pressure, flow rate, etc., as well as the statistical variation in the measurements is 16% for the $v'=0$ measurements and 18% for the $v'=1$ measurements.

IV. DISCUSSION

Table I shows that our values are substantially in disagreement with most other measurements in the literature, although our values for the rate constants for $v'=0$ and $v'=1$ deactivation bracket the other values reported. Most of the other experimenters used either NO γ-band or Hg 6^3P_1 tracers and therefore made non-state-specific measurements, although Dunn and Young[4] and Clark and Setser[11] used interference filters to isolate spectral lines or portions of the spectrum, and Dreyer, Perner, and Roy[3] used an absorption diagnostic to monitor the $N_2(A)$ number density.

The use of interference filters can be misleading in the $N_2(A)$ system because the strong possibility of NO contamination in the system can lead to NO γ-band signals within the bandpass of the interference filter which can be much stronger than the signal from the $N_2(A)$ being monitored. The NO γ bands are very strongly excited in the energy-transfer reaction between $N_2(A)$ and NO.[11] In our system, even with a 1.7 nm bandpass, signals from the NO γ 0, 4 and 0, 5 bands at NO number densi-

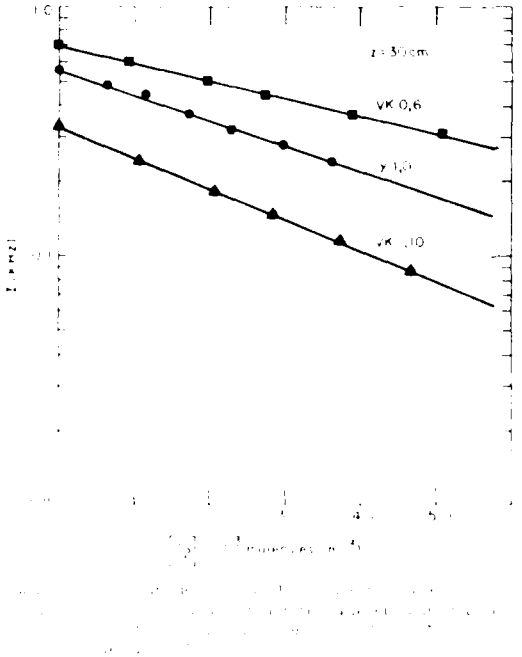

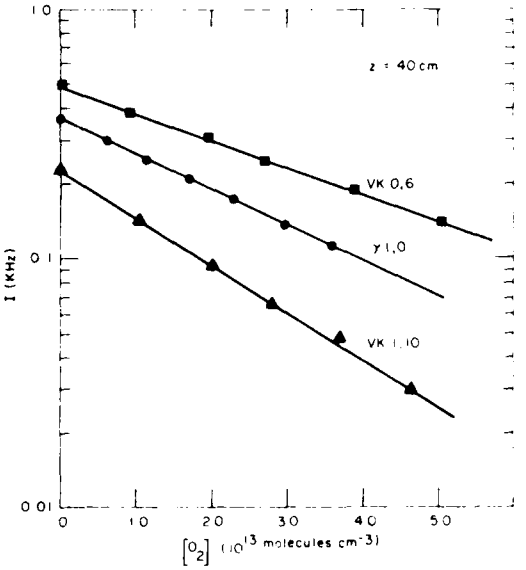

FIG. 9. Fixed-point decay of $N_2(A)$ as a function of $[O_2]$ for $v'=0$, $v'=1$ and a combination of both vibrational levels using the NO γ 1, 0 band as a tracer. P = 1.50 torr, $\bar{v}$ = 1.61 × 10^5 cm/sec, z = 40 cm. [NO] < 10^{11} molecules cm^{-3}.

ties on the order of 10^{11} molecules cm^{-3} significantly perturb the effective peak intensity of the Vegard–Kaplan 0, 6 band situated between them. The obliteration of the 1, 5 band of the Vegard–Kaplan system by the 0, 2 and 0, 3 γ bands is almost complete at such low number densities of NO. It is probably impossible in discharge-excited mixtures of N_2 and O_2 to avoid formation of significant amounts of NO. In our system, even very small leaks in the argon line, or sometimes slightly less pure gases, will give significant γ-band contamination of the Vegard–Kaplan spectrum even though the gas-handling system appears to be tight. In this case small traces of air are converted to NO in the metastable argon discharge. We therefore feel that the experiments of Dunn and Young[4] in which mixtures of N_2 and O_2 were discharged to make the $N_2(A)$ were almost certainly in fact tracer measurements.

A strong possibility also exists that the major experiments of Clark and Setser[11] were also tracer experiments because they could not spectrally scan the regions they were monitoring to ensure that they had a pure gas purity. Clark and Setser do report two direct measurements in which the 0, 6 and 1, 9 Vegard–Kaplan bands were monitored directly as a function of the quenching number density. The [illegible] were done using the five observation points [illegible] but only at the minimum observation points [illegible] so that the data could be seriously affected by [illegible] wall-deactivation corrections.

[illegible]

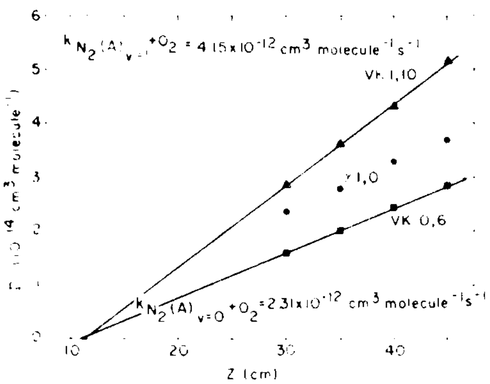

FIG. 10. Decay constants for $N_2(A)$ removal by O_2 as a function of reaction distance for $v'=0$, $v'=1$ and a mixture of vibrational levels using the NO γ 1,0 band as a tracer. P = 1.[illegible] Torr, $\bar{v}$ = 171[illegible] cm s^{-1}, [NO] ≤ [illegible] × 10$^{[illegible]}$ molecules cm^{-3}.

seriously affected by the use of a tracer or by NO impurities, which would act to make the measurements in effect tracer measurements. The one exception is the measurement of Dreyer *et al.*,[3] who used an absorption diagnostic. Our results agree with Dreyer *et al.* for $v'=0$, but they obtained a value for $v'=1$ a factor of 2 larger than ours. In general, rather larger deviations from the Beer–Lambert law can occur in absorption systems which use discharge lamps as the source of radiation,[28] and such deviations can affect strongly the analysis used to extract rate constants. Dreyer *et al.* do not discuss corrections to their lamp diagnostic. Our measurements are direct and contain no such complications in the analysis.

We designed an experiment to test the effects of using a tracer to follow $N_2(A)$ decay. We measured the decay of the 0,6 and 1,10 Vegard–Kaplan bands as a function of molecular oxygen number density, and under identical conditions, the decay of the 1,0 γ band of NO when a small trace of NO was added to the reactor. The number density of NO added to the reactor was ≲5 × 10^{10} molecules cm^{-3}, sufficient to give a strong tracer signal, but sufficiently small that NO quenching of $N_2(A)$ had little effect on the overall kinetics.

Two fixed-point decay plots are shown in Figs. 8 and 9. It is obvious from the plots that the $N_2(A)$ decay rate as monitored by the γ-band tracer is intermediate between the decays shown for the individual $N_2(A)$ vibrational levels. Figure 10 shows how the fixed-point decay constants vary with mixing distance. The γ-band-monitored decay constants are midway between the v' = 0 and v' = 1 decay constants, and at longer mixing times the tracer measurements approach more closely the decay of the v' = 0 level.

[illegible] optimum for demonstrating the tracer effect [illegible] observations are made [illegible] point of mixing [illegible] effective [illegible] from 11 to 20 ms [illegible] and our initial [illegible] 1.5[illegible] that only about 3[illegible] of the total $N_2(A)$ number density was in the v' = 1 state. In contrast to this, Clyne and Wood[?] and Young *et al.*[5] indicate that roughly two thirds of their initial $N_2(A)$ number density is in v' = 1 while Setser's group[illegible] has nearly equal number densities of the two states. Our tracer decay constants at the two shortest reaction times imply an $N_2(A)$ deactivation rate constant by O_2 of 3.3 × 10^{-12} cm^3 molecule^{-1} s^{-1} using the mixing correction determined from the VK 0,6 and 1,10 measurements.

V. SUMMARY

We have determined the rate constants for the deactivation of $N_2(A\,^3\Sigma_u^+)$ v' = 0 and 1 to be (2.3 ± 0.4) and (4.1 ± 0.7) × 10^{-12} cm^3 molecule^{-1} s^{-1}, respectively. Our rate constants for the two vibrational levels bracket the rate constants reported by most previous experimenters who used non-state-specific tracer techniques. The recent experimental observations of Zipf[12] of $k_{0,0}$ = 1.9 × 10^{-12} cm^3 molecule^{-1} s^{-1} and $k_{0,1}$ = 4.0 × 10^{-12} cm^3 molecule^{-1} s^{-1} are in excellent agreement with our own measurements.

ACKNOWLEDGMENTS

These experiments were conducted at the Air Force Geophysics Laboratories in Bedford, Mass. under AFOSR Project No. 231064. PSI participation was funded under Air Force Contract # F19628-77-C-0089. We are grateful for program support from both the Defense Nuclear Agency and the Air Force Office of Scientific Research. LGP thanks Professor E. C. Zipf (University of Pittsburgh) and Professor D. W. Setser (Kansas State University) for preprints of their work prior to publication; he also thanks Dr. W. T. Rawlins (PSI) for interesting discussions.

[1]W. Swider, [illegible] 1969.
[2]J. A. Meyer, [illegible] Setser, [illegible] Chem. 7[illegible]
[3]J. W. Dreyer, D. Perner, and [illegible] Phys. 61, [illegible] 1974.
[4]G. E. [illegible] 1966.
[5]J. A. Meyer, D. A. Setser, and D. [illegible] Astrophys. J. 157, [illegible] 1969.
[6]R. A. Young, [illegible] Phys. 50, [illegible]
[illegible]
[illegible]
[illegible]

195 (1971).
[3]L. C. Piper, J. E. Velazco, and D. W. Setser, J. Chem. Phys. 59, 3323 (1973).
[24]D. Levron and A. V. Phelps, J. Chem. Phys. 69, 2260 (1978).
[25]C. R. Roy, J. W. Drever, and D. Perner, J. Chem. Phys. 63, 2131 (1975).
[26]E. E. Ferguson, F. C. Fehsenfeld, and A. L. Schmeltekopf, in *Advances in Atomic and Molecular Physics V*, edited by D. R. Bates (Academic, New York, 1970).
[27]R. C. Bolden, R. S. Hemsworth, M. J. Shaw, and N. D. Twiddy, J. Phys. B ., 15 (1970).
[28]A. L. Farragher, Trans. Faraday Soc. 66, 1411 (1970).
[29]R. W. Huggins and J. H. Cahn, J. Appl. Phys. 38, 180 (1967).
[30]R. E. Walker, Phys. Fluids 4, 1211 (1961).
[31]R. V. Poirer and R. W. Carr, J. Phys. Chem. 75, 1593 (1971).
[32]M. Cher and C. S. Hollingsworth, Adv. Chem. Ser. 80, 118 (1969).
[33]J. H. Kolts and D. W. Setser, J. Chem. Phys. 68, 4848 (1978).
[34]W. T. Rawlins and F. Kaufman, J. Quant. Spectrosc. Radiat. Transfer 18, 561 (1977).

Appendix E

Rate Constants for Deactivation of $N_2(A\ ^3\Sigma_u^+, v' = 0,1)$ by O

Rate constants for deactivation of $N_2(A\,^3\Sigma_u^+, v'=0,1)$ by O

L. G. Piper and G. E. Caledonia

Physical Sciences Inc., Woburn, Massachusetts 01801

J. P. Kennealy

Air Force Geophysics Laboratories, Bedford, Massachusetts 01730

(Received 9 March 1981; accepted 26 May 1981)

The removal of $N_2(A\,^3\Sigma_u^+, v'=0,1)$ by O has been studied in a room temperature discharge-flow apparatus by monitoring the temporal decay of the 0,6 and 1,10 bands of the Vegard–Kaplan system. The measured rate constants are (2.8 ± 0.4) and $(3.4 \pm 0.6) \times 10^{-11}$ cm^3 molecule^{-1} s^{-1} for $v'=0$ and 1, respectively.

I. INTRODUCTION

It has been suggested that the reactions of $N_2(A^3\Sigma_u^+)$ with atomic and molecular oxygen could be significant sources of odd nitrogen and vibrationally excited NO in the upper atmosphere.[1] For the interaction between $N_2(A)$ and atomic oxygen, the possible reaction channels are as follows:

$$N_2(A\,^3\Sigma_u^+)_{v'\le 1} + O(^3P) \rightarrow N_2(X\,^1\Sigma_g^+) + O(^3P) + 6.2\ \text{eV}, \quad (1a)$$

$$N_2(X\,^1\Sigma_g^+) + O(^1D) + 4.2\ \text{eV}, \quad (1b)$$

$$N_2(X\,^1\Sigma_g^+) + O(^1S) + 2.0\ \text{eV}, \quad (1c)$$

$$NO(X\,^2\Pi) + N(^4S) + 2.9\ \text{eV}, \quad (1d)$$

$$NO(X\,^2\Pi) + N(^2D) + 0.5\ \text{eV}. \quad (1e)$$

Reactions (1d) and (1e) may be major sources of NO and $N(^2D)$ in auroras and in the quiet daytime E region[1]; in addition, some of the exothermicity of these reactions may appear as vibrational energy in the product NO molecules. The further reaction of $N(^2D)$, formed in Reaction (1e), with ambient O_2 can also produce vibrationally excited NO.

The rate constant for quenching $N_2(A\,^3\Sigma_u^+)$ by oxygen atoms has been reported to be 2.2×10^{-11} and 1.5×10^{-11} cm^3 molecule^{-1} s^{-1}.[3] However, Meyer *et al.*'s[2] number was measured relative to the rate constant for quenching $N_2(A)$ by molecular oxygen k_2, which they took to be 6.0×10^{-12} cm^3 molecule^{-1} s^{-1}, and should be reduced by a factor of 2 to conform to presently accepted values of k_2.[4] The determination of Dunn and Young[3] was made in a complicated system which could provide reactive species, in addition to $N_2(A)$, which might complicate the kinetics. Furthermore, their atomic oxygen number densities were subject to substantial uncertainties. Some aeronomic estimates[1] have favored a value closer to 10^{-13} cm^3 molecule^{-1} s^{-1}, although recent rocket measurements by Sharp *et al.*[5,6] and O'Neil *et al.*[7] are in conflict on this. Sharp *et al.*[5,6] favor a value of 2×10^{-13} cm^3 molecule^{-1} s^{-1}, while O'Neil *et al.*[7] support the earlier laboratory measurements with an estimate for k_1 of $(2 \pm 4) \times 10^{-11}$ cm^3 molecule^{-1} s^{-1}.

Only Meyer *et al.*[2] have investigated the products of the reaction between $N_2(A)$ and oxygen atoms. They observed excitation of $O(^1S)$ by its characteristic emission at 557.7 nm, and estimated that 25^{+12}_{-7}% of the total $N_2(A)$ quenching by oxygen atoms occurs via this path. This estimate is probably a lower limit since they neglected quenching of $O(^1S)$, which can be considerable in systems containing discharged oxygen. Our recent observations indicate a value much larger than this.[9] Their system was not sufficiently free from extraneous NO contamination to rule out the possibility of NO product formation as well.

During the course of a program to study product formation in Reaction (1), we remeasured the rate constants at 300 K for this reaction for both vibrational levels 0 and 1. Our results are about a factor of 2 higher than the corrected measurement of Meyer *et al.*[2] and that of Dunn and Young,[3] but a factor of 7 less than the aeronomic estimate of Sharp *et al.*[5,6] In contrast to the quenching of $N_2(A)$ by O_2, where $k_2^{v=1}/k_2^{v=0} \approx 1.8$,[4] the quenching of $N_2(A)$ by atomic oxygen shows only a 20% enhancement of $k_1^{v=1}$ over $k_1^{v=0}$.

II. EXPERIMENTAL

A. Apparatus

The experiments were done in a discharge–flow apparatus with the $N_2(A)$ number densities monitored by spectroscopic observations of individual vibrational bands of the Vegard–Kaplan $N_2(A\,^3\Sigma_u^+ - X\,^1\Sigma_g^+)$ system of nitrogen. The reactor, which has been described in detail previously,[4,10(a)] is a 2 in. diameter quartz tube which is pumped by a Roots blower that is capable of producing linear flow velocities up to 8×10^3 cm s^{-1} at pressures of 1 Torr. A 0.5 m monochromator (Minuteman) is mounted upon a set of rails parallel to the flow tube. Spectral observations of the luminous gases in the flow tube, therefore, can be made as a function of linear distance along the tube by sliding the monochromator up and down on its rails. Distances are converted to reaction times by dividing by the flow velocity. Light intensities are measured photoelectrically using a thermoelectrically cooled EMI 9558QA photomultiplier and an an SSR 1105 photon-counting rate meter.

The metastable nitrogen molecules are produced in the reaction between metastable $Ar(^3P_{0,2})$ and molecular nitrogen.[10,11] This transfer results in the production of nearly equal populations of the $C\,^3\Pi_u$ and $B\,^3\Pi_g$ states of N_2[12] which quickly cascade radiatively to the metastable $A\,^3\Sigma_u^+$ state. The metastable argon is produced

by flowing argon through a cold, hollow-cathode discharge operated at about 210 V and 3 mA. The argon was purified by flowing it through a trap filled with a 5 A molecular sieve and cooled with dry ice. Typically, the argon flow rate is ~1500 μmol s^{-1}, the nitrogen flow rate is ~250 μmol s^{-1}, and the flow tube pressure is about 1.3 Torr. Typical flow velocities ranged from 1100–1500 cm s^{-1}. These were obtained by throttling the Roots blower, or by shutting the blower off and using only the forepump on the flow tube.

Atomic oxygen was made by dissociating O_2 in a microwave discharge through a small amount of O_2 in helium (typical flows: 1 μmol s^{-1} of O_2 and 100 μmol s^{-1} of He). The oxygen atoms were injected into the flow tube through a 1 m, diameter loop fabricated from 2 mm o.d. polyethylene tubing. Number densities of atomic oxygen were determined using the air-afterglow technique,[13,14] which required the injection of NO through a second loop in the flow tube about 10 cm downstream from the oxygen injector.

The molecular oxygen was purified by pumping on liquid O_2 prior to expanding the middle portion of the liquid O_2 into a 5–1 storage bulb. The nitric oxide used in the O-number-density determinations was purified by slowly flowing NO through an ascarite trap, and then a trap at dry ice temperature prior to storage in a 5–1 bulb.

B. Determination of atomic oxygen number density

When atomic oxygen and nitric oxide are mixed, a continuum emission called the air afterglow is observed, which extends from 375 to beyond 3000 nm.[13–22] The intensity of this emission is directly proportional to the product of the number densities of atomic oxygen and nitric oxide, and independent of pressure of bath gas, at least at pressures above about 0.2 Torr. Thus, the emission intensity of the air afterglow is given by

$$I_{O/NO} = \kappa_A[O][NO], \tag{2}$$

where κ_A is a calibration constant specific to the particular viewing geometry and incorporates such things as detection system efficiency, the size of the observation volume, and the absolute air-afterglow rate constant. κ is a function of wavelength both through the detection systems' spectral response as well as through the wavelength variation of the air-afterglow rate constant. The calibration constant κ is determined experimentally by titrating atomic nitrogen with excess NO:

$$N + NO \rightarrow N_2 + O. \tag{3}$$

In the absence of added nitric oxide, N-atom recombination produces chemiluminescence from the nitrogen first-positive bands, the intensity of which is proportional to the square of the N-atom number density:

$$N + N + M \rightarrow N_2(B^3\Pi_g) + M, \tag{4}$$

$$N_2(B^3\Pi_g) \rightarrow N_2(A^3\Sigma_u^+) + h\nu \quad \text{(first positive bands)}. \tag{5}$$

Upon addition of NO, the first positive emission intensity decreases until such a point that the quantity of NO added balances the amount of N atoms initially in the flow. At this point, the end point of the NO titration,

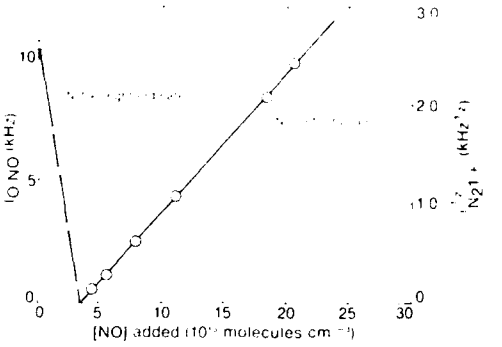

FIG. 1. Variation in emission at 580 ± 5 nm as a function of added [NO].

all N initially in the reactor has been quantitatively converted to O, and no emission is observed in the reactor. When even more NO is added to the reactor, the air-afterglow emission begins to be observed, and the intensity of the emission will vary linearly with the amount of NO added. An N-atom titration plot is shown in Fig. 1. The equation describing the change in the air-afterglow intensity as a function of added NO for NO additions beyond the titration end point is

$$I_{O/NO} = \kappa[O][NO] = \kappa[N]_0([NO]_0 - [N]_0), \tag{6}$$

where κ is the constant of proportionality relating the air-afterglow intensity to the product $[O][NO]$, $[N]_0$ is the number density of N atoms initially in the reactor prior to NO addition and the O-atom number density for NO additions beyond the titration end point, and $[NO]_0$ refers to the NO number density which would obtain in the absence of Reaction (3). The factor κ, then, is determined to be the ratio of the square of the slope to the intercept of the line describing the change in air-afterglow intensity with $[NO]_0$.[23]

O-atom number densities in the present experiments were determined by measuring the air-afterglow signal at 580 nm, with a 5 nm bandpass at at least three different NO number densities. Then [O] was taken to be the slope of the line representing the air-afterglow intensity as a function of [NO] divided by κ. Even through small amounts of ozone could be by-products of the O-atom discharge, there can be no interference from the O_3 + NO chemiluminescent reaction in the technique for determining the O-atom number density. The continuum generated from the O_3 + NO reaction has a short wavelength cutoff of 600 nm.[24]

A series of calibrations taken over a period of time established κ to ± 10%. The slopes of the $I_{O/NO}$ vs [NO] plots for the determination of [O] has standard deviations less than 5%. Thus, the determination of [O] is, in principle, accurate to ± 12%. Because the measurements of [O] were not made simultaneously with the kinetic measurements, it is possible that short-term variations in [O] could lead to differences between the number density of O measured and that actually in the reactor during the kinetic measurements. We shall

assume these differences to be random and therefore included in the experimental scatter in the data analysis.

C. Experimental technique for measurement of the quenching of $N_2(A)$ by atomic oxygen

Atomic oxygen is produced for the studies of the quenching of $N_2(A)$ by dissociating molecular oxygen in a microwave discharge of a trace of O_2 in helium. When the discharge is on, there are three important processes for $N_2(A)$ removal: deactivation at the wall (rate constant k_w), quenching by atomic oxygen (rate constant k_2), and quenching by molecular oxygen (rate constant k_3). With the discharge on, the equation describing the change in $N_2(A)$ number density with distance down the flow tube is given by

$$t \ln \frac{[N_2(A)]^{on}}{[N_2(A)]_0^{on}} = -(k_w + k_2[O] + k_3[O_2])z , \tag{7}$$

When the discharge is turned off, the $N_2(A)$ number density is given by

$$t \ln \frac{[N_2(A)]^{off}}{[N_2(A)]_0^{off}} = -(k_w + k_3[O_2])z , \tag{8}$$

When the discharge is on, the molecular oxygen number density is given by

$$[O_2] = [O_2]_0 - \tfrac{1}{2}[O] , \tag{9}$$

where $[O_2]_0$ is the number density of O_2 with the discharge off. Substituting Eq. (9) into Eq. (7) and taking the difference between Eqs. (7) and (8) results in an expression which relates the ratio of the $N_2(A)$ number density with the discharge on to that with it off to the rate constant of interest k_2, the atomic oxygen number density, and the reaction time, i.e.,

$$\ln \frac{[N_2(A)]^{on}}{[N_2(A)]_0^{on}} - \ln \frac{[N_2(A)]^{off}}{[N_2(A)]_0^{off}} = \ln \frac{[N_2(A)]^{on}}{[N_2(A)]^{off}}$$

$$= -k_2 z \frac{[O]}{v} . \tag{10}$$

Plots of the left-hand side of Eq. (10) against $[O]$ give straight lines whose slopes equal $-k_2 z/v$. Γ'. The slope from a plot of Γ' vs $[O]$ can be used to obtain the unknown rate constant k_2 given the previously determined rate constant k_w.

D. Flow analysis

In our apparatus there is essentially unit probability of $N_2(A)$ deactivation in collisions with the reactor walls. Hence, a radial gradient in $N_2(A)$ number density is set up in the flow tube, and this radial gradient, when coupled with a parabolic velocity profile resulting from laminar flow within the flow tube, affects the analysis of the rate constant measurements. The proper fluid dynamical analysis of this situation has been considered extensively in the literature [ ]. In the ideal case, the parabolic velocity profile is fully developed, and the rate constants determined under the assumption of plug flow conditions must be multiplied by a factor of 1.6 to obtain the true rate constant. The time required for the development of a parabolic velocity profile in the reactor is usually translated into a traversal distance $0.227aR$, where z is the distance from the inlet of the tube, a is the tube radius, and R is the Reynolds number of the flow. In our experiments R ranges from 35–55 and typical entry lengths vary from 20–32 cm. All our measurements were done 30–45 cm downstream of the reagent inlet, thus ensuring that the flow was fully developed even if there was some perturbation from the flow from reagent addition.

III. RESULTS

Figures 2 and 3 show the plots of the left-hand side of Eq. (10) vs $[O]$ for $N_2(A)$, $v' = 0$ at two different reaction distances, and Fig. 4 the plot of Γ' vs z for the $v' = 0$ measurements which monitored the 0, 6 Vegard–Kaplan band; Figs. 5, 6, and 7 show the similar plots for measurements made on the 1, 10 band. The slopes of the plots of Γ' vs z are $(1.7 \pm 0.1) \times 10^{-11}$ cm^3 molecule^{-1} s^{-1} for $v' = 0$ and $(2.0 \pm 0.1) \times 10^{-11}$ cm^3 molecule^{-1} s^{-1} for $v' = 1$, where the uncertainty given is one standard deviation in the least squres fit. The removal rate constants are then determined by multiplying these slopes by 1.6 to correct for flow effects (Sec. III D) and adding half of the rate constant for removal by molecular oxygen. We previously have determined these rate constants to be 2.3×10^{-12} and 4.1×10^{-12} cm^3 molecules^{-1} s^{-1} for $v' = 0$ and 1, respectively.[1] The final results for the removal of $N_2(A^3\Sigma_u^+)$ by atomic oxygen are $(2.8 \pm 0.2) \times 10^{-11}$ cm^3 molecule^{-1} s^{-1} for $v' = 0$ and $(3.4 \pm 0.2) \times 10^{-11}$ cm^3 molecule^{-1} s^{-1} for $v' = 1$. The total uncertainty (rms), including uncertainties in temperature, pressure, flow rate, O-atom number density, etc., is 15%

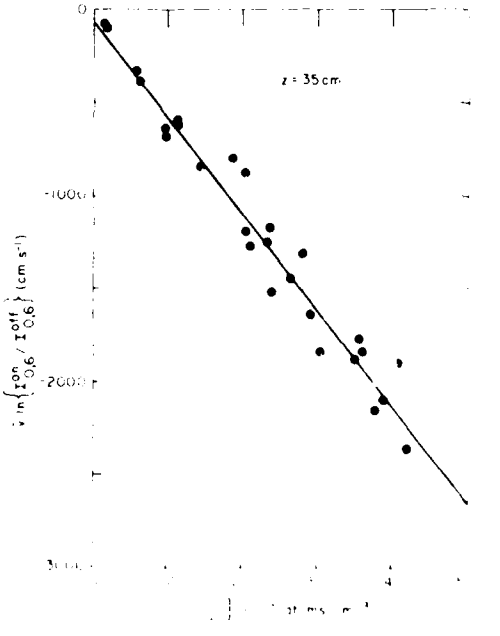

[illegible] distance [illegible]

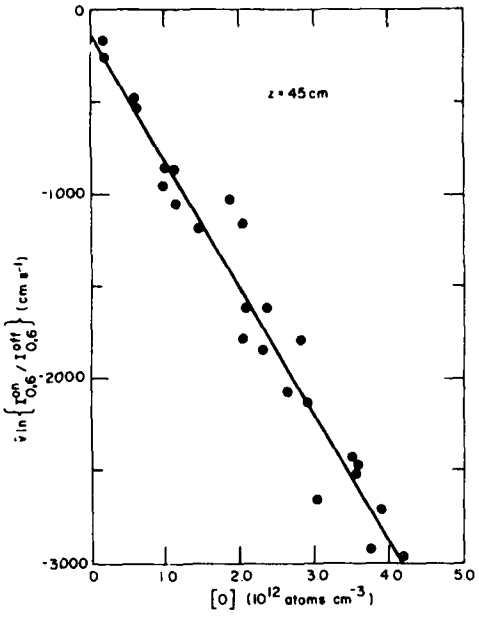

FIG. 3. The decay of $N_2(A)_{v=0}$ as a function of [O] for a mixing distance of 45 cm.

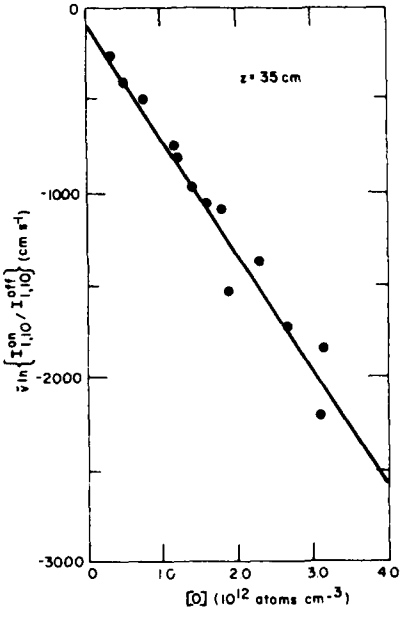

FIG. 5. The decay of $N_2(A)_{v=1}$ as a function of [O] for a mixing distance of 35 cm.

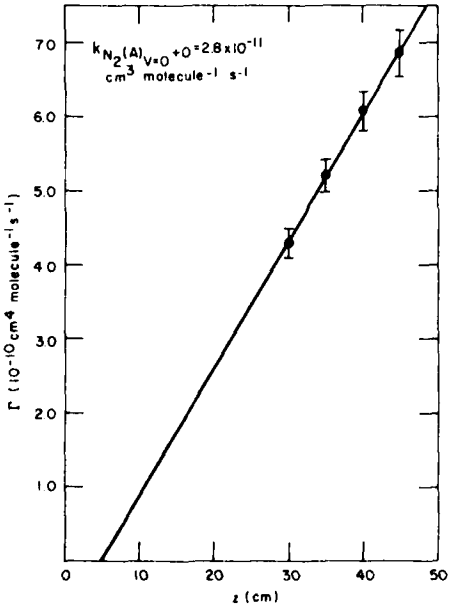

FIG. 4. Decay constants for $N_2(A)_{v=0}$ + O as a function of reaction distance.

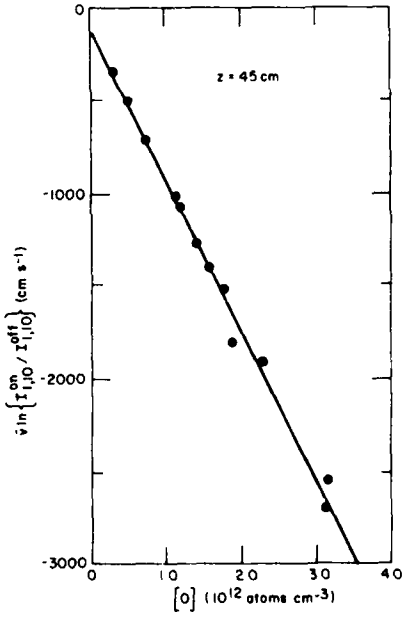

FIG. 6. The decay of $N_2(A)_{v=1}$ as a function of [O] for a mixing distance of 45 cm.

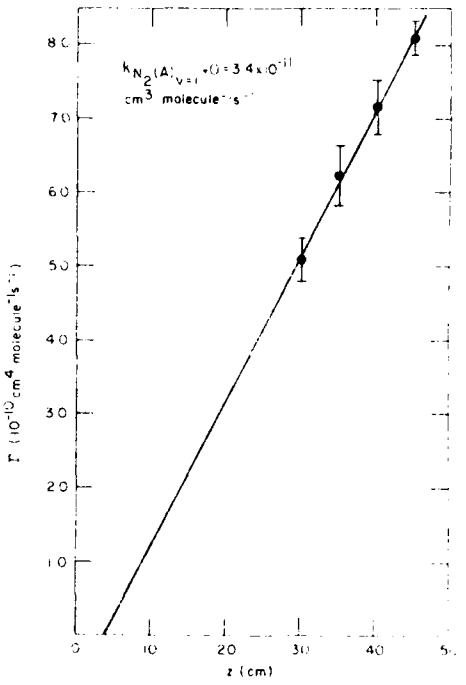

FIG. 2. Decay constants for $N_2(A^3\Sigma_u^+, v=1)$ as a function of reaction distance.

for $x' = 0$ and 19% for $x' = 4$. These results are tabulated in Table I along with some other values which have appeared in the literature.

IV. DISCUSSION

At least two other species which are known to be produced to some extent in oxygen discharges also could be potential quenchers of $N_2(A)$. These species are ozone and $O_2(a^1\Delta)$. The electronically excited molecular oxygen is formed primarily through the heterogeneous recombination of atomic oxygen, while the ozone is formed from the three body reaction

$$O + O_2 + M \rightarrow O_3 + M$$

$$k_{11} = 3.6 \times 10^{-34} \text{ cm}^6 \text{molecule}^{-2} \text{s}^{-1}; \quad \text{M} = \text{Ar}). \quad (11)$$

The ozone is destroyed by reaction with atomic oxygen

$$O + O_3 \rightarrow 2O_2$$

$$k_{12} = 8.4 \times 10^{-15} \text{ cm}^3 \text{molecule}^{-1} \text{s}^{-1},^{30} \quad (12)$$

reaction with $O_2(a^1\Delta)$,[31] and with hydrogeneous impurities in the discharged gas.[32] This latter removal process probably has the largest effect, but is the most difficult to assess. Given sufficient reaction time, Reactions (11) and (12) combine to give an upper limit to the steady-state concentration of O_3 which is governed by the ratio $k_{11}[M][O_2]/k_{12}$. We estimate that the pressure in the tube containing the atom discharge is about 1.8 Torr. Then, the ratio $[O_3]/[O_2] = k_{11}[M]/k_{12}$ is less than or equal to 0.011, where we have made the assumption that the third body efficiency of helium in Reaction (11) is similar to that for argon. This assumption probably is good to $\pm 30\%$.[33]

The point of the above argument is that, in the worst case, the ozone number density in the reactor will be only 1% of the molecular oxygen number density, whereas the atomic oxygen number density is typically about 25% of the molecular oxygen number density. Thus, even if the rate constant for quenching $N_2(A)$ by ozone is 1×10^{-11} cm^3 molecule^{-1} s^{-1}, the measurement of the rate constant for quenching of $N_2(A)$ by O will be too large by only 12%. Given that our calculated ozone number density is an upper limit because of our neglect of the removal of ozone by $O_2(a^1\Delta)$ and by hydrogeneous impurities created in the discharge, we feel confident in rejecting ozone as a significant quencher of $N_2(A)$ in this series of measurements. However, the sidearm pressure was not varied to check for this effect.

Electronically excited molecular oxygen $O_2(a^1\Delta)$ could also be a potential quencher of $N_2(A)$. This species is produced to some extent in the discharge and also in the heterogeneous recombination of atomic oxygen of the Pyrex walls of the injector.[34] The presence of significant number densities of $O_2(a^1\Delta)$ in the gas stream can have two possible effects. If the electronically excited molecular oxygen quenches or reacts with $N_2(A)$ very efficiently, our rate constant for Reaction (1) will be too large. On the other hand, if the rate constant for the interaction between $N_2(A)$ and $O_2(a^1\Delta)$ is very small

TABLE I. Rate constants for removal of $N_2(A^3\Sigma_u^+, v=1)$ by O.

Rate constant[a]	Method	Reference
$k_{N_2(A)_{v=1}+O}$	Flow-P_2 tracer value from $k_{v=4}$, $k_{v=3}$, $k_{v=2}$ and $k_{v=1}$ = $(3.6 \pm 0.6) \times 10^{-11}$ cm^3 molecule^{-1} s^{-1}. Correcting average value of $k_{N_2(A)_{v=1}+O}$ for 20% admixture of $N_2(A)$, $v=0$ and 1 gives value in parentheses.	Meyer, Setser, and Stedman[7]
1.3×10^{-10}	Looked at VK, 0,3 and 1,5 with interference filters in pulsed N_2–O discharge. Probably interference from γ bands. See essential agreement with present results.	Dunn and Young[9]
2.5×10^{-10} to 3.5×10^{-10}	Direct observation of the decay of Vegard–Kaplan emission in discharge flow reactor.	Present results
$\leq 4 \times 10^{-11}$	Estimated from upper limit to rate constant for loss of $N_2(A)$ in collisions with electronically excited argon at altitudes 100–200 km.	O'Neil, Lee, and Hunt[5]
1×10^{-10}	Estimated from rate constant for $N_2(A)$ + CO and $N_2(A)$ + O_2 and assumed $k_{N_2(A)+O} = k_{N_2(A)+CO}$	Fort and Shaw[6]

[a] The listed rate constants are in units of 10^{-10} cm^3 molecule^{-1} s^{-1} and are for 300 K.

$< 10^{-13}$ cm^3 molecule^{-1} s^{-1}) and if, in addition, a large fraction of the undissociated molecular oxygen is in the $a^1\Delta$ state, then we will have overcorrected for quenching of $N_2(A)$ by the undissociated molecular oxygen, and the rate constant we present will be smaller than the true value. However, even if 100% of the undissociated molecular oxygen is in the $a^1\Delta$ state, our rate constant will be low by less than 25%.

Although we cannot think of mechanisms that would make $O_2(a^1\Delta)$ a significantly more efficient quencher of $N_2(A)$ than $O_2(X^3\Sigma_g^-)$, the combination of more than 30% of the undissociated O_2 in the $a^1\Delta$ state *and* an $N_2(A)$ $-O_2(a^1\Delta)$ rate constant greater than 10^{-11} cm^3 molecule^{-1} s^{-1} would cause our measurement of k_1 to be high by more than 25%. As evidence that these two coincidental conditions did not obtain in the present experiments, we note that $O(^1S)$ is excited strongly in our reactor.[9] This excitation must be via Reaction (1c) because the dissociative excitation of $O_2(a^1\Delta)$ by $N_2(A)$ to make $O(^1S)$ and $O(^3P)$ is not energetically feasible. Preliminary results[9] indicate that most of the quenching of $N_2(A)$ by O leads to $O(^1S)$ excitation. Thus, the possible presence of $O_2(a^1\Delta)$ in our reactor cannot cause large errors in our measurements. Strictly speaking, however, our measurements should be considered upper limits until any effects of $O_2(a^1\Delta)$ on $N_2(A)$ quenching measurements can be demonstrated conclusively.

Our results, although of substantially improved accuracy, confirm the earlier laboratory measurements with respect to the order of magnitude of k_1. In addition, our values are in excellent agreement with the model-derived rate constants of O'Neil *et al.*[7] in their simulated-aurora, rocket experiments. The model-derived rate constant of Sharp *et al.*[5,6,35] of 2.0×10^{-10} cm^3 molecule^{-1} s^{-1} differs substantially from our measurements. The resolution of this discrepancy will require a careful reanalysis of the model and input data used by Sharp *et al.* to derive their rate constant.

ACKNOWLEDGMENTS

These experiments were conducted at the Air Force Geophysics Laboratories in Bedford, Mass. under AFOSR project No. 231064. PSI participation was funded under Air Force Contract #19628-77-C-0089. We are grateful for program support from both the Defense Nuclear Agency and the Air Force Office of Scientific Research. LGP appreciates interesting discussions with R. R. O'Neil (AFGL), T. G. Slanger (SRI, Int), F. A. Ogryzolo (University of British Columbia), and W. T. Rawlins (PSI).

[5]W. E. Sharp, M. H. Rees, and A. I. Stewart, J. Geophys. Res. 84, 1977 (1979).
[6]D. G. Torr and W. E. Sharp, Geophys. Res. Lett. 6, 969 (1979).
R. R. O'Neil, E. T. P. Lee, and E. R. Huppi, J. Geophys. Res. 84, 823 (1979).
[7]J. A. Meyer, D. W. Setser, and D. H. Stedman, Astrophys. J. 157, 1023 (1969).
[8](a) G. E. Caledonia, L. G. Piper, W. T. Rawlins, and B. D. Green, PSI TR-233 (1980), available from the authors upon request; (b) L. G. Piper (manuscript in preparation).
[9]D. W. Setser, D. H. Stedman, and J. A. Coxon, J. Chem. Phys. 53, 1004 (1970).
[11]D. H. Stedman and D. W. Setser, Chem. Phys. Lett. 2, 542 (1968).
[12]J. H. Kolts, H. C. Brashears, and D. W. Setser, J. Chem. Phys. 67, 2931 (1977).
[13]F. Kaufman, Proc. R. Soc. London Ser. A 247, 123 (1958).
[14]F. Kaufman, *Chemiluminescence and Bioluminescence*, edited by M. J. Cormier, D. M. Hercules, and J. Lee (Plenum, New York, 1973), pp. 83–100.
[15]A. T. Stair and J. P. Kenneally, J. Chim. Phys. 64, 124 (1967).
[16]A. Fontijn, C. B. Meyer, and H. I. Schiff, J. Chem. Phys. 40, 64 (1964).
[17]M. Vanpee, K. D. Hill, and W. R. Kineyko, AIAA J. 9, 135 (1971).
[18]M. F. Golde, A. E. Roche, and F. Kaufman, J. Chem. Phys. 59, 3953 (1973).
[19]D. Golomb and J. H. Brown, J. Chem. Phys. 63, 5246 (1975).
[20]G. A. Woolsey, P. H. Lee, and W. D. Slafer, J. Chem. Phys. 67, 1220 (1977).
[21]M. Sutoh, Y. Morioka, and M. Nakamura, J. Chem. Phys. 72, 20 (1980).
[22]A. M. Pravilov and L. G. Smirnova, Kinet. Catal. (USSR) 19, 202 (1978).
[23]For a more complete discussion of this calibration process including caveats, please see Ref. 9(a).
[24]P. N. Clough and B. A. Thrush, Trans. Faraday Soc. 63, 915 (1967).
[25]E. E. Ferguson, F. C. Fehsenfeld, and A. L. Schmeltekopf, Adv. At. Mol. Phys. 5, 1 (1970).
[26]R. C. Bolden, R. S. Hemsworth, M. J. Shaw, and N. D. Twiddy, J. Phys. B 3, 45 (1970).
A. L. Farragher, Trans. Faraday Soc. 66, 1411 (1970).
[28]R. W. Huggins and J. H. Cahn, J. Appl. Phys. 38, 180 (1967).
[29]R. E. Walker, Phys. Fluids 4, 1211 (1961).
[30]R. V. Poirier and R. W. Carr, J. Phys. Chem. 75, 1536 (1971).
[31]M. Cher and C. S. Hollingsworth, Adv. Chem. Ser. 80, 115 (1969).
[32]J. H. Kolts and D. W. Setser, J. Chem. Phys. 68, 4848 (1978).
[33]J. Arnold and F. J. Comes, Chem. Phys. 42, 231 (1979).
[34]K. H. Becker, W. Groth, and U. Schurath, Chem. Phys. Lett. 14, 489 (1972).
[35]J. L. McCrumb and F. Kaufman, J. Chem. Phys. 57, 1270 (1972).
[36]D. L. Baulch, D. D. Drysdale, J. Duxbury, and S. J. Grant, *Evaluated Kinetic Data for High Temperature Reactions* III *Homogeous Gas Phase Reactions of the O_2–O_3 System, the CO–O–H System and of Sulfur-containing Species* (Butterworths, London, 1976).
[37]G. Black and T. G. Slanger, J. Chem. Phys. 74, 6137 (1981).
[38]W. E. Sharp and D. G. Torr, J. Geophys. Res. 84, 534 (1979).
[3]W. Swider, Geophys. Res. Lett. 3, 335 (1976).
[4]A. A. Meyer, D. W. Setser, and D. H. Stedman, J. Phys. Chem. 74, 2238 (1970).
[10]J. Heicklen and R. A. Young, Int. J. Chem. Kinet. 5, 161 (1973).
[31]L. G. Piper, G. E. Caledonia, and J. P. Kennealy, J. Chem. Phys. 74, 2888 (1981).

Appendix F

The Excitation of $O(^1S)$ in the Reaction Between $N_2(A\ ^3\Sigma_u^+)$ and $O(^3P)$

The excitation of O(^1S) in the reaction between $N_2(A\ ^3\Sigma_u^+)$ and O(^3P)

Lawrence G. Piper

Physical Sciences Inc., Woburn, Massachusetts 01801
(Received 5 February 1982; accepted 12 May 1982)

The rate constant for the excitation of O(^1S) in the reaction between $N_2(A\ ^3\Sigma_u^+, v = 0)$ and O(^3P) has been measured in a discharge-flow reactor at room temperature to be $(2.1 \pm 0.4) \times 10^{-11}$ cm^3 molecule^{-1} s^{-1}. Combining this measurement with the previously determined rate constant for total quenching of $N_2(A)$ by O shows that the fraction of all quenching events which lead to O(^1S) excitation is 0.75 ± 0.13. These results are at variance with rate constants estimated from some auroral models and indicate that some revision of auroral models is in order.

I. INTRODUCTION

Following their observation of O(^1S) excitation in laboratory studies on the interaction between $N_2(A)$ and O(^3P), Meyer *et al.*[1] suggested that the energy-transfer reaction between $N_2(A)$ and O was an important mechanism for the production of the auroral green line O(^1S—^1D, λ 557.7 nm). Since that work controversy has raged over the relative importance of the $N_2(A)$ + O excitation mechanism compared to other possible green-line excitation channels.[2–14] Much of this controversy resulted from a state of ignorance over the magnitude of the rate constant for quenching $N_2(A)$ by O and the fraction of $N_2(A)$ + O quenching events which lead to O(^1S) excitation. A number of years ago Meyer *et al.*,[15] and Dunn and Young[16] reported rate constants for the quenching of $N_2(A)$ by O. In addition, Meyer *et al.* estimated that about 25% of the quenching collisions between $N_2(A)$ and O resulted in O(^1S) excitation, although, as they pointed out, this value is in reality a lower bound because they didn't correct for O(^1S) quenching. Although the experimental results of Meyer *et al.* and Dunn and Young agreed, several experimental uncertainties plagued both studies, and neither has been generally accepted by the aeronomic community.

A number of aeronomers[7–14] have preferred to try to infer the rate constant for quenching $N_2(A)$ by O and for excitation of O(^1S) in the $N_2(A)$ plus O reaction by varying rate constants in an auroral model until the model predictions could be made to coincide with the atmospheric observations. This process is risky, however, because some of the important parameters in the model, such as atomic oxygen number density, usually are quite uncertain.[3] In addition, some models neglect important processes such as quenching of $N_2(A)$ by NO which can be significant in a strong aurora where NO number densities can build up to levels as high as 10^{15} molecules cm^{-3}.[17] Therefore, it is not surprising that model-derived rate constants for the $N_2(A)$ plus O reaction vary by more than an order of magnitude, nor that estimates of the fraction of quenching events leading O(^1S) vary between 0.13 and unity.

We have shown recently that the rate constants for quenching $N_2(A)$ by atomic oxygen are 2.8×10^{-11} and 3.4×10^{-11} cm^3 molecule^{-1} s^{-1} for vibrational levels 0 and 1, respectively.[18] In this paper we present the results of experimental measurements on the rate constant for excitation of O(^1S) in the $N_2(A)$ plus O reaction which show that 75% of all quenching events lead to O(^1S) excitation.

II. EXPERIMENTAL

The experimental apparatus is a discharge-flow reactor in which $N_2(A)$ number densities are monitored by observing individual vibrational bands of the Vegard–Kaplan (N_2 $A\ ^3\Sigma_u^+ - X\ ^1\Sigma_g^+$) system of nitrogen. The reactor, described in detail previously by Piper *et al.*,[18,19] is a 2 in. diameter quartz tube which is pumped by a Roots blower that is capable of producing linear flow velocities up to 8×10^3 cm s^{-1} at pressures of 1 Torr. A 0.5 m monochromator (Minuteman) is mounted upon a set of rails parallel to the flow tube. Spectral observations of the luminous gases in the flow tube, therefore, can be made as a function of linear distance along the tube by sliding the monochromator up and down on its rails. The reaction time is the ratio of distance to flow velocity. A thermoelectrically cooled EMI 9558QA photomultiplier and an SSR 1105 photon-counting rate meter measure light intensities photoelectrically.

The reaction between metastable Ar($^3P_{0,2}$) and molecular nitrogen makes the metastable nitrogen molecules.[20–23] This transfer produces primarily the $C\ ^3\Pi_u$ state of N_2[22] which quickly cascades radiatively to the metastable $A\ ^3\Sigma_u^+$ state via the $B\ ^3\Pi_g$ state. A cold, hollow-cathode discharge (210 V and 3 mA) through the flowing argon produces the argon metastables. The argon was purified by flowing it through a trap filled with 5 Å molecular sieve and cooled with dry ice. Typically, the argon flow rate is ~ 1600 μmol s^{-1}, the nitrogen flow rate is ~ 100 μmol s^{-1}, the flow tube pressure about 1.3 Torr, and the flow velocities ~ 1400 cm s^{-1}.

A microwave discharge through a small amount of O_2 in helium (typical flows: 1 μmol s^{-1} of O_2 and 100 μmol s^{-1} of He) makes atomic oxygen. The oxygen atoms enter the flow tube through a 1 m. diameter loop fabricated from 2 mm o.d. polyethylene tubing. O-atom number densities were determined by measuring the air-afterglow signal at 580 nm,[23,24] with a 5 nm bandpass as a function of NO number density when NO was injected into the flow tube through a second loop 10 cm downstream from the oxygen injector. Then the slope of the line representing the air-afterglow intensity as a function of

0021-9606/82/172473-06$02.10 ©1982 American Institute of Physics 2373

$[NO]$ divided by κ, an apparatus calibration constant, gives $[O]$. We have discussed in detail previously how to determine κ.[17,18] Even though small amounts of ozone could be by-products of the O-atom discharge, there can be no interference from the O_3 + NO chemiluminescent reaction in the technique for determining the O-atom number density. The continuum generated from the O_3 - NO reaction has a short wavelength cutoff of 600 nm.[25]

A series of calibrations taken over a period of time established κ to ± 10%. The slopes of the $I_{O/NO}$ vs $[NO]$ plots for the determination of $[O]$ had standard deviations less than 5%. Thus, the determination of $[O]$ is in principle accurate to ± 12%. Because the measurements of $[O]$ were not made simultaneously with the kinetic measurements, it is possible that short-term variations in $[O]$ could lead to differences between the number density of O measured and that actually in the reactor during the kinetic measurements. We shall assume these differences to be random and, therefore, included in the experimental scatter in the data analysis.

The molecular oxygen was purified by pumping on liquid O_2 prior to expanding the middle portion of the liquid O_2 into a 5 ℓ storage bulb. The nitric oxide used in the O-number-density determinations was purified by slowly flowing NO through an ascarite trap, and then a trap at dry ice temperature prior to storage in a 5 ℓ bulb.

III. ANALYSIS AND RESULTS

We have observed variations in the ratio of the intensity of the aurora green line, $O(^1S-{}^1D)$, at 558 nm to the Vegard–Kaplan 0, 6 band as a function of atomic-oxygen number density and time. The processes which must be considered in the data analysis are

$$N_2(A) + O(^3P) \rightarrow O(^1S) + N_2(X), \tag{1a}$$

$$\rightarrow \text{other products}, \tag{1b}$$

$$N_2(A) + O_2 \rightarrow \text{products}, \tag{2}$$

$$N_2(A) + \text{wall} \xrightarrow{k_w^A} N_2(X),$$

$$O(^1S) + O(^3P) \rightarrow 2O(^3P \text{ or } {}^1D), \tag{3}$$

$$O(^1S) + O_2 \rightarrow \text{products}, \tag{4}$$

$$O(^1S) + \text{wall} \xrightarrow{k_w^S} O(^3P).$$

The differential equation which describes the change in the $N_2(A)$ number density as a function of time is

$$\frac{d[N_2(A)]}{dt} = -(k_1[O] + k_2[O_2] + k_w^A)[N_2(A)]. \tag{5}$$

Under pseudofirst-order conditions ($[N_2(A)] \ll [O]$, $[O_2]$) it has the solution

$$[N_2(A)] = [N_2(A)]_0 e^{-k_A t}, \tag{6}$$

where $k_A = k_1[O] + k_2[O_2] + k_w^A$.

The differential equation for the temporal history of $O(^1S)$ is

$$\frac{d[O(^1S)]}{dt} = k_{1a}[O][N_2(A)] - (k_3[O] + k_4[O_2] + k_w^S)[O(^1S)]. \tag{7}$$

The analytical solution to this equation is

$$[O(^1S)] = \frac{k_{1a}[O][N_2(A)]_0}{K_S - K_A}\{e^{-K_A t} - e^{-K_S t}\}, \tag{8}$$

where $K_S = k_3[O] + k_4[O_2] + k_w^S$. Using the result in Eq. (6) and rearranging slightly gives

$$\frac{[O(^1S)]}{[N_2(A)]} = \frac{k_{1a}[O]}{K_S - K_A}\{1 - e^{-(K_S - K_A)t}\}. \tag{9}$$

This result ignores differences in decay rate between the different vibrational levels of $N_2(A)$. Allowing for the vibrational-level effect gives

$$\frac{[O(^1S)]}{[N_2(A)]_{t'=0}} = \frac{k_{1a}^{v'=0}[O]}{K_S - K_{A_{v'=0}}}\{1 - \exp[-(K_S - K_{A_{v'=0}})t]\} + \frac{k_{1a}^{v'=1}[O]}{K_S - K_{A_{v'=1}}}\{1 - \exp[-(K_S - K_{A_{v'=1}})t]\} \cdot \frac{[N_2(A)]_{v'=1}^0}{[N_2(A)]_{v'=0}^0}\exp\{-\Delta k_1[O_2] + \Delta k_2[O]\}t, \tag{10}$$

where $K_{A_{v'=0,1}}$ are as given above but with state-specific rate constants k_1 and k_2. Δk_1 and Δk_2 are the differences in the respective rate constants between $v' = 1$ and 0, respectively, and the super 0 on the $N_2(A)$ number densities represent initial conditions.

Our experimental observations consisted of measurements of the decay of the 0, 6 Vegard–Kaplan band and of the $O(^1S)$ 558 nm line as a function of time over a range of O-atom number densities of $0.16 - 3.9 \times 10^{12}$ atoms cm^{-3} and effective reaction times of 18–29 ms, and a spectral scan over the Vegard–Kaplan bands at the beginning of each run to obtain a value for the ratio of $[N_2(A)]_{v'=1}^0 / [N_2(A)]_{v'=0}^0$. Although the data showed only a small or negligible change in the ratio $I_0(^1S)/I_{7,6}$ as a function of time, the exponential term in Eq. (10) did contribute significantly to the overall kinetics so that a complete analysis of the data according to Eq. (10) was necessary.

Only two of the rate constants in Eq. (10) are unknown k_{1a} the subject of this investigation, and k_3. Several values have been published for k_3[26–28] spanning a range of several orders of magnitude. Slanger and Black[29] have shown recently, however, that some of these measurements were marred by the presence of $O_2(a^1\Delta)$ in the reactor in addition to atomic oxygen. $O_2(a^1\Delta)$ quenches $O(^1S)$ at a gas kinetic rate.[29] $O_2(a^1\Delta)$ was undoubtedly present in our measurements also, but at number densities so low that we would not have been able to measure them by conventional methods. However, Oreyzko has shown that the ratio of $[O_2(a^1\Delta)]$ to $[O]$ produced in a discharge containing traces of molecular oxygen in argon or helium is constant at constant pressure, being independent of $[O_2]$. Thus $[O_2(a^1\Delta)] = C[O]$,

TABLE I. Rate constants used in data analysis.

Reaction		Rate constant[a]	Reference
(1) $N_2(A) + O$	→ products	2.8×10^{-11} ($v' = 0$) 3.4×10^{-11} ($v' = 1$)	17
(2) $N_2(A) + O_2$	→ products	2.3×10^{-12} ($v' = 0$) 4.1×10^{-12} ($v' = 1$)	19, 31, 32
(3) $O(^1S) + O(^3P)$	→ products	$< 10^{-11}$	29
(4) $O(^1S) + O_2(X\,^3\Sigma)$	→ products	$(3 \pm 1) \times 10^{-13}$	33–35
(5) $O(^1S) + O_2(a\,^1\Delta)$	→ products	1.7×10^{-10}	29

[a]Rate constants are at 298 K and are in units of cm^3 molecule^{-1} s^{-1}.

and we can treat k_3 as an effective atomic-oxygen quenching rate constant which must be determined.

We have reported previously the rate constant k_1,[17] and our value for k_2[19] agrees well with the other recent literature[31,32] (see Table I). The rate constant k_4[33–35] may safely be neglected compared to k_3. The wall-loss rate constants k_w can be calculated from the known diffusion coefficients of $N_2(A)$[36–38] and $O(^1S)$[39,40] in argon since both species are quenched with unit efficiency at the reactor walls:

$$k_w = \frac{0.62\,D_0}{\Lambda^2 P}\,, \tag{11}$$

where $\Lambda^2 = (a/\lambda_0)^2$ with λ_0 being the first root of the Bessel function J_0, a the flow tube radius, D_0 the diffusion coefficient in argon, and the factor of 0.62 is included to correct for the coupling of the parabolic velocity profile with the radial density gradient of diffusing species. Corney and Williams[39] and Zipf[40] both have measured the diffusion coefficient of $O(^1S)$ in argon at 298 K obtaining 268 ± 10 and 260 ± 6 $cm^2 s^{-1}$ at 1 Torr, respectively. We have analyzed our data with the value 265 $cm^2 s^{-1}$ at 1 Torr. Brömer and Spieweck,[37] Zipf,[36] and Levron and Phelps[38] all have determined the diffusion coefficient of $N_2(A)$ in nitrogen to be 153 $cm^2 s^{-1}$ at 1 Torr while Levron and Phelps have also measured the diffusion coefficient of $N_2(A)$ in argon to be 153 ± 10 and 169 ± 6 $cm^2 s^{-1}$ at 1 Torr for $v' = 0$ and 1 of $N_2(A)$, respectively. We have chosen to use the value 155 $cm^2 s^{-1}$ at 1 Torr for both vibrational levels. The diffusion coefficient of $O(^1S)$ in argon is 15% larger than the diffusion coefficient of $O(^3P)$ in argon measured by Morgan and Schiff,[41] while the $N_2(A)$ diffusion coefficient is 8% larger than that for ground-state nitrogen.[42]

The raw data in the form of an intensity ratio had to be corrected by the factor γ which relates intensities to populations

$$\gamma = \frac{R_\lambda^{1S}\, {}^{1}_{1S}\beta}{R_\lambda^{0,6} A_{0,6}}\,, \tag{12}$$

where R_λ^i is the relative monochromator response function and A_i is the Einstein coefficient of species i [(0.163 for the 0,6 Vegard–Kaplan band[43] and 1.18 for the $O(^1S \rightarrow {}^1D)$ transition[44]], β is a correction factor relating the measured peak height of the 0,6 band to the integrated band intensity.

The reaction time is given by $(z - z_0)/\bar{v}$ where z is the distance from the injector to the observation region, z_0 is a mixing correction of 10%–15%, and $\bar{v}$ is the bulk flow velocity. The analysis of the $N_2(A) + O$ rate constants[17] showed that $z_0 = 4.5$ cm under our experimental conditions.

We analyzed all our data using a nonlinear least-squares program based on Eq. (10) and the input parameters just discussed. The ratio k_{1a}/k_1 was assumed to be the same for both vibrational levels, even though the rate constants differ by about 20%. This assumption does not introduce significant uncertainties in the final value obtained for k_{1a}. The two parameters to be determined in the fit were $k_{1a}^{v'=0}$ and k_3.

The results of the fit gave $k_{1a}^{v'=0} = (2.1 \pm 0.2) \times 10^{-11}$ cm^3 molecule^{-1} s^{-1} and $k_3 = (5.7 \pm 0.4) \times 10^{-11}$ cm^3 molecule^{-1} s^{-1}, where the quoted uncertainty is one standard deviation from the least-squares fit. The $O(^1S)$ production ef-

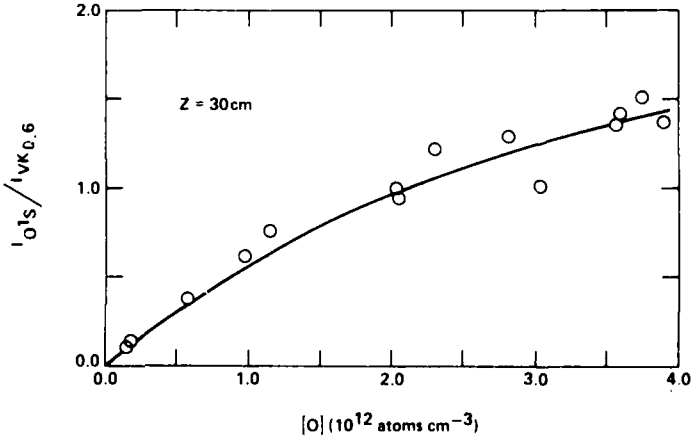

FIG. 1. Variation in ratio of $O(^1S)$ emission intensity to that of Vegard–Kaplan 0,6 band as a function of [O] for a mixing distance of 30 cm.

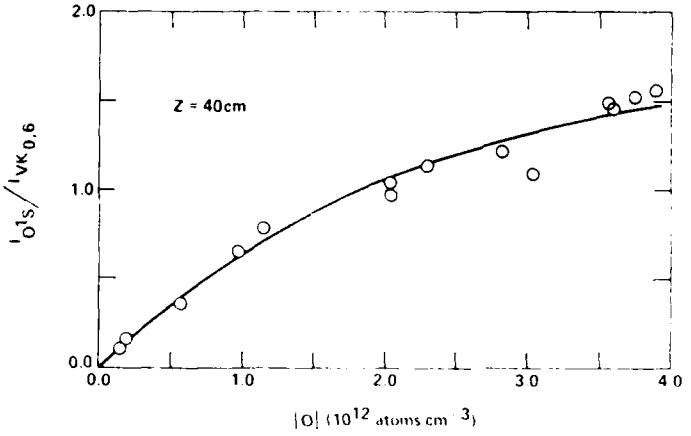

FIG. 2. Variation in ratio of $O(^1S)$ emission intensity to that of Vegard–Kaplan (0,6) band as a function of [O] for a mixing distance of 40 cm.

ficiency η from this fit is 0.75. We find a sensitivity analysis of the data by varying in turn values of the $N_2(A)$ quenching rate constants, the difference between the $O(^1S)$ and $N_2(A)$ wall loss rate constants, the ratio $[N_2(A)]^0_{t'}/[N_2(A)]^0_{t''}$, and the mixing correction while holding the other parameters fixed at their normal values. The only significant changes came in varying the wall-loss rate-constant difference, where a change of ±12% changed $k^{t'}_{1a}$ by ±5%, and the ratio $[N_2(A)]^0_{t'}/[N_2(A)]^0_{t''}$ where a ±20% variation gave a ±7% change in $k^{t'}_{1a}$. A complete error analysis in which all experimental uncertainties were estimated indicated a 17% uncertainty in the ratio η if the ±20% uncertainty in the Vegard–Kaplan transition probability is neglected, and a 27% overall uncertainty when the $A_{v,6}$ error estimate is included. The error limits on $k^{t'}_{1a}$ (19^{+}_{-}% and 28^{+}_{-}% for neglect and inclusion of $A_{v,6}$ uncertainty, respectively) are slightly larger than those for the rate-constant ratio η due primarily to a cancellation of [O] (12% uncertainty) in determining η.

Data at two reaction times are shown in Figs. 1 and 2. The line through the data is the best fit to Eq. (10) when pressure, flow velocity, and the ratio [O]/[O_2] are assumed to be the same for all points. This fit gives values of k_{1a} and k_{1b} about 10% larger than the complete fit. Our results are summarized in Table II.

TABLE II. Excitation of $O(^1S)$ in $N_2(A)+O$ reaction.

Process	Value
(1a) $N_2(A^3\Sigma^+_u, v'=0,1) + O(^3P) \rightarrow O(^1S) + N_2(X^1\Sigma^+_g)$	k_{1a} (2,1 + 0,0) $= 1.0 \times 10^{-11}$ a (2,1 + 0,0) $= 1.0 \times 10^{-11}$ b
(1b) $N_2(A^3\Sigma^+_u, v'=0,1) + O(^3P) \rightarrow$ all products	$k^{(2,1)}_{1b} = (2,1 + 0,0) = 0.3 \times 10^{-11}$ c $k^{(1,0)}_{1b} = (1,0) = 0.6 \times 10^{-11}$ c $\frac{k_{1a}}{k_{1b}} = 0.75 \pm 0.13$ $= 0.75 \pm 0.20$ d

[a] Rate constants are at 298 K and are in units of cm^3 molecule^{-1} s^{-1}.
[b] The error estimates of these values include the 20% uncertainty in $A_{VK_{0,6}}$.
[c] Reference 17.

IV. DISCUSSION

If we assume that some of the $O(^1S)$ quenching is by $O_2(a^1\Delta)$ rather than by O, then the least-squares fit k_3 represents an effective $O_2(a^1\Delta)$ quenching rate constant k_3^{eff}:

$$k_3^{eff} = k_3 + k_{3'}\frac{[O_2(a^1\Delta)]}{[O]} . \quad (13)$$

If k_3 is negligible, Slanger and Black's[23] value of $k_{3'}$ (1.7×10^{-11} cm^3 molecule^{-1} s^{-1}) along with our experimentally derived k_3^{eff} gives $[O_2(a^1\Delta)]/[O] = 0.34$. We would not have been able to measure such small amounts of $O_2(a^1\Delta)$ in our reactor using conventional techniques.

The presence of $O_2(a^1\Delta)$ in our reactor in no way affects the value obtained for k_{1a}. The reaction between $N_2(A)$ and $O_2(a^1\Delta)$ lacks sufficient energy to give $O(^1S)$ as a product. However, if $O_2(a^1\Delta)$ is a very efficient quencher of $N_2(A)$ (i.e., a rate constant $>10^{-11}$ cm^3 molecule^{-1} s^{-1}) then our previously reported rate constant for quenching $N_2(A)$ by O[17] could be too high as we have already discussed. In this event, the value of η deduced in these studies would be too low and a value closer to unity would be correct. The $[O_2(a^1\Delta)]/[O]$ ratio estimated above and the constraint that $\eta \leq 1$ limit the $N_2(A)+O_2(a^1\Delta)$ rate constant to be less than or equal to 2×10^{-11} cm^3 molecule^{-1} s^{-1}.

Within the past ten years, aeronomers have tried to explain auroral observations of Vegard–Kaplan and OI 558 nm emissions by proposing total $N_2(A)+O$ quenching rate constants between 1.5 and 40×10^{-11} cm^3 molecule^{-1} s^{-1} and $O(^1S)$ excitation efficiencies between 0.13 and unity. We feel that the present measurements on $O(^1S)$ excitation and our earlier $N_2(A)+O$ rate constant determination[17] should remove one long standing source of controversy in trying to reconcile auroral models with auroral measurements. Other parameters in auroral models such as atomic oxygen number density, $N_2(A^3\Sigma^+_u)$

excitation mechanism and $O(^1S)$ quenching rates are now less certain than the kinetics of the $N_2(A)+O$ interaction, and should receive more attention in the future.

Swider[45] suggested that the reaction between $N_2(A)$ and O could be an important source of NO in auroras and perhaps in the quiet daytime E region. The results of this study indicate that the reactive channel is minor compared to the direct energy-transfer channel. Thus NO production does not appear to be a major consequence of the $N_2(A)+O$ interaction. We do plan to investigate the importance of this reactive channel in the near future, however, as a check on the present results.

ACKNOWLEDGMENTS

These experiments were conducted at the Air Force Geophysics Laboratories in Bedford, Massachusetts, under Air Force Contract No. F19628-77-C-0089. We thank J. P. Kennealy for the use of his laboratory facilities. Interesting discussions with R. R. O'Neil (AFGL), T. G. Slanger (SRI, Int.), E. A. Ogryzolo (University of British Columbia), and W. T. Rawlins (PSI) were most helpful.

[1]L. A. Meyer, D. W. Setser, and D. H. Stedman, Astrophys. J. **157**, 1023 (1969).
[2]T. D. Parkinson and E. C. Zipf, Planet. Space Sci. **18**, 895 (1970).
[3]K. Henriksen, Planet. Space Sci. **21**, 863 (1973).
[4]A. W. Yau and G. G. Shepherd, Planet. Space Sci. **27**, 481 (1978).
[5]W. E. Sharp and D. G. Torr, J. Geophys. Res. **84**, 5345 (1979).
[6]R. R. O'Neil, E. T. P. Lee, and E. R. Huppi, J. Geophys. Res. **84**, 823 (1979).
[7]D. M. Hunten and M. B. McElroy, Rev. Geophys. **4**, 303 (1966).
[8]W. E. Sharp, J. Geophys. Res. **76**, 987 (1971).
[9]D. E. Shemansky, E. C. Zipf, and T. M. Donahue, Planet. Space Sci. **19**, 1669 (1971).
[10]A. Vallance-Jones and R. L. Gattinger, J. Geophys. Res. **81**, 497 (1976).
[11]M. H. Rees, G. G. Sivjee, and K. A. Dick, J. Geophys. Res. **81**, 6046 (1976).
[12]A. J. Deans and G. G. Shepherd, Planet. Space Sci. **26**, 319 (1978).
[13]W. E. Sharp, M. H. Rees, and A. I. Stewart, J. Geophys. Res. **84**, 1977 (1979).
[14]D. G. Torr and W. E. Sharp, Geophys. Res. Lett. **6**, 860 (1979).
[15]L. A. Meyer, D. W. Setser, and D. H. Stedman, J. Phys. Chem. **74**, 2238 (1970).
[16]G. J. Dunn and R. A. Young, Int. J. Chem. Kinet. **8**, 161 (1976).
[17]L. G. Piper, G. E. Caledonia, and J. P. Kennealy, J. Chem. Phys. **75**, 2847 (1981).
[18]G. E. Caledonia, L. G. Piper, W. T. Rawlins, and B. D. Green, PSI TR-233 (1980), available from the authors upon request.
[19]L. G. Piper, G. E. Caledonia, and J. P. Kennealy, J. Chem. Phys. **74**, 2888 (1981).
[20]D. W. Setser, D. H. Stedman, and J. A. Coxon, J. Chem. Phys. **53**, 1004 (1970).
[21]D. H. Stedman and D. W. Setser, Chem. Phys. Lett. **2**, 542 (1968).
[22]N. Sadeghi and D. W. Setser, Chem. Phys. Lett. **82**, 44 (1981).
[23]F. Kaufman, Proc. R. Soc. London Ser. A **247**, 123 (1958).
[24]F. Kaufman, *Chemiluminescence and Bioluminescence*, edited by M. J. Cormier, D. M. Hercules, and J. Lee (Plenum, New York, 1973), pp. 83–100.
[25]P. N. Clough and B. A. Thrush, Trans. Faraday Soc. **63**, 915 (1967).
[26]W. Felder and R. A. Young, J. Chem. Phys. **56**, 6028 (1972).
[27]T. G. Slanger and G. Black, J. Chem. Phys. **64**, 3763 (1976).
[28]For a review of the $O(^1S)+O$ quenching literature see D. R. Bates, Planet. Space Sci. **26**, 897 (1978).
[29]T. G. Slanger and G. Black, Geophys. Res. Lett. **8**, 535 (1981).
[30]E. A. Ogryzlo (private communication, 1980).
[31]E. C. Zipf, Nature (London) **287**, 523 (1980).
[32]M. P. Ianuzzi and F. Kaufman, J. Phys. Chem. **85**, 2163 (1981).
[33]T. G. Slanger, B. J. Wood, and G. Black, Chem. Phys. Lett. **17**, 401 (1972).
[34]S. V. Filseth, F. Stuhl, and K. H. Welge, J. Chem. Phys. **52**, 239 (1970).
[35]R. Atkinson and K. H. Welge, J. Chem. Phys. **57**, 3689 (1972).
[36]E. C. Zipf, J. Chem. Phys. **38**, 2034 (1963).
[37]H. H. Brömer and F. Spieweck, Planet. Space Sci. **15**, 689 (1971).
[38]D. Levron and A. V. Phelps, J. Chem. Phys. **69**, 2260 (1978).
[39]E. C. Zipf, Bull. Am. Phys. Soc. **14**, 264 (1969).
[40]A. C. Corney and J. Williams, J. Phys. P **5**, 686 (1971).
[41]J. E. Morgan and H. I. Schiff, Can. J. Chem. **42**, 2300 (1964).
[42]J. O. Hirschfelder, C. J. Curtiss, and R. B. Bird, *Molecular Theory of Gases and Liquids* (Wiley, New York, 1954).
[43]D. E. Shemansky, J. Chem. Phys. **51**, 689 (1969).
[44]C. Nicolaides, O. Sinanoğlu, and R. Westhouse, Phys. Rev. A **4**, 1403 (1971).
[45]W. Swider, Geophys. Res. Lett. **3**, 335 (1976).

END